Coherent and Non-coherent Techniques for Cooperative Communications

Ph.D

Kai Zhu
University of York
Electronics

May 2014

Abstract

Future wireless network may consist of a cluster of low-complexity battery-powered nodes or mobile stations (MS). Information is propagated from one location in the network to another by cooperation and relaying. Due to the channel fading or node failure, one or more relaying links could become unreliable during multiple-hop relaying. Inspired by conventional multiple-input multiple-output (MIMO) techniques exploiting multiple co-located transmit antennas to introduce temporal and spatial diversity, the error performance and robustness against channel fading of a multiple-hop cooperative network could be significantly improved by creating a virtual antenna array (VAA) with various distributed MIMO techniques. In this thesis, we concentrate on the low-complexity distributed MIMO designed for both coherent and non-coherent diversity signal reception at the destination node.

Further improvement on the network throughput as well as spectral efficiency could be achieved by extending the concept of unidirectional relaying to bidirectional cooperative communication. Physical-layer network coding (PLNC) assisted distributed space-time block coding (STBC) scheme as well as non-coherent PLNC aided distributed differential STBC system are proposed. It is confirmed by the theoretical analysis that both approaches have the potential for offering full spatial diversity gain.

Furthermore, differential encoding and non-coherent detection techniques are generally associated with performance degradation due to the doubled noise variance. More importantly, conventional differential schemes suffer from the incapability of recovering the source information in time-varying channels owing to the assumption of static channel model used in the derivation of non-coherent detection algorithm. Several low-complexity solutions are proposed and studied in this thesis, which are able to compensate the performance loss caused by non-coherent detection and guarantee the reliable recovery of information in applications with high mobility. A substantial amount of iteration gain is achieved by combining the differential encoding with error-correction code and sufficient interleaving, which allows iterative possessing at the receiver.

Contents

List of Figures

List of Tables

Acknowledgements

First and foremost, I would like to express my sincere gratitude to my supervisor, Prof. Alister, for his countless hours of work guiding me throughout the PhD study. Without the kind, generous and patient support of him, this thesis would never go this far.

I benefit a lot from his rigorous attitude for scientific research which is invaluable fortune for my future research career.

Special thanks go to my thesis advisor, Dr. Yuriy Zakharov, for his inspiring discussion and suggestion.

I am also grateful to my colleagues in the Communication Research Group for their help and assistance, the group discussions with them are quite thought-provoking.

The financial support of the EPSRC UK and British Telecom (BT) is gratefully acknowledged.

I would like, last but not the least, to thank my parents and partner for their love, care, and support; to them I dedicate this thesis.

Declaration

All work presented in this thesis is original to the best knowledge of the author. References and acknowledgements to other researchers have been given as appropriate.

Some of the research presented in this thesis has resulted in some publications. These publications are listed as follows.

- Journal Paper

  1. **K. Zhu** and A. G. Burr, "Performance Analysis of Relay Selection Aided Distributed STBC for Two-Way Relay Channel with Physical-Layer Network Coding," *IEEE Trans. Commun.*, under preparation, 2014.
  2. **K. Zhu** and A. G. Burr, "Iterative Non-coherent DPSK Detection for Fast Fading Channels," *IEEE Trans. Commun.*, under preparation, 2014.

- Conference Paper

  1. **K. Zhu** and A. G. Burr, "Relay Selection Aided Distributed Space-Time Block Code for Two-Way Relay Channel with Physical-Layer Network Coding," *Proceedings of IEEE Vehicular Technology Conference (VTC)*, pp.1-5, Budapest, Hungary, May 2011.
  2. **K. Zhu** and A. G. Burr, "Differential Distributed Space-time Block Code for Two-way Relay Channel with Physical-layer Network Coding," *Proceedings of Progress in Electromagnetics Research Symposium (PIERS)*, pp.1-5, Kuala Lumpur, Malaysia, March 2012.(Invited Paper)
  3. **K. Zhu** and A. G. Burr, "A Simple Non-Coherent Physical-Layer Network Coding for Transmissions Over Two-Way Relay Channels," *Proceedings of IEEE Global Communications Conference (GLOBECOM)*, pp.2268–2273, Anaheim, California, USA, December 2012.
  4. **K. Zhu** and A. G. Burr, "Two-Way Non-Coherent Physical-Layer Network Coded Differential Distributed Space-Time Block Coding," *Proceedings of IEEE Wireless Communications and Networking Conference (WCNC)*, pp.2416–2421, Shanghai, China, April 2013.
  5. **K. Zhu** and A. G. Burr, "Iterative Non-coherent Detection of Serially-Concatenated Codes with Differential Modulation," *Proceedings of IEEE Wireless Communications and Networking Conference (WCNC)*, pp.3969–3973, Shanghai, China, April 2013.

6. **K. Zhu** and A. G. Burr, "Iterative Non-coherent Detected DPSK Systems in Fast Fading Channels," *Proceedings of IEEE Wireless Communications and Networking Conference (WCNC)*, pp.660-665, Istanbul, Turkey, April 2014.

Chapter 1

Introduction

Contents

1.1 Historical Perspective and State-of-the-Art

Ever since the very first long-distance transatlantic radio communication was unveiled by Italian physicist Guglielmo Marconi, wireless technology has been evolving at a dramatic rate in 113 years, from transmission of simple single-bit Morse code to the 4th generation cellular system supporting H.264 high-definition multimedia streaming. The prevalence of laptop, smartphone and tablet reveals that wireless already permeates every aspect of our daily lives. In 2013, there are almost 6.8 billion mobile-cellular users in the world that implies the number of mobile subscriptions approaches the global population as published in International Telecommunication Union (ITU) annual report [1].

The first generation of mobile system using analog transmission was launched in the early 1980s. In the next decade, more sophisticated digital transmission technology was incorporated in the second generation of cellular communication system. Unfortunately,

its commercial application was mostly limited to speech only due to a theoretical transfer speed of 9.6 kilobits per second (kb/s). With supporting multimedia and other form of high bit-rate services in mind, the third generation system and its successor, 4G Long-Term Evolution (LTE), are aiming towards a peak data rate measured at several megabits per second (mb/s) or even more [2].

The main driving force that facilitates innovations in the wireless industry is the promise of accessibility, mobility and portability. While an increasing number of users are enjoying the freedom from being physically connected, the demands on bandwidth and spectral efficiency are growing in an explosive manner. However, in order to fulfill the current demand of wireless market, information throughput is required at least several orders of magnitude higher compared to the data rates made available by state-of-the-art technology.

On the other hand, radio spectrum is rare and crowded since a huge portion of spectrum is dedicated to satellite, military, broadcast radio and TV. Moreover, a large block of government reserved spectrum also needs to be taken into account. Consequently radio spectrum resource is extremely expensive, a few megahertz or even just kilohertz of bandwidth may cost billions of dollars to acquire. [1] Civilian digital mobile networks are working around the 1GHz and 2.5GHz at which signals can penetrate obstacles, at the same time there is still enough bandwidth for large amounts of data transmission.

The objective of telecommunications is to reliably transmit information between geographically separated locations via wireless medium with adequate quality at a certain rate. In practice, however, the wireless medium/channel would severely impair the transmitted signals causing the received power level fluctuates rapidly. Such undesirable interference is generally defined as channel fading. Thermal noise introduced by the electronic circuit in receivers also challenges the reliable signal detection and recovery [4]. Therefore, design of modern wireless communication system is a uphill task. The dilemma for engineers is how to cope with limited availability of radio frequency spectrum, time-varying nature of the wireless channel and many other real-world limitations, while at the same time meeting the demand for high data traffic and quality of wire-line communication.

Modern wireless communication system is under the constraint of two major resources, i.e. transmit power and spectral bandwidth. Transmitting some information to the receiver at a certain rate requires certain spectral bandwidth and power which are under

[1] British telecom company Everything Everywhere Ltd (EE) has to pay £588,876,000 for 4G spectrum license at 796-801 MHz and 837-842 MHz, 2535-2570 MHz and 2655-2690Mhz (Source: Ofcom [3]).

strict control of government organization, like Federal Communications Commission (FCC) in the U.S. In most cases, one of these resources is more precious than the other. Hence, the communication systems can be correspondingly classified as power-limited and bandwidth-limited systems. For bandwidth-limited systems, one should make the best use of bandwidth at the expense of power. Furthermore, bandwidth efficient modulation schemes are capable of improving the performance without bandwidth expansion.

1.2 MIMO and Diversity Techniques

What is the ultimate performance limit of wireless communication systems, underlying only by the fundamental physical nature? This question is addressed in Shannon's groundbreaking work in the field of information theory [5]. The maximum possible transmission rate is bounded by the channel capacity at which information can be transmitted over the channel with arbitrarily small probability of error, despite the presence of noise.

Since the available radio spectrum is limited as mentioned earlier, the solution to improving maximum data rate as well as spectral efficiency relies primarily on the design of more efficient signaling techniques. Advances in error control coding, such as turbo codes (TC) [6] and low density parity check codes (LDPC) [7, 8] are both capable of performing very close to the Shannon capacity limit in systems with a single transmit and receive antenna, generally termed single-input single-output (SISO) systems.

Further capacity gain can be achieved by increasing the number of antennas at either/both end(s) of the communication link. Systems equipped with multiple transmit and receive antennas are usually called multiple-input multiple-output (MIMO) systems. Recent research has proven from the information-theoretical viewpoint that enormous capacity gains are available for such channels due to the diversity obtained from the independent fading experienced by individual signal paths corresponding to different antennas [9–14]. It is pointed out that the capacity limit of MIMO channels scales approximately linearly with the number of antennas.

The term 'diversity' or 'diversity order' generally indicates the slope of the error probability versus signal-to-noise ratio (SNR) curve. For single-user MIMO systems, maximum available diversity order is limited by $N_t \times N_r$, where N_t is the number of transmit antennas and N_r is the number of receive antennas [15]. To define diversity quantitatively, although lacking in mathematical rigor, the relationship between the received SNR, denoted by γ, and the probability of error $P_b(e)$ is asymptotically formulated as $P_b(e) \approx \gamma^{-d}$

as $\gamma \to +\infty$ where the exponent d represents the diversity order [16], a more formal definition is given in Chapter 3.

Diversity intends to mitigate the deleterious effect of fading. Various established modern communication systems use multiple receiving antennas at the base stations to provide receive diversity, for instance a base station in the GSM systems typically has two receiving antennas [17, 18]. Such configuration enables significant improvement in data rate and spectral efficiency for the communication link from mobile station (end user) to base station. The enormous benefits as well as substantial amount of performance gain promised by using multiple antennas ignited much research interest in this area. The diversity technique was further extended to allow exploiting diversity gain when only the transmitting side is equipped with multiple antennas, hence this technique is termed transmit diversity.

In practice, the power strength of received signals might attenuate heavily during transmission due to time-variant fading and interference from other users, which could lead to unreliable recovery of transmitted information at the receiver. Fortunately, the surrounding environment generally varies quickly with time, if the radio signals emitting from different transmit antennas propagate through several independent paths before reaching the receive antenna, the combined received signals are more likely to have sufficient power strength to support reliable detection at the receiver. Transmit diversity offers potential performance increase for the downlink (from base station to end user), although portable devices are usually power, size, and complexity limited.

1.3 Space-Time Coding

Pioneering work on transmit diversity dates back to early 90's, various delay transmit modulation schemes were proposed for deployment in the base stations. By activating two or more transmit antennas interchangeably, proposed scheme in [19] was effective in terms of generating exactly the same diversity gain as that acquired with receive diversity but at a cost of less efficiency in terms of required SNR for a target bit error probability.

Space-time coding (STC) is a practical real-world application of diversity technique that is capable of providing substantial capacity gain promised by the MIMO channels. The family of STC consists of space-time trellis coding (STTC) [20], space-time block coding (STBC) [21–23] and layered space-time (LST) [24] coding schemes. As suggested by their names, these distinct coding techniques for MIMO channels are designed to achieve diversity gains and/or coding gains, as well as high spectral efficiency, by introducing

encoding operations across both space and time domains. The original scheme of STC was based on trellis code [20] until a simpler version using block code was proposed in 1998 [21].

To elaborate further, STTC and STBC focus on boosting error performance and mitigating deleterious effect of channel-induced fading by transmitting duplicated information through different paths. Both STTC and STBC are able to deliver full diversity gain. On the other hand, LST is devised for higher attainable transmission rate and full multiplexing gain, which is implemented by sending independent information in parallel across different channels. The trade-offs between diversity gain and multiplexing gain is a rather multifaceted research topic and was studied throughly in [25] and references therein.

STBC is constructed from known orthogonal designs, where data streams to be transmitted are encoded in blocks and are distributed among spaced antennas across time, but STBC suffers from a lack of coding gain because of the orthogonal nature of STBC codewords. Nonetheless, code orthogonality in return facilitates a low-complexity decoding via linear processing at the receiver. On the other hand, STTC possesses both significant diversity advantage as well as enormous coding gain, yet are complex to decode due to the joint maximum likelihood sequence estimation. Furthermore, from the viewpoint of coding theory, STTC is an error-control code with coding rate of $1/N_t$, N_t is the number of transmit antennas [26].

STBC is more appealing in practice due to ease of implementation at the transmitter side as well as simple and optimal decoding at the receiver side. The Alamouti code [21] is historically the first STBC scheme that provides simultaneous full transmit diversity and full transmission rate. In other words, the Alamouti code exploits full diversity gain without needing to sacrifice the transmission rate. Alamouti STBC was originally proposed with two transmit antennas, later Tarokh *et al.* extended the concept of STBC using theory of orthogonal designs. As a result, the Alamouti code is deemed as a special case of the orthogonal STBC (OSTBC) [23]. It is worthwhile to mention that a series of quasi-orthogonal STBC (QOSTBC) are also discussed in [27, 28], which are able to operate at higher transmission rate at the cost of inter-symbol interference (ISI). In this thesis, the term 'STBC' is referring to the orthogonal STBC unless otherwise stated.

1.4 Organization of Thesis

After brief introduction of the basic philosophy of wireless communications, MIMO and diversity techniques, including space-time coding, the outline of this thesis is presented as follows.

- **Chapter 2:** The concept of STBC and its variants, including orthogonal STBC, layered STBC and linear dispersion codes (LDC), are reviewed. Literatures on the differential STBC (DSTBC) and two variants, including orthogonal differential STBC and unitary space-time modulation (USTM), are also presented. Emphases are given to the orthogonal STBC and orthogonal DSTBC, encoding and decoding procedures, extension to multiple receiving antennas as well as performance evaluations are also detailed in this chapter.

- **Chapter 3:** Cooperative communication and relaying techniques are introduced. Two-way relay network and existing two-way relaying strategies are elaborated. The concept of physical-layer network coding (PLNC) and benefit of employing PLNC in a two-way relay network are demonstrated. Novel selection relaying aided distributed STBC scheme for two-way cooperative communication is proposed and explained in detail. Theoretical tight upper and lower bounds as well as the exact bit error probability (BEP) are analyzed and solved.

- **Chapter 4:** The principles of distributed differential STBC schemes for unidirectional and bidirectional relaying scenarios are elaborated and evaluated in this chapter. Encoding and decoding procedures for the proposed distributed DSTBC are provided. Numerical analysis of the distributed coding scheme is also presented. A novel non-coherent PLNC algorithm is devised and investigated for two-way relay network dispensing with channel information.

- **Chapter 5:** The fundamentals of iterative decoding, maximum a posteriori (MAP) algorithm as well as soft-in soft-out (SISO) decoder are revisited. Several existing differential detection approaches are investigated, emphasis is given to the error performance improvement under fast fading channels. Four distinct iterative differential detection and decoding schemes, including non-coherent differential phase shift keying (DPSK) demapper, iterative a posteriori probability (APP) DPSK decoder, decision feedback differential detection (DFDD) aided soft DPSK demapper, and DFDD aided DPSK trellis decoder, are proposed and compared. DFDD aided DPSK trellis decoder utilizing decision feedback and trellis decoding is more robust in fast fading channels.

- **Chapter 6:** The main contributions are summarized to conclude the thesis. Suggestions for future research topics are presented.

1.5 Novel Contributions

The novel contributions of this thesis are summarized as follows.

- Conventional distributed STBC systems assume that the source and/or relay nodes are equipped with multiple co-located antennas, which could inflict extra complexity and energy consumption. Proposed novel distributed STBC as well as distributed differential STBC schemes are both based on the single-antenna assisted transceiver configuration. Most importantly, full diversity order is still guaranteed when a simple selection relaying or opportunistic relaying protocol is employed in the relay nodes. Furthermore, it is important that the effective throughput of proposed schemes is doubled as compared to the conventional 4-timeslot two-way relaying.

- Theoretical end-to-end BEP of proposed distributed STBC scheme over two-way relay channel is provided. Upper and lower bounds of the end-to-end BEP are derived using moment generating function (MGF) method, which is straightforward and intuitive. Moreover, the exact BEP expression is also solved. A direct comparison of analytical and empirical results confirms that the derived upper and lower bounds are accurate and tight.

- Novel non-coherent or differential PLNC is proposed, which has a low-complexity dual-branch structure. Similar to other existing differential techniques, differential PLNC is designed to extract the network-coded symbols dispensing with the channel information. Compared with the results reported in literature, the novel differential PLNC is able to perform as well as existing non-coherent PLNC schemes in terms of error performance, but the computational complexity is much lower.

- Proposed non-coherent PLNC is combined with distributed DSTBC, a fully non-coherent two-way relaying scheme is presented. To be more specific, DPSK is employed for the source-to-relay link, whereas distributed DSTBC is constructed during the relay-to-destination transmission. Such system configuration requires accurate channel estimation at neither of the receiving nodes, hence, proposed DPSK distributed DSTBC scheme is still able to facilitate simultaneous communication in a non-coherent way when the channel estimation is difficult to perform during

both transmission periods. Again, with the assistance of selection relaying protocol, full diversity gain is achieved at the destination nodes although each node in the cooperative network is single antenna assisted.

- The performance of differential detection is studied in the context of fast fading channel. Recovery of differentially-encoded information with trellis decoding algorithm could lead to significant improvement on the error rate, allowing near-coherent performance. Four iterative DPSK detection schemes are devised with different focus and considerations, for example, DFDD aided DPSK trellis decoding is designed to provide reliable communication in fast fading scenario while the derivation of iterative APP DPSK decoder emphasizes on delivery of accurate estimation with low complexity in slowly and moderately faded channels.

- When differential modulation is combined with error-correction codes and interleaving, it does not necessarily lead to performance degradation. It is feasible for non-coherent detection scheme to outperform its coherent counterpart without inflicting additional complexity. With the assistance of state-of-the-art Turbo code, our proposed differential detection and decoding algorithm is still capable of delivering reliable results when the normalized Doppler frequency equals to 0.05.

1.6 Notations

Throughout this thesis, lowercase letter a, boldface lowercase letter $\mathbf{a}$ and boldface uppercase letter $\mathbf{A}$ represent scalar, vector in column form and matrix, respectively. $|a|$, $||\mathbf{a}||$ and $|\mathbf{A}|$ denote the absolute value of a scalar a, the Euclidean norm of a vector $\mathbf{a}$ and the determinant of a square matrix $\mathbf{A}$, respectively. $(\cdot)^*$, $(\cdot)^T$ and $(\cdot)^H$ stand for the complex conjugate, transpose and conjugate transpose, respectively. We define $\text{sign}(x) = 1$ if $x > 0$ and 0 otherwise, whilst the expectation is given by $\mathbb{E}[\cdot]$. The bit error probability of an event $\mathcal{X}$ and the probability density function (PDF) of a random variable x are denoted by $P_b(\mathcal{X})$ and $p(x)$, respectively. In this thesis, the definitions of $\mathbf{ab}$ and $\mathbf{AB}$ are the Hadamard products of two column matrices and two matrices of the same dimensions respectively; unless otherwise stated.

Chapter 2

Theory of Space-Time Block Coding

Contents

Design of optimal space-time codes (STC) is never an easy task, it depends on a series of contradictory factors, some of which are shown in Fig. 2.1.

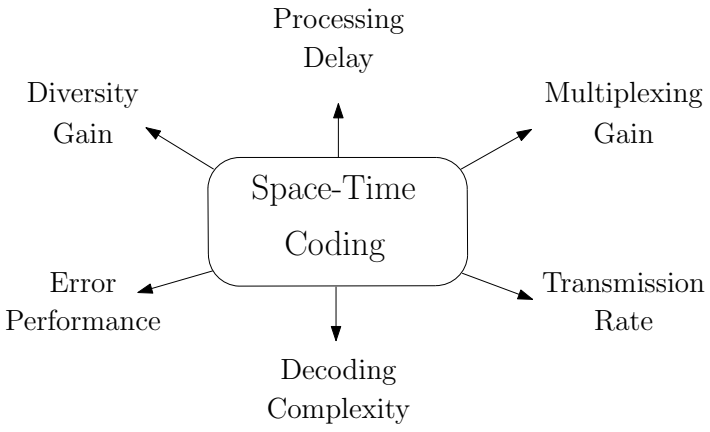

Figure 2.1: Various factors that affect the design of space-time codes (STCs).

More specifically, given different communication scenarios, STC design is aiming for optimizing different features. For example, for quality oriented application, code design is mostly concentrated on STC that is capable of achieving high levels of diversity as it is able to provide significant performance gain quantified in terms of the bit error ratio (BER) or frame error ratio (FER) reduction at certain transmission energy. On the

other hand, in a transmission rate oriented scenario, the effective throughput of the system can be increased by focusing on the multiplexing gain at the cost of error performance degradation. However, in both applications, the employment of STC implies further investments in terms of the required implementation complexity and processing delay.

The discussion in this literature review chapter starts with a brief introduction of various diversity and multiplexing techniques. We review and compare literature on the linear space-time coding for frequency flat channels in general and in particular with emphasis on orthogonal space-time block coding and orthogonal differential space-time block coding.

2.1 Space-Time Block Codes

Multi-path propagation is one of the major characteristics of the wireless channel that impairs the transmitted signal and challenges reliable transmission [29]. Various types of diversity techniques are widely used to mitigate the negative effects of multi-path fading due to their robust capabilities of improving the signal quality, reducing the effective error rate as well as providing high data rate transmission and considerable diversity gain.

A class of space time coding schemes such as space-time trellis coding (STTC) [20] and space-time block coding (STBC) [21–23, 30, 31], which combine the remarkable benefits of both spatial and temporal diversity, have the potential for achieving outstanding performance in a multi-path fading channel by employing multiple antennas at the transmitter and/or receiver.

Although a well-designed STTC, which is beneficial from simultaneous coding gain and diversity gain, has the potentiality of achieving near-capacity performance, the decoding complexity increases exponentially as the total number of trellis states increases for a given number of transmit antennas due to the joint maximum likelihood sequence detection. On the contrary, space-time block coding, in which the multiple redundant copies of data streams are encoded in blocks and transmitted among spaced antennas across time over independent channels, is less complex compared with STTC. Therefore, STBC is more appealing in terms of the simplicity of implementation and cost-effectiveness. Note that the promise of significant amount of gain associated with STBC is based on the fact that channel exhibits rich scattering so that transmission path for given pair of transmit antenna and receive antenna is independent [15]. In practice, Rayleigh fading channel models are realistic for environments with a large number of scatterers. Fail to comply

with this assumption would cause signals at the receiver become correlated and impossible to recover the original transmitted signal.

2.1.1 Evolution of Space-Time Coding

The design of space-time coding is a rather complicated and multifaceted topic. At early stage of STC research, attention is concentrated on employing extra transmit antennas for the sake of maximizing the improvement of error performance and link reliability in fading channels. Later the focus is shifted to attain maximum transmission rate promised by information theoretical analysis with extra antennas.

2.1.1.1 STBC from Orthogonal Design

Consider a MIMO communication system with N_t transmit antennas and N_r receive antennas. OSTBC is an effective diversity technique having maximum information rate of unity. OSTBC schemes are able to achieve full diversity order of ideally $N_t N_r$, which significantly improve error performance of existing systems, at the cost of providing no multiplexing gain.

The first STBC scheme working with two transmit antennas was originally proposed by Alamouti [21]. The Alamouti STBC is capable of achieving full rate (transmission rate equals to unity) and full diversity gain with a simple maximum likelihood (ML) decoding algorithm assuming the channel variation is accurately tracked. More specifically, two complex data streams are encoded and transmitted via two orthogonal channels where we assume the receiver has perfect knowledge of the channel state information (CSI) as well as the Rayleigh fading experienced by each channel is independent. His work was later extended and generalized by Tarokh *et al.* [23] to a more complex scenario where the transmitters were equipped with more than two antennas. The resultant generalized STBC theory subsumes the original Alamouti G2 scheme as a special case. One of the most important properties of the STBC mentioned here is the orthogonality; therefore, all these schemes are classified as orthogonal STBC (OSTBC).

2.1.1.2 Space-Time Code from Layered Design

In this subsection, we review and examine another distinct class of multiple-antenna schemes devised for yielding full multiplexing gain at the cost of no transmit diversity gain. The attainable information rate for these spatial multiplexing techniques reaches as high as N_t. Compared with OSTBC, the significant improvement in transmission rate is made available by transmitting N_t independent data streams from each transmit antenna.

The family of layered space-time (LST) codes primarily consists of horizontal layered space-time (HLST) codes as well as vertical layered space-time (VLST) codes. The very first space-time code based on layered architecture, hence termed layered space-time (LST) code, was proposed by Foschini [24]. In a LST coded MIMO system, the information data stream is split into several sub-streams with serial to parallel converter. Each of these sub-streams is referred to as a *layer*, operations in an individual layer are independent from others. Each layer is processed as a conventional single-layer scheme and the information sequence from each layer is encoded with error-correction code and modulated using digital modulation. The resultant modulated symbols are assigned to different transmit antennas. Therefore, the information rate is N_t. LST receiver positioned on the other end of the communication link separates the signals exploiting a combination of interference suppression and interference cancellation. The separated signals are then decoded by using conventional decoding algorithms. The separation operation leads to much lower complexity compared to maximum likelihood decoding used in, for example, STTC. Note that the complexity of the LST receivers grows linearly with the data rate. It is also worth noticing that each transmitted stream is received by N_r antennas in this scheme leading to attainable receive diversity order of N_r. Since the maximum available diversity order for a MIMO system with N_t transmit antennas and N_r receive antennas is N_tN_r, HLST seems to be a sub-optimal scheme. Two variants of HLST, named diagonal layered space-time (DLST) code or diagonal Bell laboratories layered space-time (D-BLAST) code [24, 32] and threaded layered space-time (TLST) code [33] are later proposed with improved diversity gain. DLST is designed to delay the element in row i by $i-1$ symbol periods, so that the first non-zero entries in each row lie on the diagonal of the codeword matrix. Symbols located in the j-th diagonal are then transmitted from the j-th transmit antenna. In the DLST scenario, bits from one codeword spread across N_t transmit antennas, hence extra space diversity introduced in the delayed transmission could bring performance improvement. On the other hand, the disadvantage of the delayed transmission used in DLST is the waste of transmission time, which further causes spectral efficiency loss, as the entries below the diagonal are padded by zeros indicating no transmission takes place.

In order to overcome the inefficiency of DLST, a novel threaded layered space-time (TLST) structure is devised from DLST. The principle of exploiting space diversity to guarantee better performance is similar to DLST, but the implementation is different in TLST scheme. A spatial interleaver, usually a cyclic-shift interleaver, is introduced to scramble the symbols prior to the time interleaver. To be more specific, instead of shifting the first non-zero entries to the diagonal and replacing those below the diagonal with zeros, spatial interleaver assures entries in the i-th column are shifted by $i-1$ times in a cyclic manner. In this way, space diversity is achieved without the need of inserting zero-entry, in other words, no spectral efficiency loss.

Vertical layered space-time (VLST) code or vertical Bell laboratories layered space-time (V-BLAST) code [34–36] is another popular candidate of LST coding schemes. As opposed to HLST where input data stream is divided into shorter sub-streams prior to encoding and modulation, data sequence in a VLST system is encoded, interleaved, and mapped before being fed to a demultiplexer or S/P converter. This arrangement enables the introduction of space diversity when transmitting from N_t antennas. Furthermore, since signal from each transmit antenna is picked up by N_r receive antennas, the attainable diversity order for a MIMO system employing VLST is $N_t N_r$.

2.1.1.3 Linear Dispersion Codes

In last subsection, we introduced and reviewed several distinct LST schemes and their variants. Existing LST techniques have focused primarily on multiplexing for support of high transmission rate. For example, V-BLAST is contrived for theoretical spectral efficiency up to 42 bits/s/Hz. Unfortunately, the original proposal of LST poses an implementational limitation that the number of receive antennas should be equal or greater than the number of transmit antennas. The implication of such assumption is that LST is not suitable for the downlink transmission of cellular systems as the mobile handsets are generally single-antenna aided, whilst it is common nowadays to equip base stations with multiple antennas. Moreover, detection and decoding of many existing STCs, such as OSTBC, requires an exhaustive maximum-likelihood (ML) search at the receiver that is often computationally infeasible for the scenario involving a large number of antennas.

In order to solve this problem and salvage the benefit provided by LST, Hassibi and Hochwald proposed a revolutionary theory of linear dispersion code (LDC) in [37]. LDC is considered as a more generalized version of existing space-time codes supporting any configuration of transmit and receive antennas. Therefore, LDC inherently subsumes OSTBC and LST as special cases. The proposed LDC design offers a compromise for the

diversity and multiplexing trade-off.

Recall that the V-BLAST architecture splits the original data stream into several sub-streams which are further encoded independently and assigned to individual antennas. Similarly, to construct LDC codewords, dispersion matrices are generated from each of sub-streams with certain weights, which are complex scalars typically chosen from PSK or QAM constellations. The resultant dispersion matrices and weighting components are combined in a linear fashion so that data in each sub-streams is dispersed linearly over space and time for exploiting both the spatial as well as temporal diversity. In the meanwhile, since LDC inherits the linear structure of VLST, desirable features like low-complexity decoding of VLST still remains. Also, many recently developed codes, such as TVLT [38], TASTBC [39], and those proposed in [40] and reference therein, are all subsets of the LDC framework.

It is pointed out in [41–43] that, although the original design of LDC performs well from an ergodic capacity (also referred to as the CCMC capacity) point of view, it does not necessarily perform well in terms of the average pairwise error probability (PEP). In [42], a diverse class of LDC is proposed based on the frame theory that exhibits tremendous improvement in terms of both ergodic capacity and error probability.

In this subsection, we discussed several popular diversity schemes, including orthogonal and non-orthogonal space-time codes such as OSTBC and LDC. Another class of spatial multiplexing techniques, such as those belonging to the general framework of BLAST architectures, which sacrifice the achievable diversity potential of the channel in exchange for very high throughput close to the MIMO channel capacity.

Tab. 2.1 summarizes the maximum code rate as well as the maximum achievable diversity order for various multiple-antenna transmission schemes. For a given arbitrary signal constellation, the coding rate of LDC is defined as Q/T, which represents the linear combination of Q input symbols are transmitted within T symbol intervals.

Table 2.1: Comparison of maximum code rate and maximum diversity order for various multiple-antenna transmission schemes.

	Maximum Code Rate	Maximum Diversity Order
OSTBC	1	$N_t N_r$
HLST	N_t	N_r
VLST	N_t	$N_t N_r$
LDC	$\frac{Q}{T}$	$N_r \min(N_t, T)$

2.1.2 Orthogonal Space-Time Block Codes

In this section, we discuss a simple two-branch transmit diversity scheme, namely, Alamouti space-time block coding. This part includes the encoding and decoding algorithms and its bit error ratio (BER) performance. Orthogonal space-time block code for two transmit antennas is usually referred to as the Alamouti space-time code or G2 space-time code.

2.1.2.1 Alamouti Space-Time Encoding

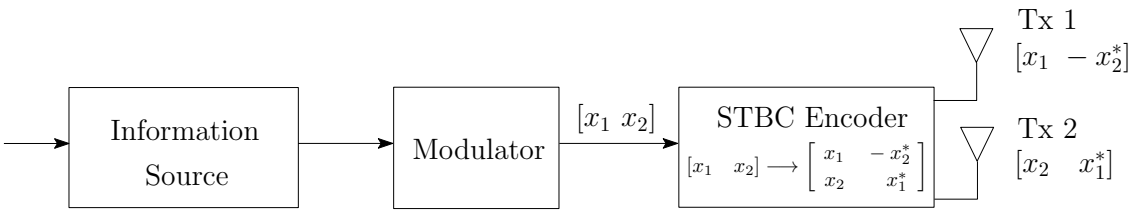

Figure 2.2: The schematic of a two-branch Alamouti transmit diversity scheme encoder.

Fig. 2.2 is the baseband representation of the Alamouti space-time encoder, showing that before performing the space-time encoding, the m number of information bits are first modulated using an $\mathcal{M}$-ary modulation scheme, where we have $m = \log_2(\mathcal{M})$. Then, according to the procedure proposed in [21], the space-time encoder groups the incoming $\mathcal{M}$-ary symbols into pairs and encodes a block of two consecutive modulated symbols x_1 and x_2 into a valid space-time code matrix

$$\mathbf{X} = \begin{bmatrix} x_1 & -x_2^* \\ x_2 & x_1^* \end{bmatrix} . \tag{2.1}$$

After the code matrix is generated based on Eq. (2.1), it is then fed to the transmit antennas and propagated to the receiver in two consecutive time slots. At a given symbol period, two signals are simultaneously transmitted from two antennas. During the first transmission slot, x_1 is transmitted from the first antenna and x_2 is transmitted from the second antenna simultaneously. In the second time slot, the signals simultaneously transmitted from antenna one and antenna two are $-x_2^*$ and x_1^*, respectively. Note that x_i^* represents the complex conjugate of x_i, $i = 1, 2$.

It is clear that each row of the codeword matrix represents the encoding operation taking place on different antennas; namely, in the space domain. At the same time, each column represents diverse transmission period; in other words, the encoding is carried out in the time domain. And the encoder takes a block of two consecutive symbols at each time; hence, this simple twin-antenna aided transmit diversity scheme is called space-time block code. Tab. 2.2 demonstrates the principle of encoding and transmissions for the Alamouti space-time code.

Table 2.2: Demonstration of encoding principle and transmissions for the Alamouti space-time code.

	Antenna 1	**Antenna 2**
Time index t	x_1	x_2
Time index $t + T$	$-x_2^*$	x_1^*

As mentioned above, the Alamouti STBC is one kind of orthogonal STBCs. The property of orthogonality can be proved by calculating the inner product of the transmit sequences from the first antenna $[x_1 \quad -x_2^*]$ and the one from the second antenna $[x_2 \quad x_1^*]$, this yields

$$x_1 x_2^* - x_2^* x_1 = 0 \, . \tag{2.2}$$

The result of Eq. (2.2) is zero, this indicates that the transmit sequences from two transmit antennas are indeed orthogonal.

2.1.2.2 Alamouti Space-Time Decoding Using ML Algorithm

Alamouti STBC is an approach designed to achieve full transmit diversity by utilizing multiple transmit antennas, but with optionally multiple receive antennas. In this subsec-

tion, the decoding principle of Alamouti STBC proposed in [21] is reviewed, including the combining and maximum likelihood (ML) decoding. This part starts from the case where a single receive antenna is employed at the receiver and then is extended to multiple receive antennas scenario.

The complex-valued fading channel coefficients experienced by the first and second transmit antenna with respect to the receive antenna at time index t are denoted as $h_1(t)$ and $h_2(t)$, respectively. The channel coefficients are assumed to remain constant over two consecutive transmission slots, but vary from block to block. Therefore, $h_1(t)$ and $h_2(t)$ can be described as

$$h_1(t) = h_1(t+T) = h_1 = |h_1|e^{j\theta_1} \,, \tag{2.3}$$

$$h_2(t) = h_2(t+T) = h_2 = |h_2|e^{j\theta_2} \,, \tag{2.4}$$

where $|h_i|$ and θ_i $(i = 1, 2)$ are the amplitude and phase shift of the fading channels between the ith transmit antenna and the receive antenna. T is the symbol duration.

As depicted in Fig. 2.3, the signals from two transmit antennas are compromised by the fading channels. Assuming the baseband signals received at two adjacent symbol periods t and $t+T$ are denoted by r_1 and r_2, they can be formulated as

$$r_1 = r(t) = h_1 x_1 + h_2 x_2 + n_1 \,, \tag{2.5}$$

$$r_2 = r(t+T) = -h_1 x_2^* + h_2 x_1^* + n_2 \,, \tag{2.6}$$

where n_1 and n_2 represent the Additive White Gaussian Noise (AWGN) induced in the receiver with zero mean and a power spectral density (PSD) of $N_0/2$ per dimension at time instant t and $t+T$, respectively.

If the fading channel coefficients h_1 and h_2 are assumed to be perfectly recovered by the channel estimator shown in Fig. 2.3, this means that the receiver has the knowledge of the channel state information (CSI) which could help the receiver to improve the decoding performance. The perfectly estimated fading coefficients $\hat{h}_1$ and $\hat{h}_2$ are sent to the signal combiner to combine with the received signals r_1 and r_2 and generate two decision statistics denoted by $\tilde{x}_1$ and $\tilde{x}_2$ as follows

$$\tilde{x}_1 = \hat{h}_1^* r_1 + \hat{h}_2 r_2^* \,, \tag{2.7}$$

$$\tilde{x}_2 = \hat{h}_2^* r_1 - \hat{h}_1 r_2^* \,. \tag{2.8}$$

Substituting Eq. (2.5) and Eq. (2.6) into the decision statistics above, then Eq. (2.7) and

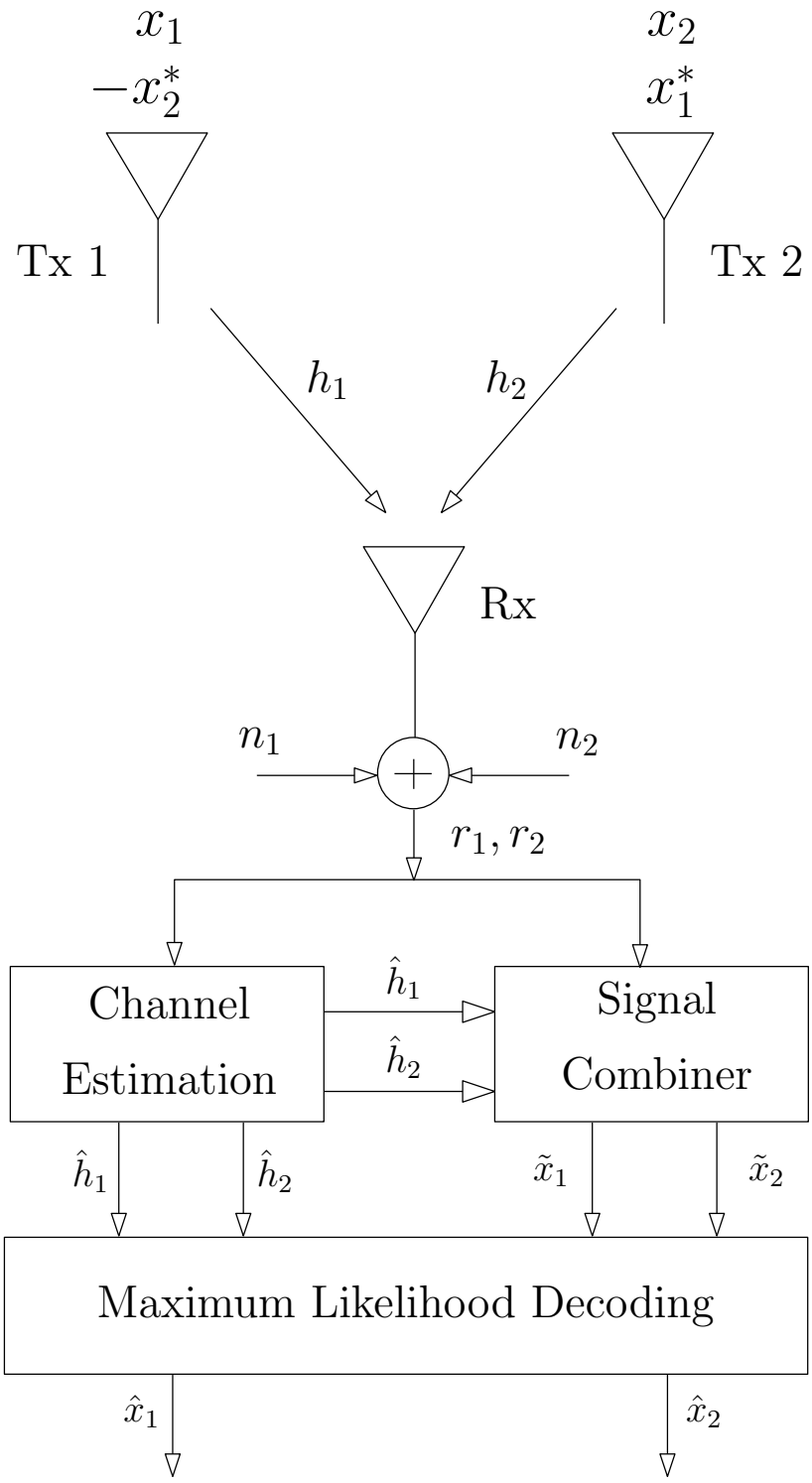

Figure 2.3: The schematic of a two-branch Alamouti transmit diversity scheme receiver.

Eq. (2.8) can also be expressed as

$$\tilde{x}_1 = (|\hat{h}_1|^2 + |\hat{h}_2|^2)x_1 + \hat{h}_1^* n_1 + \hat{h}_2 n_2^* \,, \tag{2.9}$$

$$\tilde{x}_2 = (|\hat{h}_1|^2 + |\hat{h}_2|^2)x_2 - \hat{h}_1 n_2^* + \hat{h}_2^* n_1 \,. \tag{2.10}$$

The fading coefficient estimates $\hat{h}_1$ and $\hat{h}_2$ are also used by the maximum likelihood decoder to find the most likely transmitted signal based on the decision rule of choosing a specific pair of signals $(\hat{x}_1, \hat{x}_2)$ from the signal modulation constellation to minimize the following distance metric

$$d^2(r_1, \hat{h}_1\hat{x}_1 + \hat{h}_2\hat{x}_2) + d^2(r_2, -\hat{h}_1\hat{x}_2^* + \hat{h}_2\hat{x}_1^*) \,, \tag{2.11}$$

over all possible values of $\hat{x}_1$ and $\hat{x}_2$. $d^2(x, y)$ is the squared Euclidean distance between two complex-valued signals x, y and calculated by the following expression

$$d^2(x, y) = (x - y)(x^* - y^*) = |x - y|^2 \,. \tag{2.12}$$

Note that Eq. (2.11) is based on the assumption that all of the signals in the constellation are equi-probable.

Substituting the definition of squared Euclidean distance shown in Eq. (2.12) into Eq. (2.11), the decision criterion can be written as

$$\begin{aligned}
&d^2(r_1, \hat{h}_1\hat{x}_1 + \hat{h}_2\hat{x}_2) + d^2(r_2, -\hat{h}_1\hat{x}_2^* + \hat{h}_2\hat{x}_1^*) \\
&= (r_1 - \hat{h}_1\hat{x}_1 - \hat{h}_2\hat{x}_2)(r_1^* - \hat{h}_1^*\hat{x}_1^* - \hat{h}_2^*\hat{x}_2^*) + (r_2 + \hat{h}_1\hat{x}_2^* - \hat{h}_2\hat{x}_1^*)(r_2^* + \hat{h}_1^*\hat{x}_2 - \hat{h}_2^*\hat{x}_1) \\
&= (|\hat{h}_1|^2 + |\hat{h}_2|^2)(|\hat{x}_1|^2 + |\hat{x}_2|^2) - \hat{h}_1^* r_1\hat{x}_1^* - \hat{h}_2 r_2^*\hat{x}_1^* - \hat{h}_1 r_1^*\hat{x}_1 - \hat{h}_2^* r_2\hat{x}_1 \\
&- \hat{h}_2^* r_1\hat{x}_2^* + \hat{h}_1 r_2^*\hat{x}_2^* - \hat{h}_2 r_1^*\hat{x}_2 + \hat{h}_1^* r_2\hat{x}_2 + |r_1|^2 + |r_2|^2 \,.
\end{aligned} \tag{2.13}$$

Using Eq. (2.12) along with Eq. (2.7) and Eq. (2.8), we can define $d^2(\tilde{x}_1, \hat{x}_1)$ and $d^2(\tilde{x}_2, \hat{x}_2)$ and express them as follows

$$\begin{aligned}
d^2(\tilde{x}_1, \hat{x}_1) &= (\tilde{x}_1 - \hat{x}_1)(\tilde{x}_1^* - \hat{x}_1^*) \\
&= |\tilde{x}_1|^2 + |\hat{x}_1|^2 - \hat{h}_1^* r_1\hat{x}_1^* - \hat{h}_2 r_2^*\hat{x}_1^* - \hat{h}_1 r_1^*\hat{x}_1 - \hat{h}_2^* r_2\hat{x}_1 \,.
\end{aligned} \tag{2.14}$$

Similarly,

$$\begin{aligned}
d^2(\tilde{x}_2, \hat{x}_2) &= (\tilde{x}_2 - \hat{x}_2)(\tilde{x}_2^* - \hat{x}_2^*) \\
&= |\tilde{x}_2|^2 + |\hat{x}_2|^2 - \hat{h}_2^* r_1\hat{x}_2^* - \hat{h}_1 r_2^*\hat{x}_2^* - \hat{h}_2 r_1^*\hat{x}_2 - \hat{h}_1^* r_2\hat{x}_2 \,.
\end{aligned} \tag{2.15}$$

Combining Eq. (2.14) and Eq. (2.15) with Eq. (2.13) as well as ignoring all terms that are independent of $\hat{x}_1$ or $\hat{x}_2$, the ML decision rule now becomes

$$(\hat{x}_1, \hat{x}_2) = \arg \min_{(\hat{x}_1, \hat{x}_2) \in \chi} (|\hat{h}_1|^2 + |\hat{h}_2|^2 - 1)(|\hat{x}_1|^2 + |\hat{x}_2|^2) + d^2(\tilde{x}_1, \hat{x}_1) + d^2(\tilde{x}_2, \hat{x}_2) \,, \tag{2.16}$$

where χ is the set of all possible modulated symbol pairs $(\hat{x}_1, \hat{x}_2)$.

For a pair of given fading channels, the decision statistics $\tilde{x}_i$ is a function of x_i, $i = 1, 2$. Therefore, the ML decision rule of minimizing the distance metric in Eq. (2.16) can be separated into two independent decoding criteria for x_1 and x_2 given by

$$\hat{x}_1 = \arg\min_{\hat{x}_1 \in \mathcal{S}} (|\hat{h}_1|^2 + |\hat{h}_2|^2 - 1)|\hat{x}_1|^2 + d^2(\tilde{x}_1, \hat{x}_1) \ , \tag{2.17}$$

$$\hat{x}_2 = \arg\min_{\hat{x}_2 \in \mathcal{S}} (|\hat{h}_1|^2 + |\hat{h}_2|^2 - 1)|\hat{x}_2|^2 + d^2(\tilde{x}_2, \hat{x}_2) \ , \tag{2.18}$$

where $\mathcal{S}$ is the legitimate constellation set. Note that for all $\mathcal{M}$-ary PSK signal constellations, the amplitude of all modulated signal points $(|\hat{h}_1|^2 + |\hat{h}_2|^2 - 1)|\hat{x}_i|^2$, $i = 1, 2$ is constant for specific channel coefficients. Hence, the decision criteria above can be simplified to

$$\hat{x}_1 = \arg\min_{\hat{x}_1 \in \mathcal{S}} d^2(\tilde{x}_1, \hat{x}_1) \ , \tag{2.19}$$

$$\hat{x}_2 = \arg\min_{\hat{x}_2 \in \mathcal{S}} d^2(\tilde{x}_2, \hat{x}_2) \ . \tag{2.20}$$

2.1.2.3 Alamouti Scheme Decoding with Multiple Receive Antennas

In this subsection, the Alamouti scheme with configuration of two transmit antennas and N_r number of receive antennas as the work presented in [21] is revisited. In such case, the diversity gain provided by the Alamouti STBC is $2N_r$.

The encoding and transmission arrangement are identical to previous case where only a single receive antenna is employed, the only difference is the decoding algorithm.

The signals received by the jth antenna at time interval t and $t + T$ are denoted as $r_{1,\,j}$ and $r_{2,\,j}$, respectively and are described by

$$r_{1,\,j} = h_{1,\,j}x_1 + h_{2,\,j}x_2 + n_{1,\,j} \ , \tag{2.21}$$

$$r_{2,\,j} = -h_{1,\,j}x_2^* + h_{2,\,j}x_1^* + n_{2,\,j} \ , \tag{2.22}$$

where $h_{i,\,j}$, $i = 1, 2$ and $j = 1, 2, \ldots, N_r$, is the notation for the complex-valued fading coefficients of the channel between the ith transmit antenna and the jth receive antenna; while $n_{1,\,j}$ and $n_{2,\,j}$ represent the complex-valued AWGN added by the jth receiver at time index t and $t + T$, respectively.

Assuming the channel coefficients $\hat{h}_{1,j}$ and $\hat{h}_{2,j}$ are perfectly estimated, the signal combiner will produce two new decision statistics $\tilde{x}_1$ and $\tilde{x}_2$, which are combination of the

received signals, as follows

$$\tilde{x}_1 = \sum_{j=1}^{N_r} \hat{h}^*_{1,\,j} r_{1,\,j} + \hat{h}_{2,\,j} r^*_{2,\,j} = \sum_{j=1}^{N_r} \left[(|\hat{h}_{1,\,j}|^2 + |\hat{h}_{2,\,j}|^2) x_1 + \hat{h}^*_{1,\,j} n_{1,\,j} + \hat{h}_{2,\,j} n^*_{2,\,j} \right] , \tag{2.23}$$

$$\tilde{x}_2 = \sum_{j=1}^{N_r} \hat{h}^*_{2,\,j} r_{1,\,j} - \hat{h}_{1,\,j} r^*_{2,\,j} = \sum_{j=1}^{N_r} \left[(|\hat{h}_{1,\,j}|^2 + |\hat{h}_{2,\,j}|^2) x_2 + \hat{h}^*_{2,\,j} n_{1,\,j} - \hat{h}_{1,\,j} n^*_{2,\,j} \right] . \tag{2.24}$$

Finally, the two independent decision criteria for x_1 and x_2 using the ML decoding algorithm are now adapted to

$$\hat{x}_1 = \arg\min_{\hat{x}_1 \in \mathcal{S}} \left[\left(\sum_{j=1}^{N_r} (|\hat{h}_{1,\,j}|^2 + |\hat{h}_{2,\,j}|^2) - 1 \right) |\hat{x}_1|^2 + d^2(\tilde{x}_1, \hat{x}_1) \right] , \tag{2.25}$$

$$\hat{x}_2 = \arg\min_{\hat{x}_2 \in \mathcal{S}} \left[\left(\sum_{j=1}^{N_r} (|\hat{h}_{1,\,j}|^2 + |\hat{h}_{2,\,j}|^2) - 1 \right) |\hat{x}_2|^2 + d^2(\tilde{x}_2, \hat{x}_2) \right] . \tag{2.26}$$

Similar to Eq. (2.19) and Eq. (2.20), for the case of $\mathcal{M}$-ary PSK modulation, each constellation point has equal energy. Therefore, the above formula can also be simplified to

$$\hat{x}_1 = \arg\min_{\hat{x}_1 \in \mathcal{S}} d^2(\tilde{x}_1, \hat{x}_1) , \tag{2.27}$$

$$\hat{x}_2 = \arg\min_{\hat{x}_2 \in \mathcal{S}} d^2(\tilde{x}_2, \hat{x}_2) . \tag{2.28}$$

2.1.2.4 Performance Evaluation of Alamouti STBC Scheme

The bit error performance of the Alamouti STBC scheme is discussed in this subsection. The major advantages of the Alamouti STBC can be summarized as follows. To begin with, the Alamouti STBC is a simple two-branch transmit diversity technique, which is widely used to improve the quality of propagation links without any bandwidth expansion. Secondly, there is no CSI feedback from the receiver, the channel information is retrieved from the signal estimator and fed to the combiner and ML decoder. Thirdly, the Alamouti STBC is capable of achieving full transmit diversity order only with a low complexity decoding. Therefore, it is easy to incorporate the Alamouti STBC technique in many existing systems without the need of re-design or major system modifications.

Note that, although the Alamouti STBC encoder takes two modulated symbols as input and converts them to one STBC codeword, it still needs two transmission slots to send

the codeword matrix. Therefore, the overall data rate of the Alamouti STBC using two transmit antennas is unity. Another important assumption is that the channel experienced between each transmit and receive antenna is randomly varying in time; however, the channel is assumed to remain constant over two symbol periods.

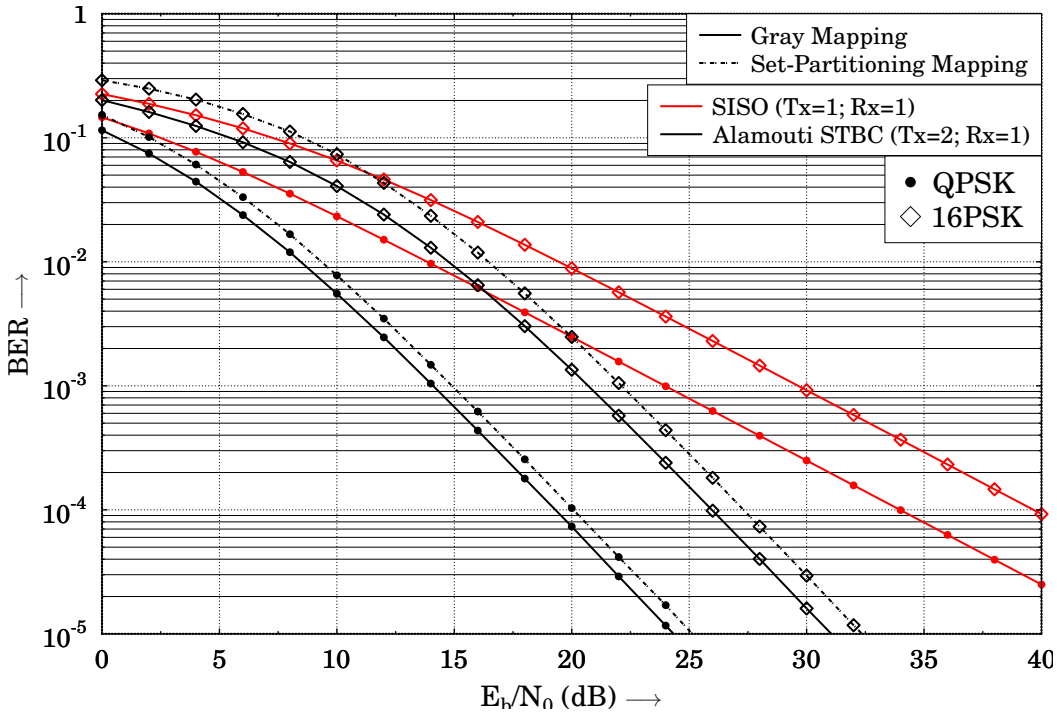

Figure 2.4: E_b/N_0 versus BER performance of Alamouti STBC invoking 2 transmit antennas and single receive antenna in quasi-static flat Rayleigh-fading channel. QPSK and 16PSK with Gray/SP mapping are investigated.

Fig. 2.4 shows the BER performance of the Alamouti STBC with QPSK/16PSK modulation and coherent detection in Rayleigh-fading channel. Combination of different modulation and symbol mapping schemes, including Gray mapping and set-partitioning (SP) mapping, are simulated in order to provide a thorough comparison. Moreover, the BER of a communication system with only one transmit antenna and one receive antenna, namely the single-input single-output (SISO) scheme is also presented as a benchmark. It is shown in Fig. 2.4, as expected, the SISO system can only achieve first order diversity due to the lack of any kind of diversity transmissions. As a result, the Alamouti schemes employing QPSK and 16PSK modulation outperform the SISO system by approximately 14.5 and 13.5 dB respectively, at BER of 10^{-4}. This outstanding performance gain is contributed by the fact that the channel experienced by one transmit antenna is spatially uncorrelated and independent from the channels experienced by other transmit antennas; hence, even if one path is deeply faded, other paths are still likely to provide high-reliability links for the transmission.

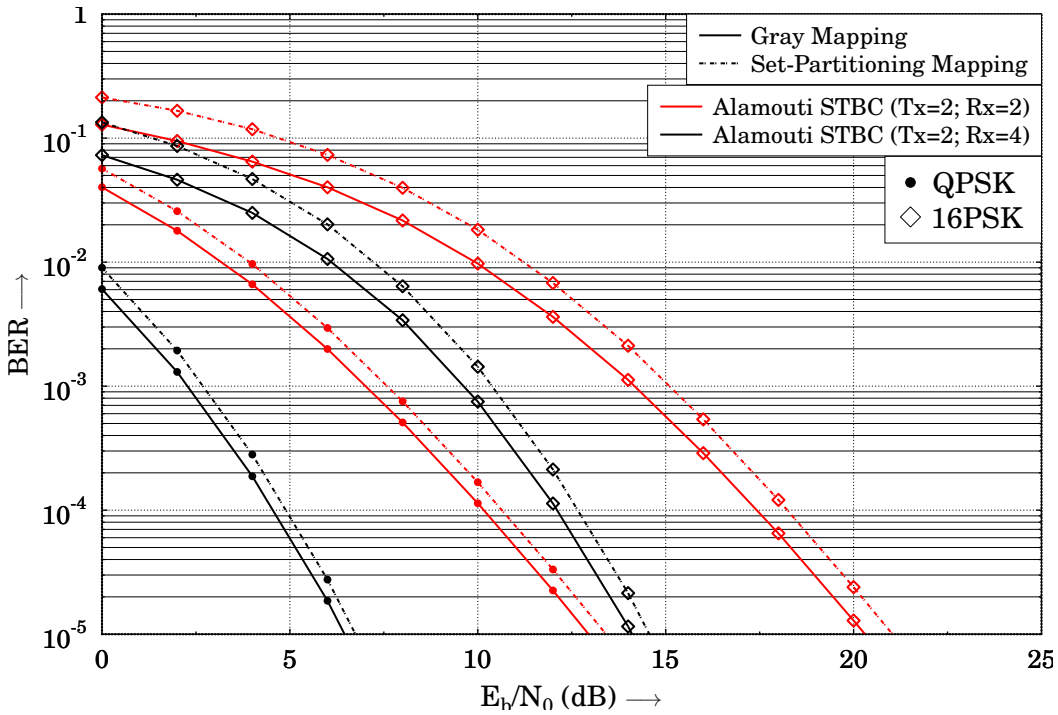

Figure 2.5: E_b/N_0 versus BER performance of Alamouti STBC invoking 2 transmit antennas and 2/4 receive antennas in quasi-static flat Rayleigh-fading channel. QPSK and 16PSK with Gray/SP mapping are investigated.

It is also illustrated in Fig. 2.4 that the Alamouti STBC invoking SP mapping is approximately 1.0 dB inferior to its counterpart with Gray mapping for QPSK-modulated scheme whereas the performance degradation is escalated to 1.5 $\sim$ 2.0 dB if higher-order modulation such as 16PSK is employed, both measured at BER = 10^{-4}. Furthermore, it is clearly evidenced in Fig. 2.4 that the bit error rate would drop by 2 order of magnitude if 10.0 dB extra transmit energy is provided, this fact indicates that the Alamouti STBC schemes having two transmit antennas and one receive antenna is capable of attaining full diversity order of 2.

Fig. 2.5 depicts the BER performance of the Alamouti STBC with multiple receive antennas. The total number of propagation paths is proportional to the number of receivers N_r, namely $2N_r$ independent propagation channels are available in this scenario. In general, the theoretical diversity order of the Alamouti STBC invoking 2 transmit antennas as well as N_r receive antennas is defined as $2N_r$.

In the following simulations, $N_r = 2$ as well as $N_r = 4$ receive antennas are investigated; hence, the independent transmission paths are 4 and 8, respectively. When the number of receive antennas is doubled, the Alamouti STBC could benefit even more from a significant deduction of required SNR per bit (E_b/N_0) due to extra diversity gain. To be

more specific, a E_b/N_0 of 10.0 dB and 17.0 dB would be sufficient for QPSK and 16PSK with Gray mapping to deliver a bit error probability of 10^{-4}, which is 9.5 dB and 8.5 dB less than their counterparts having single receive antenna. Similarly, if SP mapping is employed, the corresponding BER performance suffers from certain degradation about 0.5-1.0 dB. Furthermore, when the number of receive antennas increases to 4, as the black curves in Fig. 2.5 indicate, an additional diversity gain of approximately 5.0 and 6.0 dB is attained at BER of 10^{-4} for Gray- and SP-mapped QPSK/16PSK schemes.

2.2 Differential Space-Time Block Codes (DSTBCs)

Previous section mostly concentrated on the theory of space-time block coding, encoding procedure of the Alamouti OSTBC as well as optimum decoding with multiple receive antennas. So far, the discussions are based on the assumption of perfect channel knowledge at the receiving end, namely coherent decoding is performed. This section is devoted to differential space-time coding (DSTC) with non-coherent decoding algorithm, which dispenses with accurate channel state information (CSI) acquisition.

It is demonstrated in the previous section that OSTBC and other variants are capable of effectively mitigating multipath fading and improving the reliability and performance of digital communication over radio channels. The benefits of OSTBC in part stem from the optimal coherent decoding of the combined signal with maximum-likelihood (ML) algorithm, which relies on the availability of channel information at the receiver. However, accurate estimation of channel coefficients is never an easy task in practice.

Conventional channel estimation techniques are generally performed through sending a short segment of preambles (known to the receiving side) prior to the transmission of data symbols so that channel coefficients are in turn computed correspondingly with the assistance of these training symbols. Although the training-based channel estimation scheme offers a solution for the case of stationary and slowly-faded channels with relatively high accuracy, it could become less effective and tend to fail yielding an irreducible error floor in other applications such as high-mobility scenarios.

To be more specific, it is always difficult and costly to estimate the channel accurately when the surroundings are changing at a rapid rate as the previous estimates become outdated after several symbol periods and need to be refreshed in a very frequent fashion. Hence, for the purpose of delivering reliable channel estimates in fast-faded channels, an excessive number of training symbols are transmitted which would in turn reduce the

achievable data rate.

Moreover, the difficulty of getting access to accurate channel information is increased in multiple-antenna systems. Take Alamouti OSTBC scheme with 2 transmit antennas and 4 receive antennas as example signals from each transmitter propagate through independent paths before arriving at the receivers. In order to recover the transmitted information optimally with coherent decoding algorithm, a total of $2 \times 4 = 8$ individual complex-valued channels are estimated from the training symbols. MIMO channel estimation involves a substantial amount of high-complexity signal processing as well as arithmetic computation, which consumes extra power and introduces processing delay.

Since design of state-of-the-art radio communication systems imposes stringent limitations on the available power and spectrum resources, it is unwise to dedicate precious transmit energy as well as valuable bandwidth for transmission of training symbols. Hence, in general, this dilemma makes coherently decoded STC schemes less attractive in practice.

In this section, we review differential space-time codes (DSTC) which are dispensing with channel estimation and are decoded non-coherently without channel information. Our discussion commences from a brief introduction of differential techniques, then we carry on to explore several practical multiple-antenna differential schemes.

2.2.1 Evolution of DSTCs

The family of DSTC primarily consists of two members with distinct characteristics, namely differential space-time block codes based on orthogonal designs (DOSTBC) as well as differential unitary space-time modulation (USTM). The underlying assumption of a coherent MIMO system is that the fading envelop experienced during specific symbol period has negligible difference. In the case where fading rate is greater than symbol rate, the aforementioned assumption becomes no longer valid. DSTC is well-tailored for radio communication over fading channels where the channel coefficients are available at neither the transmitting side nor receiving side. In other words, recovery of transmitted information relies on non-coherent detection. Similar to coherent STC schemes, differential STC is also able to deliver low probability of error by exploiting high levels of diversity in comparison to single-antenna systems. A brief summary of related schemes is provided in the following subsections.

2.2.1.1 Differential Unitary Space-Time Modulation

The proposal of differential unitary space-time modulation (USTM) extends the concept of differential modulation designed for single-antenna aided communication systems to multiple-antenna scenarios. The USTM proposed in [44] is defined by a set of distinct unitary space-time constellation matrices, the size of which increases exponentially with the effective throughput. Therefore, although the presented results prove that USTM could become a highly effective non-coherent signaling scheme for MIMO channels, encoding and decoding complexity of USTM with large constellation size imposes formidable implementation challenges.

Later, in [45], the construction of unitary space-time constellation matrices has been modified and improved. Low-complexity Fourier-transform based construction scheme originated from signal processing theory as well as algebraic encoding method based on coding theory were proposed, which result in simpler encoding complexity. However, no effort was devoted to simplification of the decoding procedure, hence exponential decoding complexity makes USTM less appealing in practice.

Another novel differential space-time modulation scheme based on group codes was reported in [46]. In the mean time, similar work of [46] was also proposed independently in [47]. In order to make USTM easier for implementation, [48] focused on a simpler but suboptimal decoding algorithm for USTM schemes. The complexity of the resultant decoding scheme is proportional to the number of antennas and transmission rate instead of increasing exponentially with respect to the effective throughput. Other related novel construction methods for USTM with the goal of reducing the exponential decoding complexity were also presented in [49–52] and references therein.

2.2.1.2 Differential STBC from Orthogonal Design

Apart from USTM, a different class of differential coding scheme based on orthogonal designs was devised in [53]. The proposed differential space-time block coding (DSTBC) scheme evolves from the Alamouti code with two transmit antennas, which inherits superior features of OSTBC owing to the orthogonal structure of DSTBC codewords. Since its inception, there was misunderstanding in the research community that earlier research work on differential STBC with two transmit antennas was not applicable to the case with multiple transmit antennas. This problem was answered and clarified in [54]. Another approach to designing differential detection based on orthogonal STBCs is suggested

in [55, 56], which has been confirmed later as a special case of the scheme proposed in [54].

2.2.2 Orthogonal Differential Space-Time Block Codes (O-DSTBC)

2.2.2.1 Differential Technique for Single-antenna Transmission: DPSK

Differential techniques for single-transmit-antenna scenarios were standardized several decades ago, since then differential encoding and non-coherent decoding schemes have been widely implemented in commercial radio communication systems. For instance, $\pi/4$-DPSK was incorporated in IEEE IS-54 standard in the early 90's and applied in second-generation digital cellular system in North America.

In a single-antenna system, it is well-known that phase-shift keying (PSK) is a favored means of digital modulation. Since the information is carried in the phase of the modulated signal, coherent detection of absolutely-encoded PSK becomes much more difficult when transmitting over fading channel with uncertain phase response. Furthermore, in high-mobility scenarios, the existence of Doppler shift usually makes coherent detection of PSK complicated and less efficient.

The deficiencies inherent in coherent detection of absolutely-encoded PSK could be readily eliminated by differentially encoding the source message before transmission and detecting it non-coherently. Such modulation scheme is generally designated as differential PSK (DPSK). In a DPSK-modulated system, information resides in phase differences between two adjacent symbols rather than absolute phase, hence it could be readily extracted from the current and previous received symbols without the knowledge of channel state information. This unique property facilitates simple yet effective non-coherent detection for DPSK signals.

In this subsection, we review the theory of DPSK, including encoding procedures as well as derivation of non-coherent decoding algorithm. After that, we consider extensions of differential schemes to MIMO system in the following subsection and present details of differential space-time block codes based on orthogonal designs.

Consider a DPSK-modulated system with a single transmit antenna and a single receive antenna, the schematic of which is illustrated in Fig. 2.6. The notation s_k represents the $\mathcal{M}$-ary complex-valued PSK symbols at epoch k, which is taken from a finite alphabet $\mathcal{S}$

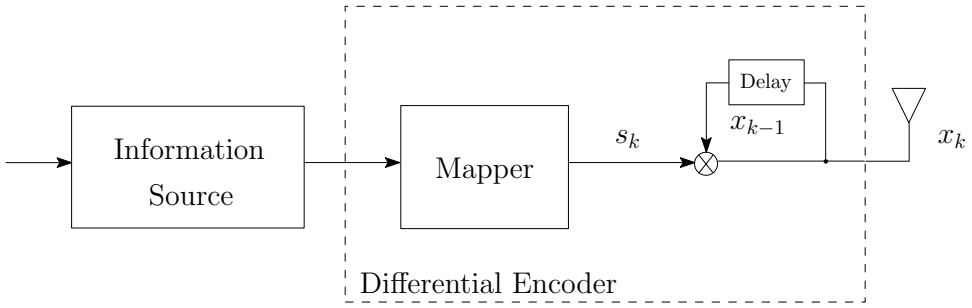

Figure 2.6: The transmitter schematic of differentially-encoded PSK modulation.

with $\mathcal{M}$ legitimate phasor combinations. $\mathcal{S}$ is defined as

$$\mathcal{S} = \exp\left(\frac{2\pi n j}{\mathcal{M}}\right) \ , n = 0, 1, 2, ..., \mathcal{M} - 1 \ . \tag{2.29}$$

At the beginning of each transmission period, an arbitrary symbol s_0 is sent at epoch 0 to initialize differential encoding process by providing reference for forthcoming PSK symbols. As demonstrated in Fig. 2.6, DPSK symbol transmitted at time k is the product of current PSK symbol s_k and previous DPSK symbol x_{k-1}. Mathematically speaking,

$$x_k = \begin{cases} s_k & \text{if } k = 1, \\ x_{k-1} \cdot s_k & \text{if } k > 1. \end{cases} \tag{2.30}$$

The resultant differentially-encoded PSK symbols are generated recursively in a similar manner. After propagating through hostile radio channel, the received signal is corrupted by fading and contaminated by noise. At time instant k, it is written as

$$y_k = h_k x_k + n_k \ . \tag{2.31}$$

Similarly, the received signal at the previous epoch $k-1$ can be expressed as

$$y_{k-1} = h_{k-1} x_{k-1} + n_{k-1} \ . \tag{2.32}$$

It is usually assumed that phase response of fading channel retains approximately constant from one symbol period to the next, namely $h_{k-1} \approx h_k$. We can therefore define $\hat{y}_k$ using the following rule

$$\begin{aligned} y_k y_{k-1}^* &= (h_k x_k + n_k)\left(h_{k-1}^* x_{k-1}^* + n_{k-1}^*\right) \\ &= h_k h_{k-1}^* x_k x_{k-1}^* + h_{k-1}^* x_{k-1}^* n_k + h_k x_k n_{k-1}^* + n_k n_{k-1}^* \ . \end{aligned} \tag{2.33}$$

Applying the constraint that $h_{k-1} \approx h_k$, Eq. (2.33) can be re-written as

$$\hat{y}_k = y_k y_{k-1}^* = |h_k|^2 x_k x_{k-1}^* + \hat{n}_k \ , \tag{2.34}$$

where $\hat{n}_k$ is the equivalent Gaussian noise containing all terms related to original noise n_k. Substitute Eq. (2.30) into Eq. (2.34), this yields

$$\hat{y}_k = y_k y_{k-1}^* = |h_k|^2 x_{k-1} x_{k-1}^* s_k + \hat{n}_k \ . \tag{2.35}$$

Since all PSK signal points are from unitary constellation with unity energy, in other words, $x_{k-1}x_{k-1}^* = |x_{k-1}|^2 = 1$, Eq. (2.35) is further simplified into

$$\hat{y}_k = y_k y_{k-1}^* = |h_k|^2 s_k + \hat{n}_k \ . \tag{2.36}$$

Upon observing Eq. (2.36), the optimal estimate of s_k is found using ML algorithm, which is formulated as

$$\tilde{s_k} = \arg\{ \min_{s_k \in \mathcal{M}-\text{PSK}} |y_k y_{k-1}^* - |h_k|^2 s_k|^2 \} \ . \tag{2.37}$$

Note that the term $|h_k|^2$ is considered as a scaling factor that does not affect the geometry of the detection regions provided that all PSK constellation points are on the same circle. Hence, the non-coherent detection criterion of minimizing Eq. (2.37) is equivalent to minimizing the following function

$$\tilde{s_k} = \arg\{ \min_{s_k \in \mathcal{M}-\text{PSK}} |y_k y_{k-1}^* - s_k|^2 \} \ . \tag{2.38}$$

This implies that optimum non-coherent detection of DPSK signal is to find the hypothesis symbol from $\mathcal{M}$-ary PSK constellation that is the closet point to $y_k y_{k-1}^*$. Observing the equivalent noise term $\hat{n}_k$, it is clear that energy level of $\hat{n}_k$ is approximately $2|h_k|^2$ times larger than that of conventional coherent PSK counterpart. Since average fading power is normalized to unity, this translates to half of received SNR for differential detection scheme which leads to 3-dB performance degradation. Non-coherently-detected DPSK scheme no longer requires the availability of channel information for data recovery, the advantage of DPSK results from trading extra 3-dB transmit energy for exemption of channel knowledge.

2.2.2.2 Differential Technique for Multiple-antenna Transmission: ODSTBC

Differential transmission and non-coherent reception scheme for the single-antenna scenario is revisited in the last subsection, it is natural to consider extensions to MIMO channels with similar properties. In this subsection, we primarily concentrate on a simple differential scheme that is originated from classic orthogonal STBC. Differential approaches based on other structures, for example unitary space-time modulation (USTM), will also be presented in general.

2.2.2.3 Encoding of Differential Alamouti Code

Fig. 2.7 depicts a differentially-encoded Alamouti orthogonal STBC scheme consisting of two transmit antennas. Compared with schematic of differential PSK encoding shown in Fig. 2.6, an extra step is added to generate intermediate symbols that have orthonormal feature. Assuming $\mathcal{M}$-PSK modulation with $\mathcal{M}$ constellation points in total is employed, each modulated symbol corresponds to $\log_2 \mathcal{M} = m$ data bits. Furthermore, it is worth noticing that transmitted DPSK codewords are comprised of complex scalars; however, DSTBC codewords are $N_t \times N_t$ complex matrices in the case of multiple-antenna systems. In order to assure total transmit power of the baseband signals from N_t transmit antennas is normalized to unity, we divide signal amplitude by a factor of $\sqrt{N_t}$.

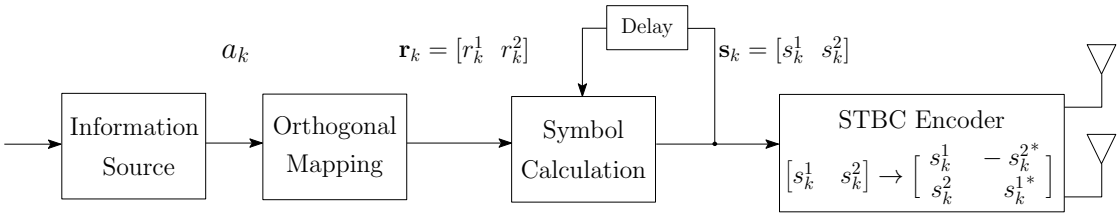

Figure 2.7: The schematic of differential Alamouti STBC employing two transmit antennas.

Suppose a stream of information bits $\mathbf{a}$ ($\mathbf{a} = \{a_1, a_2, a_3, ...\}$) are to be transmitted, each block of $2m$ bits are grouped into pairs and mapped into PSK symbols subsequently. The resultant pair of two modulated symbols from the k-th block is denoted as a vector as follows

$$\mathbf{c}_k = [c_k^1 \quad c_k^2] \,, \tag{2.39}$$

where c_k^1 and c_k^2 represent the first and second element of $\mathbf{c}_k$ respectively. Furthermore, c_k^1 and c_k^2 are taken from a finite alphabet $\mathcal{C}$ given by

$$\mathcal{C} = \frac{\exp\left(2\pi n j/\mathcal{M}\right)}{\sqrt{2}} \,, n = 0, 1, 2, ..., \mathcal{M} - 1 \,. \tag{2.40}$$

Differential encoding procedure is initialized with the calculation of complex-valued coefficients vector $\mathbf{r}_k$ using a one-to-one orthogonal mapping function, which is defined as

$$r_k^1 = c_k^1 (c_{k-1}^1)^* + c_k^2 (c_{k-1}^2)^* \,, \tag{2.41}$$

$$r_k^2 = -c_k^1 c_{k-1}^2 + c_k^2 c_{k-1}^1 \,, \tag{2.42}$$

where $\mathbf{r}_k = [r_k^1 \quad r_k^2]$ are chosen from set $\mathcal{V}$. Apparently, there are in total 2^{2m} number of distinct and unique $\mathbf{r}_k$ vectors.

Similar to the DPSK encoding invoking current data symbol and previously transmitted differential codeword, the intermediate symbols prepared for transmission through multiple antennas also depend on the grouped PSK-modulated symbol block from previous interval as well as the coefficients vector $\mathbf{r}_k$, which is further determined by current input data bits. The difference between two differential schemes is that DPSK codeword is the product of two terms while, in the case of DSTBC, each pair of transmitted symbols is calculated as the linear combination of two corresponding terms. That is

$$\mathbf{s}_k = r_k^1 \cdot \begin{bmatrix} c_{k-1}^1 \\ c_{k-1}^2 \end{bmatrix} + r_k^2 \cdot \begin{bmatrix} (c_{k-1}^2)^* \\ -(c_{k-1}^1)^* \end{bmatrix} . \tag{2.43}$$

Note that the initial two blocks, $\mathbf{s}_0$ and $\mathbf{s}_1$, provide reference for the differential transmission, which do not carry any information. The rest blocks are encoded recursively in a differential manner, the resultant intermediate symbols are prepared for subsequent Alamouti encoding as follows

$$\mathbf{X}_k = \begin{bmatrix} s_k^1 & -s_k^{2*} \\ s_k^2 & s_k^{1*} \end{bmatrix} , \tag{2.44}$$

where s_k^1 and s_k^2 represent the first and second element of $\mathbf{s}_k$ respectively.

In order to provide better understanding of differential encoding procedure, we demonstrate how to generate DSTBC codewords using two transmit antennas and BPSK modulation. Extension to multiple transmit antennas and higher order modulation is straightforward.

To begin with, a number of $2\log_2(\mathcal{M}) = 2\log_2(2) = 2$ successive information bits are grouped into pairs and mapped into BPSK symbols. There are two legit phasor combinations in total for BPSK signal constellation $+\frac{1}{\sqrt{2}}$ and $-\frac{1}{\sqrt{2}}$, which yield four possible coefficients vectors shown in Tab. 2.3.

In this example, it is assumed that the intermediate symbols from $(k-1)$-th block are $\left(+\frac{1}{\sqrt{2}} \quad -\frac{1}{\sqrt{2}}\right)$. At next time interval, the k-th block $\mathbf{c}_k = \left(+\frac{1}{\sqrt{2}} \quad +\frac{1}{\sqrt{2}}\right)$ arrives at the differential encoder, which is corresponding to a pair of information bits of $(0 \;\; 0)$.

According to the orthogonal mapping function described in Eq. (2.43), the coefficients used to compute the intermediate symbols for next differential transmission are $r_k^1 = 1$

Table 2.3: Demonstration of computing coefficients vectors for given input data bits.

Input data bits	$\mathbf{r}_k = [r_k^1 \quad r_k^2]$
(0 0)	(1 0)
(0 1)	(0 -1)
(1 0)	(0 1)
(1 1)	(-1 0)

and $r_k^2 = 0$, respectively. Thus, for the k-th block, we have

$$\begin{aligned}\mathbf{s}_k &= r_k^1 \cdot \begin{bmatrix} c_{k-1}^1 \\ c_{k-1}^2 \end{bmatrix} + r_k^2 \cdot \begin{bmatrix} (c_{k-1}^2)^* \\ -(c_{k-1}^1)^* \end{bmatrix} , \\ &= 1 \cdot \begin{bmatrix} +\frac{1}{\sqrt{2}} \\ -\frac{1}{\sqrt{2}} \end{bmatrix} + 0 \cdot \begin{bmatrix} -\frac{1}{\sqrt{2}} \\ -\frac{1}{\sqrt{2}} \end{bmatrix} , \\ &= \begin{bmatrix} +\frac{1}{\sqrt{2}} \\ -\frac{1}{\sqrt{2}} \end{bmatrix} . \end{aligned} \tag{2.45}$$

After Alamouti STBC encoding, $+\frac{1}{\sqrt{2}}$ and $-\frac{1}{\sqrt{2}}$ are sent from antenna one and two at the first transmission slot, $+\frac{1}{\sqrt{2}}$ and $+\frac{1}{\sqrt{2}}$ are sent from antenna one and two at the second transmission slot, respectively.

$$\begin{aligned}\mathbf{X}_k &= \begin{bmatrix} s_k^1 & -s_k^{2*} \\ s_k^2 & s_k^{1*} \end{bmatrix} , \\ &= \begin{bmatrix} +\frac{1}{\sqrt{2}} & +\frac{1}{\sqrt{2}} \\ -\frac{1}{\sqrt{2}} & +\frac{1}{\sqrt{2}} \end{bmatrix} . \end{aligned} \tag{2.46}$$

The relationship between input data bits and intermediate symbols from previous block is summarized in Tab. 2.4.

Table 2.4: Calculation of intermediate symbols for given input data bits and intermediate symbols from previous block.

Data bits	$(s_{k-1}^1 \quad s_{k-1}^2)$	$(s_k^1 \quad s_k^2)$
$(0 \quad 0)$	$\left(+\frac{1}{\sqrt{2}} \quad +\frac{1}{\sqrt{2}}\right)$	$\left(+\frac{1}{\sqrt{2}} \quad +\frac{1}{\sqrt{2}}\right)$
$(0 \quad 0)$	$\left(+\frac{1}{\sqrt{2}} \quad -\frac{1}{\sqrt{2}}\right)$	$\left(+\frac{1}{\sqrt{2}} \quad -\frac{1}{\sqrt{2}}\right)$
$(0 \quad 0)$	$\left(-\frac{1}{\sqrt{2}} \quad +\frac{1}{\sqrt{2}}\right)$	$\left(-\frac{1}{\sqrt{2}} \quad +\frac{1}{\sqrt{2}}\right)$
$(0 \quad 0)$	$\left(-\frac{1}{\sqrt{2}} \quad -\frac{1}{\sqrt{2}}\right)$	$\left(-\frac{1}{\sqrt{2}} \quad -\frac{1}{\sqrt{2}}\right)$
$(0 \quad 1)$	$\left(+\frac{1}{\sqrt{2}} \quad +\frac{1}{\sqrt{2}}\right)$	$\left(+\frac{1}{\sqrt{2}} \quad -\frac{1}{\sqrt{2}}\right)$
$(0 \quad 1)$	$\left(+\frac{1}{\sqrt{2}} \quad -\frac{1}{\sqrt{2}}\right)$	$\left(-\frac{1}{\sqrt{2}} \quad -\frac{1}{\sqrt{2}}\right)$
$(0 \quad 1)$	$\left(-\frac{1}{\sqrt{2}} \quad +\frac{1}{\sqrt{2}}\right)$	$\left(+\frac{1}{\sqrt{2}} \quad +\frac{1}{\sqrt{2}}\right)$
$(0 \quad 1)$	$\left(-\frac{1}{\sqrt{2}} \quad -\frac{1}{\sqrt{2}}\right)$	$\left(-\frac{1}{\sqrt{2}} \quad +\frac{1}{\sqrt{2}}\right)$
$(1 \quad 0)$	$\left(+\frac{1}{\sqrt{2}} \quad +\frac{1}{\sqrt{2}}\right)$	$\left(-\frac{1}{\sqrt{2}} \quad +\frac{1}{\sqrt{2}}\right)$
$(1 \quad 0)$	$\left(+\frac{1}{\sqrt{2}} \quad -\frac{1}{\sqrt{2}}\right)$	$\left(+\frac{1}{\sqrt{2}} \quad +\frac{1}{\sqrt{2}}\right)$
$(1 \quad 0)$	$\left(-\frac{1}{\sqrt{2}} \quad +\frac{1}{\sqrt{2}}\right)$	$\left(-\frac{1}{\sqrt{2}} \quad -\frac{1}{\sqrt{2}}\right)$
$(1 \quad 0)$	$\left(-\frac{1}{\sqrt{2}} \quad -\frac{1}{\sqrt{2}}\right)$	$\left(+\frac{1}{\sqrt{2}} \quad -\frac{1}{\sqrt{2}}\right)$
$(1 \quad 1)$	$\left(+\frac{1}{\sqrt{2}} \quad +\frac{1}{\sqrt{2}}\right)$	$\left(-\frac{1}{\sqrt{2}} \quad -\frac{1}{\sqrt{2}}\right)$
$(1 \quad 1)$	$\left(+\frac{1}{\sqrt{2}} \quad -\frac{1}{\sqrt{2}}\right)$	$\left(-\frac{1}{\sqrt{2}} \quad +\frac{1}{\sqrt{2}}\right)$
$(1 \quad 1)$	$\left(-\frac{1}{\sqrt{2}} \quad +\frac{1}{\sqrt{2}}\right)$	$\left(+\frac{1}{\sqrt{2}} \quad -\frac{1}{\sqrt{2}}\right)$
$(1 \quad 1)$	$\left(-\frac{1}{\sqrt{2}} \quad -\frac{1}{\sqrt{2}}\right)$	$\left(+\frac{1}{\sqrt{2}} \quad +\frac{1}{\sqrt{2}}\right)$

2.2.2.4 Receiver and Non-coherent Decoding

In this subsection, we discuss the decoding algorithm for the differential Alamouti code using two transmit antennas. For the sake of simplicity of presentation, the number of receive antenna is limited to one. This limitation is lifted later enabling recovery of the transmitted information employing N_r receive antennas.

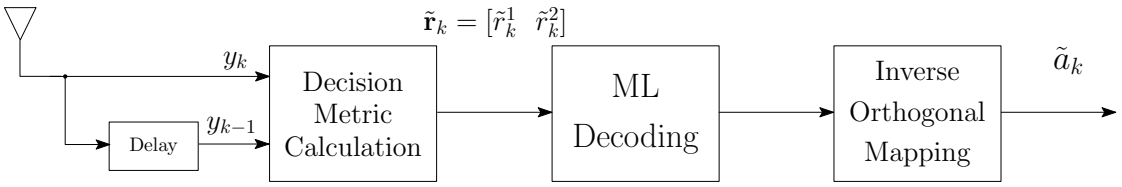

Figure 2.8: The receiver schematic of differential Alamouti STBC employing one receive antenna.

If the notation y_k^i represents the i-th element ($i = 1, 2$ when $N_t = 2$) from the k-th received symbol block, the received symbols for two successive blocks can be expressed as

$$y_{k-1}^1 = s_{k-1}^1 h_{k-1}^1 + s_{k-1}^2 h_{k-1}^2 + n_{k-1}^1 \,, \tag{2.47}$$

$$y_{k-1}^2 = -(s_{k-1}^2)^* h_{k-1}^1 + (s_{k-1}^1)^* h_{k-1}^2 + n_{k-1}^2 \,, \tag{2.48}$$

$$y_k^1 = s_k^1 h_k^1 + s_k^2 h_k^2 + n_k^1 \,, \tag{2.49}$$

$$y_k^2 = -(s_k^2)^* h_k^1 + (s_k^1)^* h_k^2 + n_k^2 \,, \tag{2.50}$$

where h_k^i is the Rayleigh fading coefficient experienced by the i-th element of the k-th block. Under the assumption of quasi-static fading, channel coefficients appear almost constant for consecutive blocks, $h_{k-1}^1 \approx h_k^1 = h_1$ and $h_{k-1}^2 \approx h_k^2 = h_2$. Moreover, n_k^i denotes the Gaussian noise added to the i-th element of the k-th block, which has zero mean and variance of $1/N_0$ per dimension.

For the ease of illustration, we further define the vector representations of the received signals as follows

$$\begin{pmatrix} y_{k-1}^1 & (y_{k-1}^2)^* \end{pmatrix} = \begin{pmatrix} s_{k-1}^1 & s_{k-1}^2 \end{pmatrix} \underbrace{\begin{pmatrix} h_1 & h_2^* \\ h_2 & -h_1^* \end{pmatrix}}_{\mathcal{H}} + \underbrace{\begin{pmatrix} n_{k-1}^1 & (n_{k-1}^2)^* \end{pmatrix}}_{\mathcal{N}_{k-1}^1} \,. \tag{2.51}$$

Similarly,

$$\begin{pmatrix} y_{k-1}^2 & -(y_{k-1}^1)^* \end{pmatrix} = \begin{pmatrix} -(s_{k-1}^2)^* & (s_{k-1}^1)^* \end{pmatrix} \underbrace{\begin{pmatrix} h_1 & h_2^* \\ h_2 & -h_1^* \end{pmatrix}}_{\mathcal{H}} + \underbrace{\begin{pmatrix} n_{k-1}^2 & -(n_{k-1}^1)^* \end{pmatrix}}_{\mathcal{N}_{k-1}^2}, \tag{2.52}$$

$$\begin{pmatrix} y_k^1 & (y_k^2)^* \end{pmatrix} = \begin{pmatrix} s_k^1 & s_k^2 \end{pmatrix} \underbrace{\begin{pmatrix} h_1 & h_2^* \\ h_2 & -h_1^* \end{pmatrix}}_{\mathcal{H}} + \underbrace{\begin{pmatrix} n_{k-1}^1 & (n_{k-1}^2)^* \end{pmatrix}}_{\mathcal{N}_k^1}. \tag{2.53}$$

Construction of the decision statistics is based on the inner product of two adjacent received symbol blocks given in Eq. (2.51) and Eq. (2.53).

$$\begin{aligned} \begin{pmatrix} y_k^1 & (y_k^2)^* \end{pmatrix} \cdot \begin{pmatrix} y_{k-1}^1 & (y_{k-1}^2)^* \end{pmatrix} &= y_k^1 (y_{k-1}^1)^* + (y_k^2)^* y_{k-1}^2 , \\ &= \begin{pmatrix} s_k^1 & s_k^2 \end{pmatrix} \mathcal{H}\mathcal{H}^\dagger \begin{pmatrix} s_{k-1}^1 & s_{k-1}^2 \end{pmatrix}^* + \\ &\quad \underbrace{\begin{pmatrix} s_k^1 & s_k^2 \end{pmatrix} \mathcal{H} (\mathcal{N}_{k-1}^1)^* + \mathcal{N}_k^1 \mathcal{H}^\dagger \begin{pmatrix} s_{k-1}^1 & s_{k-1}^2 \end{pmatrix}^* + \mathcal{N}_k^1 (\mathcal{N}_{k-1}^1)^*}_{\widetilde{\mathcal{N}}_1}, \end{aligned} \tag{2.54}$$

$$\tilde{r}_k^1 = \left(|h_1|^2 + |h_2|^2\right) \left(s_k^1 (s_{k-1}^1)^* + s_k^2 (s_{k-1}^2)^*\right) + \widetilde{\mathcal{N}}_1 . \tag{2.55}$$

Similarly

$$\begin{aligned} \begin{pmatrix} y_k^1 & (y_k^2)^* \end{pmatrix} \cdot \begin{pmatrix} y_{k-1}^2 & -(y_{k-1}^1)^* \end{pmatrix} &= y_k^1 (y_{k-1}^2)^* - (y_k^2)^* y_{k-1}^1 , \\ &= \begin{pmatrix} s_k^1 & s_k^2 \end{pmatrix} \mathcal{H}\mathcal{H}^\dagger \begin{pmatrix} -s_{k-1}^2 & s_{k-1}^1 \end{pmatrix}^* + \\ &\quad \underbrace{\begin{pmatrix} s_k^1 & s_k^2 \end{pmatrix} \mathcal{H} (\mathcal{N}_{k-1}^2)^* + \mathcal{N}_k^1 \mathcal{H}^\dagger \begin{pmatrix} -s_{k-1}^2 & s_{k-1}^1 \end{pmatrix}^* + \mathcal{N}_k^1 (\mathcal{N}_{k-1}^2)^*}_{\widetilde{\mathcal{N}}_2} \end{aligned} \tag{2.56}$$

$$\tilde{r}_k^2 = \left(|h_1|^2 + |h_2|^2\right) \left(-s_k^1 s_{k-1}^2 + s_k^2 s_{k-1}^1\right) + \widetilde{\mathcal{N}}_2 . \tag{2.57}$$

Summarize Eq. (2.55) and Eq. (2.57), we can write the decision statistics in a vector form

$$\begin{pmatrix} \tilde{r}_k^1 & \tilde{r}_k^2 \end{pmatrix} = \left(|h_1|^2 + |h_2|^2\right) \begin{pmatrix} r_k^1 & r_k^2 \end{pmatrix} + \begin{pmatrix} \widetilde{\mathcal{N}}_1 & \widetilde{\mathcal{N}}_2 \end{pmatrix} . \tag{2.58}$$

For a given channel realization h_1 and h_2, the decision statistics $\tilde{r}_1$ and $\tilde{r}_2$ only depend on the differential coefficients r_1 and r_2, respectively. Since all the coefficients vectors in the set $\mathcal{V}$ have equal lengths, the receiver now chooses the closest coefficient vector from $\mathcal{V}$ to the decision statistics signal vector $(\tilde{r}_1, \tilde{r}_2)$ as the decoding output. Then the inverse mapping of Eq. (2.41) and Eq. (2.42) is applied to recover the transmitted block of bits.

2.2.2.5 Decoding with Multiple Receive Antennas

In this subsection, we extend the concept of non-coherent DSTBC reception to support multiple receive antennas, which could in return benefit from higher level of diversity. The differential encoding and transmission arrangement are identical to the case of employing a single receive antenna; however, the combining and diversity reception algorithm on the receiving side are different.

To begin with, transmitted DSTBC symbols picked up by the j-th receive antenna during two successive symbol intervals $(k-1)$-th and k-th are denoted as follows

$$y^1_{j,k-1} = s^1_{k-1}h^1_{j,k-1} + s^2_{k-1}h^2_{j,k-1} + n^1_{j,k-1} \ , \tag{2.59}$$

$$y^2_{j,k-1} = -(s^2_{k-1})^* h^1_{j,k-1} + (s^1_{k-1})^* h^2_{j,k-1} + n^2_{j,k-1} \ , \tag{2.60}$$

$$y^1_{j,k} = s^1_k h^1_{j,k} + s^2_k h^2_{j,k} + n^1_{j,k} \ , \tag{2.61}$$

$$y^2_{j,k} = -(s^2_k)^* h^1_{j,k} + (s^1_k)^* h^2_{j,k} + n^2_{j,k} \ , \tag{2.62}$$

where $h^i_{j,k}$ $(i = 1, 2; j = 1, 2, ..., N_r)$ is the notation for the complex-valued Rayleigh fading coefficients of the channel between the i-th transmit antenna and the j-th receive antenna experienced by the k-th symbol block; while $n^i_{j,k}$ represents the AWGN added to the k-th symbol block at the j-th receiver.

Since the quasi-static channel model is assumed for DSTBC transmission, $h^i_{j,k}$ could be replaced with $h_{j,i}$ in the rest of this subsection to keep the presentation concise. Following the same steps formulated in Eq. (2.51)-Eq. (2.57), two decision metrics correspond to the j-th receiver are written as

$$\tilde{r}^1_{j,k} = \left(|h_{j,1}|^2 + |h_{j,2}|^2\right)\left(s^1_k (s^1_{k-1})^* + s^2_k (s^2_{k-1})^*\right) + \widetilde{\mathcal{N}}_{j,1} \ , \tag{2.63}$$

$$\tilde{r}^2_{j,k} = \left(|h_{j,1}|^2 + |h_{j,2}|^2\right)\left(-s^1_k s^2_{k-1} + s^2_k s^1_{k-1}\right) + \widetilde{\mathcal{N}}_{j,2} \ . \tag{2.64}$$

Summarize Eq. (2.63) and Eq. (2.64), the final decision statistics are now adapted to

$$\begin{pmatrix} \tilde{r}^1_k & \tilde{r}^2_k \end{pmatrix} = \left(\sum_{j=1}^{N_r} \left(|h_{j,1}|^2 + |h_{j,2}|^2\right)\right) \begin{pmatrix} r^1_k & r^2_k \end{pmatrix} + \sum_{j=1}^{N_r} \begin{pmatrix} \widetilde{\mathcal{N}}_{j,1} & \widetilde{\mathcal{N}}_{j,2} \end{pmatrix} \ . \tag{2.65}$$

2.2.2.6 Performance Evaluation of Differential STBC Scheme

In this subsection, we present some simulation results of the differential STBC introduced previously. It is assumed that $N_t = 2$ antennas are used in the transmitting side, we focus on the bit error performance for scenarios with different numbers of receive antennas $N_r = 1, 2, 4$. Since various kinds of differential STBCs are derived from classic Alamouti code, the terms 'differential STBC' and 'differential Alamouti code' are used interchangeably.

The following simulation results are based on the quasi-static flat Rayleigh-fading channel model. This implies that the path gains of the fading channel, which are independent complex Gaussian random variables, remain constant during the transmission of one frame. We also provide the simulation results for corresponding coherent Alamouti code with exactly the same configurations as comparison benchmarks.

Fig. 2.9 plots the BER versus transmitted E_b/N_0 when BPSK-modulated symbols are emitted from two transmit antennas in two successive transmission periods, the overall transmission rate is therefore equivalent to 1 bit/sec/Hz. As denoted by red solid-line and black dashed-line in Fig. 2.9, the BER curves corresponding to orthogonal Alamouti STBC and the differential one share the same slope indicating that differential Alamouti code is also capable of performing at full diversity order, albeit this is achieved at the cost of approximately 3.0 dB degradation due to the doubled noise variance incurred during non-coherent decoding. It is natural to find such observation is consistent with systems employing differential PSK at the transmitter, since differential Alamouti STBC is in fact an extension of DPSK to multiple-antenna scenarios. It is illustrated in Fig. 2.9 that significant performance improvement of roughly 10.5 dB is attained at BER of 10^{-5} from incorporating an extra antenna in the receiving side, while a further reduction of about 6.50 dB transmit power is witnessed with two additional receive antennas.

It is worth noticing that the assumption of constant path gains during transmission of entire frame is somewhat unrealistic, however, an irreducible error floor is incurred when such assumption is not satisfied. For the purpose of eliminating the underlying assumption, a variety of solutions are contrived in literature, where using more than two received symbol blocks to facilitate the detection seems perform effectively and efficiently. For more detailed discussion, one can refer to [57] and reference therein.

Fig. 2.10 and Fig. 2.11 depict the comparison of BER versus E_b/N_0 performance for a similarly-configured differential STBC scheme with transmission rate of 2 bits/sec/Hz, which is achieved by utilizing Gray- and SP-mapped QPSK symbols for two successive

transmission periods, respectively. Full diversity order is also observed in these figures. When aiming at a bit error probability of 10^{-5}, an additional SNR of 3.0 dB is required for systems invoking $N_r = 1, 2, 4$ receiving antennas in comparison to 1 bits/sec/Hz case. As expected, for SP-mapped scheme, the performance is slightly degraded by about 1.0 $\sim$ 2.0 dB at BER $= 10^{-5}$. Fig. 2.12 and Fig. 2.13 provide similar results for differential Alamouti scheme transmitting at 3 bits/sec/Hz under the same simulation conditions. The resulting differential scheme, which also has the ability to acquire full spatial diversity gain, is $35.0 - 27.0 = 8.0$ dB and $35.0 - 30.0 = 5.0$ dB inferior in terms of the required SNR compared to the 1 bit/sec/Hz and 2 bits/sec/Hz at BER $= 10^{-5}$, respectively.

According to the results presented in Fig. 2.9-Fig. 2.14, differential Alamouti codes exhibit many desirable properties, including straightforward and simple encoding, full spatial diversity gain, non-coherent decoding dispensing with channel information at the receiver. However, on the other hand, the construction procedure of differential Alamouti codes imposes limitations. For instance, when aiming at transmission rate of 2 bits/sec/Hz, QPSK-modulated symbols are invoked to compute the intermediate symbol set $\mathbf{s}_k$ following Eq. (2.41)-Eq. (2.43) defined in subsection 2.2.2.3. Note that the aforementioned encoding procedure significantly expands the signal constellation for non-binary signalling. As a consequence, the resulting intermediate symbols are taken from an irregular 9QAM constellation with more than four points instead of QPSK constellation. This translates to some inconvenience for incorporating differential Alamouti STBC in existing communication systems.

Some results for USTM schemes based on group codes are considered in order to provide a comprehensive comparison between distinct differential techniques. For instance, the bit error performance of unity-rate as well as 3/2-rate USTM employing $N_t = 2$ transmit antennas as well as N_r receive antennas ($N_r = 1, 2, 4$) are shown in Fig. 2.14 and Fig. 2.15, respectively. It is clearly shown that the unique feature of USTM schemes also enable non-coherent detection in the receiver without the knowledge of channel coefficients. Furthermore, USTM is capable of performing as well as the differential Alamouti codes. Note that USTM schemes generally suffer from rate deficiency. To elaborate further, according to encoding rule of USTM, the overall coding rate is defined as $\log_2(2 * 2^2)/N_t = \log_2(2 * 2^2)/2 = 1.5$ bits/sec/Hz, which leads to a lower coding rate in comparison to differential Alamouti STBC.

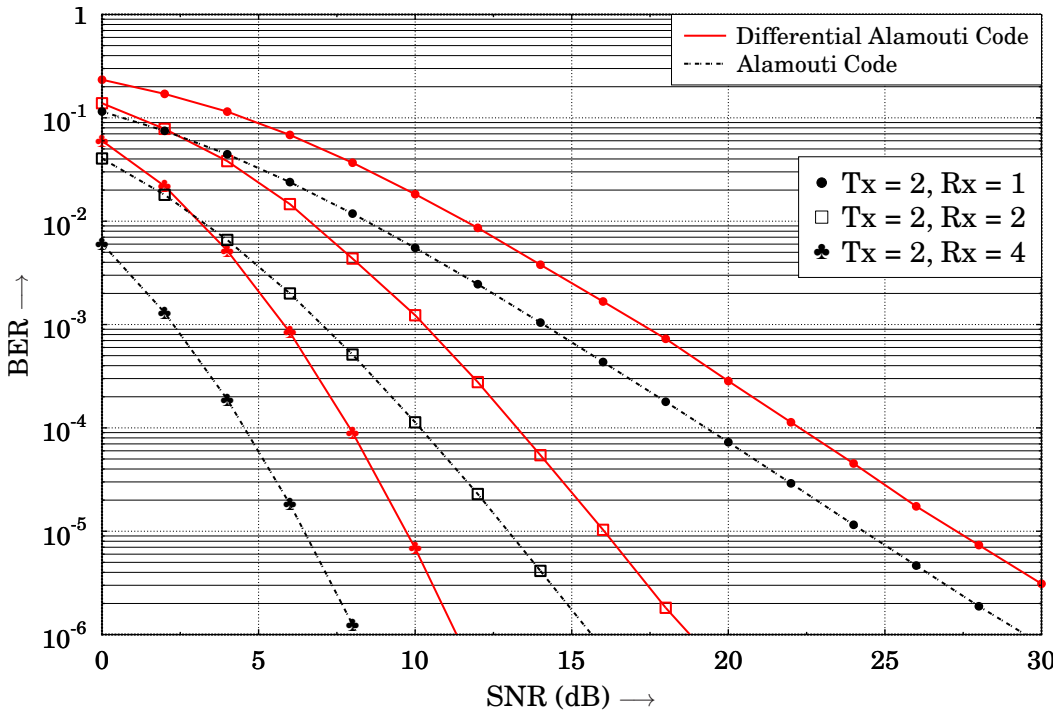

Figure 2.9: Error rate performance comparison between Alamouti STBC with coherent decoding and differential Alamouti STBC with non-coherent decoding. $N_t = 2$ transmit antennas and $N_r = 1/2/4$ receive antennas are employed for transmission at 1 bit/sec/Hz over quasi-static flat Rayleigh-fading channel.

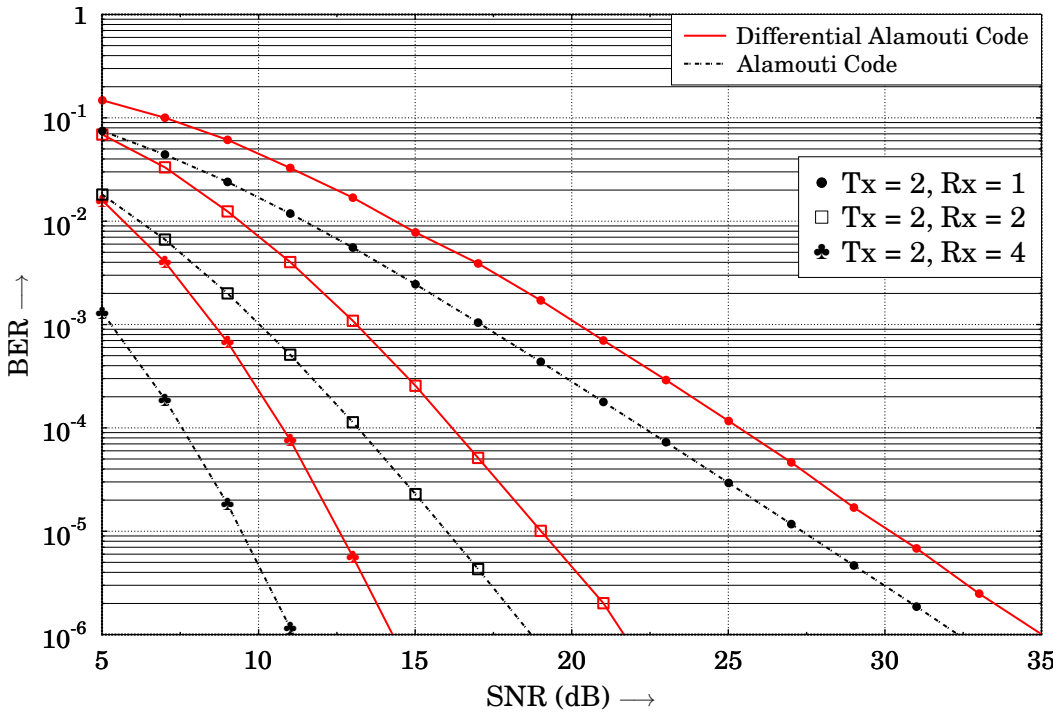

Figure 2.10: Error rate performance comparison between Alamouti STBC with coherent decoding and differential Alamouti STBC with non-coherent decoding. $N_t = 2$ transmit antennas and $N_r = 1/2/4$ receive antennas are employed for transmission at 2 bit/sec/Hz with Gray mapping over quasi-static flat Rayleigh-fading channel.

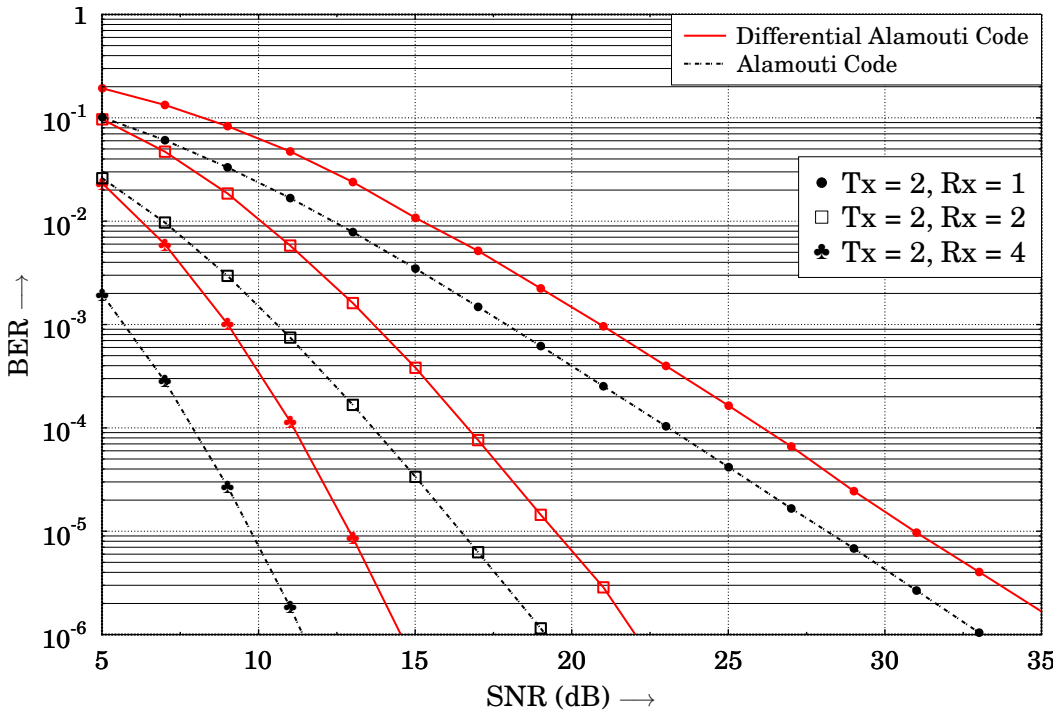

Figure 2.11: Error rate performance comparison between Alamouti STBC with coherent decoding and differential Alamouti STBC with non-coherent decoding. $N_t = 2$ transmit antennas and $N_r = 1/2/4$ receive antennas are employed for transmission at 2 bit/sec/Hz with SP mapping over quasi-static flat Rayleigh-fading channel.

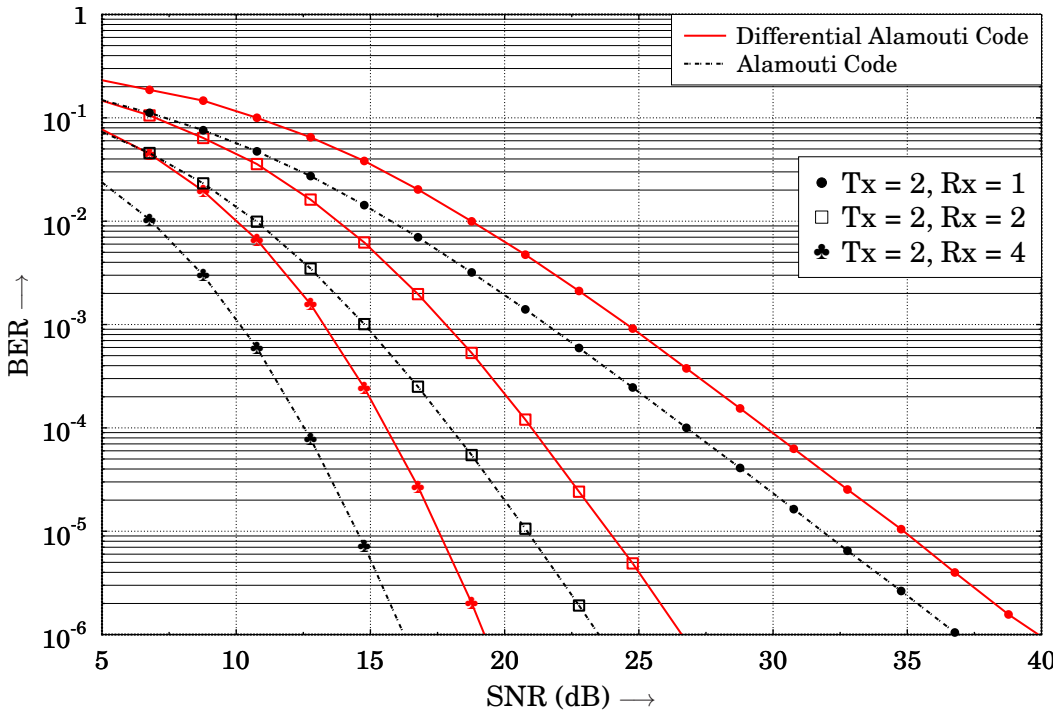

Figure 2.12: Error rate performance comparison between Alamouti STBC with coherent decoding and differential Alamouti STBC with non-coherent decoding. $N_t = 2$ transmit antennas and $N_r = 1/2/4$ receive antennas are employed for transmission at 3 bit/sec/Hz with Gray mapping over quasi-static flat Rayleigh-fading channel.

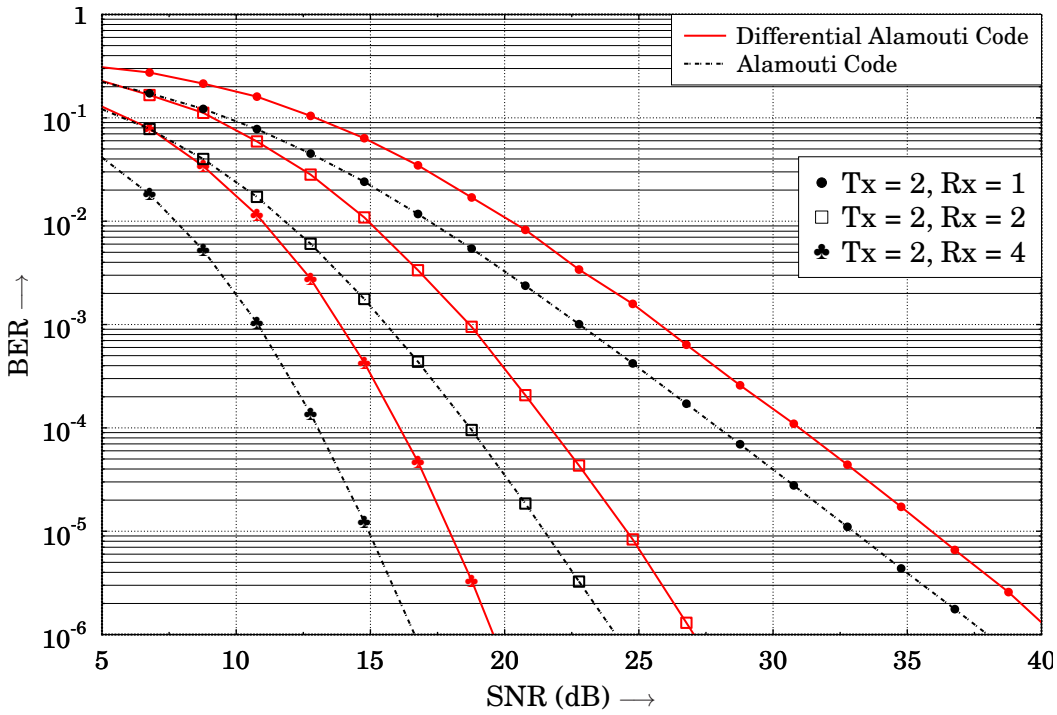

Figure 2.13: Error rate performance comparison between Alamouti STBC with coherent decoding and differential Alamouti STBC with non-coherent decoding. $N_t = 2$ transmit antennas and $N_r = 1/2/4$ receive antennas are employed for transmission at 3 bit/sec/Hz with SP mapping over quasi-static flat Rayleigh-fading channel.

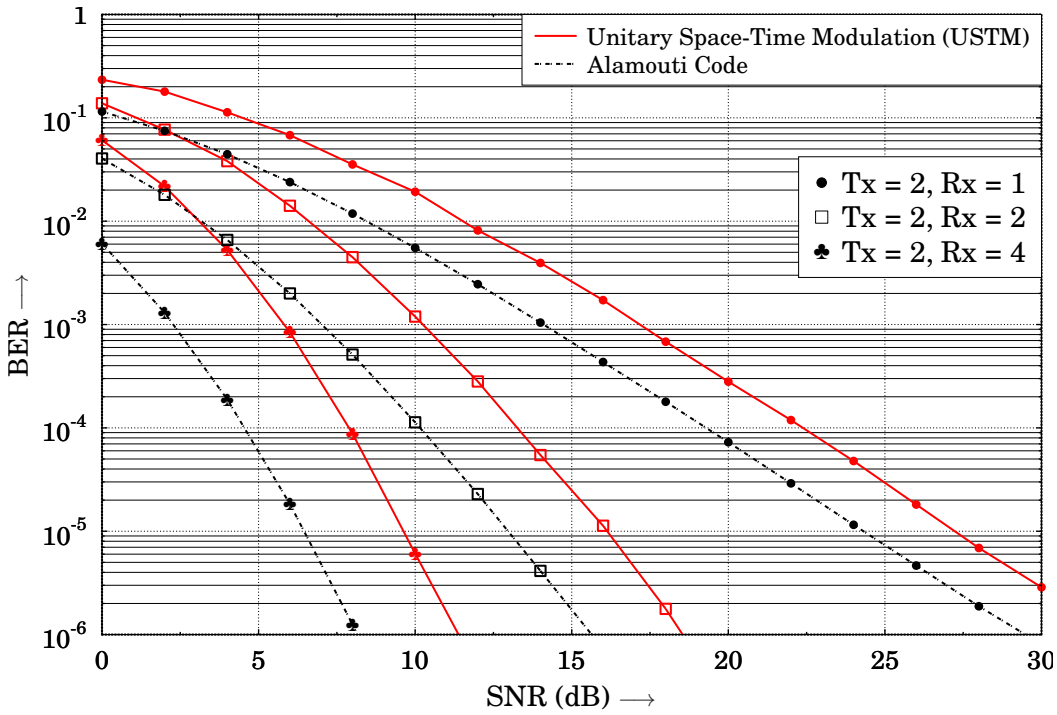

Figure 2.14: Error rate performance comparison between Alamouti STBC with coherent decoding and USTM with non-coherent decoding. $N_t = 2$ transmit antennas and $N_r = 1/2/4$ receive antennas are employed for transmission at 1 bit/sec/Hz over quasi-static flat Rayleigh-fading channel.

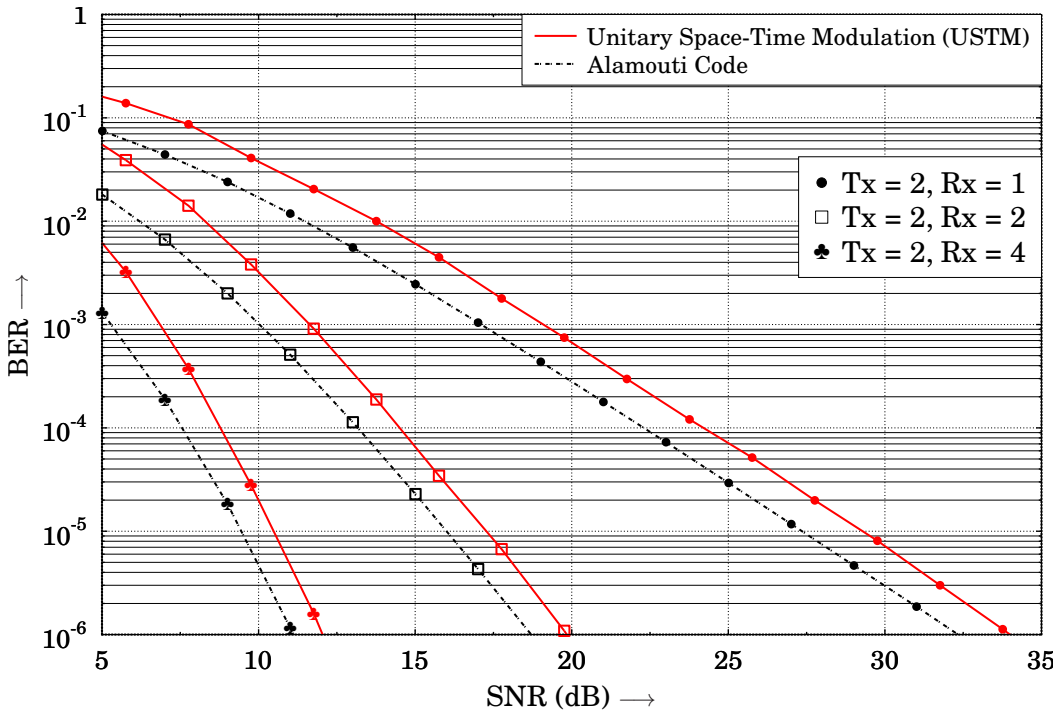

Figure 2.15: Error rate performance comparison between Alamouti STBC with coherent decoding and USTM with non-coherent decoding. $N_t = 2$ transmit antennas and $N_r = 1/2/4$ receive antennas are employed for transmission at 1.5 bit/sec/Hz with Gray mapping over quasi-static flat Rayleigh-fading channel.

2.3 Conclusion

In this literature review chapter, some basic principles of space-time coding as well as differential space-time coding are revisited and reviewed. Discussions in this chapter involve the following aspects

- General introduction of various types of diversity and multiplexing techniques, including orthogonal space-time block code, layered space-time code as well as linear dispersion code are given. Desirable properties and features of each scheme are explored and studied.
- The simplest orthogonal space-time block code with two transmit antennas, Alamouti code, is discussed in detail. Alamouti STBC encoding procedure is first presented, then explanation of non-coherent decoding algorithm starts with single receive antenna and later extends to multiple receive antennas. Performance results of the Alamouti STBC are also provided and compared.
- Differential space-time coding is originated from classic space-time coding but eliminating the channel estimation component, hence it is more appealing in practice due to the simplicity of implementation. Similarity and difference between the differential unitary space-time modulation and orthogonal differential STBC are investigated and discussed.
- Examples of differential encoding and non-coherent decoding techniques are provided for single-antenna as well as multiple-antenna scenarios in the rest part of Chapter 2. Similarly, performance evaluations are also demonstrated.

Chapter 3

Cooperative Space-Time Block Codes

Contents

3.1 Cooperative Communication and Relaying

As discussed in Chapter 1, at present, the demand for mobile multimedia services is exploding at an exponential rate. In addition, the energy consumed to support the networks delivering this kind of high-data-rate services is continuously rising. To create a state-of-the-art broadband wireless communication network, the main focus needs to be shifted to a new paradigm which could not only meet the increasing demand for data throughput but also reduce the energy consumption. Multiple-input and multiple-output (MIMO) system provides a good solution to meet these requirements by employing multiple transmit/receive antennas. In the last decade, we have tasted many benefits of MIMO systems, such as substantial increases in the channel capacity as well as high transmit/receive diversity gain [9, 13, 14].

However, a practical problem arises when implementing MIMO systems. It is difficult

to integrate more than one antenna in a mobile handset or wireless node (in the context of wireless sensor network (WSN)) due to stringent limitation imposed on the available power and hardware complexity. Most importantly, it is difficult to eliminate the correlations between the received signals, which arrive at the antennas simultaneously via different propagation paths, when multiple antennas are deployed in a size-limited mobile handset. This makes the recovery of the original signal almost impossible; hence, system performance will be highly degraded.

Under such circumstances, user cooperation or cooperative communication [58–64], which introduces a large number of low-power nodes/users to cooperate and relay signals for others, is a promising approach to balance the tradeoff between high network throughput and energy conservation. Furthermore, by creating a virtual antenna array (VAA), where each mobile unit is capable of collaborating with one partner or a few partners, cooperative communication has the potential for increasing the achievable capacity, spectrum efficiency, coverage area and quality of experience.

Considering these attractive benefits and the trend of future generation radio networks, an increasing number of researchers are endeavoring to develop and establish novel multihop cooperative wireless networks. More explicitly, optimization of distributed coding, joint channel and network coding design, development of new relaying protocols and cooperative transmission schemes, resource and power allocations, and cross-layer optimization are key issues in the design of cooperative wireless networks. Much ongoing research on cooperative communication and relaying techniques involving the deployment of fixed or nomadic relay nodes reveals a bright future of cooperative communications. In 2009, the IEEE standard 802.16j was approved by IEEE-SA Standards Board as an amendment to IEEE standard 802.16-2009.

Based on the behaviour of relaying terminals, the cooperative protocols can be generally classified as transparent relaying and regenerative relaying [65]. The former basically implies that the transformations of received signals in the relay nodes simply take place in the analog domain. For instance, the well-known amplify-and-forward (AF) scheme, which only amplifies the signal amplitude before forwarding to the destination nodes, is a typical representative of transparent relaying strategy. On the other hand, in the latter scenario, the received signals in relay nodes are processed in the digital domain resulting in the waveform and information are totally changed. A popular approach called decode-and-forward (DF) falls into this category.

3.1.1 Distributed Space-Time Coding

The distributed nature of the cooperative wireless networks provides unique opportunities for designing efficient distributed signal processing and coding techniques which could potentially lead to significant energy saving and performance gain. Distributed space-time block coding schemes were developed for cooperative communications in a multi-user environment to achieve extra spatial diversity by exploiting a collection of distributed antennas belonging to different users. It allows a group of conventional single-antenna aided mobile units to collaborate with each other by sharing their antennas so that a VAA could be created to perform various kinds of space-time coding schemes. In order to achieve the cooperative diversity in distributed space-time coding scenarios, the space-time codewords are constructed by different users and transmitted through statistically independent fading channels. Hence, comparing to traditional single-user non-cooperative space-time coded wireless MIMO networks, the construction of distributed coding poses more challenges than ordinary code design.

Distributed space-time coding integrates the following three major advantages.

- To begin with, the distributed STBC inherits all characteristics of the original STBC and naturally has the potentiality of achieving significant performance gain in a multi-path fading channel.
- The second advantage of distributed STBC is that, unlike the original STBC scheme with co-located multiple antennas, mobile units in a distributed STBC network only need to be equipped with a single antenna. This feature could result in more compact size for future handsets and more importantly, simpler structure could effectively extend the battery life.
- Thirdly, with the assistance of distributed STBC, the cooperating users are capable of helping the senders to forward and relay the signals to the destination. In this manner, the coverage of wireless network could be extended without any further infrastructure investment.

These benefits brought by distributed STBC seem very attractive; however, two crucial problems need to be solved in order to implement distributed STBC. The first is error propagation induced in the decoding and forward stage in the relay nodes. If error-free decoding could not be guaranteed, the decoded signal containing errors will be re-encoded and forwarded during next transmission period. This would cause serious problems when the detector and decoder in the destination node try to recover the original information

and lead to severe degradation of the system performance. It is shown in [66, 67] that the orthogonality of the distributed space-time coded signals constructed and transmitted by multiple relay nodes in a distributed manner is not preserved due to the error propagation experienced by the relay-to-destination link. The second key issue needs to be addressed is the synchronization problem among all the collaborative relaying users, which is also referred to as inter-relay-node synchronization. If the destination node picks up several signals from different users without sufficient synchronization, it is extremely difficult to perform an accurate decision.

Although both have N independent transmission routes from the transmitter to receiver, two distinct differences between the relaying network having N number of relay nodes and conventional multi-antenna system with N co-located transmit antennas and one receive antenna make them have their unique characteristics. To begin with, in a conventional multi-antenna system, antennas are connected by cables enabling full cooperation. However, in the context of a distributed relaying network, they could only coordinate in a distributed fashion since antennas belonging to different users are geographically separated. Secondly, the destination node is always able to exploit full spatial diversity gain using conventional co-located STBC schemes; however, for decode-and-forward relaying scenarios, this argument is no longer satisfied as construction of valid distributed STBC codewords requires each relay node performs error-free recovery of the transmitted information symbols. In fact, the signals observed by the relay nodes are noisy version of the transmitted ones, the integrity of estimates recovered from these noisy signals is not guaranteed. In this case, the destination could not attain any spatial diversity gain from the employment of distributed STBC.

There are many existing works related to the topic of distributed STBC, for example, in [68], the authors proposed a distributed linear dispersion (DLD) code aided multi-relay cooperative communication system. When the AF protocol is employed, the relay node is only required to re-encode the received signal with DLD code and transmit the resultant DLD signal to the destination node. If we use the notation N_{relay} to represent the total number of relay nodes in the network topology, when the relays have the knowledge of the channels between source and relay nodes h_{sr} and the channels between relay and destination node h_{rd}, the capacity varies as a function of $\log(N_{relay})$ and the power efficiency varies as $\sqrt{N_{relay}}$. The work of [69] is also heuristic, in which two terminals focus on the exchange of Alamouti space-time coded information symbols simultaneously via a single partner with the aid of PLNC, which has the constraint that the source nodes have to be equipped with multiple co-located antennas to avoid inducing error propagation in the relaying process. Other cooperative strategies for two-way relaying schemes, including the denoise-and-forward method [70], also achieve the maximum diversity gain offered

by the fading channel.

3.1.2 Two-way Relay Channel and Existing Two-way Relaying Strategies

The direction of signal flow in conventional cooperation schemes is generally considered as one-way mode. To be more specific, the relay nodes receive the incoming signals from the source nodes, which are subsequently amplified or decoded/re-encoded and finally forwarded to the destination nodes. The hardware used in all relaying nodes is designed under an important assumption that the transmission and reception of radio signals are not allowed at the same time. In other words, they operate in time-division half-duplex. This kind of unidirectional cooperative communication system usually suffers from spectral efficiency loss.

The two-way communication channel was first introduced in the early 1960s. The property and capacity bound of two-way communication channel were fully investigated and calculated in [71]. After that, there was not much progress or significant breakthrough in the field of two-way communication until the advent of network coding (NC) [72–75]. Network coding was originally proposed to save the bandwidth and increase the network throughput for multiple access channels. Network coding arithmetic, which exploits the broadcast nature of mobile radio channels, is carried out at the bit level after the received signals have been separately detected and decoded in the relay nodes.

Recently, the unidirectional-relay assisted cooperative communication strategies have been extended to transmit over two-way relay channels [76]. The schematic of a classic three-node two-way cooperative communication system is shown below.

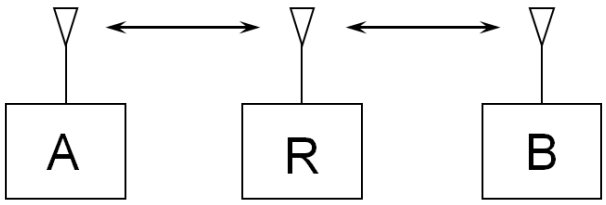

Figure 3.1: Schematic of a two-way cooperative communication system.

Node $\mathbf{A}$ and node $\mathbf{B}$ are ordinary time-division half-duplex wireless terminals, which intend to simultaneously exchange information with the assistance of a cooperating relay node $\mathbf{R}$. Each terminal node $\mathbf{A}$ or node $\mathbf{B}$ acts as a source node as well as a destination

node. As the name suggests, the two-way relaying network takes advantage of the bidirectionality of radio channels to overcome the bandwidth inefficiency problem experienced in one-way relaying case. It is proven in [76] from the viewpoint of information theory that the spectral efficiency of two-way relaying system is significantly higher than that of one-way counterpart.

Recall the two-way communication system illustrated in Fig. 3.1. In general, existing two-way relaying protocols can be classified into two major categories based on the time slots needed to complete the information exchange process between two nodes.

The first approach is referred to as the conventional 'physical-layer' two-way relaying protocol. It is the simplest and most straightforward approach to exchange data between two terminals. A vivid illustration of this method is depicted in Fig. 3.2 below. During the first and second time slot, node $\mathbf{A}$ transmits to relay $\mathbf{R}$ and then $\mathbf{R}$ forwards the signal to node $\mathbf{B}$. Subsequently, node $\mathbf{B}$ sends the signal to relay $\mathbf{R}$ and $\mathbf{R}$ relays it to destination $\mathbf{A}$. Therefore, the total number of transmission slots is four.

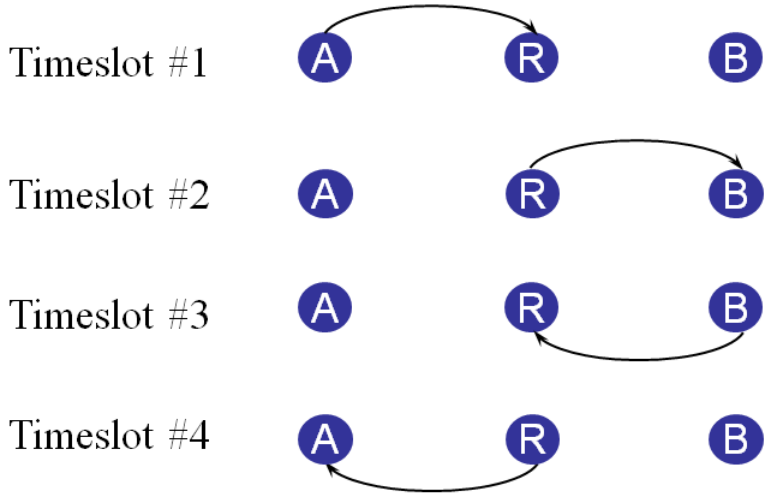

Figure 3.2: Illustration of a two-way cooperative communication system using four time slots.

The number of steps could be reduced to three if the network coding is employed to assist the information exchange between node $\mathbf{A}$ and node $\mathbf{B}$ as shown in Fig. 3.3. The first step is similar to the previous case. The difference is that the relay node $\mathbf{R}$ will keep the signal from node $\mathbf{A}$ in its buffer before it is ready to receive signals from other users. In the second time slot, node $\mathbf{B}$ transmits to relay $\mathbf{R}$ and $\mathbf{R}$ also save the data into its buffer. Next, $\mathbf{R}$ performs the network coding to calculate the bit-wise exclusive or of two data streams and then forwards the product to node $\mathbf{A}$ and $\mathbf{B}$ simultaneously. While the overall

time slots needed are reduced from four to three, the network throughput is increased by approximately 33%.

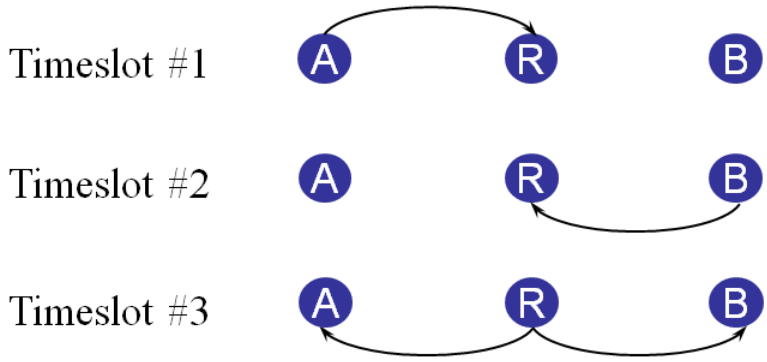

Figure 3.3: Illustration of a two-way cooperative communication system using three time slots.

3.2 Cooperative Space-Time Block Codes for Bidirectional Relaying

Recall that in the last subsection we discussed two kinds of existing two-way relaying strategies.

The second approach combining the network coding with two-way relaying effectively improves the system throughput and reduces the number of steps for exchanging information between two nodes. It is natural to ask the question that is it possible to do it more efficiently? We introduce the physical-layer network coding (PLNC) assisted two-way cooperative system in this subsection, which is capable of fulfilling the whole process within two time slots.

3.2.1 Physical-Layer Network Coding (PLNC)

Physical-layer network coding, first proposed in [77], is capable of transforming the superimposed signals directly into network-coded symbols without knowing the explicit data bits from two source nodes by exploiting the additive nature of EM waves. In brief,

as the name implied, the motivation of using PLNC is to perform the conventional network coding equivalently in physical layer (PHY). The spectral efficiency as well as the achievable channel capacity are significantly increased by deploying PLNC in the relaying protocol without additional power and any sacrifice in the bandwidth.

An example of PLNC assisted two-way cooperative system is illustrated in Fig. 3.4. During the first step, node **A** and node **B** transmit to relay **R** at the same time, relay **R** then employs PLNC to process the superimposed signal and sends the equivalent network-coded signal back to node **A** and node **B** simultaneously. Obviously, with the assistance of PLNC, the overall throughput is doubled when compared against the traditional two-way relaying protocol using four time slots.

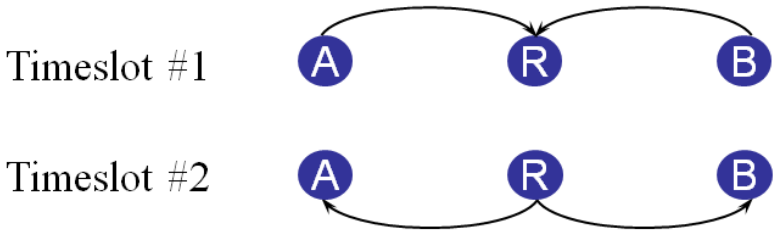

Figure 3.4: Illustration of a two-way cooperative communication system using two time slots.

The principle of PLNC is quite straightforward and can be briefly stated as follows. Imagine that the relaying user is located and fixed in the middle of terminal nodes T_1 and T_2. When T_1 and T_2 transmit BPSK symbols s_1, s_2 simultaneously, the received signal y in each relay is a superimposition of two BPSK signals having three constellation points: $\{-2, 0, +2\}$.

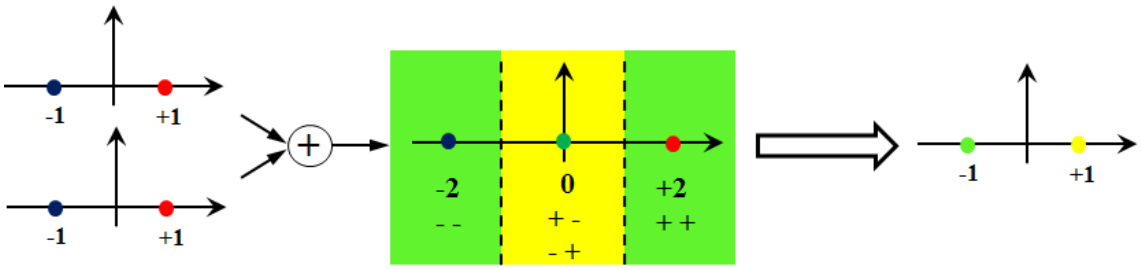

Figure 3.5: Principle of PLNC mapping with two BPSK signals.

Case 1: If $\{+1, +1\}$ are the transmitted symbols, then we have $\{+2\}$ in the relay.

Case 2: If the symbols from T_1, T_2 are {-1, -1}, then the received signal is {-2}.

Case 3 and 4: If the terminal nodes T_1, T_2 send {-1, +1} or {+1, -1}, the result of y is 0.

It is noticed that, in *case 1* and *case 2*, although the received symbols are different in these two cases, the exclusive or results of the transmitted symbols are identical, both equal to 0. Similarly, we could find in *case 3* and *case 4* that no matter T_1 and T_2 send $\{-1, +1\}$ or $\{+1, -1\}$, their exclusive or outcomes are both 1. To summarize, if the received symbol falls into the green area, the outcome of PLNC is bit 0. Otherwise, if symbols from received signal y belong to the yellow region, then the PLNC would give bit 1 as the network-coded symbol. Consequently, the network-coded symbols could be re-mapped in order to generate new BPSK symbols for the cooperating phase.

3.2.2 Design of Distributed STBC aided Two-way Relaying System

3.2.2.1 System Model

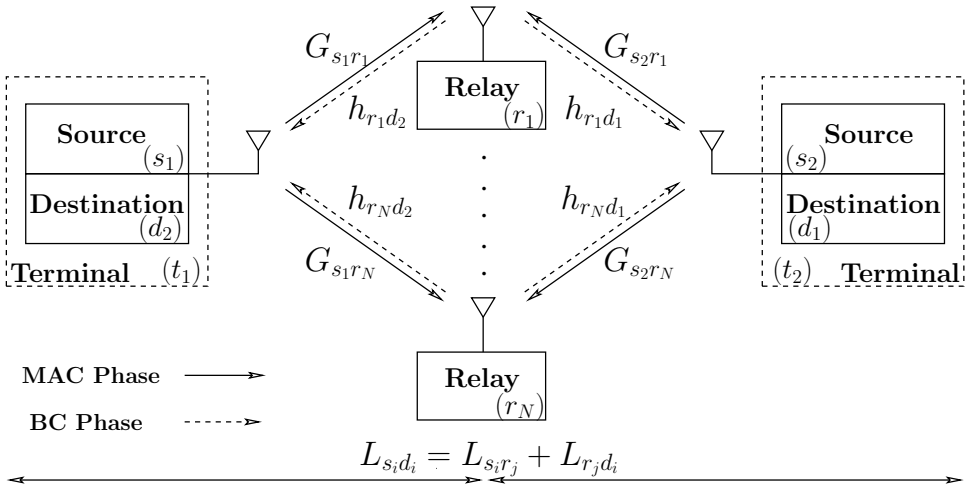

Figure 3.6: The symmetric structure of a typical multi-relay aided two-way cooperative communication system, where each terminal node is single-antenna aided and is serving as a source node as well as a destination node.

The schematic of the multi-relay aided two-way cooperative communication system is depicted in Fig. 3.6, where two terminal nodes (t_1, t_2), are capable of simultaneously exchanging information with the assistance of N parallel single-antenna aided cooperating relay nodes $(r_1, r_2, ..., r_N)$. Each terminal node basically consists of a co-located source node (s) and destination node (d) which share a single antenna. It is assumed that each

node operates in time-division half-duplex so that the source for the data stream transmitted from t_1 also serves as the destination for the signal flow emanating from t_2, and vice-versa.

Our proposed scheme is based on the assumption that the direct communication link between two terminal nodes t_1 and t_2 is unavailable, however the cooperating nodes have reliable radio connections with both terminal nodes. All propagation links in Fig. 3.6 are subject not only to long-term free-space path loss, but also to short-term frequency non-selective Rayleigh fading. If L_{ab} represents the geometrical distance between arbitrary nodes a and b, the path loss between them could be modelled as

$$P(ab) = K/L_{ab}^{\alpha} \,, \tag{3.1}$$

where K is a constant determined by the transmission environment while α is the path-loss exponent, which gives $\alpha = 2$ if a free-space path loss model is invoked. The geometrical-gain or path-gain [78] experienced by the channel between the ith source node and the jth relay node with respect to the source-to-destination link could be formulated as

$$G_{s_i r_j} = \left(\frac{L_{s_i d_i}}{L_{s_i r_j}} \right)^{\alpha} \,, \tag{3.2}$$

where $i = \{1, 2\}$, $j = \{1, 2, \ldots, N\}$.

Similarly, the geometrical-gain of the jth relay to the ith destination link with respect to the source-to-destination link could be computed as

$$G_{r_j d_i} = \left(\frac{L_{s_i d_i}}{L_{r_j d_i}} \right)^{\alpha} \,. \tag{3.3}$$

As illustrated in Fig. 3.6, the communication between t_1 and t_2 involves two stages, namely, the multiple access (MAC) phase and broadcast (BC) phase. Assume that the information bits at source node s_i are denoted by $\mathbf{x}_{s_i}$, which are modelled as uncorrelated uniformly distributed binary sequence vector $\mathbf{x}_{s_i} = \{x_{s_i,1}, x_{s_i,2}, \ldots\}$, $i = \{1, 2\}$. During the MAC phase, $\mathbf{x}_{s_i}$ is modulated into a frame of $\mathcal{M}$-ary PSK symbols $\mathbf{v}_{s_i}$ and simultaneously transmitted to N relay nodes. The received signal at the jth relay node is a superposition of the transmitted signals from two source nodes contaminated by the fading channel and noise, which could be formulated as

$$\mathbf{y}^{(r_j)} = \sum_{i=1}^{2} \left(\sqrt{G_{s_i r_j}} \mathbf{h}_{s_i r_j} \mathbf{v}_{s_i} \right) + \mathbf{n}^{(r_j)} \,, \tag{3.4}$$

where $j \in \{1, 2, \ldots, N\}$. Furthermore, the complex-valued vector $\mathbf{h}_{s_i r_j}$ denotes the quasi-static frequency-flat Rayleigh fading coefficients of the communication link between the ith source node and the jth relay node which remain constant over two symbol intervals, while the complex-valued vector $\mathbf{n}^{(r_j)}$ is the additive white Gaussian noise (AWGN) introduced in the jth relay node with zero mean and variance of $N_0/2$ per dimension.

It is assumed that the DF relaying strategy is incorporated in our system. Therefore, during the BC stage, a CRC-based selective relaying algorithm is employed in each relay node to eliminate error propagation. More specifically, only correctly estimated bits are re-encoded and transmitted to the destination nodes. A frame of virtual STBC codewords $\mathbf{w}^{(r_j)}$ are constructed by N cooperating relay nodes in a distributed fashion, yielding

$$\mathbf{w}^{(r_j)} = [w^{(r_1)}, w^{(r_2)}, \ldots, w^{(r_N)}]^T , \tag{3.5}$$

where the notation $w^{(r_j)}$ represents the distributed STBC symbols contributed from the jth relay node after the PLNC mapping. The received signal at the ith destination node is given by

$$\mathbf{y}^{(d_i)} = \sum_{j=1}^{N} \left(\sqrt{G_{r_j d_i}} \mathbf{h}_{r_j d_i} \mathbf{w}^{(r_j)} \right) + \mathbf{n}^{(d_i)} , \tag{3.6}$$

where $i \in \{1, 2\}$. A similar vector $\mathbf{h}_{r_j d_i}$ denotes the complex-valued Rayleigh block fading coefficients of the channel between the jth relay node and the ith destination node, while the complex-valued vector $\mathbf{n}^{(d_i)}$ is the AWGN induced in the ith destination node having zero mean and variance of $N_0/2$ per dimension.

At the destination node, a serially-concatenated conventional STBC decoder, PSK demapper and PLNC demapper are invoked to perform the final decision and recover the information transmitted from the source nodes. Note that we assume the transmit power of each node is normalized to unity. Hence, each relay node transmits at $1/N$ of the overall power to ensure that $\sum_{j=1}^{N} |\mathbf{w}^{(r_j)}|^2 = 1$ for the purpose of offering a fair comparison.

3.2.2.2 Principle of CRC-based Selective Relaying

Fig. 3.7 illustrates the architecture of source and relay nodes for the proposed CRC-based relay selection aided distributed STBC scheme. For ease of analysis, in this subsection, we consider a two-way cooperative STBC system with $N = 2$ relay nodes, which is capable of achieving full diversity order with a relatively low complexity. Also, we assume

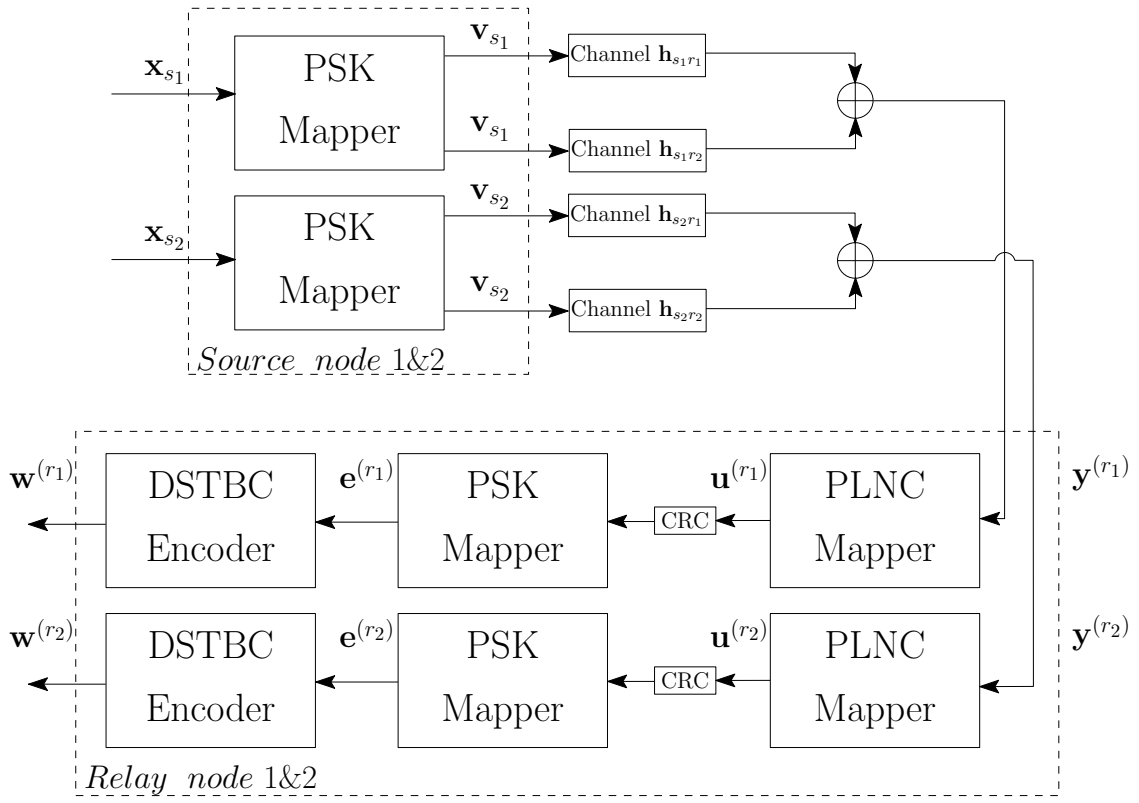

Figure 3.7: The schematic of the source and relay nodes for the proposed novel PLNC aided distributed STBC scheme with selection relaying strategy, where two distributed source and relay nodes are drawn in parallel for simplicity.

binary phase shift keying (BPSK) is employed as the modulation scheme in all source and relay nodes. The cooperating users are located mid way between t_1 and t_2, so that

$$L_{s_i r_j} = L_{r_j d_i} = \frac{L_{s_i d_i}}{2} \, . \tag{3.7}$$

Hence, according to Eq. (3.2) and Eq. (3.3), we have

$$G_{s_i r_j} = G_{r_j d_i} = 2^2 = 4 \, . \tag{3.8}$$

As discussed earlier, the signal received by each relay node is the superposition of two noise-corrupted BPSK-modulated signals simultaneously transmitted from s_1 and s_2, which could be formulated as Eq. (3.4). In order to make sure the destination nodes can successfully extract the useful information, the received superimposed signal has to be transformed to network-coded symbols which are then transmitted by the relay during the broadcast phase. The most straightforward method is that each relay node detects and recovers the explicit information bits $\hat{\mathbf{x}}_{s1}^{(r_j)}$ and $\hat{\mathbf{x}}_{s2}^{(r_j)}$ from the superimposed signal individually and then performs bit-wise exclusive or (XOR) arithmetic over the estimated data bits to acquire the network-coded symbol sequence. At the jth relay node, if $\hat{\mathbf{x}}_{s_i}^{(r_j)}$ is the estimate of information bits transmitted from the ith source node, the result of network coding could be expressed as

$$\mathbf{u}^{(r_j)} = \hat{\mathbf{x}}_{s_1}^{(r_j)} \oplus \hat{\mathbf{x}}_{s_2}^{(r_j)} \, , \tag{3.9}$$

where $\oplus$ represents the addition operation in the Galois field GF(2^m), which can be simplified to the exclusive or (XOR) arithmetic when $m = 1$.

It is clear that the responsibility of a relay node is to facilitate the final decision at the destination and make sure that the information of interest could be extracted correctly, and hence to fully detect the received signal at the relay node is unnecessary and could make proposed scheme inferior in terms of spectral efficiency. The unique nature of PLNC makes it possible to transform the estimate of two superimposed BPSK-modulated signals directly to the equivalent network-coded symbols shown in Eq. (3.9) instead of detecting the information separately. In other words, the PLNC mapping is fulfilled within two time slots, the reduction of intermediate processing steps could potentially lead to significant spectral efficiency gain and energy saving. For a BPSK-modulated symbol, there are two possible phasor combinations, namely, $\mathbf{v}_{s_i} \in \{-1, +1\}$, where $i = \{1, 2\}$. Therefore, the constellation of the summation of two BPSK symbols could be described as $\mathbf{z} = (\mathbf{v}_{s_1} + \mathbf{v}_{s_2}) \in \chi$, where $\chi = \{-2, 0, +2\}$. If the superposition of two BPSK symbols is denoted by $\mathbf{z}^{(r_j)}$ at the jth relay node, then the estimate of $\mathbf{z}^{(r_j)}$ is computed as

$$\hat{\mathbf{z}}^{(r_j)} = \arg \min_{\mathbf{z} \in \chi} \left\| \mathbf{y}^{(r_j)} - \sum_{i=1}^{2} \left(\sqrt{G_{s_i r_j}} \mathbf{h}_{s_i r_j} \mathbf{v}_{s_i} \right) \right\|^2 , \tag{3.10}$$

where $j \in \{1, 2\}$ and $||(\cdot)||$ is the Frobenius norm of variable $(\cdot)$.

After the summation of two BPSK-modulated signals is estimated, PLNC is applied to obtain the network-coded bits $\mathbf{u}^{(r_j)}$ as follows

$$\mathbf{u}^{(r_j)} = \mathrm{mod}\left(\frac{\hat{\mathbf{z}}^{(r_j)}}{2} - 1, 2\right) = \hat{\mathbf{x}}_{s1}^{(r_j)} \oplus \hat{\mathbf{x}}_{s2}^{(r_j)}, \tag{3.11}$$

where $\mathrm{mod}\ (a, b)$ represents the modulus after division between a and b. For example, if we assume $\hat{\mathbf{z}}^{(r_j)} = \{-2, 0, +2\}$, the network-coded bits $\mathbf{u}^{(r_j)}$ could be calculated based on Eq. (3.11), which gives $\mathbf{u}^{(r_j)} = \{0, 1, 0\}$.

In view of the potential error propagation introduced in the decoding and re-encoding process, an error-detecting code based selective relaying or opportunistic relaying strategy is deployed in each relay node. Since CRC has been widely implemented in many commercial mobile networks, it would not significantly decrease the data rate or exert additional complexity on the system design. The construction of a robust error-detecting code, such as CRC code, primarily lies in the selection of an appropriate generator polynomial which should be designed to maximize the error detecting capabilities. We use the CRC-8 algorithm, a well-known and commonly used polynomial with excellent error detecting capability which has been adopted in the WCDMA cellular network [79]. The generator polynomial of CRC-8 algorithm is given by $\Gamma = [x^8 + x^7 + x^4 + x^3 + x + 1]$, which corresponds to the 9-bit string $\{110011011\}$.

In the source nodes, the 9-bit CRC algorithm is carried out automatically to compute the CRCs of each frame of information bits before transmission. The PLNC-coded data stream could be treated as the XOR combination (modulo-2 sum) of two estimated information sequences transmitted from both source nodes.

The linearity of the CRC [80] implies that if two sequences pass the same CRC, their modulo-2 sum will also pass. Moreover if one is in error, or both are in error but in different positions, the validation will fail. Hence if the CRCs computed from the PLNC-coded signal perfectly match that acquired by performing the XOR operation on the CRCs provided by the source nodes, the relay nodes will map $\mathbf{u}^{(r_j)}$ to BPSK-modulated symbols $\mathbf{e}^{(r_j)}$ and feed $\mathbf{e}^{(r_j)}$ to the distributed STBC encoder. On the other hand, if those two values are not identical, the relay node is instructed to maintain silence during that transmission period. The re-modulated BPSK symbols in $\mathbf{e}^{(r_j)}$ are then grouped into pairs in order to construct distributed STBC codewords in the next step. One of the most distinct characteristics differentiating the distributed STBC from conventional STBC using co-located antennas is that each column of the distributed STBC codewords is constituted by a different relaying user and is transmitted through an independent antenna.

As portrayed in Fig. 3.7, two cooperating relay nodes act like a twin-antenna aided MIMO transmitter, although both of them are equipped with a single antenna. The design of the distributed STBC encoder is based on the Alamouti scheme with two transmit antennas and one receive antenna, which could be described as follows at time index T

$$\mathcal{G}_{\mathbf{2}} = \begin{bmatrix} g_1 & -g_2^* \\ g_2 & g_1^* \end{bmatrix} = \begin{bmatrix} e^{(r_1)}|_T & -e^{(r_2)^*}|_T \\ e^{(r_1)}|_{T+1} & e^{(r_2)^*}|_{T+1} \end{bmatrix} . \tag{3.12}$$

In the destination node shown in Fig. 3.8, a conventional Alamouti STBC decoder as well as a BPSK demapper are employed to recover the PLNC-coded symbols $\hat{\mathbf{u}}^{(r_j)}$. Then each destination node could extract the useful information transmitted by the corresponding source node with the assistance of their local information as follows

$$\hat{\mathbf{x}}_{s_1} = \hat{\mathbf{u}}^{(r_j)} \oplus \mathbf{x}_{s_2} . \tag{3.13}$$

Similarly, we have

$$\hat{\mathbf{x}}_{s_2} = \hat{\mathbf{u}}^{(r_j)} \oplus \mathbf{x}_{s_1} , \tag{3.14}$$

where $j = 1$ or 2.

In the event that both relay nodes fail to transmit in the BC phase, the destination nodes will make arbitrary assumptions about that pair of transmitted bits. In our simulations $\{0, 0\}$ is assumed. Note that the choice will not influence the end-to-end BER performance significantly since we assume the information sources in t_1 and t_2 are equiprobable.

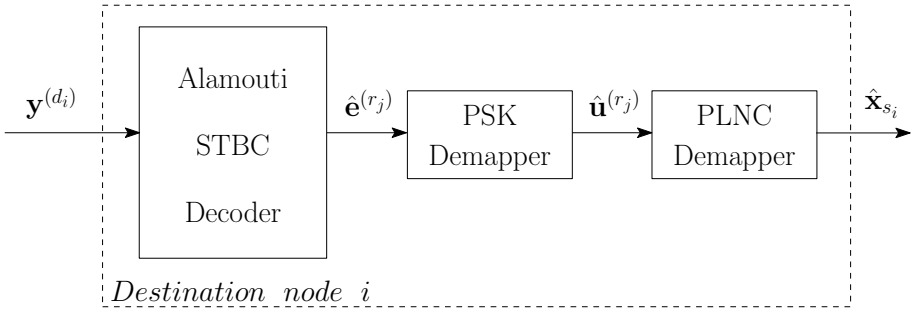

Figure 3.8: The schematic of the ith destination node for the proposed novel PLNC aided distributed STBC scheme with selection relaying strategy when both relay nodes can correctly decode the signals transmitted from two source nodes, where $i, j \in \{1, 2\}$.

3.2.3 Performance Results, Comparison and Discussion

In this subsection, we evaluate and analyze the BER performance of our proposed two-way selection relaying assisted distributed STBC scheme. It is confirmed by the Monte Carlo simulation results that our proposed system is able to achieve full diversity order and outperform the non-cooperative counterpart when communicating over two-way relay channel. A simple CRC-based selection relaying strategy is proposed to mitigate the potential error propagation so that deployment of any sophisticated forward error correction codes in the source nodes is no longer necessary. The transmission is assumed over bidirectional Rayleigh fading channels, where the magnitude of the fading envelope remains near-constant within one block but varies from block to block. The frame length involved in all simulations is fixed at 2×10^6 BPSK-modulated distributed STBC symbols. Detailed simulation configuration is listed in Tab. 3.1.

Table 3.1: Simulation parameters for the following BER performance evaluation.

Simulation Parameters	
Parameters	**Values**
Modulation Scheme	BPSK
Path-gain of Source-to-Relay Link	4 or 1.7778 or 16
Path-gain of Relay-to-Destination Link	4 or 1.7778 or 16
CRC Generator Polynomial	$[x^8 + x^7 + x^4 + x^3 + x + 1]$
Maximum Length of Frame	2000000
Eb/N0 Range	0–40 dB
Channel Type	Quasi-static Rayleigh Fading Channel

We first consider the scenario illustrated in Fig. 3.6, where $N = 2$ relay nodes are located and fixed in the mid-way of the source-to-destination link. Hence, the geometrical-gain for the source-to-relay link as well as the relay-to-destination link both equal to 4. As we can see from Fig. 3.9, the BER of the distributed STBC with selection relaying (DSTBC-SR) shares the same slope with the conventional Alamouti STBC scheme having two co-located transmit antennas and a single receive antenna, which is chosen as the benchmark. Clearly, our proposed DSTBC-SR scheme is capable of achieving second order diversity with the aid of a simple CRC-based selection relaying algorithm.

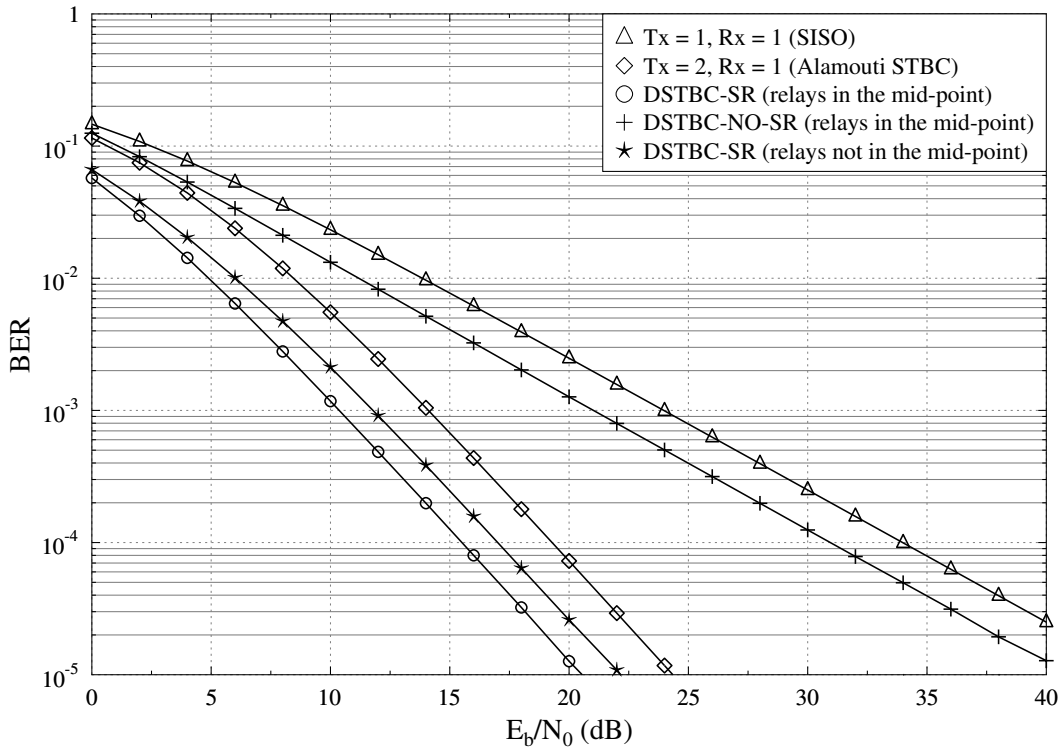

Figure 3.9: BER versus E_b/N_0 performance of the proposed novel PLNC aided distributed STBC scheme with selection relaying strategy when communicating over Rayleigh block fading channel, where the frame length is 2×10^6.

Furthermore, the DSTBC-SR scheme outperforms the non-cooperative benchmark by approximately 4.0 dB at BER = 10^{-4}. This performance gain demonstrates that the CRC-based selection relaying protocol is a low-complexity but efficient solution to preserving the orthogonality of the distributed space-time coded signals when transmitted by a group of cooperating relay nodes.

Fig. 3.9 also shows that, even though the cooperation stage is assisted by multiple relay nodes, the performance of distributed STBC scheme without an appropriately designed selection relaying strategy (DSTBC-NO-SR) is similar to that of a single antenna system providing only first order diversity. This detrimental effect generally results from error propagation in the relay nodes, which degrades the BER performance by more than 11.0 dB in comparison to its counterpart employing a selection relaying protocol at BER = 10^{-3}.

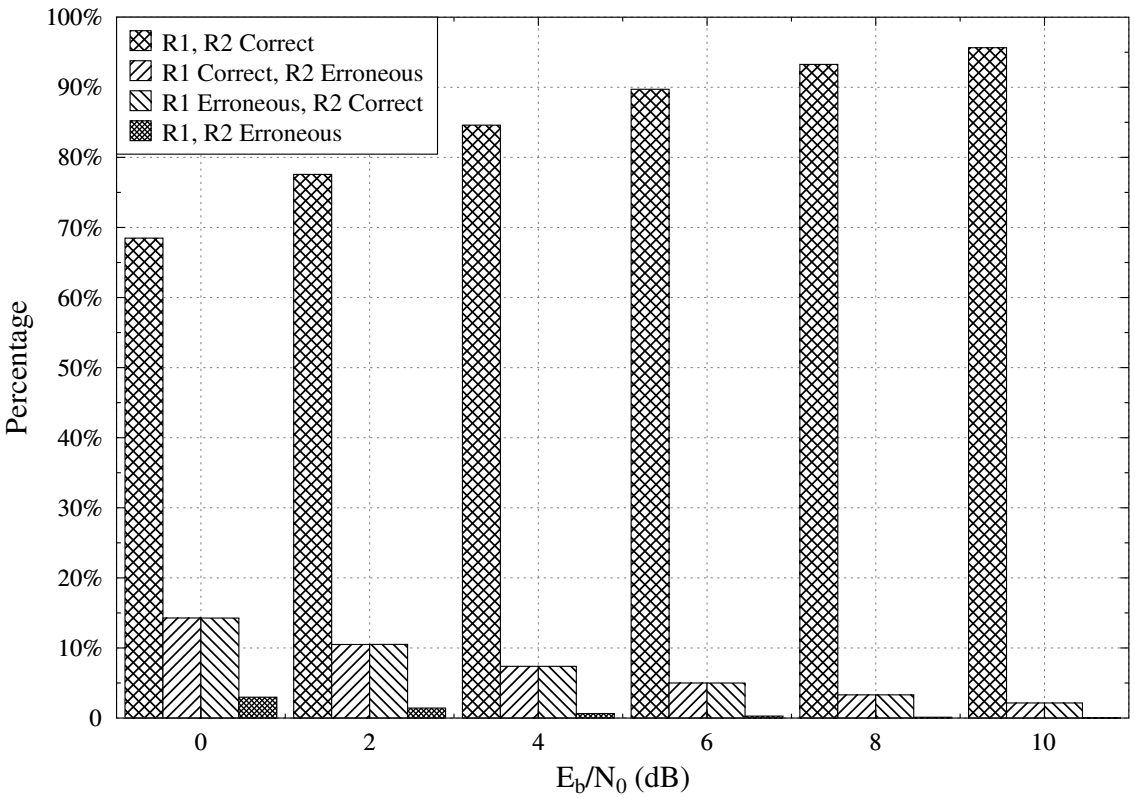

Figure 3.10: Bar chart for the percentage of correctly and erroneously decoded bits in two relay nodes at different E_b/N_0, where the total number of bits is fixed to 2×10^6.

Fig. 3.10 demonstrates the percentage of correctly and erroneously decoded bits in two relay nodes when the E_b/N_0 is increasing from 0.0 dB to 10.0 dB. For $N = 2$ relay nodes, four different relaying scenarios could be generalized as follows:

1) Relay 1 (R1) and Relay 2 (R2) both decode correctly;
2) R1 decodes correctly while R2 decodes erroneously;
3) R1 decodes erroneously while R2 decodes correctly;
4) Neither R1 nor R2 decode correctly.

As shown in Fig. 3.10, more than 68% of the total bits transmitted from the source nodes can be decoded correctly using PLNC in both relay nodes even when the $E_b/N_0 = 0.0$ dB, while the percentage soars to almost 100% when the E_b/N_0 grows to 10.0 dB. On the other hand, the percentage of erroneously decoded bits in both relay nodes is less than 5% in the worst case when the $E_b/N_0 = 0.0$ dB. In other words, more than 68% of the PLNC-coded bits transmitted from two relay nodes could be used to construct valid distributed Alamouti space-time codewords. There is a higher probability (more than 95%) that at least one of the two relay nodes will be active and help other users to forward their information.

We also investigate an asymmetric system architecture, where relay node r_1 moves towards destination node d_1, while the other relay r_2 moves towards d_2. We assume the distance between each relay node and the nearest destination node is one quarter of that between two terminal nodes t_1 and t_2. In other words, we could define $L_{r_1d_1} = L_{r_2d_2} = L_{t_1t_2}/4$. Then, the geometrical-gain experienced by each mobile channel could be computed based on Eqs. (3.2), (3.3), yielding:

$$G_{s_1r_1} = G_{s_2r_2} = G_{r_1d_2} = G_{r_2d_1} = (1/0.75)^2 = 1.7778\ . \tag{3.15}$$

Similarly, we have:

$$G_{s_2r_1} = G_{s_1r_2} = G_{r_1d_1} = G_{r_2d_2} = (1/0.25)^2 = 16\ . \tag{3.16}$$

It is shown in Fig. 3.9 that the DSTBC-SR scheme with new relay locations is also capable of achieving second order transmit diversity, although the performance is approximately 1.0 dB worse than in the previous scenario. During the MAC as well as the BC stages, although half of the communication links are improved, having a geometrical-gain of 16; the remaining half, having a gain of 1.7778, are unable to provide reliable transmission. This leads to the decoding performance in one relay node being better than that in the other. As discussed above, a valid space-time codeword could be constructed only when both of the relay nodes achieve error-free decoding. Hence, the BER performance of the new case slightly degrades by about 1.0 dB compared with the DSTBC-SR with centrally located relay nodes.

3.3 Numerical Analysis of Distributed STBC aided Two-way Relaying System

After the discussion of system model and principle of relay selection assisted distributed STBC over the bidirectional relay channel in subsection 3.2.2.1 and subsection 3.2.2.2, in this subsection our focus is shifted to the analytical evaluation of the proposed scheme. Compared with the traditional probability distribution function (PDF) based approach, it is more convenient to analyze and solve the theoretical error performance by utilizing the moment generating function (MGF) method. It provides a unified way to measure the bit error probability (BEP) or pairwise error probability (PEP) of a specific system communicating over diverse fading channels such as Rayleigh fading, Nakagami-n (Rician) and Nakagami-m. This subsection commences from the introduction of mathematical preliminaries, and then concentrates on the error probability analysis of the average end-to-end BEP performance based on a bound approach, where tight upper and lower bounds are derived. After that, the analysis is extended to obtain the exact expression of the average end-to-end BEP.

3.3.1 Mathematical Preliminaries

In general, average signal-to-noise ratio and average bit error probability are widely used to reflect the performance of a specific system. The average SNR measured at the output of the receiver is able to give an immediate reflection of the quality of a communication system. If it is assumed that the instantaneous SNR is denoted by γ, according to [16], the average SNR can be defined as

$$\overline{\gamma} \triangleq \int_0^\infty \gamma p_\gamma(\gamma)\,\mathrm{d}\gamma\,, \tag{3.17}$$

where $p_\gamma(\gamma)$ represents the probability distribution function of γ.

Note that the term 'average' means statistically average γ over the probability distribution of the fading.

The other criterion is the average BEP, which is the most commonly used in the literature to reveal the nature of a radio communication system. Average BEP can be computed by using the following formula given in [16]

$$P_b(E) \triangleq \int_0^\infty P_b(E|\gamma)p_\gamma(\gamma)\,\mathrm{d}\gamma\,, \tag{3.18}$$

where $P_b(E|\gamma)$ is the conditional BEP of the received signal, which, take PSK modulation for example, is written as Q-function. Therefore, the evaluation of average BEP over fading channel now becomes averaging the Q-function over the probability distribution of fading.

The Gaussian Q-function is defined in the form of a semi-infinite integral as shown in [16]

$$Q(x) \triangleq \int_x^\infty \frac{1}{\sqrt{2\pi}} \exp\left(-\frac{y^2}{2}\right) \mathrm{d}y \,. \tag{3.19}$$

The difficulty of evaluating the average BEP primarily lies in the fact that the conditional BEP is generally a non-linear function of the instantaneous SNR γ. Furthermore, from the expression of the Q-function, we note that the argument of the function is in the lower limit of the integral, which poses analytical difficulties when averaging statistically over its probability distribution. As a solution, Craig's Q-function [16] offers an alternative.

$$Q(x) = \frac{1}{\pi} \int_0^{\frac{\pi}{2}} \exp\left(-\frac{x^2}{2\sin^2\theta}\right) \mathrm{d}\theta \,. \tag{3.20}$$

Now the expression of this Q-function is more desirable because the argument of this function is in neither the upper nor lower limits of the integral and the integrand is an elementary function. More importantly, the upper and lower limits are finite. As a result, the calculation of average BEP can be significantly simplified as

$$\begin{aligned} P_b(E) &= \int_0^\infty Q(a\sqrt{\gamma}) p_\gamma(\gamma)\, \mathrm{d}\gamma \\ &= \int_0^\infty \frac{1}{\pi} \int_0^{\frac{\pi}{2}} \exp\left(-\frac{a^2\gamma}{2\sin^2\theta}\right) \mathrm{d}\theta\, p_\gamma(\gamma)\, \mathrm{d}\gamma \\ &= \frac{1}{\pi} \int_0^{\frac{\pi}{2}} \left[\int_0^\infty \exp\left(-\frac{a^2\gamma}{2\sin^2\theta}\right) p_\gamma(\gamma)\, \mathrm{d}\gamma\right] \mathrm{d}\theta \\ &= \frac{1}{\pi} \int_0^{\frac{\pi}{2}} M_\gamma\left(-\frac{a^2}{2\sin^2\theta}\right) \mathrm{d}\theta \,, \end{aligned} \tag{3.21}$$

where $M_\gamma(s) = \int_0^\infty e^{s\gamma} p_\gamma(\gamma)\, \mathrm{d}\gamma$ denotes the moment generating function of the instantaneous SNR, which only depends on the fading channel model , whereas the scalar a is a constant depending on the modulation scheme.

If compare the MGF of the instantaneous SNR γ with the definition of Laplace transform

$$\mathscr{L}\{f(t)\} = \int_0^\infty e^{-st} f(t)\, \mathrm{d}t \,, \tag{3.22}$$

we can interestingly find that the MGF of the instantaneous SNR γ is the Laplace transform of $P_b(E|\gamma)$, but reversing the sign of exponent, namely

$$\mathscr{L}\{p_\gamma(\gamma)\} = M_\gamma(-s) \,. \tag{3.23}$$

3.3.2 Upper and Lower Bound of Average End-to-End BEP for Proposed Distributed STBC System

The average end-to-end error probability measured at the output of the receiver, is defined as the average of the instantaneous end-to-end BEP over all possible random channel coefficients. Mathematically, if P_{EtoE} denotes the instantaneous end-to-end BEP, the desired average end-to-end error probability $\overline{P_{EtoE}}$ is computed as the statistical expectation of the instantaneous end-to-end BEP, namely,

$$\overline{P_{EtoE}} = \mathbb{E}\left[P_{EtoE}\right] \ . \tag{3.24}$$

In addition, recall the structure of cooperative STBC scheme depicted in subsection 3.2.2.1. The instantaneous end-to-end BEP P_{EtoE} represents the average of the instantaneous error probabilities at terminal node t_1 and t_2 denoted as $P_{EtoE}^{t_i}$, this yields

$$\begin{aligned} P_{EtoE} &= \mathbb{E}\left[P_{EtoE}^{t_i}\right], \qquad i = 1, 2 \\ &= \frac{1}{2}\sum_{i=1}^{2} P_{EtoE}^{t_i} \ . \end{aligned} \tag{3.25}$$

Furthermore, as mentioned in subsection 3.2.2.2, the transmissions of the re-encoded signals in the BC phase involve four different opportunistic relaying scenarios, corresponding to the results of the CRC verification. Hence the instantaneous end-to-end error probability at terminal node t_i $(i = 1, 2)$ can be formulated as follows

$$\begin{aligned} P_{EtoE}^{t_i} = &\underbrace{P_{DSTBC}^{t_i}(1 - P_{MAC,r_1})(1 - P_{MAC,r_2})}_{r_1,\, r_2 \text{ both decode correctly}} + \underbrace{P_{BPSK}^{r_1 \to t_i}(1 - P_{MAC,r_1})P_{MAC,r_2}}_{r_1 \text{ decodes correctly, } r_2 \text{ decodes erroneously}} \\ &+ \underbrace{P_{BPSK}^{r_2 \to t_i} P_{MAC,r_1}(1 - P_{MAC,r_2})}_{r_1 \text{ decodes erroneously, } r_2 \text{ decodes correctly}} + \underbrace{\frac{1}{2} P_{MAC,r_1} P_{MAC,r_2}}_{r_1,\, r_2 \text{ both decode erroneously}} \ , \end{aligned} \tag{3.26}$$

where the notations used in Eq. (3.26) are summarized as follows:

- P_{MAC,r_1} and P_{MAC,r_2} are the instantaneous error probabilities of the received signals at relay node r_1 and r_2 during the MAC phase, respectively.
- $P_{DSTBC}^{t_i}$ represents the instantaneous BEP of the distributed Alamouti STBC received at terminal node t_i $(i = 1, 2)$ during the BC phase, which corresponds to the case when both relay nodes r_1 and r_2 successfully decode the signal. In this case, both relay nodes are capable of transmitting and forwarding the re-encoded signals to destination nodes. Hence, the virtual distributed Alamouti STBC frame is jointly constructed.

- $P_{BPSK}^{r_1 \to t_i}$ and $P_{BPSK}^{r_2 \to t_i}$ denote the instantaneous BEP of the BPSK signals received at terminal node t_i ($i = 1, 2$) during the BC phase. This corresponds to the case when either relay node r_1 or r_2 successfully decode the signal; therefore, only one relay node is able to forward the re-encoded signal to destination nodes and the received signal at the destination seems like a BPSK-modulated signal while the other relay node stays silent.

- For the case when none of the two relay nodes achieves error-free decoding, the transmission from the relay is halted during the BC stage and the destination nodes assume (as discussed above) that the pair of information bits contained in the missing packet is $\{0, 0\}$. Therefore, the probability of making an erroneous judgment for each bit is 0.5.

If z represents the exclusive or combination of the information bits from two source nodes, where $z = x_{s_1} \oplus x_{s_2}$, the definition of the instantaneous BEP of the MAC phase at relay node r_1 can be described as the probability that symbols from $u^{(r_1)}$ are not identical to those transmitted in z for given complex-valued fading channel coefficients $h_{s_1 r_1}$ and $h_{s_2 r_1}$. Thus we have

$$P_{MAC,r_1} \triangleq \Pr\left[z \neq u^{(r_1)} | h_{s_1 r_1}, h_{s_2 r_1}\right] , \tag{3.27}$$

where $h_{s_i r_j}$ is the complex-valued fading coefficients of the channel between s_i and r_j, $i = j = 1, 2$.

Similarly, the instantaneous BEP of the MAC phase at relay node r_2 is given by

$$P_{MAC,r_2} \triangleq \Pr\left[z \neq u^{(r_2)} | h_{s_1 r_2}, h_{s_2 r_2}\right] . \tag{3.28}$$

According to the analysis in [81], we know that P_{MAC,r_i} is upper bounded by $P_{MAC,r_i}^{(U)}$ which is given by the sum of the instantaneous BEP of the propagation paths from two source nodes to relay nodes; while it is lower bounded by $P_{MAC,r_i}^{(L)}$ which is determined by the instantaneous BEP of the weaker link ($i = 1, 2$). Since simple BPSK modulation is used in source and relay nodes, the tight upper bound and tight lower bound can be expressed as

Tight Upper Bound:

$$P_{MAC,r_1} < P_{MAC,r_1}^{(U)} = Q\left(\sqrt{2\gamma_{s_1 r_1}}\right) + Q\left(\sqrt{2\gamma_{s_2 r_1}}\right) , \tag{3.29}$$

$$P_{MAC,r_2} < P_{MAC,r_2}^{(U)} = Q\left(\sqrt{2\gamma_{s_1 r_2}}\right) + Q\left(\sqrt{2\gamma_{s_2 r_2}}\right) , \tag{3.30}$$

Tight Lower Bound:

$$P_{MAC,r_1} > P^{(L)}_{MAC,r_1} = Q\left(\sqrt{2\min[\gamma_{s_1r_1}, \gamma_{s_2r_1}]}\right) , \tag{3.31}$$

$$P_{MAC,r_2} > P^{(L)}_{MAC,r_2} = Q\left(\sqrt{2\min[\gamma_{s_1r_2}, \gamma_{s_2r_2}]}\right) , \tag{3.32}$$

where $\gamma_{s_ir_j} = G_{s_ir_j}|h_{s_ir_j}|^2 E_{s_i}/\sigma^2$ is the linear signal-to-noise ratio (SNR) measured at the transmitter when source node s_i is communicating with relay node r_j. Furthermore, E_{s_i} denotes the transmit power which is normalized to unity, while σ^2 is the variance of the AWGN, $i = j = 1, 2$.

Therefore, Eq. (3.26) can now be re-written and the average end-to-end error probability of the novel bidirectional relaying aided distributed STBC system is upper bounded and lower bounded by

$$\begin{aligned}\overline{P^{(U)}_{EtoE}} = \mathbb{E}\Bigg\{\frac{1}{2}\Bigg[&\overbrace{\left(1 - P^{(L)}_{MAC,r_1}\right)\left(1 - P^{(L)}_{MAC,r_2}\right)\left(P^{t_1}_{DSTBC} + P^{t_2}_{DSTBC}\right)}^{\text{Part I}} \\ &+ \underbrace{\left(1 - P^{(L)}_{MAC,r_1}\right) P^{(U)}_{MAC,r_2}\left(P^{r_1\to t_1}_{BPSK} + P^{r_1\to t_2}_{BPSK}\right)}_{\text{Part II}} \\ &+ \underbrace{P^{(U)}_{MAC,r_1}\left(1 - P^{(L)}_{MAC,r_2}\right)\left(P^{r_2\to t_1}_{BPSK} + P^{r_2\to t_2}_{BPSK}\right)}_{\text{Part III}} + \underbrace{P^{(U)}_{MAC,r_1} P^{(U)}_{MAC,r_2}}_{\text{Part IV}}\Bigg]\Bigg\} ,\end{aligned} \tag{3.33}$$

$$\begin{aligned}\overline{P^{(L)}_{EtoE}} = \mathbb{E}\Bigg\{\frac{1}{2}\Bigg[&\overbrace{\left(1 - P^{(U)}_{MAC,r_1}\right)\left(1 - P^{(U)}_{MAC,r_2}\right)\left(P^{t_1}_{DSTBC} + P^{t_2}_{DSTBC}\right)}^{\text{Part I}} \\ &+ \underbrace{\left(1 - P^{(U)}_{MAC,r_1}\right) P^{(L)}_{MAC,r_2}\left(P^{r_1\to t_1}_{BPSK} + P^{r_1\to t_2}_{BPSK}\right)}_{\text{Part II}} \\ &+ \underbrace{P^{(L)}_{MAC,r_1}\left(1 - P^{(U)}_{MAC,r_2}\right)\left(P^{r_2\to t_1}_{BPSK} + P^{r_2\to t_2}_{BPSK}\right)}_{\text{Part III}} + \underbrace{P^{(L)}_{MAC,r_1} P^{(L)}_{MAC,r_2}}_{\text{Part IV}}\Bigg]\Bigg\} .\end{aligned} \tag{3.34}$$

Next, we expand Eq. (3.33) and Eq. (3.34), then solve the expectations term by term due to the linearity of the integrals. The final expression of the average end-to-end BEP can

be obtained by summing up all individual terms. The detailed derivation is provided in Appendix A.

$$\begin{aligned}\overline{P_{EtoE}^{(U)}} = &\frac{1}{4}\left(\frac{1-\lambda}{2}\right)^2(\lambda+2)\,\Gamma(\overline{\Psi}_2)\left[1+\Gamma(\overline{\Psi}_1)\right] \\ &+\frac{1}{8}\left[2-\Gamma(\overline{\gamma}_{s_1r_2})-\Gamma(\overline{\gamma}_{s_2r_2})\right]\left[1-\Gamma(\overline{\gamma}_{r_1d_1})\right]\left[1+\Gamma(\overline{\Psi}_1)\right] \\ &+\frac{1}{8}\left[2-\Gamma(\overline{\gamma}_{s_1r_1})-\Gamma(\overline{\gamma}_{s_2r_1})\right]\Bigg\{\left[1-\Gamma(\overline{\gamma}_{r_2d_1})\right]\left[1+\Gamma(\overline{\Psi}_2)\right] \\ &+\left[1-\frac{1}{2}\Gamma(\overline{\gamma}_{s_1r_2})-\frac{1}{2}\Gamma(\overline{\gamma}_{s_2r_2})\right]\Bigg\}, \end{aligned} \tag{3.35}$$

$$\begin{aligned}\overline{P_{EtoE}^{(L)}} = &\frac{1}{2}\left(\frac{1-\lambda}{2}\right)^2(\lambda+2)\Big\{\Gamma(\overline{\gamma}_{s_1r_1})+\Gamma(\overline{\gamma}_{s_1r_2})+\Gamma(\overline{\gamma}_{s_2r_1})+\Gamma(\overline{\gamma}_{s_2r_2}) \\ &+\frac{1}{2}\left[2-\Gamma(\overline{\gamma}_{s_1r_1})-\Gamma(\overline{\gamma}_{s_1r_2})\right]\left[2-\Gamma(\overline{\gamma}_{s_2r_1})-\Gamma(\overline{\gamma}_{s_2r_2})\right]-2\Big\} \\ &+\frac{1}{8}\left[\Gamma(\overline{\gamma}_{s_1r_1})+\Gamma(\overline{\gamma}_{s_2r_1})\right]\Big\{\left[1-\Gamma(\overline{\Psi}_1)\right]\left[1-\Gamma(\overline{\gamma}_{r_2d_1})\right]+\left[1-\Gamma(\overline{\Psi}_2)\right]\left[1-\Gamma(\overline{\gamma}_{r_1d_1})\right]\Big\} \\ &+\frac{1}{16}\left[1-\Gamma(\overline{\Psi}_1)\right]\left[1-\Gamma(\overline{\Psi}_2)\right], \end{aligned} \tag{3.36}$$

where $\Gamma(a)$ is defined as $\sqrt{\frac{a}{1+a}}$ and $\lambda = \sqrt{\frac{\overline{\gamma}_{DSTBC}}{2+\overline{\gamma}_{DSTBC}}}$. Moreover, $\overline{\gamma}_{DSTBC}$ is the average received SNR at the destinations when distributed STBC scheme is invoked during the BC phase. $\overline{\gamma}_{ab}$ represents the average received SNR at node b for the transmission between a and b. $\overline{\Psi}_1$ is defined as $\frac{\overline{\gamma}_{s_1r_1}\overline{\gamma}_{s_2r_1}}{\overline{\gamma}_{s_1r_1}+\overline{\gamma}_{s_2r_1}}$. Similarly, $\overline{\Psi}_2$ is equivalent to $\frac{\overline{\gamma}_{s_1r_2}\overline{\gamma}_{s_2r_2}}{\overline{\gamma}_{s_1r_2}+\overline{\gamma}_{s_2r_2}}$.

3.3.3 Exact Average End-to-End BEP for Proposed Distributed STBC System

In this subsection we extend the basic principles used in the previous subsection and derive the exact average end-to-end BEP in a similar way. The derivation steps are different from Eq. (3.33), where we replace the upper and lower bounds of the instantaneous BEP at relay nodes with the exact instantaneous BEP of the MAC phase denoted by P_{MAC,r_j}. According to the investigation in [82, 83], we have

$$\begin{aligned}P_{MAC,r_j} = &\frac{2}{\pi}\int_0^{\frac{\pi}{2}}\exp\left(-\frac{|h_{s_2r_j}|^2}{2\sin^2\delta}\right)\mathrm{d}\delta+\frac{1}{\pi}\int_0^{\frac{\pi}{2}}\exp\left(-\frac{|2h_{s_1r_j}-h_{s_2r_j}|^2}{2\sin^2\delta}\right)\mathrm{d}\delta \\ &-\frac{1}{\pi}\int_0^{\frac{\pi}{2}}\exp\left(-\frac{|2h_{s_1r_j}+h_{s_2r_j}|^2}{2\sin^2\delta}\right)\mathrm{d}\delta\,. \end{aligned} \tag{3.37}$$

We substitute the above equation into Eq. (3.26) and expand Eq. (3.26). The following steps are exactly the same as those used in the previous derivation. Specifically we calculate the expectation for each term and sum them up. After some manipulation the exact average end-to-end BEP of our proposed novel distributed STBC system is given by

$$\begin{aligned}\overline{P_{EtoE}^{(exact)}} = &\frac{1}{32}\left[2-2\Gamma(\overline{\gamma}_{s_2r_1})-\Gamma(\overline{\gamma}_{s_1r_1})+\Lambda(\overline{\gamma}_{s_1r_1})\right]\left[2-2\Gamma(\overline{\gamma}_{s_2r_2})-\Gamma(\overline{\gamma}_{s_1r_2})+\Lambda(\overline{\gamma}_{s_1r_2})\right]\\ &+\frac{(1-\lambda)^2(\lambda+2)-4+4\Gamma(\overline{\gamma}_{r_1d_1})}{64}\left[2+2\Gamma(\overline{\gamma}_{s_2r_1})+\Gamma(\overline{\gamma}_{s_1r_1})-\Lambda(\overline{\gamma}_{s_1r_1})\right]\\ &\times\left[2+2\Gamma(\overline{\gamma}_{s_2r_2})+\Gamma(\overline{\gamma}_{s_1r_2})-\Lambda(\overline{\gamma}_{s_1r_2})\right]\ , \qquad (3.38)\end{aligned}$$

where the definitions of $\Gamma(a)$ as well as $\Lambda(a)$ are given by $\Gamma(a)=\sqrt{\frac{a}{2+a}}$ and $\Lambda(a)=\sqrt{\frac{9a}{2+9a}}$, respectively. The results shown in Fig. 3.11 and Fig. 3.12 indicate the derived analytical upper and lower bounds of the average end-to-end BEP are fairly accurate and tight. The theoretical curves perfectly match those obtained by Monte Carlo simulations.

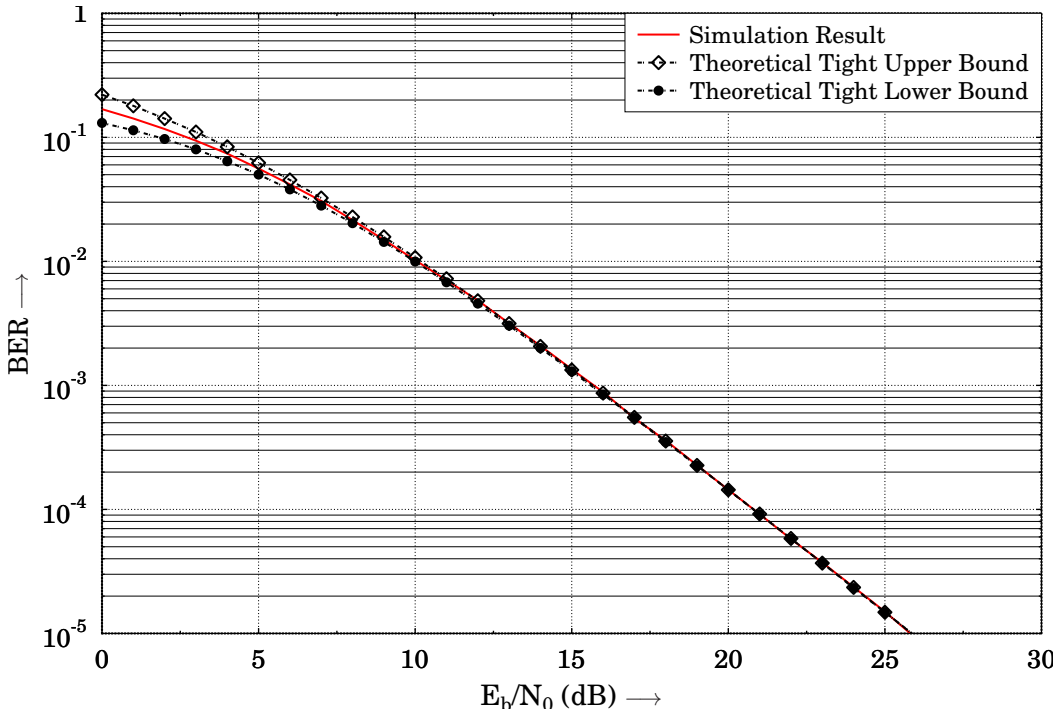

Figure 3.11: Tight upper and lower bounds of the average end-to-end BEP of the proposed distributed STBC scheme.

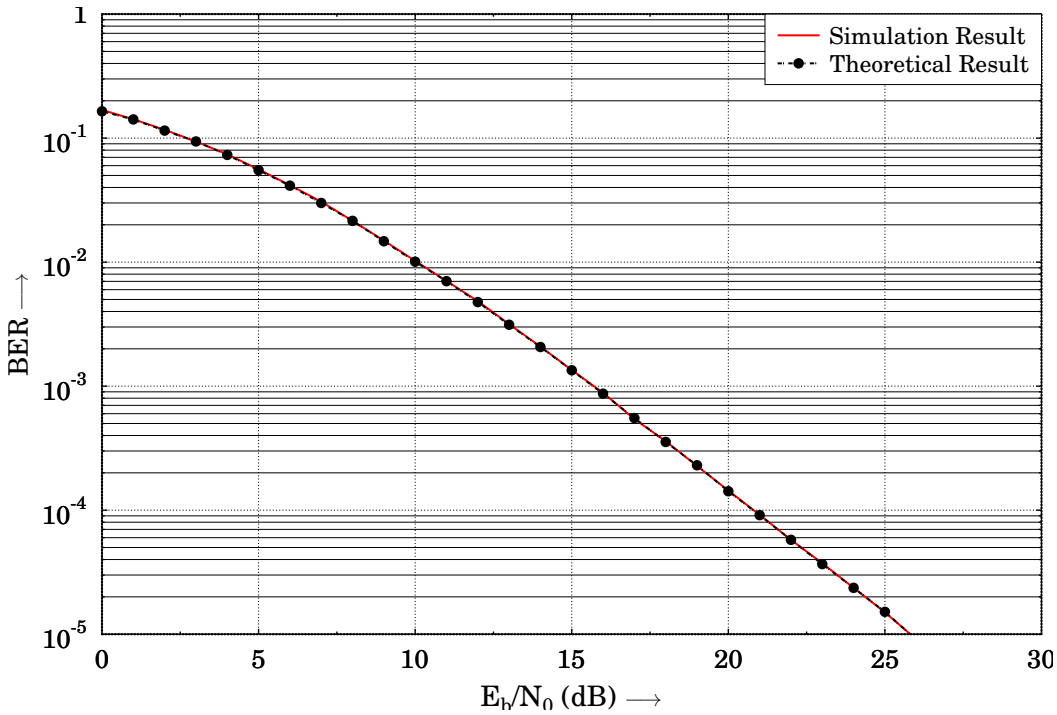

Figure 3.12: Exact average end-to-end BEP of the proposed distributed STBC scheme.

3.4 Conclusion

A novel distributed space-time block coding scheme using 'decode-and-forward' relaying protocol for multi-relay assisted two-way cooperative communication is presented in this chapter. Some distinguished contributions of this scheme are summarized as follows:

- The network topology is similar to the one in [69] where two users simultaneously exchange Alamouti space-time coded signals via a relaying partner with the aid of PLNC, however we eliminate the constraint that the source nodes have to be equipped with multiple antennas. In this chapter, we show that our proposed scheme can still achieve full diversity order when each node acts as a single-antenna assisted mobile unit.

- A simple selection relaying or opportunistic relaying protocol is appropriately designed to effectively circumvent the error propagation inflicted by the relay nodes. More specifically, an error detection code (such as CRC) based selection relaying strategy is proposed to retain the orthogonality of the distributed STBC codewords as well as guarantee the full diversity order is achieved at the destination without employing any sophisticated channel codes to protect the source-to-relay link.

- PLNC is employed to guarantee that the information exchange between two users

via a single or multiple relays can be fulfilled within two time slots. Hence, this novel cooperative communication scheme for two-way relay channels can achieve significant throughput and spectral efficiency improvements.

- Theoretical end-to-end bit error probability (BEP) performance of our proposed distributed STBC scheme over two-way relay channel is investigated using the well-known MGF based approach. Tight upper and lower bounds of the average end-to-end BEP are first derived and solved. Then, the analysis is extended to obtain a more accurate expression of the exact BEP.

Chapter 4

Cooperative Differential Space-Time Block Codes

Contents

In the previous chapter, we focused on the discussion of distributed STBC scheme in the context of two-way cooperative communication. This chapter is devoted to the cooperative differential STBC (DSTBC) system under two-way relay scenario.

A novel distributed DSTBC structure is first studied, which enables construction of DSTBC codewords from cooperation of multiple relaying partners at scattered geographic locations in a distributed manner. We then apply the differential algorithm to the PLNC employed in the two-way relaying network illustrated in Fig. 3.6 and propose a novel low-complexity differential PLNC, which also facilitates the extraction of information of interest from the superimposed signal at relay nodes, as for coherent PLNC but dispensing with channel state information at the receiving side.

The proposed distributed DSTBC aided bidirectional relaying scheme is based on the framework developed in Chapter 3, where a similar selective relaying protocol is utilized to guarantee the orthogonality of the distributed DSTBC codewords during the broadcast

stage of two-way cooperative communication. Discussions in this chapter begin with an introduction of the distributed DSTBC scheme for unidirectional relay channels, and extend it to the bidirectional scenario in the following part of the chapter.

4.1 Cooperative Differential Space-Time Block Codes for Unidirectional Relaying

Modern telecommunication systems mostly concentrate on transmission of speech and data using the star topology [84]. The trend of future wireless applications, for instance smart grid and body area network, results in user cooperation among a large number of battery-powered network devices or communication nodes, following a peer-to-peer or heterogeneous mesh topology [84]. Consequently, data flowing in such configuration is more likely to be forwarded in a relaying manner from node to node through the network.

Similar to the case for non-cooperative systems, fading or node failure could also lead to unreliable links in the relaying networks. Cooperative diversity [59, 61, 85] provided by multiple cooperating users or nodes is capable of remedying the network instability and effectively improving network robustness. It is possible to exploit further performance gain by implementing the concept of temporal and spatial diversity with the assistance of distributed DSTBC schemes. The maximum achievable diversity gain is identical to that promised in conventional multiple-antenna communication systems.

Under the circumstance that neither the transmitter nor the receiver has knowledge of the channel coefficients, it is a preferable choice to incorporate differential encoding at the transmitting side and non-coherent detection at the receiving side. Differential STBC for co-located multiple-antenna system was first introduced and investigated in [53]. It is demonstrated in [53] that the unique properties of the DSTBC scheme significantly simplify the complexity of receiver and save precious spectrum resources otherwise required for training-based channel estimation.

Motivated by the work in [86,87], we generalize and extend the principle of the distributed STBC scheme to distributed DSTBC allowing non-coherent detection at the receiver. Owing to the redundancy introduced during the differential encoding, it becomes feasible to detect the original information bits conveyed by the distributed DSTBC signal dispensing with the channels' fading coefficients. On the other hand, the proposed distributed DSTBC scheme offers the same amount of spatial and temporal diversity gain as in the

corresponding coherently-detected distributed STBC scenario.

4.1.0.1 System Model

In this subsection, we consider the system model of a multi-hop relaying cooperative communication system. An example of a typical two-hop relaying model with N relay nodes $(r_1, r_2, ..., r_N)$ located and fixed between the source node (s) and the destination node (d) is illustrated in Fig. 4.1. Moreover, it is assumed that there is no direct line-of-

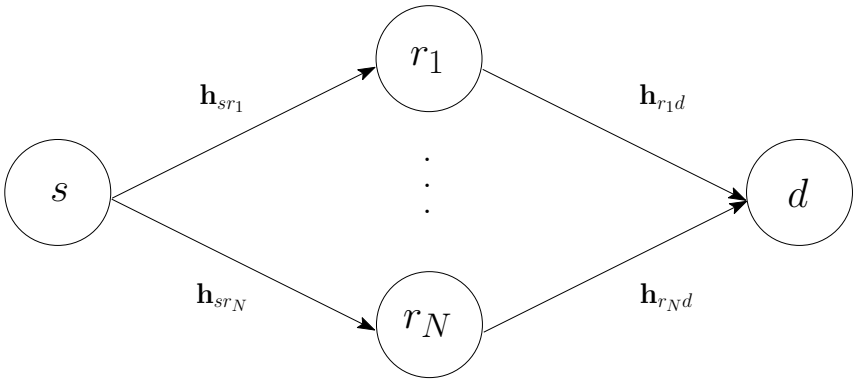

Figure 4.1: Schematic of a typical two-hop multi-relay cooperative communication system.

sight between the source and destination node while the source-to-relay links as well as the relay-to-destination links are subject to Rayleigh fading. All wireless nodes shown in Fig. 4.1 are single-antenna supported half-duplex devices.

The relaying scheme consists of two stages, during the first transmission period, the source node transmits a frame of $\mathcal{M}$-ary differential phase-shift keying (DPSK) symbols $\mathbf{x}_s$ to all relay nodes. If the notation $\mathbf{h}_{sr_i}\,(i = 1, 2, ..., N)$ represents the vector of Rayleigh fading coefficients, the received signal in the ith relay node is given by

$$\mathbf{y}_i = \mathbf{h}_{sr_i}\mathbf{x}_s + \mathbf{m}_i\ , \tag{4.1}$$

where $\mathbf{m}_i$ is the additive white Gaussian noise having zero mean and variance of $N_0/2$ per dimension.

The DF cooperative protocol imposes the requirement of fully recovering the transmitted information bits at each relay node, hence a non-coherent differential detector is employed to generate the estimates of the original information bits. An additional distributed DSTBC encoder prepares the relay nodes for transmission in the second time slot. At the

destination node, a conventional DSTBC decoder is invoked to recover the information bits from the received signal $\mathbf{y}_d$, which is expressed as

$$\mathbf{y}_d = \sum_{i=1}^{N} \mathbf{h}_{r_i d} \mathbf{v}_{r_i} + \mathbf{n}_d \ , \tag{4.2}$$

where $\mathbf{v}_{r_i}$ represents the distributed DSTBC symbols transmitted from the relay nodes during the BC phase, whereas $\mathbf{h}_{r_i d}$ indicates the Rayleigh block fading coefficients between the ith relay node and the destination node whereas $\mathbf{n}_d$ is the AWGN introduced at the destination node having zero mean and variance of $N_0/2$ per dimension.

4.1.0.2 Proposed Two-hop Cooperative DSTBC Scheme with Selection Relaying

A detailed block diagram of the proposed two-hop distributed DSTBC scheme with $N = 2$ relay nodes is demonstrated in Fig. 4.2.

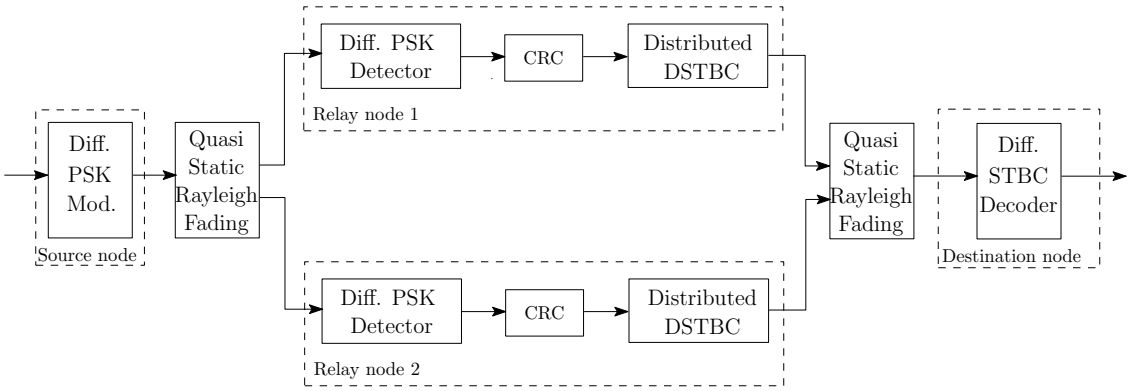

Figure 4.2: Schematic of the proposed two-hop distributed DSTBC aided unidirectional cooperative communication scheme.

It is worth pointing out that, since the antenna array is constructed in a distributed fashion, it is unable to guarantee full diversity order at the destination if the re-encoded network-coded symbols are simply forwarded without certain protection mechanism. In order to enhance the error-resilience against potential error propagation, one popular solution is to protect the source-to-relay link by introducing redundancy using a channel code, with high decoding complexity at the relay nodes. A more appealing alternative is to invoke a low-complexity frame-by-frame (or packet-by-packet) based relay selection strategy, similar to the one used in Section 3.2.2.2.

The negative effects of error propagation induced in the decoding and re-encoding stage can now be effectively circumvented at each relay node. To elaborate further, a CRC

error-detecting checksum is conducted prior to re-encoding the network-coded symbols into the distributed DSTBC frame. The generator polynomial for CRC is $\Gamma = [x^8 + x^7 + x^4 + x^3 + x + 1]$, which corresponds to the 9-bit string $\{110011011\}$. Depending on the results of CRC validation, each cooperating node can decide whether to become active during the second transmission period or just keep silent. For $N = 2$ relay nodes, there are four different relaying scenarios summarized as follows in Tab. 4.1.

Table 4.1: Demonstration of the transmission schedule used in selective relaying for $N = 2$ relay nodes.

Relay 1	**Relay 2**	**Transmission Mode**
Pass	Pass	Distributed DSTBC
Pass	Fail	Differential PSK
Fail	Pass	Differential PSK
Fail	Fail	No transmission

4.1.0.3 Design of Distributed DSTBC Encoding and Decoding

In this subsection, we elaborate on the detailed encoding and decoding procedure of the proposed distributed DSTBC scheme, the schematic of which is illustrated in Fig. 4.3.

Several distributed DSTBC proposals from other contributors can be found in the literature [88, 89] and references therein. It is noteworthy that existing techniques simply incorporate conventional differential STBC in one or more cooperating nodes in order to support diversity reception at the destination, which requires multiple co-located antennas at relay nodes. On the contrary, our proposed scheme takes advantage of the distributed nature inherent in the cooperative network allowing multiple single-antenna aided low-complexity low-power nodes to fully cooperate and exploit the same amount of spatial and temporal diversity gain.

The encoding procedure for the proposed distributed DSTBC scheme incorporating $N = 2$ relay nodes and a PSK signal constellation with 2^L elements is stated as follows. To begin with, the encoding process is initialized by modulating the estimated information bits at the ith relay node into a sequence of L-ary PSK symbols. For ease of presentation,

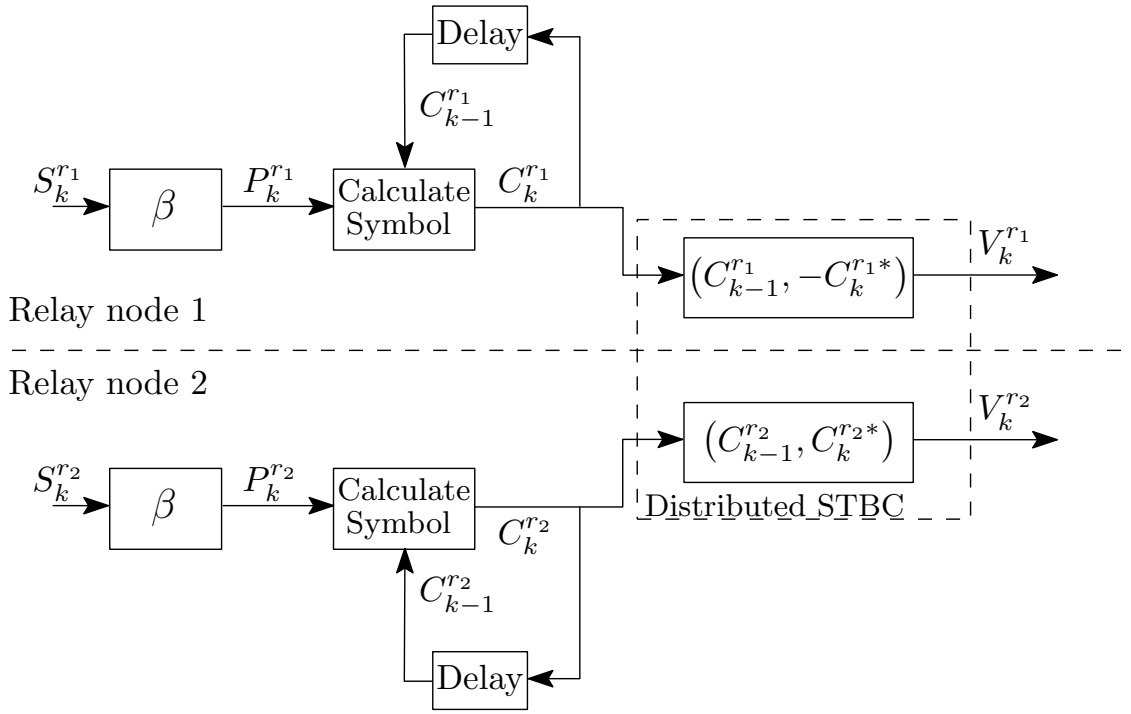

Figure 4.3: The schematic of the proposed distributed DSTBC encoder.

each pair of two adjacent PSK-modulated symbols is grouped into a block. To be more specific, the kth block for the ith relay node is written as

$$S_k^{r_i} = \begin{bmatrix} s_{k,1}^{r_i} & s_{k,2}^{r_i} \end{bmatrix} , \tag{4.3}$$

where $s_{k,1}^{r_i}$ and $s_{k,2}^{r_i}$ represent the first and second element of $S_k^{r_i}$ respectively.

For a given complex-valued set $\mathcal{P}$ consisting of 2^{2L} distinct 1×2 coefficient vectors, the input symbols at the ith relay node are mapped onto the constellation $\mathcal{P}$, where the first and second element of the resultant coefficient vector corresponding to the kth block at the ith relay node are denoted as $P_k^{r_i} = \begin{bmatrix} p_{k,1}^{r_i} & p_{k,2}^{r_i} \end{bmatrix}$. The design of the mapping function β is arbitrary as long as all coefficient vectors in $\mathcal{P}$ are unique and a one-to-one mapping is guaranteed. In this work, an orthogonal mapping function is employed, which gives

$$p_{k,1}^{r_i} = s_{k,1}^{r_i} \left(s_0^{r_i}\right)^* + s_{k,2}^{r_i} \left(s_1^{r_i}\right)^* , \tag{4.4}$$

$$p_{k,2}^{r_i} = -s_{k,1}^{r_i} s_1^{r_i} + s_{k,2}^{r_i} s_0^{r_i} , \tag{4.5}$$

where $s_0^{r_i}$ and $s_1^{r_i}$ are the notations for the first and second element of the reference block at the ith relay node.

An example of the one-to-one mapping function β and the complex-valued finite set $\mathcal{P}$ is demonstrated as follows. Assume the PSK constellation consists of two points $1/\sqrt{2}$ and

$-1/\sqrt{2}$ and the set $\mathcal{P}$ is defined as $\mathcal{P} = \{(1,0),(0,1),(0,-1),(-1,0)\}$. The encoding commences from the transmission of a pair of arbitrary reference symbols $s_0^{r_i}$ as well as $s_1^{r_i}$ which do not carry any information. The orthogonal mapping β maps a block of two input bits onto $\mathcal{P}$ using Eq. (4.4) and Eq. (4.5). As a result, the one-to-one relationship between input data bits and coefficient vector $P_k^{r_i}$ is summarized in Tab. 4.2 below.

Table 4.2: Demonstration of computing coefficient vectors $P_k^{r_i}$ for given input data bits.

Input data bits	$P_k^{r_i} = [p_{k,1}^{r_i} \quad p_{k,2}^{r_i}]$
(0 0)	(1 0)
(0 1)	(0 -1)
(1 0)	(0 1)
(1 1)	(-1 0)

At time interval k, each relay node calculates a 1×2 differential codeword vector, denoted by $C_k^{r_i}$, in a recursive fashion. The corresponding differential symbols depend on the one generated in the previous block at time $k-1$, mathematically speaking

$$C_k^{r_i} = p_{k,1}^{r_i} O_1(S_{k-1}^{r_i}) + p_{k,2}^{r_i} O_2(S_{k-1}^{r_i}) \,, \tag{4.6}$$

where $O_1(S_{k-1}^{r_i})$ and $O_2(S_{k-1}^{r_i})$ are two vectors constructed on an orthogonal basis

$$O_1(S_{k-1}^{r_i}) = S_k^{r_i} = \left[s_{k,1}^{r_i} \quad s_{k,2}^{r_i} \right] \,, \tag{4.7}$$

$$O_2(S_{k-1}^{r_i}) = \left[\left(s_{k,2}^{r_i}\right)^* \quad -\left(s_{k,1}^{r_i}\right)^* \right] \,. \tag{4.8}$$

Subsequently, a distributed Alamouti STBC encoder is invoked to generate the distributed DSTBC codewords $V_k^{r_1} = \left[c_{k,1}^{r_1} \quad -\left(c_{k,2}^{r_1}\right)^* \right]$ for the kth block transmitted by the first relay node, whilst $V_k^{r_2} = \left[c_{k,1}^{r_2} \quad \left(c_{k,2}^{r_2}\right)^* \right]$ is transmitted by the second relay node.

4.1.0.4 Performance Results and Discussion

The BER performance of the proposed selection relaying aided DPSK-DDSTBC scheme for the unidirectional relaying scenario is examined and quantified using Monte-Carlo simulation as shown in Fig. 4.4 and Fig. 4.5. It is assumed that the number of DPSK/distributed DSTBC symbols used for transmission from the source/relay node is

defined as $N_s = N_r = 50, 100, 300$ DPSK/DDSTBC symbols with BPSK modulation. Simulation results are based on the quasi-static Rayleigh fading channel model, which implies all DPSK/distributed DSTBC symbols from one frame experience the same fading amplitude and phase. The detailed simulation configuration is given in Tab. 4.3.

Table 4.3: Simulation parameters for the following BER performance evaluation.

Simulation Parameters	
Parameters	**Values**
Modulation Scheme	BPSK
Path-gain of Source-to-Relay Link	1
Path-gain of Relay-to-Destination Link	1
CRC Generator Polynomial	$[x^8 + x^7 + x^4 + x^3 + x + 1]$
Maximum Length of Frame	50/100/300
Eb/N0 Range	0–40 dB
Channel Type	Quasi-static Rayleigh Fading Channel

BER performance of the distributed DSTBC scheme with selection relaying (DDSTBC-SR) is illustrated in Fig. 4.4. Since the achievable diversity order can be roughly identified from the slope of the BER curve, it can be seen that the proposed DDSTBC-SR scheme is also capable of exploiting full diversity order when compared against the conventional non-cooperative differential STBC scheme with two co-located transmit antennas and a single receive antenna. On the other hand, although multiple number of cooperating nodes are incorporated to relay the signal from source to destination node using proposed distributed DSTBC approach, only first order diversity is observed leading to a BER degradation of more than 5.0 dB at BER = 10^{-3} due to the lack of an appropriately-designed selection relaying strategy (denoted as DDSTBC-NO-SR shown in Fig. 4.4) to effectively alleviate the detrimental effect of error propagation.

It is also worth noticing the impact of different frame lengths on the end-to-end BER performance. As we can see from Fig. 4.4, as the transmitted DPSK sequence length increases from 50 to 300, the BER performance suffers from a slight degradation. This limitation results from the employment of distributed DSTBC encoding at the relay nodes and is inherent in the proposed selective relaying strategy. According to the principle of

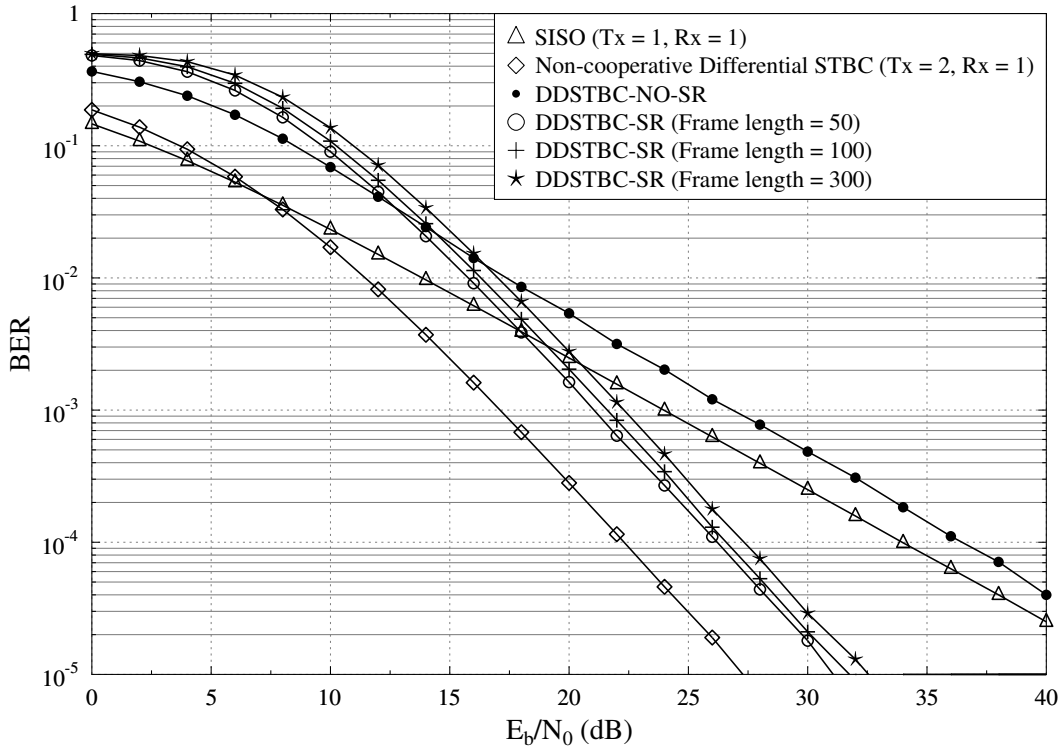

Figure 4.4: BER versus E_b/N_0 performance of the proposed novel DPSK-DDSTBC scheme with selection relaying strategy when communicating over quasi-static Rayleigh fading channel, where the frame length is $50, 100, 300$.

selective relaying, received symbols at the destination node are valid DSTBC codewords if and only if the DPSK symbols transmitted from the source node are all correctly detected at both relay nodes. Such a condition becomes more difficult to satisfy when longer frame length is used. However, compared with the substantial benefits brought by distributed DSTBC, the performance degradation is negligible.

Moreover, as shown in Fig. 4.5, when the $E_b/N_0 = 0.0$ dB, almost 90% of the total transmitted frames from the source node are detected erroneously leading to a high error rate, which is also confirmed by the BER simulation result. The percentage of erroneous detection begins to drop when the E_b/N_0 increases from 0.0 dB to 20.0 dB. At approximately $E_b/N_0 = 8.0$ dB, the percentage of performing error-free detection at both relay nodes starts to dominate and increases to 90% when the E_b/N_0 increases.

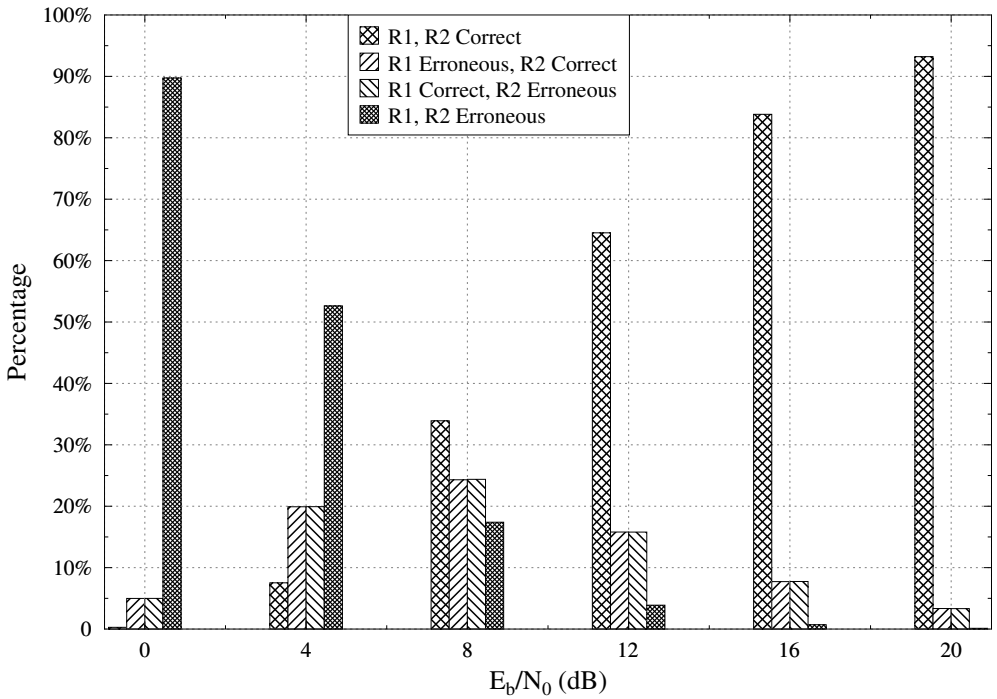

Figure 4.5: Bar chart for the percentage of correctly and erroneously detected bits at two relay nodes with different E_b/N_0.

4.1.0.5 Theoretical Performance Analysis

In this subsection, the performance of proposed DPSK-DDSTBC two-hop unidirectional relaying scheme is investigated from an analytical perspective. Similar to the theoretical analysis for the distributed STBC scenario presented in Chapter 3, the derivation of the

average end-to-end error probability based on the moment generating function is straightforward and intuitive.

Since the analysis methodology is very similar to that used in Section 3.3, the derivation steps are described in brief in order to keep the presentation concise and compact. The instantaneous end-to-end BEP measured at the destination node, denoted by $P_{b,EtoE}$, consists of four parts depending on the different statuses of selective relaying during the cooperating stage, which are summarized in Tab. 4.1. It is straightforward to define the instantaneous end-to-end BEP $P_{b,EtoE}$ with the following formula

$$P_{b,EtoE} = \underbrace{(1-P_{F,DPSK}^{r_1})(1-P_{F,DPSK}^{r_2})P_{b,DSTBC}}_{r_1,\, r_2 \text{ both decode correctly}} + \underbrace{(1-P_{F,DPSK}^{r_1})P_{F,DPSK}^{r_2}P_{b,DPSK}}_{r_1 \text{ decodes correctly, } r_2 \text{ decodes erroneously}} + \underbrace{P_{F,DPSK}^{r_1}(1-P_{F,DPSK}^{r_2})P_{b,DPSK}}_{r_1 \text{ decodes erroneously, } r_2 \text{ decodes correctly}} + \underbrace{\frac{1}{2}P_{F,DPSK}^{r_1}P_{F,DPSK}^{r_2}}_{r_1,\, r_2 \text{ both decode erroneously}}, \tag{4.9}$$

where the notations used in Eq. (4.9) are explained as follows:

- To begin with, the term $P_{F,DPSK}^{r_i}(i = 1, 2)$ denotes the frame error rate of the received DPSK signal measured at the ith relay node, which is used to indicate the probability of whether one specific DPSK frame transmitted from the source node is correctly detected at the ith relay node.
- Assume both relay nodes r_1, r_2 succeed in making correct detection, a frame of distributed DSTBC symbols are transmitted to the destination node at the second hop. $P_{b,DSTBC}$ represents the instantaneous BEP of the received distributed DSTBC signal estimated at the destination node.
- If the estimation of DPSK signal is erroneous at either of the relay nodes r_1, r_2, the performance of the relay-to-destination link is identical to that of DPSK scheme providing only first order diversity as the diversity reception would fail when only one row or one column of the DSTBC codewords arrive at the destination node. Therefore, $P_{b,DPSK}$ is used to denote the instantaneous BEP of the received signal for the scenario of only one relay node is activated.
- In the last scenario, none of the relay nodes r_1, r_2 detects the DPSK symbol sequence successfully, which results in complete radio silence during the second transmission period. Destination node has to pick an arbitrary pair of binary bits as the estimation. Hence, this leads to a bit error rate of $1/2$ as observed in Eq. (4.9).

The frame error probability of receiving K number of sequential DPSK symbols is given by [16]

$$P_{F,DPSK}^{r_i} = 1 - (\frac{1}{2})^K \left[1 + \sum_{k=1}^{K} \prod_{j=1}^{k} \frac{K+1-j}{j+\frac{1}{\gamma_i}} \right] , \tag{4.10}$$

where we have $i = \{1, 2\}$ in this work since two relay nodes are considered in the network topology and γ_i is the average received SNR at the ith relay node.

On the other hand, the bit error probability of the differential STBC scheme $P_{b,DSTBC}$ with non-coherent detection is studied in [27] and can be expressed as

$$P_{b,DSTBC} = \lambda^2 \left[1 + 2(1-\lambda) \right] , \lambda = \frac{1}{2} - \frac{1}{2} \left(1 + \frac{1}{\gamma} \right)^{-1/2} , \tag{4.11}$$

where γ denotes the average received SNR at the destination node.

Moreover, the bit error probability of receiving a frame of DPSK symbols with non-coherent detection at the destination node can be easily obtained by letting the frame length $K = 1$ and replacing γ_i with γ, which yields

$$P_{b,DPSK} = \frac{1}{2(1+\gamma)} . \tag{4.12}$$

Finally, the average end-to-end bit error probability of the novel unidirectional distributed DSTBC relaying scheme is acquired by calculating the statistical expectation of the instantaneous end-to-end BEP, where the expectation is conditioned on the distribution of the fading channel, which gives

$$\overline{P_{b,EtoE}} = \mathbb{E}\big[P_{b,EtoE} \big] . \tag{4.13}$$

A closed-form expression is difficult to find for Eq. (4.13), hence the well-known numerical integration approach is employed to evaluate the expectation of Eq. (4.13). The analytical evaluation of the average end-to-end bit error probability of the proposed DPSK-DDSTBC scheme is plotted and verified against the simulation results for different frame lengths as illustrated in Fig. 4.6.

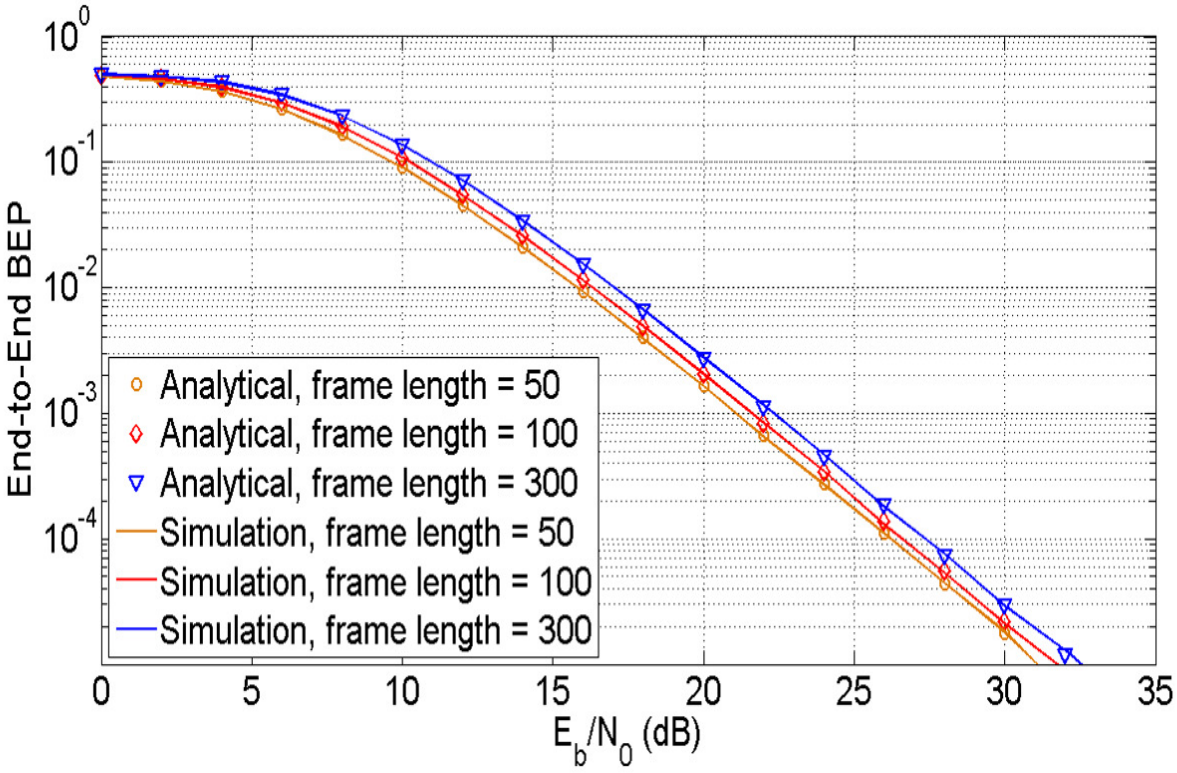

Figure 4.6: Comparison of the analytical and empirical average end-to-end BEP of the proposed DPSK-DDSTBC unidirectional relaying scheme with different frame lengths.

4.1.0.6 Extension to Turbo-coded Distributed DSTBC Scheme

In the previous subsection, we proposed and investigated a novel distributed DPSK-DSTBC two-hop relaying scheme for unidirectional cooperative communications. Observations from analytical and empirical results both confirm the fact that the bit error performance of the proposed distributed scheme varies with respect to the frame length. The likelihood of making correct detection for the received DPSK symbol sequence at the relay nodes becomes smaller if longer frame length is involved in the source-to-relay link. As a result, implementation of the proposed scheme is constrained by this undesirable property in practice.

The practical limitation is circumvented by incorporating a certain level of temporal redundancy using FEC codes in order to reinforce the reliability of the source-to-relay link. Moreover, the error rate degradation of an uncoded distributed DSTBC lacking sufficient protection is proportional to the frame length. Fortunately, the coding gain associated to the FEC codes also grows as an increasing number of information bits are encoded providing a higher level of redundancy. Hence, the employment of FEC codes in the source node offers an efficient and effective countermeasure.

In this subsection, a half-rate Turbo-coded DPSK scheme is introduced for suppressing the sensitivity to the frame length. To elaborate further, a quadratic polynomial permutation (QPP) interleaver [90, 91], which has been standardized into the 3GPP LTE specification, is considered as the internal interleaver for the Turbo code at the source node; whereas a random block interleaver is employed at both source and relay nodes to fully scramble the coded symbols and eliminate the correlation between adjacent symbols. A QPP interleaver defines the relationship between the output bit index i and the input index $\pi(i)$, which satisfies the following equation

$$\pi(i) = \left(f_1 i + f_2 i^3\right) \mathrm{mod} K \ , \tag{4.14}$$

where K is the block size, f_1 and f_2 are the coefficients that characterize the rule of permutation. For example, if block size $K = 1088$, coefficients f_1 and f_2 are given in 3GPP technical specification [92] as follows: $f_1 = 171$; $f_2 = 204$; while $K = 3072$, $f_1 = 47$; $f_2 = 96$.

The schematic of the Turbo-coded DPSK-DDSTBC scheme with selection relaying strategy for one-way relaying case is depicted in Fig. 4.7, in which it is assumed that two single-antenna assisted relay nodes ($i = \{1, 2\}$) are situated between the source and destination node.

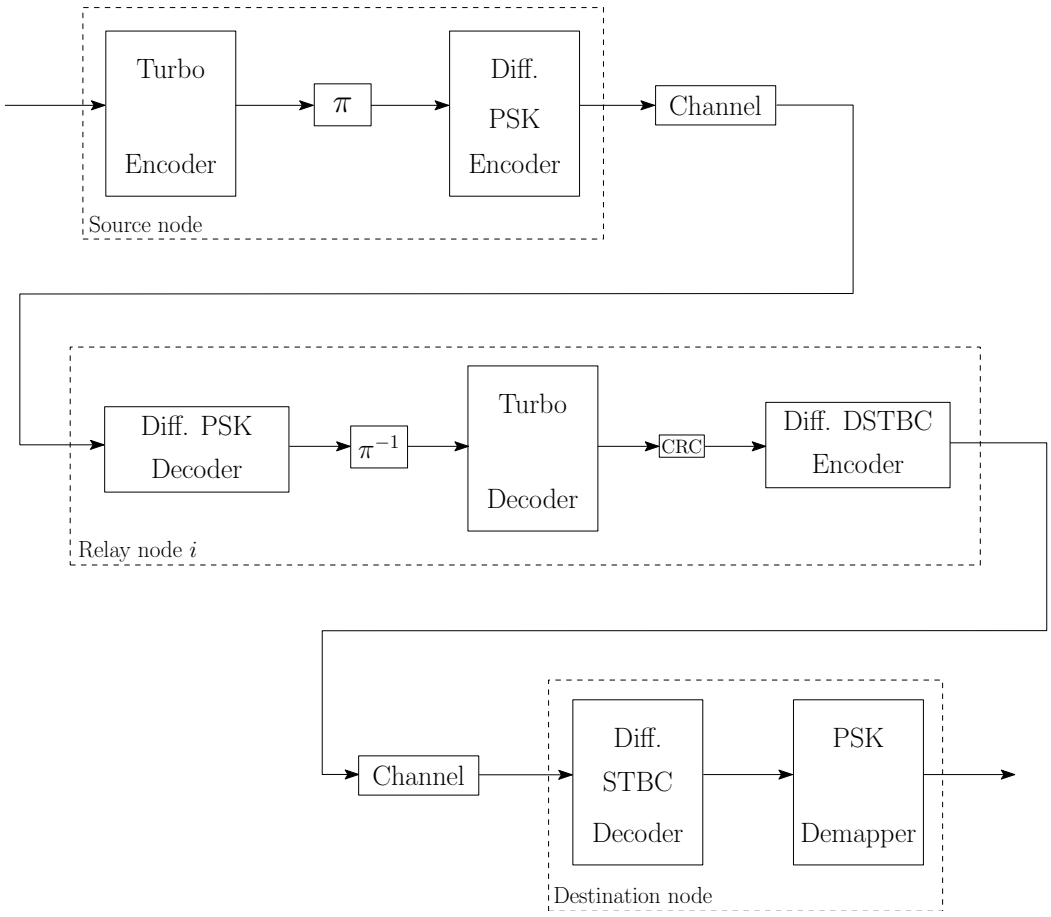

Figure 4.7: The schematic of the Turbo-coded DPSK-DDSTBC scheme with selection relaying strategy for one-way relaying case.

As shown in Fig. 4.7, a $1/2$-rate Turbo code encodes the input binary bits and introduces redundancy. Next, the resultant Turbo-coded symbols are interleaved and further modulated with differential PSK. After propagating through quasi-static Rayleigh fading channel, the interleaved version of Turbo-coded symbols are estimated in a non-coherent fashion at the ith cooperating node based on the distorted received signal. Recovered symbols are further de-interleaved and decoded with optimal Log-MAP algorithm. A simple CRC checksum guarantees only correctly decoded information bits are re-encoded with distributed DSTBC and relayed to the destination node during the second hop.

Diversity reception technique combines the distributed DSTBC symbols emitted from each relay node and exploits the transmit diversity gain, even though the destination node is equipped with a single receiving antenna. A conventional DSTBC decoder followed by a PSK demapper performs final decoding and detection for retrieving the original information bits from the source node.

Two identical recursive systematic convolutional (RSC) codes operating in parallel are employed as the constituent codes for the Turbo code. In this work, we consider rate $R_{tc} = 0.5$ memory-three Turbo code [93] having a generator polynomial of $[13\ 15]_8$ expressed in octal format. Furthermore, 4 iterations are considered for the internal Turbo decoding between two component RSC decoders for the purpose of balancing the trade-off of error correction capability and decoding complexity. The rest simulation configurations are similar to those mentioned in Tab. 4.3.

The Monte Carlo simulation of BER versus E_b/N_0 performance of Turbo-coded DPSK-DDSTBC one-way cooperative communication scheme is shown in Fig. 4.8. It is clearly demonstrated in Fig. 4.8 that, when transmitting a series of consecutive 1088 or 3072 DPSK symbols from the source node using uncoded DPSK-DDSTBC scheme, the end-to-end BER versus E_b/N_0 curves, denoted by pink and red solid-lines with circle marker respectively, exhibit slight performance degradation of 0.5 dB at BER$= 10^{-3}$ as the frame length increases from 1088 to 3072. On the other hand, the degraded error probability can be compensated by encoding the information bits with Turbo code prior to differential modulation. The comparison of a DPSK signal containing 1088 (blue, triangle solid-line) and 3072 DPSK symbols (purple, pentagram solid-line) indicates that the proposed Turbo-coded DPSK-DDSTBC design not only effectively resolves the frame length limitation experienced in uncoded system, but also provides simultaneous coding gain and full transmit diversity gain. When the frame length grows from 1088 to 3072, an improvement of approximately 2.0 dB is noticed at BER $= 10^{-4}$ as expected. It is noteworthy that the well-known turbo cliff of coded DPSK-DDSTBC scheme is not observed in Fig. 4.8. Owing to the assumption of quasi-static fading channel model in both source-to-relay and

relay-to-destination links, stringent limitation is imposed on the available coding gain provided by the channel codes including Turbo code, due to lack of time diversity.

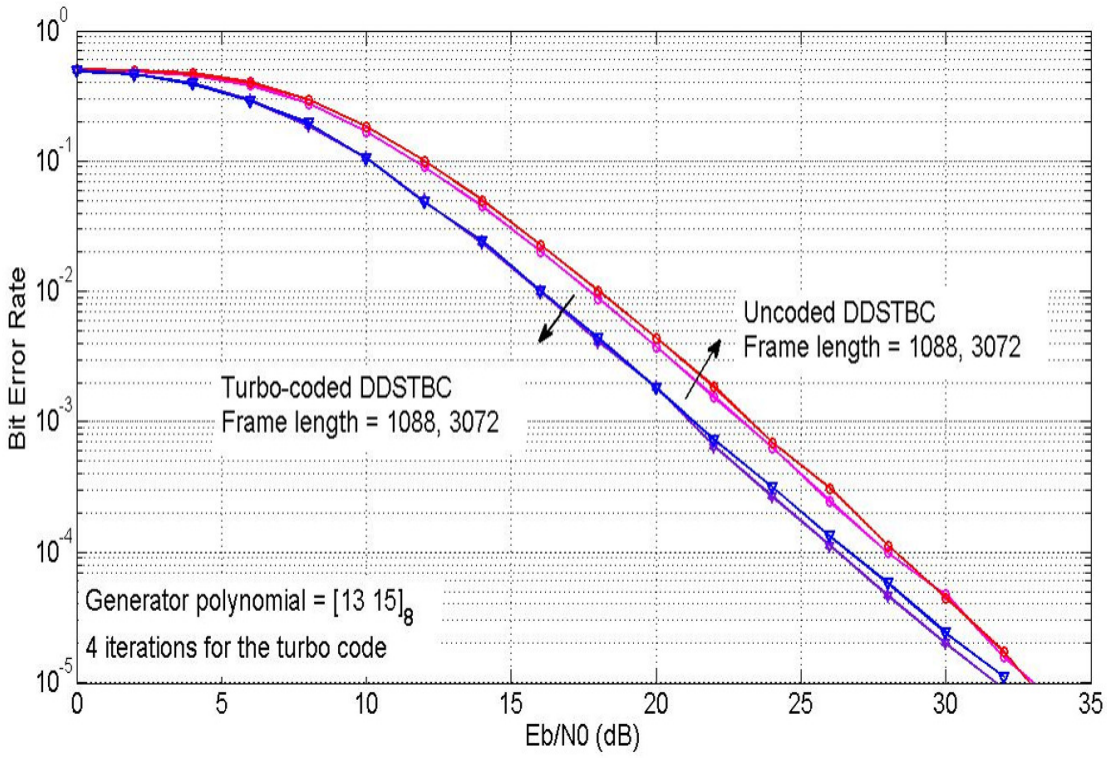

Figure 4.8: BER versus E_b/N_0 performance of the Turbo-coded distributed DSTBC scheme with selection relaying strategy when communicating over quasi-static Rayleigh fading channel.

4.2 Cooperative Differential Space-Time Block Codes for Bidirectional Relaying

In the previous subsection, we investigated a fully non-coherent distributed differential STBC scheme in the context of two-hop unidirectional cooperative communication. Although the decoding and detection at both relay and destination nodes are independent with channel's fading coefficients, it is still capable of attaining full transmit diversity gain. In this subsection, we take one step further by extending the unidirectional DPSK-DDSTBC scheme to bidirectional relaying scenario.

A low-complexity non-coherent physical-layer network coding (PLNC) algorithm is first proposed and studied. Similar to the conventional PLNC, a non-coherent PLNC detection approach is designed to perform a direct extraction of the network-coded symbols from the received superimposed signal at the relay nodes when channel coefficients are unavailable.

Moreover, compared with the conventional cooperative system under half-duplex constraint requiring four time slots for two-way relaying, the employment of non-coherent PLNC at all cooperating nodes significantly improves overall throughput and network capacity by allowing simultaneous information exchange between two users. To be more specific, a simple non-coherent PLNC detector with a low-complexity dual-branch structure is devised and incorporated to support bidirectional distributed coding.

It is worth pointing out that several existing distributed DSTBC systems have been presented in the literature. For instance, a cooperative DSTBC based on AF collaborative protocol is found in [88]. On the other hand, the work in [89] is similar to ours, unfortunately multiple number of transmitting antennas at the source and relay nodes incur extra power consumption and high implementation complexity. The proposed novel distributed DSTBC scheme is designed to be deployed in the two-way relaying network consisting of single-antenna nodes.

In this subsection, our attention is concentrated on the construction of a two-way communication system utilizing DF relaying protocol from a cluster of low-complexity single-antenna assisted mobile handsets or wireless nodes. The architecture of our proposed distributed coding scheme leads to substantial energy saving and performance gain. In addition, an error-detecting code based selective relaying protocol is also invoked in each cooperating node to prevent potential error propagation.

4.2.1 System Model and Design

A multi-relay aided two-way cooperative communication network architecture, illustrated in Fig. 4.9, is used throughout this chapter for the investigation of the proposed two-way distributed DSTBC scheme. To be more specific, a classic two-way cooperative network consists of two ordinary time-division half-duplex terminals (t_1, t_2) situated in symmetric locations and N parallel wireless nodes $(r_1, r_2, ..., r_N)$ supporting simultaneous exchange of information between the source and destination designated as the cooperating relays.

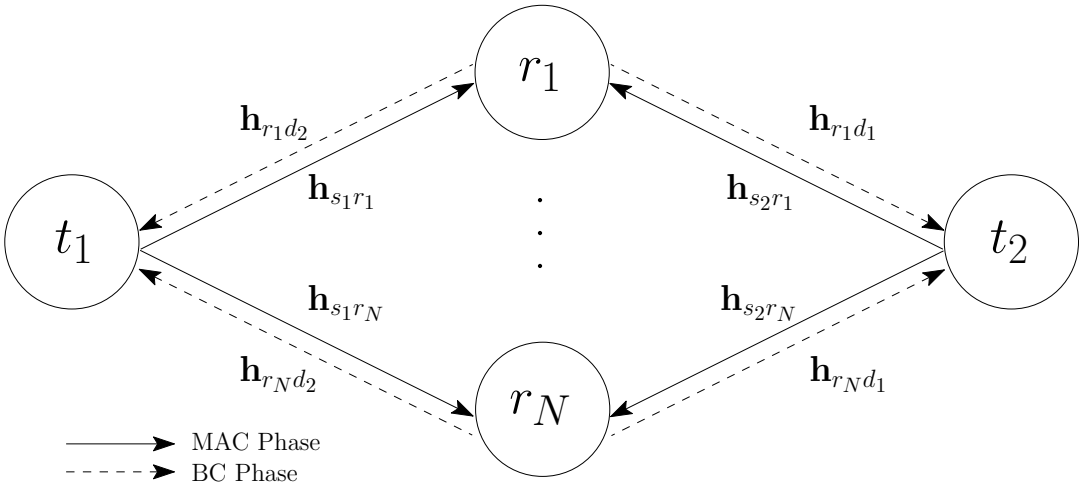

Figure 4.9: The schematic of the proposed DPSK-DDSTBC scheme for two-way relaying case.

Each terminal node operates as a source node (s) as well as a destination node (d); however transmitting and receiving at the same time slot is restrained due to the half-duplex limitation. It is noteworthy that all $N + 2$ nodes as seen in Fig. 4.9 are single-antenna wireless units with relatively low implementation complexity compared with conventional MIMO devices with multiple co-located antennas.

Furthermore, the classic unidirectional relaying protocol is extended in order to support simultaneous transmission from multiple users. Two-way relaying is realized by our novel superposition coding technique called differential physical-layer network coding (DPLNC), the primary interest of which is to directly extract the network-coded symbols from the superimposed received signals at the relay nodes rather than explicitly detecting the individual symbols when the channel information is unknown. Substantial amount of error performance and spectral efficiency improvement could be expected when proposed DPLNC is deployed in a cooperative DSTBC network. In this subsection we combine the advantage of distributed DSTBC with novel DPLNC-assisted bidirectional relaying, and propose a differential two-way relay scheme based on the DF protocol.

Transmission schedule in bidirectional cooperative scenarios has been well explained in Section 3.2.2, hence it is only briefly stated in this subsection as follows. The information emitted from one user takes two transmission slots to reach the destination via relay nodes, namely the multiple access (MAC) phase as well as the broadcast (BC) phase. To begin with, during the MAC phase, information sequence with equal-probability $\mathbf{x}_{s_i}$ is modulated into a frame of $\mathcal{M}$-ary PSK symbols $\mathbf{p}_{s_i}$ and further differentially-encoded into DPSK symbols $\mathbf{c}_{s_i}$ before being transmitted by t_1 and t_2 simultaneously. As a result, the received signal at the jth relay node is essentially the noisy version of the superposition

of two channel-corrupted $\mathcal{M}$-DPSK signals, which is written as

$$\mathbf{y}_{r_j} = \sum_{i=1}^{2} \left(\mathbf{h}_{s_i r_j} \mathbf{c}_{s_i} \right) + \mathbf{v}_{r_j} \ , \tag{4.15}$$

where $j \in \{1, 2, \ldots, N\}$ and $\mathbf{h}_{s_i r_j}$ is the Rayleigh block fading coefficients of the transmission link between the ith source node and the jth relay node implying that L symbols in one block are subject to the same Rayleigh fading. Moreover, $\mathbf{v}_{r_j}$ denotes the complex-valued AWGN imposed at the jth relay node with zero mean and variance $\sigma_I^2 = \sigma_Q^2 = N_0/2$ for both real and imaginary part.

Information bits transmitted from the ith source node could be estimated at the jth relay node, denoted as $\hat{\mathbf{x}}_{s_i}^{(r_j)}$, by treating signals from other source as interference. Therefore, the corresponding network-coded symbols are defined as

$$\mathbf{u}_{r_j} = \hat{\mathbf{x}}_{s_1}^{(r_j)} \oplus \hat{\mathbf{x}}_{s_2}^{(r_j)} \ , \tag{4.16}$$

where $\oplus$ indicates an element-by-element modulo-two addition performed in the Galois field GF(2^m), which can be simplified to the exclusive or arithmetic when $m = 1$. Fortunately, after the advent of differential PLNC, calculation of the network-coded symbols $\mathbf{u}_{r_j}$ becomes more efficient, since differential PLNC is able to generate corresponding network-coded symbols immediately from the superimposed signal $\mathbf{y}_{r_j}$. Due to the differential feature, the generation of network-coded symbols is implemented in a non-coherent fashion and is independent of the availability of channel coefficients. The detailed principle of differential PLNC is elaborated in following subsection.

During the BC phase, only correctly estimated network-coded symbols are re-encoded into distributed DSTBC symbols $\mathbf{w}_{r_j}$ and broadcasted to the destination nodes. Although each cooperating relay node only carries one row of the DSTBC code matrix, the combined received signals at the destination nodes are still valid DSTBC codewords. The received signal at the ith destination node can be expressed as:

$$\mathbf{y}_{d_i} = \sum_{j=1}^{N} \left(\mathbf{h}_{r_j d_i} \mathbf{w}_{r_j} \right) + \mathbf{v}_{d_i} \ , \tag{4.17}$$

where $i \in \{1, 2\}$ and $\mathbf{h}_{r_j d_i}$ denotes the complex-valued Rayleigh block fading coefficients of the channel between the jth relay node and the ith destination node, while $\mathbf{v}_{d_i}$ represents the AWGN induced at the ith destination node with zero mean and variance $\sigma_I^2 = \sigma_Q^2 = N_0/2$. It is noteworthy that the overall transmit power for the relay-to-destination link is normalized so that the average energy of the distributed DSTBC codewords is $\sum_{j=1}^{N} |\mathbf{w}_{r_j}|^2 = 1$.

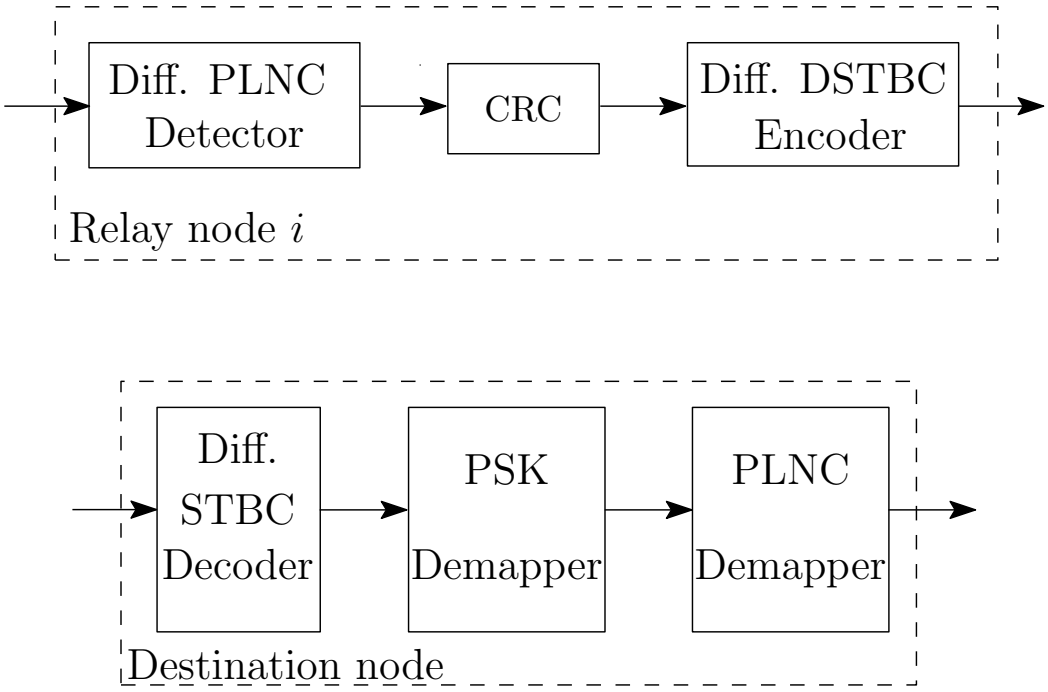

Figure 4.10: System structure for the differential PLNC aided two-way DPSK-DDSTBC scheme.

At the destination node, a conventional differential STBC decoder as proposed in [53] is invoked to obtain the estimate of the network-coded symbols $\hat{\mathbf{u}}_{r_j}$. Applying the exclusive-or arithmetic again between the estimated network-coded symbols and the information bits transmitted at the MAC phase so that each destination node is capable of retrieving the interested information transmitted from the source node by

$$\hat{\mathbf{x}}_{s_1} = \hat{\mathbf{u}}_{r_j} \oplus \mathbf{x}_{s_2} \ . \tag{4.18}$$

Similarly, for the information bits transmitted from s_2, we have:

$$\hat{\mathbf{x}}_{s_2} = \hat{\mathbf{u}}_{r_j} \oplus \mathbf{x}_{s_1} \ , \tag{4.19}$$

where $j \in \{1, 2, \ldots, N\}$. Owing to the linearity of the cyclic codes, each relay node is capable of distinguishing the integrity of the network-coded symbols generated from $\mathbf{y}_{r_j}$ by comparing the CRC of $\mathbf{u}_{r_j}$ with the 'modulo-two sum' of two CRCs corresponding to the information streams $\mathbf{x}_{s_1}$ and $\mathbf{x}_{s_2}$ from the source nodes. In other words, if the estimated information sequences pass the same CRC with identical generator polynomial, their modulo-two sum at the relay nodes will also pass. On the other hand, when one is in error, or both are in error but in different positions, the check will fail.

4.2.1.1 Differential Physical-layer Network Coding for Two-way Fading Channel

The principle and design procedure of the novel non-coherent or differential PLNC is elaborated and studied in this subsection. Non-coherent PLNC is evolved from the classic coherent PLNC with the same objective, that is to support bidirectional communication and recover the spectral efficiency loss caused by half-duplex constraint by calculating the network-coded symbols directly from the linear superposition of multiple complex-valued signals from source nodes.

One of the major limitations regarding the existing coherently-detected PLNC schemes is the requirement of prior knowledge of the channel state information at each receiving node. In general, the problem of accurate estimation of fading channel coefficients is solved by inserting pilot symbols periodically, which leads to spectral efficiency loss.

The contrivance of the novel non-coherent PLNC has drawn the inspiration from the differential demodulation, in which the channel information estimation is avoided by taking advantage of the connection between two adjacent symbols and processing the received signal successively.

Two similar research works on non-coherent transmission schemes for two-way relay channels are proposed recently in [94, 95]. However, existing schemes are less appealing in practice as a sophisticated ML-based sequence estimation is used to extract the network-coded symbols at each relay node inflicting high computational complexity. Furthermore, a Turbo-coded differential PLNC system utilizing frequency shift keying (FSK) modulation is presented in [96]. Although this scheme is less complex than [94, 95], FSK suffers from bandwidth inefficiency making it also less attractive in practice.

For ease of analysis, it is assumed that 2-level DBPSK modulation is invoked at two source nodes. Letting the differential encoding at the ith source node is initialized by the reference symbol $\mathbf{v}_{s_i}[0] = +1$, the received signal at the jth relay node is apparently the superposition of two DBPSK-modulated symbol sequences. For a DBPSK-modulated signal, there are three possible phasor combinations described as $\Lambda = (\mathbf{v}_{s_1} + \mathbf{v}_{s_2}) \in \tau$, where $\tau = \{-2, 0, +2\}$ for the case $\mathbf{h}_{s_1 r_j} = \mathbf{h}_{s_2 r_j} = 1$. As mentioned earlier, the principle of non-coherent PLNC relies on exploiting the dependence between the current received symbol and the previous one. The connection between the superimposed signal $\mathbf{y}_{r_j}$ and the desired network-coded symbols $\mathbf{u}_{r_j}$ is listed in Tab. 4.4.

After careful analysis of Tab. 4.4, the non-coherent PLNC decision rule is generalized as follows. The network-coded symbol at time instant T is uniquely defined by the modulus

Table 4.4: An example of non-coherent PLNC for detecting two superimposed DBPSK-modulated symbol sequences. The reference symbols for s_1 and s_2 are assumed to be $[+1, +1]$, and it is assumed that $\mathbf{h}_{s_1 r_j} = \mathbf{h}_{s_2 r_j} = 1$.

	Info. Bit		**Diff. Symbol**		$\mathbf{y}_{r_j}$	**Network-coded**
	$\mathbf{x}_{s_1}$	$\mathbf{x}_{s_2}$	$\mathbf{v}_{s_1}$	$\mathbf{v}_{s_2}$		**Symbol** $\mathbf{u}_{r_j}$
Time *T*	**0**	**0**	**+1**	**+1**	**+2**	**0**
	0	0	+1	+1	+2	0
Time	0	1	+1	-1	0	1
T + 1	1	0	-1	+1	0	1
	1	1	-1	-1	-2	0
Time *T*	**0**	**1**	**+1**	**-1**	**0**	**1**
	0	0	+1	-1	0	0
Time	0	1	+1	+1	+2	1
T + 1	1	0	-1	-1	-2	1
	1	1	-1	+1	0	0
Time *T*	**1**	**0**	**-1**	**+1**	**0**	**1**
	0	0	-1	+1	0	0
Time	0	1	-1	-1	-2	1
T + 1	1	0	+1	+1	+2	1
	1	1	+1	-1	0	0
Time *T*	**1**	**1**	**-1**	**-1**	**-2**	**0**
	0	0	-1	-1	-2	0
Time	0	1	-1	+1	0	1
T + 1	1	0	+1	-1	0	1
	1	1	+1	+1	+2	0

of two adjacent received DBPSK symbols. Specifically speaking, the resultant network-coded symbol acquired at time interval $T+1$ is equal to 0, if and only if the absolute value or modulus (for a complex-valued constellation) of the received superimposed symbols $|\mathbf{y}_{r_j}|$ at time $T+1$ is identical to that at time T. On the other hand, the corresponding network-coded symbol is calculated as 1 when the value of $|\mathbf{y}_{r_j}|$ is observed swapping from one to the other.

Moreover, the assumption of $\mathbf{h}_{s_1r_j} = \mathbf{h}_{s_2r_j} = 1$ is relaxed in following discussion to allow extensions to the fading channel h, which is generally expressed as $h = |a|e^{j\theta}$ with the fading amplitude $|a|$ and phase shift of θ. In order to provide better understanding of the proposed non-coherent PLNC detector, Fig. 4.11 demonstrates the constellation diagram of the superimposed signal at the jth relay node with the absence of noise for different channel realizations. It is important to notice that the solid and dashed lines in Fig. 4.11 are for demonstration purpose and are not indication of the actual decision regions.

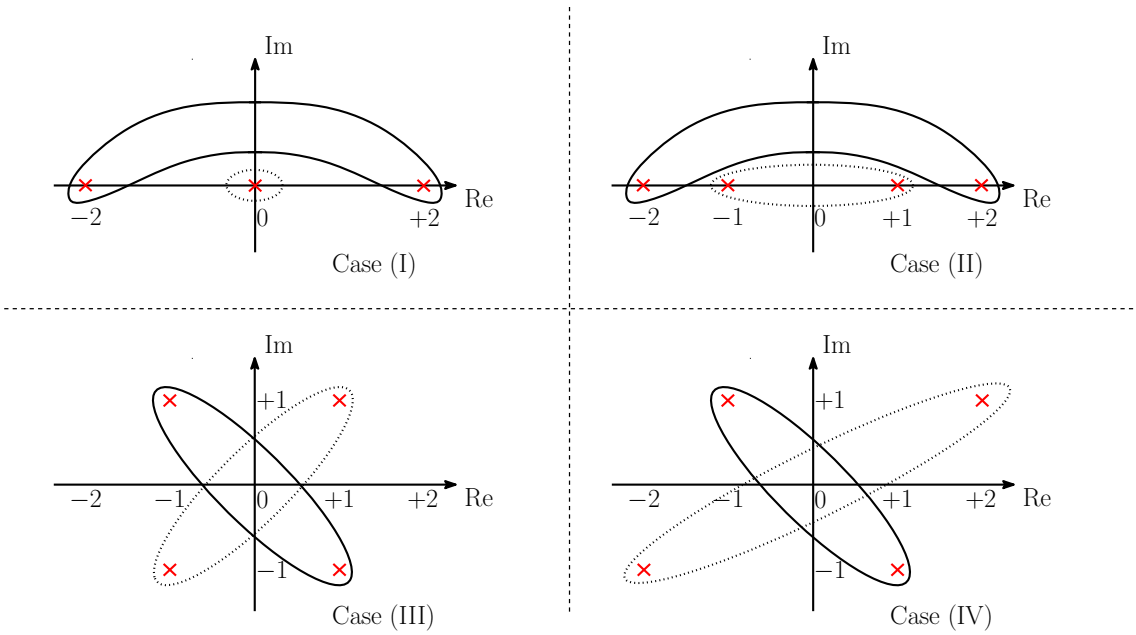

Figure 4.11: The constellation diagrams of the superimposed signal received by the relay node in a noise-free scenario.

Four specific channel conditions denoted as Case (I) – (IV) are summarized as follows:

- Case (I): $|h_{s_1r_j}| = |h_{s_2r_j}|$, $|\theta_1 - \theta_2| = n\pi$;
- Case (II): $|h_{s_1r_j}| \neq |h_{s_2r_j}|$, $|\theta_1 - \theta_2| = n\pi$;
- Case (III): $|h_{s_1r_j}| = |h_{s_2r_j}|$, $|\theta_1 - \theta_2| = \frac{(2n+1)\pi}{2}$;

- Case (IV): $|h_{s_1r_j}| \neq |h_{s_2r_j}|$, $|\theta_1 - \theta_2| \neq \frac{n\pi}{2}$;

where the integer $n = \{0, 1, 2, \ldots\}$.

As we can see from Fig. 4.11, constellation points are classified into two distinct groups delineated by the solid lines and the dashed lines. Recall that the non-coherent PLNC detection operates on pairs of two consecutive received symbols. Therefore, when two adjacent received symbols from one pair both fall into the same group indicating the modulus of two recently received symbols is identical, which results in a network-coded symbol 0. On the contrary, if two successively received symbols belong to different groups, the corresponding network-coded symbol is thereby detected as 1.

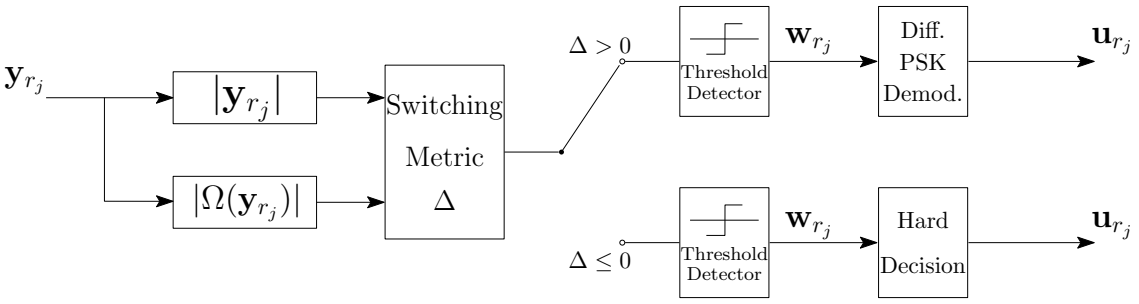

Figure 4.12: The schematic of the proposed non-coherent PLNC detector with a low-complexity dual-branch structure.

The schematic of the proposed dual-branch non-coherent PLNC detector is depicted in Fig. 4.12. The detection procedure is interpreted into the upper-branch of the non-coherent PLNC detector shown in Fig. 4.12. To elaborate further, each superimposed symbol is appropriately assigned to one group by a simple threshold detector, where the choice of threshold is determined by the mean of $|\mathbf{y}_{r_j}|$ denoted as ψ. It can be obtained by taking the average over all elements of $|\mathbf{y}_{r_j}|$ within one frame. Therefore, the product of the threshold detector, $\mathbf{w}_{r_j}$, can be mathematically described as

$$\mathbf{w}_{r_j}[n] = \begin{cases} -1 & \text{if } |\mathbf{y}_{r_j}[n]| > \psi, \\ 1 & \text{if } |\mathbf{y}_{r_j}[n]| \leq \psi, \end{cases}$$

where n is the symbol index. After that, a conventional DPSK demodulator is invoked to accurately estimate the network-coded symbols by comparing the modulus of one specific symbol to that of the previous one and determining whether two neighboring symbols from $\mathbf{w}_{r_j}$ are assigned to the same group.

Unfortunately, it is noteworthy that this detection rule would not succeed for Case (III) in Fig. 4.11, since it is unable to distinguish the four constellation points due to identical amplitude. As a remedy, the lower branch is specially devised to cope with scenario like Case (III). Instead of computing the modulus of $\mathbf{y}_{r_j}$, a threshold detector is applied to the modulus of $\Omega(\mathbf{y}_{r_j})$, namely $|\Omega(\mathbf{y}_{r_j})|$ and categorizes symbols from $|\Omega(\mathbf{y}_{r_j})|$ into two different groups. The nth received symbol at the jth relay node is expressed as

$$\mathbf{y}_{r_j}[n] = \mathbf{h}_{s_1 r_j}[n]\mathbf{v}_{s_1}[n] + \mathbf{h}_{s_2 r_j}[n]\mathbf{v}_{s_2}[n] + \mathbf{m}_{r_j}[n] \, . \tag{4.20}$$

Similarly, the received symbol at the previous transmission slot is given by

$$\mathbf{y}_{r_j}[n-1] = \mathbf{h}_{s_1 r_j}[n-1]\mathbf{v}_{s_1}[n-1] + \mathbf{h}_{s_2 r_j}[n-1]\mathbf{v}_{s_2}[n-1] + \mathbf{m}_{r_j}[n-1] \, . \tag{4.21}$$

The definition of function $\Omega(\cdot)$ is formulated by Eq. (4.22), Eq. (4.23) and Eq. (4.24) as follows. Note that all noise related terms are neglected for a concise presentation.

$$\begin{aligned}
\mathbf{y}_{r_j}[n]\mathbf{y}^*_{r_j}[n-1] &= \mathbf{h}_{s_1 r_j}\mathbf{v}_{s_1}[n]\mathbf{h}^*_{s_1 r_j}\mathbf{v}^*_{s_1}[n-1] + \mathbf{h}_{s_1 r_j}\mathbf{v}_{s_1}[n]\mathbf{h}^*_{s_2 r_j}\mathbf{v}^*_{s_2}[n-1] \\
&\quad + \mathbf{h}^*_{s_1 r_j}\mathbf{v}^*_{s_1}[n-1]\mathbf{h}_{s_2 r_j}\mathbf{v}_{s_2}[n] + \mathbf{h}_{s_2 r_j}\mathbf{v}_{s_2}[n]\mathbf{h}^*_{s_2 r_j}\mathbf{v}^*_{s_2}[n-1] \, , \\
&= |\mathbf{h}_{s_1 r_j}|^2\mathbf{p}_{s_1} + \mathbf{h}_{s_1 r_j}\mathbf{h}^*_{s_2 r_j}\mathbf{v}_{s_1}[n]\mathbf{v}^*_{s_2}[n-1] + \mathbf{h}^*_{s_1 r_j}\mathbf{h}_{s_2 r_j}\mathbf{v}^*_{s_1}[n-1]\mathbf{v}_{s_2}[n] \\
&\quad + |\mathbf{h}_{s_2 r_j}|^2\mathbf{p}_{s_1} \, ,
\end{aligned} \tag{4.22}$$

$$\begin{aligned}
\mathbf{y}^*_{r_j}[n]\mathbf{y}_{r_j}[n-1] &= \mathbf{h}^*_{s_1 r_j}\mathbf{v}^*_{s_1}[n]\mathbf{h}_{s_1 r_j}\mathbf{v}_{s_1}[n-1] + \mathbf{h}^*_{s_1 r_j}\mathbf{v}^*_{s_1}[n]\mathbf{h}_{s_2 r_j}\mathbf{v}_{s_2}[n-1] \\
&\quad + \mathbf{h}_{s_1 r_j}\mathbf{v}_{s_1}[n-1]\mathbf{h}^*_{s_2 r_j}\mathbf{v}^*_{s_2}[n] + \mathbf{h}^*_{s_2 r_j}\mathbf{v}^*_{s_2}[n]\mathbf{h}_{s_2 r_j}\mathbf{v}_{s_2}[n-1] \, , \\
&= |\mathbf{h}_{s_1 r_j}|^2\mathbf{p}^*_{s_1} + \mathbf{h}_{s_1 r_j}\mathbf{h}^*_{s_2 r_j}\mathbf{v}_{s_1}[n-1]\mathbf{v}^*_{s_2}[n] + \mathbf{h}^*_{s_1 r_j}\mathbf{h}_{s_2 r_j}\mathbf{v}^*_{s_1}[n]\mathbf{v}_{s_2}[n-1] \\
&\quad + |\mathbf{h}_{s_2 r_j}|^2\mathbf{p}^*_{s_2} \, ,
\end{aligned} \tag{4.23}$$

$$\begin{aligned}
\Omega(\mathbf{y}_{r_j}) &= \mathbf{y}_{r_j}[n]\mathbf{y}^*_{r_j}[n-1] - \mathbf{y}^*_{r_j}[n]\mathbf{y}_{r_j}[n-1] \\
&= |\mathbf{h}_{s_1 r_j}|^2\mathbf{p}_{s_1} + \mathbf{h}_{s_1 r_j}\mathbf{h}^*_{s_2 r_j}\mathbf{v}_{s_1}[n]\mathbf{v}^*_{s_2}[n-1] + \mathbf{h}^*_{s_1 r_j}\mathbf{h}_{s_2 r_j}\mathbf{v}^*_{s_1}[n-1]\mathbf{v}_{s_2}[n] \\
&\quad + |\mathbf{h}_{s_2 r_j}|^2\mathbf{p}_{s_2} - (|\mathbf{h}_{s_1 r_j}|^2\mathbf{p}^*_{s_1} + \mathbf{h}_{s_1 r_j}\mathbf{h}^*_{s_2 r_j}\mathbf{v}_{s_1}[n-1]\mathbf{v}^*_{s_2}[n] \\
&\quad + \mathbf{h}^*_{s_1 r_j}\mathbf{h}_{s_2 r_j}\mathbf{v}^*_{s_1}[n]\mathbf{v}_{s_2}[n-1] + |\mathbf{h}_{s_2 r_j}|^2\mathbf{p}^*_{s_2}) \\
&= 2(\mathbf{p}_{s_1} - \mathbf{p}_{s_2})\mathrm{Im}\Big\{\mathbf{h}_{s_1 r_j}\mathbf{h}^*_{s_2 r_j}\mathbf{v}_{s_1}[n-1]\mathbf{v}^*_{s_2}[n-1]\Big\} \, .
\end{aligned} \tag{4.24}$$

Owing to the fact that $\mathbf{v}_{s_1}[n-1]$ and $\mathbf{v}_{s_2}[n-1]$ are real-valued DBPSK symbols and channel coefficients $\mathbf{h}_{s_1 r_j}$ and $\mathbf{h}_{s_2 r_j}$ are constant during the whole frame under quasi-static channel assumption, $2\mathrm{Im}\{\mathbf{h}_{s_1 r_j}\mathbf{h}^*_{s_2 r_j}\mathbf{v}_{s_1}[n-1]\mathbf{v}^*_{s_2}[n-1]\}$ is considered as a scaling factor.

Furthermore, the one-to-one mapping between $\mathbf{p}_{s_1} - \mathbf{p}_{s_2}$ and network-coded symbols $\mathbf{u}_{r_j}$ is outlined in Tab. 4.5, which facilitates the extraction of network-coded symbols with a simple hard-decision device as illustrated in the lower-branch of Fig. 4.12.

$$\mathbf{u}_{r_j}[n] = \begin{cases} 1 & \text{if } \mathbf{w}_{r_j}[n] = -1, \\ 0 & \text{if } \mathbf{w}_{r_j}[n] = 1. \end{cases}$$

Table 4.5: The relationship between the BPSK-modulated symbols $\mathbf{p}_{s_1}$, $\mathbf{p}_{s_2}$ and network-coded symbols $\mathbf{u}_{r_j}$.

$\mathbf{p}_{s_1}$	$\mathbf{p}_{s_2}$	$\mathbf{p}_{s_1} - \mathbf{p}_{s_2}$	Network-coded symbols $\mathbf{u}_{r_j}$
1	1	0	0
1	-1	+2	1
-1	1	-2	1
-1	-1	0	0

Finally, a switching metric Δ is incorporated to decide which branch is more appropriate for the detection of the network-coded symbols $\mathbf{u}_{r_j}$. The switching metric Δ is defined as follows

$$\Delta = \mathrm{Var}\{|\mathbf{y}_{r_j}|\} - \mathrm{Var}\{|\Omega(\mathbf{y}_{r_j})|\} \,, \tag{4.25}$$

where $\mathrm{Var}\{a\}$ is the variance of sequence a. If $\Delta > 0$, the upper branch is selected; while $\Delta \leq 0$, the lower branch would be more appropriate.

4.2.1.2 Performance Results and Discussion

The error performances of the novel non-coherent PLNC as well as the proposed distributed DSTBC aided two-way relaying communication scheme are evaluated in this subsection. System robustness against fading and other interferences is investigated under quasi-static Rayleigh fading channels where the fading coefficients experienced by one frame are near-constant, but vary from frame to frame. As shown in the network topology in Fig. 4.9, it is assumed that the two relay nodes are situated in the mid-way of direct line-of-sight path between terminal nodes t_1 and t_2 with reliable communication links. In order to make fair comparison, the energy used for the transmission of DPSK

Table 4.6: Simulation parameters for the following BER performance evaluation.

Simulation Parameters	
Parameters	**Values**
Modulation Scheme	DBPSK
Path-gain of Source-to-Relay Link	1
Path-gain of Relay-to-Destination Link	1
CRC Generator Polynomial	$[x^8 + x^7 + x^4 + x^3 + x + 1]$
Maximum Length of Frame	200/500/1000
Eb/N0 Range	0–30 dB
Channel Type	Quasi-static Rayleigh Fading Channel

signals at source nodes as well as transmission of distributed DSTBC codewords from relay nodes is normalized to unity. Detailed simulation configuration is given in Tab. 4.6.

To begin with, the error performance of the proposed non-coherent PLNC aided bidirectional cooperative network under Rayleigh fading channel is depicted in Fig. 4.13. Bit error rate of the MAC phase measured at intermediate relaying nodes is compared with its coherent counterpart. As we can see from Fig. 4.13, the error probability of the proposed scheme is capable of decreasing as rapidly as the coherent PLNC when the E_b/N_0 grows; however, a performance degradation of 6.5 dB is witnessed at BER$= 10^{-2}$ due to the non-coherent detection of network-coded symbols from the superimposed signal.

Moreover, the end-to-end BER calculated at the destination node is also presented in Fig. 4.13 and compared against the coherent scenario. Note that, at this moment, DPSK is used to modulate the network-coded symbols during BC stage and later DPSK modulator is replaced with the novel distributed DSTBC encoder. The end-to-end error performance is quantified and measured based on the statistical average of the bit error probability at t_1 and t_2. Similar to the results obtained for the MAC phase, although the BER curves of coherent and non-coherent PLNC schemes share the same slope, non-coherent scheme is approximately 5.5 dB inferior due to the lack of accurate channel information.

The results of other coherent bidirectional collaborative protocols that are designed and

employed in the relay nodes to support simultaneous information exchange, including 4-timeslot traditional scheduling and 3-timeslot network coding approach, are also provided for comparative purpose. Since different number of transmission slots are involved in three cases, for the sake of giving a fair comparison, the overall transmit energy is scaled and equally split among the source and relay nodes.

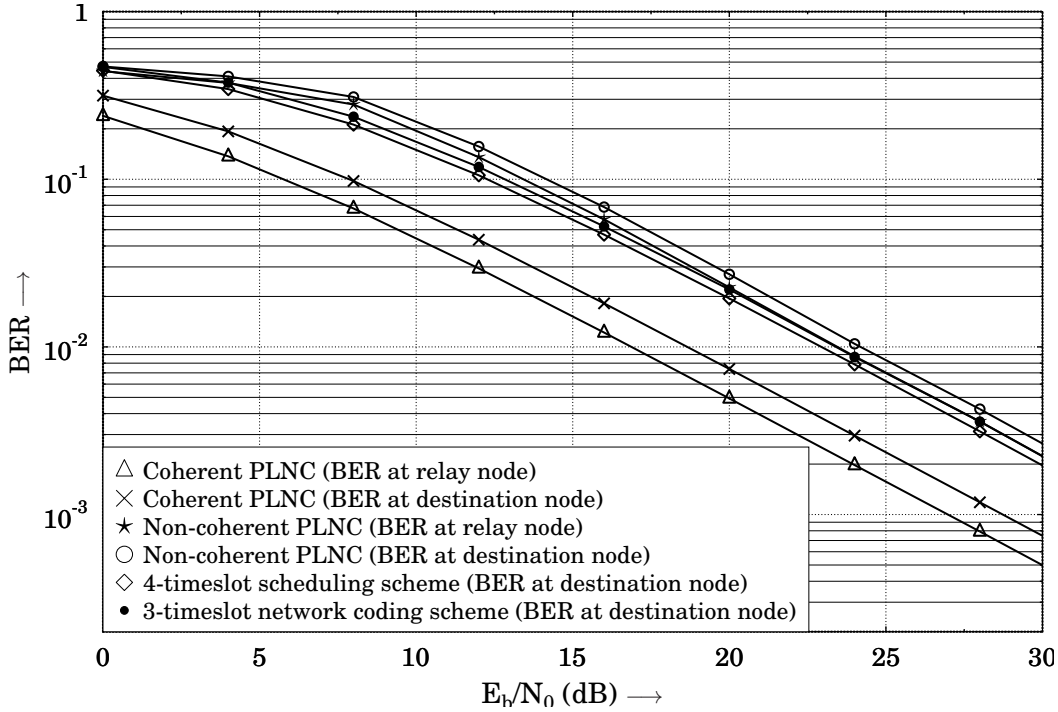

Figure 4.13: BER versus E_b/N_0 performance of the proposed novel non-coherent PLNC aided two-way cooperative system when communicating over quasi-static Rayleigh fading channel, where the frame length is 1×10^4.

As illustrated in Fig. 4.13, the 4-timeslot cooperative scheme is viewed as the succession of two independent conventional unidirectional transmissions in each direction; hence it is superior in terms of the end-to-end BER performance. On the other hand, the 3-timeslot network coding assisted relaying protocol, in which the MAC phase is fulfilled within two channel uses, may yield a higher network throughput compared with 4-timeslot scheme, albeit this is achieved at the cost of about 1.0 dB performance degradation. Last but not the least, as suggested in Fig. 4.13, if allowing another 0.2 dB extra energy at the source transmitters, non-coherent PLNC is also capable of performing as well as the 4-timeslot relaying scheme in terms of the end-to-end BER while at the same time doubling the spectral efficiency and throughput.

Next, our scheme is compared with other existing approaches developed in the literature [94, 95]. In order to make a fair comparison, we duplicate their differential PLNC detectors, incorporate into current simulation model and make sure all simulation parameters

are identical. As illustrated in Fig. 4.14, although the novel non-coherent PLNC detector has poorer BER performance at low E_b/N_0 regime (smaller than 10.0 dB), the slope of corresponding BER curve is steeper than those using sequence estimation. Furthermore, at higher E_b/N_0, our scheme can outperform the existing non-coherent approaches by 1.0 dB and 2.5 dB respectively, at BER $= 10^{-2}$.

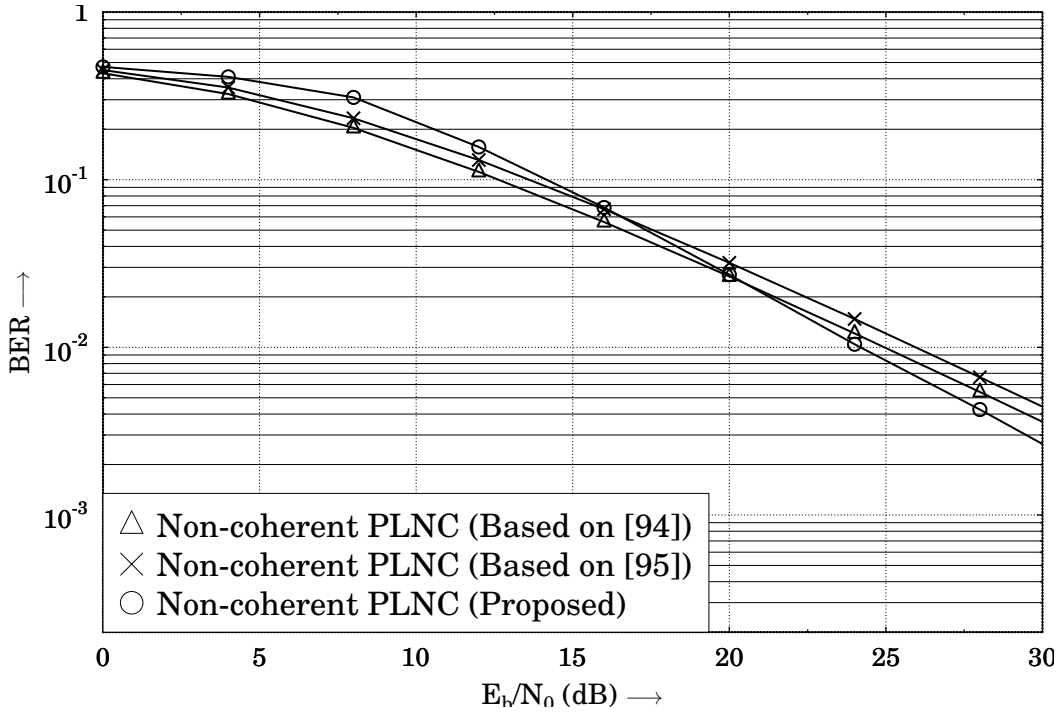

Figure 4.14: Comparison of end-to-end BER performance between the proposed novel non-coherent PLNC scheme and other existing approaches.

In the rest of this subsection, we combine the benefits of distributed DSTBC with non-coherent two-way relaying techniques, and propose a selective relaying aided DPSK-DDSTBC scheme for two-way cooperative communication. By applying the novel differential PLNC discussed in the last subsection as well as selective relaying strategy at each relay node, we show that our proposed scheme with high-throughput is capable of approaching full diversity order without accurate estimation of the CSI in two-way relaying scenarios.

Fig. 4.15 portrays the end-to-end BER comparison of proposed fully non-coherent distributed coding scheme and distributed STBC scheme with coherent PLNC introduced in [97]. Although multiple number of co-located antennas and channel state information are available at neither the relay nor destination nodes, it is confirmed in Fig. 4.15 that full diversity order is still achievable albeit approximately 6.0 dB degradation due to the non-coherent signal detection conducted at both relay and destination nodes.

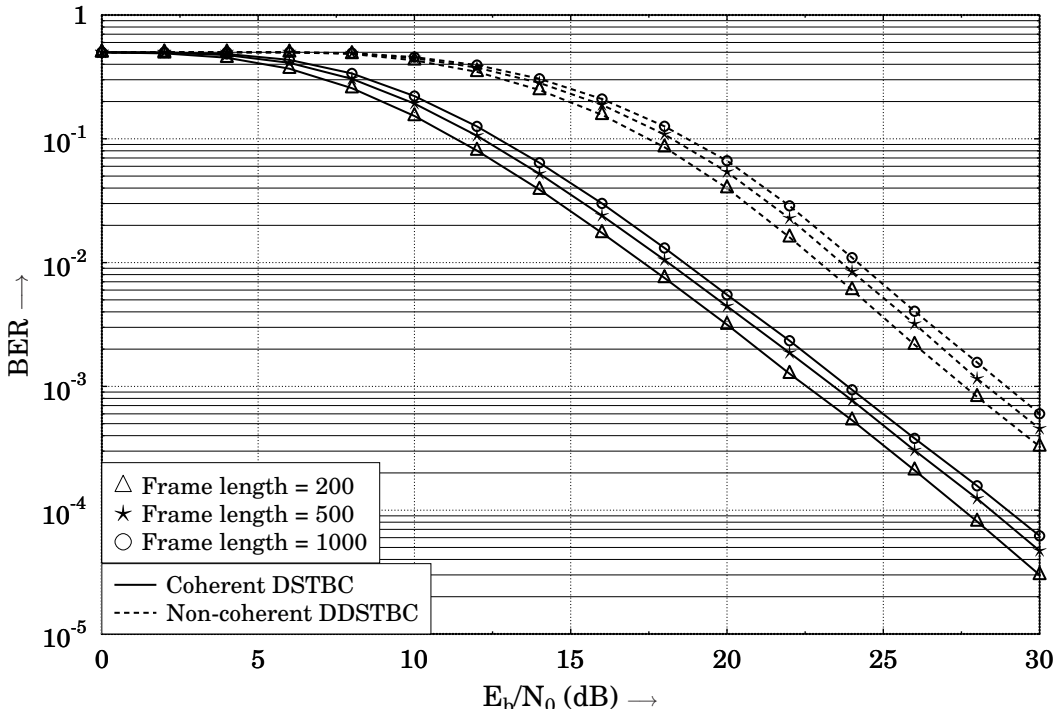

Figure 4.15: BER versus E_b/N_0 performance of the proposed novel non-coherent PLNC aided distributed DSTBC scheme with selection relaying strategy when communicating over quasi-static Rayleigh fading channel.

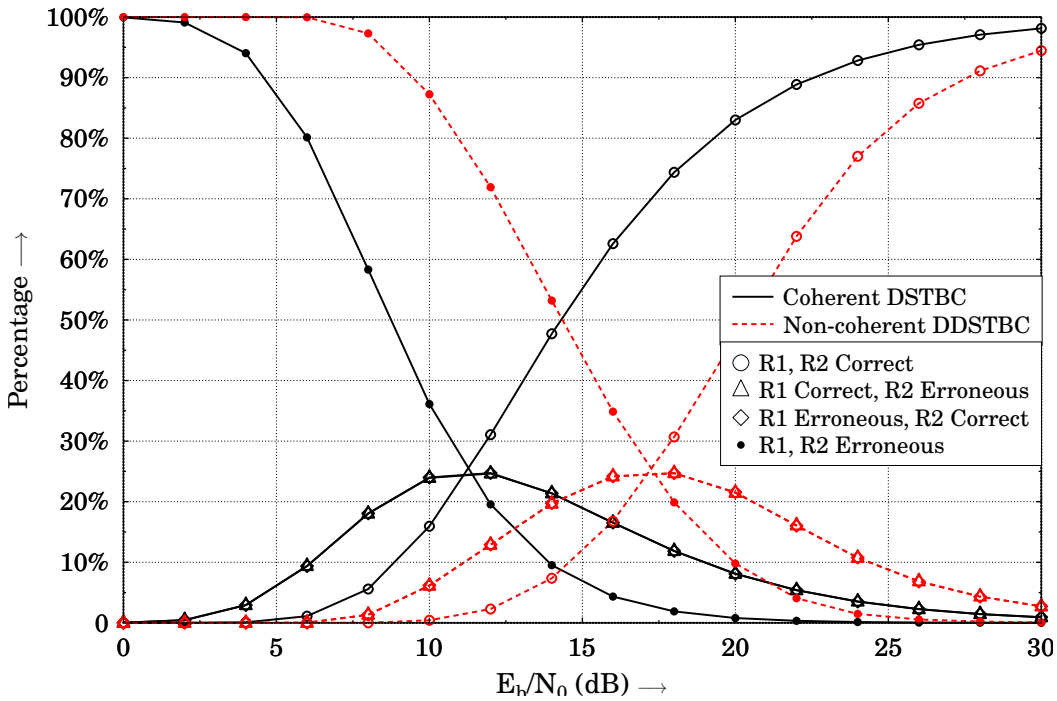

Figure 4.16: Percentage of correctly and erroneously detected network-coded symbols in two relay nodes at different E_b/N_0, when the frame length is 500.

Similar to the distributed DSTBC relaying scheme in one-way scenario, the novel bidirectional distributed DSTBC system is also sensitive to the frame length as it increases from 200 to 1000. The underlying reason is that the number of valid distributed DSTBC codewords constructed by two relay nodes would decline as the block size is relatively large.

Take a fixed frame length of 500 DPSK symbols for example, Fig. 4.16 demonstrates the percentage of correctly and erroneously estimated network-coded symbols in two relay nodes. As shown in Fig. 4.16, when E_b/N_0 is smaller than 6.0 dB, neither of the two relay nodes succeed in generating the network-coded symbols without error, which leads to a extremely high end-to-end error rate as confirmed by Fig. 4.15.

As the E_b/N_0 increases to 15.0 dB, the percentage of incorrect detection decreases to less than 50%. When keeping increasing E_b/N_0 to 25.0 dB, the percentage of both relay nodes produce correct estimation of the network-coded symbols is rising and exceeding 80%, which in return implies that more than 80% of the network-coded symbols are re-encoded and transmitted from two relay nodes during BC phase using distributed DSTBC.

4.3 Conclusion

A novel distributed differential STBC scheme for multi-relay assisted unidirectional as well as bidirectional cooperative communication systems based on 'decode-and-forward' relaying protocol are introduced and studied in this chapter. Some distinguished contributions of these schemes can be summarized as follows:

- The novel CRC-based selection relaying aided distributed DSTBC cooperative scheme is still capable of exploiting full transmit diversity gain utilizing non-coherent decoding and detection, even if the network only consists of a cluster of mobile units having single antenna.
- Numerical analysis of the end-to-end bit error probability for the proposed DPSK-DDSTBC two-hop scheme is given in this chapter. The well-known MGF approach is employed to derivate the theoretical results. Comparison of analytical and empirical results confirms that the analysis is accurate and precise.
- In order to mitigate the performance degradation with respect to the frame length in a uncoded distributed coding system, a Turbo-coded DPSK-DDSTBC scheme

is devised for the one-way cooperation scenario. Redundancy introduced from the Turbo encoding readily overcomes the problem of frame length limitation. More importantly, the substantial coding gain provided by Turbo code could effectively boost the performance.

- A novel non-coherent PLNC scheme is investigated in the context of bidirectional relaying. It is designed to cope with the simultaneous transmission of radio signals from two users when the CSI is not available. Our scheme using a dual-branch non-coherent PLNC detector imposes lower complexity in the intermediate relay nodes, but is still able to achieve similar performance, compared with other existing approaches.

- Finally, the advantage of distributed DSTBC is combined with two-way relaying techniques to support high network throughput. Previously-proposed non-coherent PLNC is invoked at each cooperating node to estimate the network-coded symbols, which are later re-encoded by distributed DSTBC for transmission during BC phase. It is shown that our novel two-way DPSK-DDSTBC with opportunistic relaying is capable of doubling the network throughput, while retaining full diversity gain.

Chapter 5

Iterative Detection of Channel-coded Differential Schemes in Fast Fading Channels

Contents

5.1 Principle of Iterative Decoding

Iterative decoding and detection technique, also referred to as "turbo principle", has been applied to various state-of-the-art coding schemes. Modern telecommunication systems incorporating serial or parallel concatenation of multiple component encoders in the transmitter and iterative (turbo) decoding in the receiver could bring significant performance gain at the cost of increased complexity to the decoder but still at reasonable level. The fundamental of turbo principle is the exchange of soft information (probability or log-likelihood ratio (LLR)) among component decoders/detectors. A detector or decoder that operates with soft information, is generally termed as a soft-in/soft-out (SISO) detector or decoder. In next subsection, we review and investigate some basics of the SISO decoder and the principles of iterative decoding and detection.

5.1.1 Log-Likelihood Ratio (LLR)

The concept of log-likelihood ratio was introduced by Robertson in 1994 [98] to simplify the description of information flowing from one component decoder to the other in the context of iterative decoding. The LLR of a data bit u_k, denoted as $L(u_k)$, is defined as the logarithmic ratio of the probabilities of u_k equals to $+1$ and -1, which is written as [26]

$$L(u_k) \triangleq \ln\left(\frac{P(u_k=+1)}{P(u_k=-1)}\right) . \tag{5.1}$$

The likelihood of either the data bit is $+1$ or -1 can be interpreted from Eq. (5.1), since the sign of the LLR gives an indication of polarity whereas the magnitude of the LLR shows how likely the estimation is. Note that, $L(u_k) \approx 0$, when $P(u_k=+1) \approx P(u_k=-1) \approx 0.5$, which implies a zero LLR represents the original data bit could be either $+1$ or -1 with equal probability.

On the other hand, for a given LLR value $L(u_k)$, we can also calculate the probability of u_k equals to $+1$ or -1 from the LLR inversely using the following formula

$$P(u_k=\pm 1) = \left(\frac{e^{-L(u_k)/2}}{1+e^{-L(u_k)}}\right) \cdot e^{\pm L(u_k)/2} . \tag{5.2}$$

Similar to the LLR computation based on the unconditional probabilities $P(u_k=\pm 1)$, LLRs calculated from the conditional probabilities are also useful for the design of SISO decoding algorithm, it gives [26]

$$L(u_k|\underline{y}) \triangleq \ln\left(\frac{P(u_k=+1|\underline{y})}{P(u_k=-1|\underline{y})}\right) , \tag{5.3}$$

where the term $P(u_k=\pm 1|\underline{y})$ is defined as the *a-posteriori* probabilities of the bit u_k conditioned on the received signal sequence $\underline{y}$. Furthermore, with the assistance of the Bayes' theorem, the conditional LLR calculated at the output of matched filter y_k in the receiver with respect to the transmitted bit $x_k=\pm 1$ is defined as

$$L(y_k|x_k) \triangleq \ln\left(\frac{P(y_k|x_k=+1)}{P(y_k|x_k=-1)}\right) . \tag{5.4}$$

Example

Let us consider a BPSK transmission over AWGN or fading channel, the probability of matched filter output y_k is given by the PDF of the Gaussian noise

$$P(y_k|x_k=\pm 1) = \frac{1}{\sigma\sqrt{2\pi}} \exp\left(-\frac{E_b}{2\sigma^2}(y_k \mp h)^2\right) , \tag{5.5}$$

where E_b is the bit energy, σ^2 is the variance of noise and h is the coefficient of channel fading.

Hence, the soft output of the channel is described by the conditional LLR as follows

$$L(y_k|x_k) \triangleq \ln\left(\frac{P(y_k|x_k=+1)}{P(y_k|x_k=-1)}\right) = \ln\left(\frac{\exp\left(-\frac{E_b}{2\sigma^2}(y_k-h)^2\right)}{\exp\left(-\frac{E_b}{2\sigma^2}(y_k+h)^2\right)}\right) = \frac{2hE_b}{\sigma^2}\cdot y_k\ , \quad (5.6)$$

where the constant $2hE_b/\sigma^2$ is referred to as the channel reliability value which is related to the SNR and fading coefficient of the channel.

5.1.2 Maximum A-Posteriori (MAP) Algorithm

Maximum A-Posteriori (MAP) algorithm was originally designed by Bahl *et al* in 1974 [99] to decode both block and convolutional codes with the objective of minimizing the symbol error rate (SER) when systems are subject to memoryless noise. At early stages of the coding history, MAP algorithm did not exhibit its powerful decoding capability as it had almost the same performance compared with Viterbi algorithm [100] yet higher implementation complexity since MAP is devised to examine every possible path in the trellis. Moreover, MAP algorithm is less efficient when processing the received signal sequence with long frame length as the required memory would increase rapidly with the sequence length.

MAP algorithm has become popular after the advent of the ground-breaking Turbo code in 1993 [101], some unique characteristics of it greatly facilitate the iterative decoding for the serial and parallel concatenation of several component codes, such as Turbo code. For instance, MAP decoder is capable of providing not only the estimated data sequence, but also calculating the likelihood of one specific bit has been decoded correctly. Since then, MAP algorithm and MAP decoder are widely used in various applications.

In [102], a revision of the original MAP algorithm was introduced, the proposed MAP algorithm operates in logarithmic-domain, hence termed Log-MAP algorithm. The problem of high computational complexity of the original MAP algorithm as well as numerical issues experienced in computer simulation are successfully resolved.

5.1.2.1 Principle of MAP Algorithm

Prior to explaining the principle of MAP algorithm, we define the following notations.

Definition of Notations

u_k Information symbols with M different values, where $k = 1, 2, \ldots, N$.

x_k Coded symbols generated from encoder.

y_k Received symbols, $y_k = x_k + n_k$ when transmitted over AWGN channel, n_k is the complex AWGN sample.

m Possible values of the information symbol given by the received sequence, where $m = 0, 1, \ldots, M-1$.

$s_{k-1} = j$ Trellis state j at time index $k-1$.

$s_k = i$ Trellis state i at time index k.

$P(i, m)$ Trellis transition function: from current state i to previous state, when the input value is m.

$N(j, m)$ Trellis transition function: from current state j to next state, when the input value is m.

$L(j, m)$ Symbol transmitted when one specific branch in the trellis is encountered. For example, if the branch emitting from state $s_{k-1} = j$ to $s_k = N(j, m)$ is encountered, the corresponding input symbol is $u_k = m$ and transmitted symbol is $L(j, m)$, respectively.

The objective of the MAP decoding is to calculate the *a-posteriori* probability (APP) of the transmitted symbols from the observed sequence, i.e. $A_{k,m} = p(u_k = m|y_k)$ for $m = \{0, 1, \ldots, M-1\}, k = \{1, 2, \ldots, N\}$ based on the channel value and *a-priori* probability provided by other SISO constituent decoder. The MAP decoder can therefore determine the one having the largest APP is the transmitted information symbol. It is abovementioned that the MAP algorithm is able to minimize the SER by searching all legitimate paths in the trellis and selecting the one that is most likely. On the contrary, the Viterbi algorithm (VA) [100] generally guarantees the minimized frame error as it only searches for the most likely transmitted symbol sequence.

The principle of MAP decoding is briefly summarized in the following steps:

Step 1 It is assumed that the *a-priori* probabilities of the information symbols, denoted by Π_k, are known. We calculate the probabilities of channel metric $\eta_k(j, m)$ which

indicate the conditional probabilities of receiving the sample y_k given the previous state $s_{k-1} = j$ and the encountered information symbol $u_k = m$ by the following formula [26, 103]

$$\eta_k(j,m) = p(y_k|u_k = m, s_{k-1} = j) = \exp\left(\frac{-|y_k - L(j,m)|^2}{2\sigma^2}\right), \tag{5.7}$$

where σ^2 is the variance of the noise.

Step 2 Based on the *a-priori* probability of the kth information symbol $\Pi_{k,m}$ and Eq. (5.7) obtained in Step 1, the **branch transition metric** $\gamma_k(j,m)$, which only depends on the current received symbol y_k ($k = 1, 2, \ldots, N$), is calculated as

$$\gamma_k(j,m) = p(y_k, u_k = m|s_{k-1} = j) = \Pi_{k,m} \cdot \eta_k(j,m) . \tag{5.8}$$

Step 3 Subsequently, the **forward recursion metric** $\alpha_{k-1}(j)$ as well as the **backward recursion metric** $\beta_k(i)$ are computed in a recursive manner as follows

$$\alpha_k(i) = \sum_{m=0}^{M-1} \alpha_{k-1}\big(P(i,m)\big) \cdot \gamma_k\big(P(i,m), m\big) , \tag{5.9}$$

similarly,

$$\beta_{k-1}(j) = \sum_{m=0}^{M-1} \beta_k\big(N(j,m)\big) \cdot \gamma_k(j,m) . \tag{5.10}$$

Step 4 Gathering Eq. (5.8)-Eq. (5.10), the desired APP is defined as the product of channel metric, forward recursion as well as backward recursion metrics, which yields

$$\bar{A}_{k,m} = \Pi_{k,m} \cdot \sum_{j=0}^{S-1} \alpha_{k-1}(j) \cdot \beta_k\big(N(j,m)\big) \cdot \eta_k(j,m) , \tag{5.11}$$

where the integer S represents the total number of trellis states.

5.1.2.2 Logarithmic MAP Algorithm

As mentioned earlier, a feasible solution to reducing the computational complexity and computer overflow issue is to replace the original MAP algorithm with the Log-MAP algorithm [102], which is evolved from the former and maintains all superiority of the original scheme. As the name suggests, calculations in the Log-MAP algorithm are conducted in the logarithmic domain instead of the linear domain. Since the essential of the novel Log-MAP algorithm is a mathematical transformation carried out in the logarithmic domain, the performance is expected to be identical to that of the MAP decoding.

To elaborate further, from the mathematical perspective, in the logarithmic domain, the operation of multiplication could be simplified to addition. Therefore, the total amount of computational load could be highly compressed while maintaining the same decoding performance.

In order to pursue further simplification of the Log-MAP scheme, two additional sub-optimal Log-MAP algorithms are proposed based on the Jacobian logarithmic approximation. The benefit primarily results from the replacement of summation with a simple selection of the maximum value out of multiple candidates. When comparing between two elements, the Jacobian logarithm [104] can be demonstrated in the following example

$$\begin{aligned} \text{Jac}(\Phi_1, \Phi_2) &= \ln(e^{\Phi_1} + e^{\Phi_2}) \\ &= \max\{\Phi_1, \Phi_2\} + \ln(1 + e^{-|\Phi_1 - \Phi_2|}) \\ &= \max\{\Phi_1, \Phi_2\} + f_c(|\Phi_1 - \Phi_2|) \ . \end{aligned} \tag{5.12}$$

Furthermore, for the case with more than two elements, Eq. (5.12) can be extended using the following approach

$$\ln(\sum_{i=1}^{I} e^{\Phi_i}) = \text{Jac}\left(\Phi_I, \text{Jac}(\Phi_{I-1}, \ldots, \text{Jac}(\Phi_3, \text{Jac}\left(\Phi_2, \Phi_1\right)) \ldots)\right) \ , \tag{5.13}$$

where f_c is a correction term. In practice, f_c can be computed in three different manners leading to three distinct variants of the logarithmic approximation scenarios, which are generalized as follows

Exact-Log-MAP algorithm No approximation is invoked, f_c intends to compute the exact value of $\ln(1 + e^{-|\Phi_1 - \Phi_2|})$. Therefore, the decoding performance is exact the same as the MAP algorithm.

Max-Log-MAP algorithm Approximation formulated in Eq. (5.12) is invoked to provide simpler decoding. Complexity is reduced significantly at the cost of slight performance degradation. It also has the lowest implementational complexity compared with others.

Approx-Log-MAP algorithm f_c is determined by looking up a pre-stored coefficients table [104]. This scheme is able to perform as well as the Exact-Log-MAP algorithm.

5.1.3 SISO APP Decoder

In this subsection, we review the general principle of SISO[1] decoder and iterative decoding. The theory of SISO decoding technique was proposed by S. Benedetto *et al* in [105, 106]. Compared with the conventional hard-decision decoder (HDD) which only generates an 'one-off' estimation of the transmitted data bits, SISO decoding allows passing the probabilities from one constituent decoder to the other and accepting feedback of probabilities from others in an iterative fashion.

The schematic of a SISO decoder is shown in Fig. 5.1. A four-terminal SISO decoder consists of two inputs, which are referred to as the *a-priori* probabilities $p_a(x_k)$/$p_a(u_k)$, and also two outputs, namely the *a-posterior* probabilities $p_o(x_k)$/$p_o(u_k)$. Moreover, u_k is the information bit while x_k represents the coded symbol. It is noteworthy that both *a-priori* probabilities and *a-posterior* probabilities are computed in the logarithmic domain.

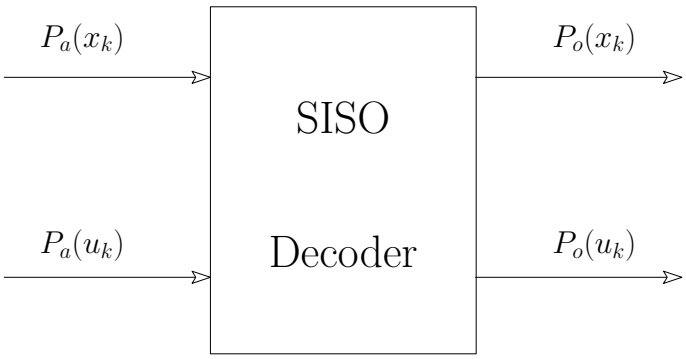

Figure 5.1: A four-terminal soft-in soft-out (SISO) decoding module.

A SISO APP decoder takes advantage of the code trellis representation and utilizes the Log-MAP algorithm to label each path in the code trellis with corresponding probability values. In the concatenated coding scenario, the *a-priori* bit/symbol probabilities from the soft-decision output of other component decoders are used to generate the *a-posterior* probabilities for both information bits and coded symbols. In other words, the *a-priori* information of a specific bit refers to the information it carries prior to arriving at the decoder, whereas the information at the output of a SISO decoder is termed as the *a-posterior* information. In general, the *extrinsic* information, which does not depend on the *a-priori* information, is defined as the subtraction of the *a-priori* information from the

[1]Note that, in this chapter, the acronym 'SISO' refers to Soft-In Soft-Out instead of Single-Input Sinlge-Output.

a-posterior information.

5.2 Low-complexity Iterative Non-coherent Detection of Differential Schemes in Fast Fading Channels

Differential phase-shift keying (DPSK), a popular digital modulation scheme debuted several decades ago [107], has been widely deployed in modern telecommunication, deep-space and satellite applications. DPSK signal carries the information in relative phase (or phase transition) between two adjacent symbols rather than absolute phase, which effectively resolves the $2\pi/M$ phase ambiguity issue experienced in coherently-detected M-PSK systems. To be more specific, coherent detection of PSK depends on the availability of reference phase. Phase ambiguity associated with coherent PSK receiver is caused by the carrier recovery circuit locking onto a wrong phase instead of the correct reference phase of the carrier [108]. Differential encoding also enables simpler implementation of receivers as carrier synchronization is no longer required. Phase reference could be acquired from the previously-detected symbol due to the unique feature of differential encoding.

In existing technical literature, the construction of non-coherently detected differential systems that are dispensing with channel information, is generally based on the assumption that phase rotation is constant or near-constant over several symbol intervals. Typically, this assumption is valid only for very slow fading. The contribution of this chapter is that we consider a more realistic fading channel assumption and we propose the use of a simple differential detector and channel interleaver in conjunction with Turbo code to improve the reliability of non-coherent decoding and detection under fast fading channels. As a result, several novel differential schemes proposed in this chapter are suitable for implementation in high mobility applications, such as radio communication between base station and high-speed train.

5.2.1 Historical Review of Differential Schemes under Fast Fading Channels

In general, DPSK systems are optimally detected if multiplicative interferences, such as fading induced by wireless medium, retain constant during observation period. However,

a practical differential communication system needs to accommodate the Doppler shift caused by the movement of mobile station (MS). Unfortunately, conventional DPSK detectors usually fail to recover the information in such scenario, this motivates the quest for novel DPSK detection algorithms that are suitable for high mobility scenarios under fast-faded channels.

The capacity of non-coherent channels is comprehensively studied in [109], information theoretic analysis has proved it to be very similar to that of coherent channels. Since then, a growing effort has been devoted toward the derivation of improved non-coherent detection or decoding schemes. In the open technical literature, this problem is addressed in two distinct manners.

Since the error rate of DPSK-modulated systems severely degrades under time-varying channel, first solution concentrates on using iteration gain offered from iterative processing to compensate the performance loss. For instance, in [110], serial concatenation of convolutional and DPSK encoders allows iterative detection and decoding which progressively improves the error performance. To be more specific, a novel soft-decision differential sequential decoder was presented, which exploited the redundancy inherent in the differentially encoded signal. [111] proposed a different non-coherent detection of DPSK signal using Viterbi algorithm under AWGN channel. Improved version of Viterbi algorithm assisted differential detection was later presented in [112] that was capable of dealing with frequency-flat Rayleigh fading channel. A more unified and general non-coherent detector was published in [113]. The resulting receiver was optimal in the maximum likelihood detection sense and had demonstrated significant error rate improvement for a non-selective fading channel with stationary users.

So far, the abovementioned research works at early stage either consider only Gaussian noise or assume constant fading process. The ground-breaking work devised in [114] deliveries reliable communication in the presence of Doppler shift by utilizing so-called 'Turbo DPSK' scheme, which is essentially a serial concatenation of FEC code and DPSK, separated by interleaving. The proposed *a-posteriori* probability (APP) DPSK soft demodulator operates following the well-known Bahl-Cocke-Jelinek-Raviv (BCJR) algorithm and is suitable for stationary and time-varying channel. Channel estimator incorporates linear prediction together with per-survivor processing. This technique hence results in an exponential expansion of the decoding trellis. Simulations indicate that it is capable of performing asymptotically as well as coded coherent PSK in a Gaussian channel, while marginally outperforming the corresponding coded coherent PSK in a flat Rayleigh fading channel due to time diversity introduced by fading. [115] is another low-complexity solution to detecting Turbo-coded differential PSK signals under corre-

lated flat-fading channels. The proposed scheme consists of both forward and backward detection processes. By removing the duplicated components in the forward and backward processes and assigning a proper combining weight, it is claimed that proposed sub-optimal detector is able to perform as well as, or even outperform, existing scheme at high signal-to-noise ratio.

On the other hand, non-coherent detection of DPSK signal based on multiple symbol intervals, therefore termed multi-symbol differential detection (MSDD), is also a favored means of data recovery technique when transmitting over fast fading channels. Pioneering work on MSDD can be traced back to late 80's [57]. Divsalar and Simon presented their maximum-likelihood non-coherent sequence estimation algorithm aided MSDD for detecting DPSK signals over AWGN channel, which yielded optimum performance by employing a block of $N+1$ measurements to produce N data decisions. Hence, the deficiency suffered from using DPSK signaling is effectively resolved. Simulation and analytical results indicate multi-symbol differential detector closes the gap between conventional (two-symbol interval) non-coherent DPSK detection and ideal coherently-detected PSK with differential encoding (usually designated as DEPSK). MSDD proposed by Divsalar and Simon was later extended to trellis coded amplitude modulation and Rayleigh/Rician fading channels [116]. Wilson [117] also presented his independent work on MSDD. Two heuristic sub-optimal solutions with far less computational complexity were also derived, which offered excellent complexity and performance trade-off. Theoretical bit error rate of DBPSK and DQPSK with multi-symbol differential decision under AWGN channel and correlated Rayleigh fading channel were given in [118] and [119], respectively. MSDD was further improved to accommodate soft input as well as generate soft output, which is ideal for iterative detection of convolutionally-coded, interleaved, DPSK systems.

Furthermore, another sub-optimal but simpler variant of MSDD was proposed in [120]. In this new approach, search space for the maximum-likelihood estimation is limited to a spherical region within certain radius, hence termed multiple-symbol differential sphere decoding (MSDSD). Later, the idea of MAP MSDSD was further extended in order to allow iterations with other soft-in soft-out decoder.

It should be pointed out that the performance improvement brought by MSDD and its reduced-complexity variants, such as MSDSD, is attributed to the extended decision window length. Theoretically, error rate of DPSK system with non-coherent detection could be identical to that of coherently-detected DEPSK as observation interval approaches infinity. It is known that the detection complexity increases exponentially as the window size becomes larger. On the contrary, although MSDSD offers an attractive trade-off be-

tween performance and complexity, implementation of such algorithm in practice is still problematic as it quickly becomes computationally intractable when either the alphabet size or observation interval grows.

Unique feature of DPSK makes it invariant to phase rotation of multiple of $2\pi/M$, this implies channel coefficients could be efficiently estimated with linear prediction in conjunction with per-survivor processing. Linear prediction demonstrates its powerful ability to track rapid phase variations by taking advantage of the statistical correlation(memory) exhibited by transmission channel. Since the concept of surviving-path is not applicable to MAP algorithm, we have to alter the original principle of per-survivor processing by expanding the number of trellis states. The corresponding decoding trellis after expansion consists of M^N states with M branches per state. Apparently, the expanded decoding trellis states increase exponentially with respect to the prediction order. Hence, the complexity issue is also endured in the iterative non-coherent DPSK detection scenario. As the predictor order becomes larger, increasing number of received samples are involved in decision-making process, hence the performance of coded DPSK scheme is more robust against impairments caused by the time-varying nature of the channel. As a result, the decoding complexity soon becomes prohibitively high. Note that, since channel coefficients are not explicitly calculated by means of inserting training symbols, it is still reasonable to define the iterative DPSK detection as 'non-coherent' scheme.

For those research works from other contributors not mentioned above, we summarize their contributions in Tab. 5.1-Tab. 5.4 below in chronological order.

Table 5.1: Major contributions of differential technique for fast fading channel (Part I).

Year	Author(s)	Contribution
1988	Makrakis *et al* [110]	A novel soft-decision sequential decoder, which exploited the redundancy introduced by the differential encoder, was presented for differentially-coded PSK signals.
1992	F. Adachi and M. Sawahashi [111]	Proposed differential detection of DPSK signal using Viterbi algorithm. The proposed approach was limited to AWGN channel.
1994	Makrakis *et al* [113]	A more unified and improved version was later published in [113]. The resulting receiver was optimal in the maximum likelihood detection sense and had demonstrated significant error rate improvement for non-selective fading channels with stationary users.
1995	G.M. Vitetta and D.P. Taylor [112]	Improved version of Viterbi decoding assisted differential detection that was capable of dealing with frequency-flat Rayleigh fading channel.
1999	P. Hoeher and J. Lodge [114]	'Turbo DPSK' was developed, which was essentially a serial concatenation of FEC code and DPSK, separated by interleaving. The proposed APP DPSK demodulator operates under BCJR algorithm and is suitable for stationary and time-varying channel. Channel state estimator incorporates linear prediction together with per-survivor processing. Note that this technique results in an exponential expansion of the decoding trellis.

Table 5.2: Major contributions of differential technique for fast fading channel (Part II).

Year	Author(s)	Contribution
1999	K.R. Narayanan and G.L. Stuber [121]	This paper investigated iterative demodulation and decoding of convolutionally-encoded data used with differential modulation. It demonstrated that DBPSK, DQPSK, CPM, etc. could be modeled as a recursive rate-1 convolutional code followed by a memoryless mapper. Note that the work presented in this paper was limited to AWGN channel only.
2000	M. Peleg *et al* [115]	Proposed a serially-concatenated system using half-rate convolutional code with M-DPSK modulation. Channel phase was discretized into N states, resulting in a linear trellis expansion of MN states.
2000	G. Colavolpe *et al* [122]	Authors in [122] studied non-coherent version of BCJR algorithm, which follows minimum symbol-error probability criterion under the assumption of constant and uniformly distributed phase variations. Note that amplitude fluctuation of transmission channel is not considered in their work.
2006	S.L. Howard and C. Schlegel [123]	Instead of expanding decoding trellis to highly-complicated 'super-trellis', proposed APP DPSK detector taking advantage of the APP provided by inner (DPSK) soft detector. However, this approach only works when channel phase information is unknown at the receiver, amplitude of the fading process is not taken into account.
2009	C.C. Lo and S.L. Su [124]	Proposed reduced-complexity solution consists of both forward and backward detection processes. By removing the duplicated component in the forward and backward processes and assigning a proper combining weight, authors claim that proposed sub-optimal scheme is able to perform as well as, or even outperform, MSDD at high signal-to-noise.

Table 5.3: Major contributions of differential technique for fast fading channel based on MSDD (Part I).

Year	Author(s)	Contribution
1989	D. Divsalar and M. K. Simon [57]	Authors presented the ground-breaking work on non-coherent detection of DPSK signal over AWGN channel. In [57], optimal detection algorithm making use of maximum-likelihood sequence estimation was derived and studied. By employing a block of $N+1$ measurements to produce N data decisions, the deficiency suffered from using DPSK signaling is effectively resolved.
1989	S.G. Wilson *et al* [117]	Wilson presented his independent work on MSDD in [117]. Two heuristic sub-optimal solutions with far less computational complexity were proposed, which offered great complexity and performance trade-off.
1990	D. Makrakis and K. Feher [125]	Makrakis and Feher proposed a similar multiple-symbol interval aided non-coherent sequential receiver that theoretically approached the performance of coherently-detected DEPSK over static channels.
1994	D. Divsalar and M. K. Simon [116]	MSDD proposed by Divsalar and Simon was later extended to trellis coded amplitude modulation and Rayleigh/Rician fading channel.

Table 5.4: Major contributions of differential technique for fast fading channel based on MSDD (Part II).

Year	Author(s)	Contribution
1994	K.M. Mackenthun [126]	Low-complexity and faster implementation of MSDD algorithm. Unfortunately, proposed scheme in [126] only works for AWGN channel and quasi-static Rayleigh fading channel that is time-invariant over the decision period.
1997	M. Peleg and S. Shamai [127]	MSDD was further improved to accommodate soft input and generate soft output. Novel iterative receiver for convolutionally-coded, interleaved, DPSK system was proposed.
2005	L. Lampe *et al* [120]	A sub-optimal but simpler version of MSDD was proposed. In this new approach, search space for the ML estimation is limited to a circle within certain radius.
2006	V. Pauli *et al* [128]	The idea of MAP multiple-symbol differential sphere decoding (MSDSD) was further extended in order to allow iteration with other soft-in soft-out decoder. The extrinsic information transfer (EXIT) characteristic of the proposed SISO-MSDSD module was throughly analyzed. Best code design yielding maximum coding gain was achieved from the analysis of EXIT function.

5.2.2 Log-MAP Decoding of Uncoded DPSK Signal: A Near-Coherent Performance Approach

In this subsection, we revisit the encoding and decoding procedures for DPSK signal as discussed in Section 2.2.2.1. We then introduce the concept of trellis representation of the differentially-encoded PSK symbols. The trellis structure of DPSK greatly facilitates the Log-MAP decoding in a non-coherent receiver.

5.2.2.1 Trellis Representation of Differentially-encoded PSK Signal

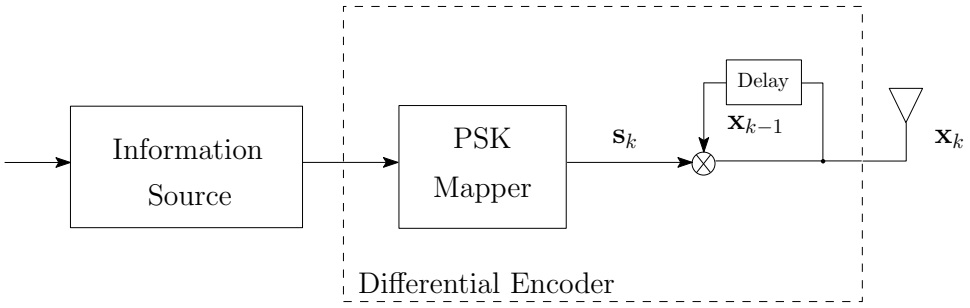

Figure 5.2: The transmitter schematic for differentially-encoded PSK modulation.

The schematic of a uncoded DPSK encoding scheme is illustrated in Fig. 5.2. When a sequence of information bits arrive at the DPSK encoder, the binary bits are first modulated to $\mathcal{M}$-ary complex-valued PSK symbols using a conventional PSK mapper shown in Fig. 5.2. It is assumed that the kth PSK-modulated symbol is taken from a finite alphabet $\mathcal{S} = \exp\left(\frac{2\pi nj}{\mathcal{M}}\right)$, $n = \{0, 1, 2, ..., \mathcal{M}-1\}$ with $\mathcal{M}$ legitimate phasor combinations.

Each transmission period is initialized at epoch 0 with an arbitrary reference symbol $\mathbf{s}_0$, the differential encoding process is conducted in a recursive fashion. As depicted in Fig. 5.2, the calculation of the DPSK symbol at time k, denoted as $\mathbf{x}_k$, is the product of current PSK symbol $\mathbf{s}_k$ and the previous DPSK symbol $\mathbf{x}_{k-1}$, which is written as

$$\mathbf{x}_k = \begin{cases} \mathbf{s}_k & \text{if } k = 1, \\ \mathbf{x}_{k-1} \cdot \mathbf{s}_k & \text{if } k > 1. \end{cases} \tag{5.14}$$

The current DPSK symbol depends on the previous one, differential encoding is repeated in a similar manner until the end of frame.

Since the DPSK-encoded symbols are taken from a complex-valued set with finite number of candidates, the dependence between two adjacent DPSK symbols could be modeled by

the state transition in an Markov process. The trellis diagrams of the differential BPSK as well as differential QPSK schemes are demonstrated in Fig. 5.3 and Fig. 5.4 respectively. Note that the term 'Codewords' in Fig. 5.4 indicate the symbol index in the QPSK constellation set.

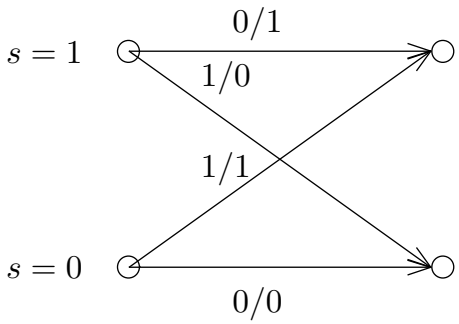

Figure 5.3: Trellis representation for the differential BPSK scheme.

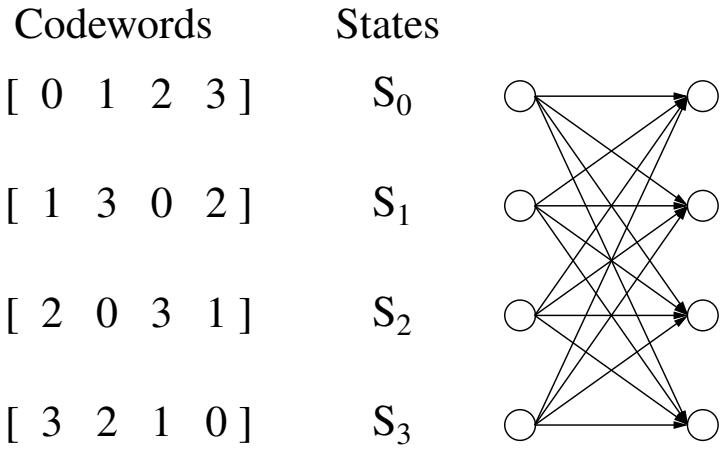

Figure 5.4: Trellis representation for the differential QPSK scheme.

According to the trellis diagrams, for a $\mathcal{M}$-ary DPSK signal, there are in total $\mathcal{M}$ trellis states and $\mathcal{M}$ branches per state. Therefore, differential encoder could be viewed from the coding perspective as the simplest rate-1 recursive non-systematic convolutional encoder with one memory element. Hence, it is feasible to decode the differential signal with trellis-based decoding schemes, for example, the Log-MAP algorithm.

After transmission through hostile environment, the DPSK signal received on the other

end of the communication link $\mathbf{y}_k$ is defined by

$$\mathbf{y}_k = \mathbf{h}_k \mathbf{x}_k + \mathbf{n}_k \ , \tag{5.15}$$

where $\mathbf{h}_k$ is the Rayleigh fading coefficient at time interval k and $\mathbf{n}_k$ represents the Gaussian noise. The well-known Jake's land-mobile model is used to characterize and reflect the time-variant nature of the fading process $\mathbf{h}_k$. This channel model implies that both amplitude as well as phase of the signal are distorted when transmitting through the fading channel. The corresponding normalized auto-correlation function $R(l)$ is expressed as [29]

$$R(l) = J_0(2\pi f_{max} T_s l) \ . \tag{5.16}$$

At epoch k, the conditional probability of receiving $\mathbf{y}_k$, conditioned on the transmitted DPSK symbol $\mathbf{x}_k$ and correlated Rayleigh fading channel coefficient $\mathbf{h}_k$, is determined by the PDF of the noise, which gives

$$p\{\mathbf{y}_k|\mathbf{h}_k, \mathbf{x}_k\} \propto \exp\Big\{ -\frac{1}{N_0} ||\mathbf{y}_k - \mathbf{h}_k \mathbf{x}_k)||^2 \Big\} \ , \tag{5.17}$$

After obtaining the channel metric, the Log-MAP decoding is carried out to estimate PSK-modulated symbol $\hat{\mathbf{s}}_k$ in the usual way as in a coherent system with the *a-posteriori* LLR vector of the data bits set to zeros.

5.2.2.2 APP DPSK Decoder

It can be seen from Eq. (5.17), accurate calculation of the channel metric relies on the availability of channel information. Acquisition of channel estimate is difficult at the receiver when the channel is rapidly changing or the system is operating at low SNR. Furthermore, low complexity is one of the most important design considerations in this work. Hence, in order to keep the selected channel estimator as simple as possible, neither the training-based approach nor optimal linear estimator, for example, minimum mean-square error (MMSE) estimator is employed.

Moreover, the symmetrical property of the DPSK trellis results in the DPSK trellis decoder is invariant to phase rotations as confirmed in [123]. This unique feature significantly simplifies the requirement on the channel estimation accuracy as the decoding is still correct even if the phase of the estimated channel coefficient is slipped by multiples of $2\pi/\mathcal{M}$. As a remedy, the estimated channel coefficient at epoch $k+1$, denoted as $\hat{\mathbf{h}}_{k+1}$, is calculated with the *a-posteriori* probability of the kth symbol at the output of

DPSK Log-MAP decoder. $\hat{\mathbf{h}}_{k+1}$ is then incorporated in the computation of *a-posteriori* probability for the $(k+1)$th received symbol. A up-to-date channel estimate is generated with the latest *a-posteriori* symbol probabilities. This approach is therefore termed APP non-coherent decoding.

A more formal description of the APP non-coherent decoding procedure is detailed in the rest part of this subsection. At the beginning of transmission, the channel coefficients are completely unknown. Hence, an initial assumption of $\mathbf{h}_k = 1$ is proposed. If we denote the output *a posteriori* probability for the kth received symbol as $p_o(\mathbf{x}_k)$, the expectation over $p_o(\mathbf{x}_k)$ defines the estimated soft symbol or expected symbol $\tilde{\mathbf{x}}_k$.

$$\tilde{\mathbf{x}}_k = E[\mathbf{x}_k] = \sum_{i=0}^{\mathcal{M}-1} \exp\left(\frac{j2\pi i}{\mathcal{M}}\right) p_o\left(\mathbf{x}_k = \exp\left(\frac{j2\pi i}{\mathcal{M}}\right)\right) . \tag{5.18}$$

In the following steps, the instantaneous channel estimate is calculated as

$$\hat{\mathbf{h}}_k = \mathbf{y}_k \tilde{\mathbf{x}}_k^* , \tag{5.19}$$

where $(\cdot)^*$ is the complex conjugate.

In the case of static channels or slowly-faded channels, the final channel estimate is simply the average of the instantaneous channel estimates, which gives

$$\tilde{\mathbf{h}}_k = \frac{\sum_{k=1}^{N} \hat{\mathbf{h}}_k}{N} . \tag{5.20}$$

For fast fading channels, the instantaneous channel estimate is passed through a smoother with forgetting factor α, the smoothed final channel estimate is invoked to decode the transmitted symbol at next time slot. The definition of the smoother is expressed as

$$\tilde{\mathbf{h}}_k = \frac{\sum_{i=-N_p}^{N_f} \alpha^{(N_w - i)} \hat{\mathbf{h}}_k(k+i)}{N_w} , \tag{5.21}$$

where α is the forgetting factor, a small number between 0 and 1. N_p and N_f are the number of past symbols and the number of future symbols, while $N_w = N_p + N_f + 1$ is the total number of samples used in each smoothing operation.

5.2.2.3 Decision Feedback Differential Detection (DFDD) aided DPSK Decoder

Recall the transmission model used in Eq. (5.15) is under the assumption of correlated Rayleigh fading following classical Jake's model. We could define the estimated channel coefficient as a noisy version of the original one, that is

$$\hat{\mathbf{h}}_k = \mathbf{h}_k + \mathbf{e}_k . \tag{5.22}$$

Correspondingly, Eq. (5.15) is re-written as

$$\begin{aligned}\mathbf{y}_k &= \mathbf{h}_k\mathbf{x}_k + \mathbf{n}_k \\ &= \hat{\mathbf{h}}_k\mathbf{x}_k + \mathbf{n}_k - \mathbf{e}_k\mathbf{x}_k \\ &= \hat{\mathbf{h}}_k\mathbf{s}_k\mathbf{x}_{k-1} + \hat{\mathbf{n}}_k \ .\end{aligned} \tag{5.23}$$

At epoch k, the estimate of channel coefficient $\hat{\mathbf{h}}_k$ involving current received symbol and multiple detected at previous time slots is defined by

$$\hat{\mathbf{h}}_k = \sum_{m=1}^{M} a_m \mathbf{x}^*_{k-m}\mathbf{y}_{k-m} \ , \tag{5.24}$$

where M is the order of the predictor, it also specifies the number of previously detected symbols that are used for current symbol detection. The predictor coefficient a is a constant that minimizes the mean square of detection error.

The optimal predictor coefficient is found by solving the well-known Wiener-Hopf equation

$$\begin{bmatrix} a_1 \\ a_2 \\ \vdots \\ a_m \end{bmatrix} = \Phi^{-1} \begin{bmatrix} t_1 \\ t_2 \\ \vdots \\ t_M \end{bmatrix} \ , \tag{5.25}$$

where Φ is given by

$$\Phi = \begin{bmatrix} t_0 + 2\sigma^2 & t_1 & \dots & t_{M-1} \\ t_1 & t_0 + 2\sigma^2 & \dots & t_{M-2} \\ \vdots & \vdots & \ddots & \vdots \\ t_{M-1} & t_{M-2} & \dots & t_0 + 2\sigma^2 \end{bmatrix} \ , \tag{5.26}$$

where σ^2 is defined as the power spectral density of the noise N_0 and

$$t_l = E[\mathbf{h}_k\mathbf{h}^*_{k-l}] = J_0(2\pi f_{max}T_s l) \ . \tag{5.27}$$

The Log-MAP algorithm is applied to generate the *a-posteriori* symbol probabilities using forward and backward recursions, at the output of the DFDD aided DPSK decoder, the

a-posteriori symbol probabilities are formulated by

$$p\left(\mathbf{x}_k = \mathbf{x}_k(n)\right) = \sum \Big(p(\mathbf{y}_k|\mathbf{x}_k, \mathbf{h}_k) \prod_{m \neq n}^{all\ m} p(\mathbf{x}_k(m)) \Big) \quad n = \{0, 1, 2, ..., \mathcal{M}-1\}\ , \tag{5.28}$$

where $\mathbf{x}_k(n)$ implies the nth symbol in the DPSK constellation set assigned to the kth symbol in the transmitted DPSK sequence. Moreover, the conditional probability of $p(\mathbf{y}_k|\mathbf{x}_k, \mathbf{h}_k)$ indicates the probability of receiving $\mathbf{y}_k$, given that the transmitted DPSK symbol is $\mathbf{x}_k$ as well as the Rayleigh fading channel $\mathbf{h}_k$, which is determined by the PDF of the noise, it gives

$$p(\mathbf{y}_k|\mathbf{x}_k, \mathbf{h}_k) = \frac{1}{\pi N_0} \exp\Big(- \frac{||\mathbf{y}_k - \mathbf{h}_k\mathbf{x}_k||^2}{N_0} \Big)\ , \tag{5.29}$$

Substituting Eq. (5.24) into Eq. (5.29), the resultant channel metric for the Log-MAP decoding of DPSK symbols is defined as

$$p\{\mathbf{y}_k|\hat{\mathbf{h}}_k, \mathbf{s}_k, \mathbf{x}_{k-1}\} \propto \exp\Big\{ - \frac{1}{N_0} ||\mathbf{y}_k - \mathbf{s}_k(\hat{\mathbf{h}}_k\mathbf{x}_{k-1})||^2 \Big\}\ , \tag{5.30}$$

Further substituting Eq. (5.24), Eq. (5.25), Eq. (5.26) and Eq. (5.27) into Eq. (5.30), after some manipulation and simplification, it yields the non-coherent detection metric that is independent of the channel coefficients, giving

$$\exp\left\{ \frac{1}{N_0} \Re\Big\{ \sum_{m=1}^{M} a_m \mathbf{y}_k^* \mathbf{s}_k \Big(\prod_{j=1}^{m-1} \mathbf{s}_{k-j} \Big) \mathbf{y}_{k-m} \Big\} \right\}\ . \tag{5.31}$$

The interpretation of Eq. (5.31) is two-fold. For minimizing the decoding error rate and achieving the best decoding performance, all legitimate PSK-modulated symbols $\{\mathbf{s}_k, \mathbf{s}_{k-1}, ..., \mathbf{s}_{k-m+1}\}$ are exhaustively searched and examined for the recovery of $\mathbf{s}_{k+1}$ leading to a sophisticated decoding structure. On the other hand, as a simpler alternative, the previously-detected symbols $\{\hat{\mathbf{s}}_{k-1}, \hat{\mathbf{s}}_{k-2}, ..., \hat{\mathbf{s}}_{k-m+1}\}$ are substituted into Eq. (5.31) to compute $\hat{\mathbf{s}}_{k+1}$ at time instant $k+1$.

5.2.2.4 Performance Results and Observations

In this subsection, we evaluate the error performance of the differentially-encoded PSK using Log-MAP algorithm when communicating over AWGN channel and correlated Rayleigh fading channel with normalized Doppler frequency $f_{dop} = 0.002$. We assume

perfect channel estimation and examine the performance of Log-MAP detection of uncoded DPSK signal. The discussion is then extended to imperfect channel estimation scenario. Since the DPSK is now considered as a convolutional code, the availability of channel knowledge is mandatory for the Log-MAP decoder. Therefore, the APP channel estimation is invoked at the receiver in latter case.

As illustrated in Fig. 5.5, although encoding the information in a differential manner could facilitate the non-coherent reception at the receiver, the BPSK with differential encoding is about 0.5 dB inferior to BPSK scheme in AWGN channel due to the error propagation introduced in differential detection. On the other hand, the performance degradation of DPSK with coherent detection is escalated to approximately 2.0 dB in correlated Rayleigh fading channel compared with coherently- detected BPSK. A performance gap of roughly 3.0 dB is witnessed when comparing DBPSK using conventional non-coherent detection to BPSK scheme having perfect channel information.

In Fig. 5.6, the DBPSK signal is decoded as a trellis code with Log-MAP algorithm. It can be seen from Fig. 5.6 that performance loss resulting from the non-coherent detection is fully recovered with Log-MAP decoding, the performance of DBPSK is capable of approaching that of DBPSK using coherent detection under both AWGN channel and correlated Rayleigh fading channel.

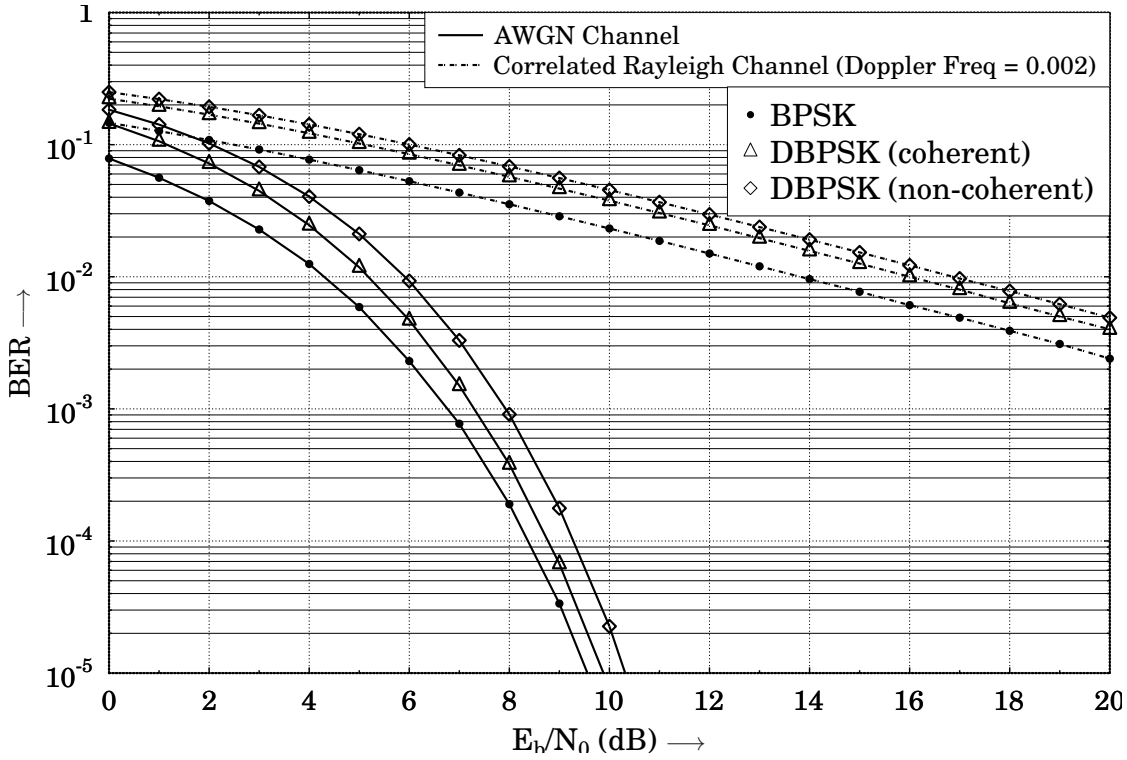

Figure 5.5: BER versus E_b/N_0 performance of DBPSK using coherent and non-coherent detection.

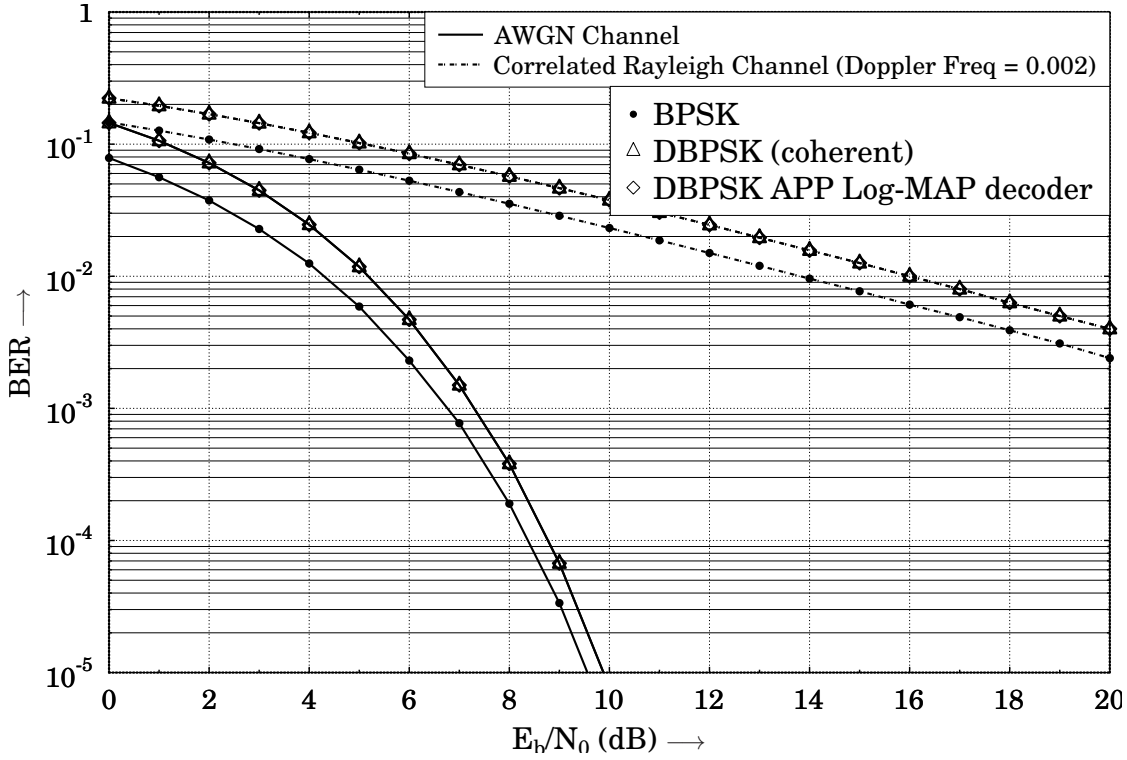

Figure 5.6: BER versus E_b/N_0 performance of uncoded DBPSK using Log-MAP decoding with APP channel estimation.

5.2.3 Turbo Principle aided Detection and Decoding of Channel-coded Differential PSK

5.2.3.1 System Model

Consider a serially-concatenated coding system with differential PSK modulation as illustrated in Fig. 5.7, which consists of a convolutional or Turbo encoder, a differential encoder and a PSK mapper. In order to provide additional protection against fading as well as eliminate the correlation of adjacent coded bits, a bit interleaver π is placed between two component codes to re-order the transmission of the symbols.

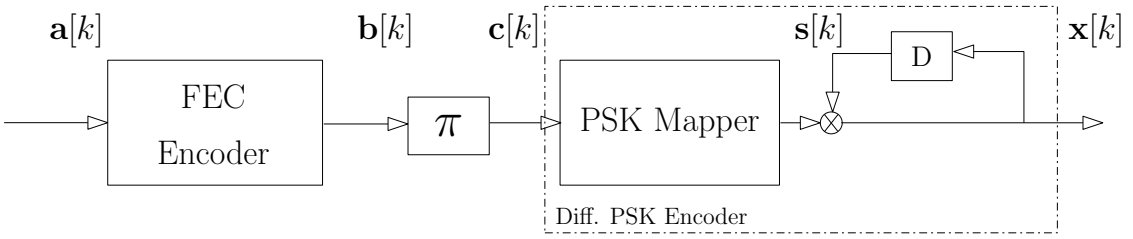

Figure 5.7: The schematic of a FEC-coded differential PSK transmitter.

The input to the FEC encoder is independent and equipropable i-bit information words $\mathbf{a}_k = \{\mathbf{a}[1], \mathbf{a}[2], .., \mathbf{a}[k]\}$. The output of the encoder is n-bit coded words $\mathbf{b}_k = \{\mathbf{b}[1], \mathbf{b}[2], .., \mathbf{b}[k]\}$. The code rate is therefore defined as i/n. The resultant convolutional or Turbo codewords are subsequently permuted and modulated to complex-valued PSK symbols $\mathbf{s}_k$ with various signal labeling, which are further encoded by outer rate-1 convolutional encoder, i.e. differential encoder. At epoch k, the differentially-modulated FEC-coded symbols are generated recursively as

$$\mathbf{x}[k] = \begin{cases} \mathbf{s}[k] & \text{if } k = 1, \\ \mathbf{x}[k-1] \cdot \mathbf{s}[k] & \text{if } k > 1. \end{cases} \tag{5.32}$$

The radio signal is distorted and contaminated by rapidly time-variant fading incurred during transmission, along with Gaussian noise imposed at the receiver. Transmission channel is modeled as frequency non-selective band-limited correlated Rayleigh fading defined by Jake's model. Note that, as there is no universally accepted definition of fast fading, we consider the communication channel is fast-faded when normalized Doppler frequency is greater than 0.05.

The corresponding received signal at the matched filter output at time instant k can be written as

$$\mathbf{y}[k] = \mathbf{h}[k]\mathbf{x}[k] + \mathbf{n}[k] \,, \tag{5.33}$$

where $\mathbf{h}_k$ is the complex-valued correlated Rayleigh fading coefficients, while $\mathbf{n}_k$ denotes the AWGN induced at the receiver having zero mean and variance of $N_0/2$ per dimension. Received signal is differentially detected with non-coherent approach as well as semi non-coherent methods based on the estimated channel, including APP channel estimation and DFDD aided channel estimation in following two subsections.

5.2.3.2 Non-coherent DPSK Demapper

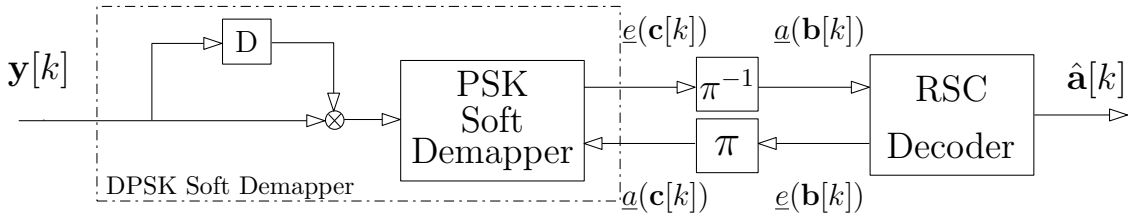

Figure 5.8: The proposed receiver structure for jointly detecting and decoding the serial concatenation of RSC and DPSK modulation.

The received samples are differentially detected by multiplying each sample by the complex conjugate of the previous one, recall that the kth received symbol is expressed as

$$\mathbf{y}[k] = \mathbf{h}[k]\mathbf{x}[k] + \mathbf{n}[k] \,, \tag{5.34}$$

The previous received sample at epoch $k-1$ is given in a similar way

$$\mathbf{y}[k-1] = \mathbf{h}[k-1]\mathbf{x}[k-1] + \mathbf{n}[k-1] \,, \tag{5.35}$$

Subsequently, the product of Eq. (5.34) and Eq. (5.35) is used to define the equivalent version of the received signal when the channel states at epoch $k-1$ and k are identical, namely $\mathbf{h}_k = \mathbf{h}_{k-1}$, which gives

$$\begin{aligned}
\tilde{\mathbf{y}}[k] &= \mathbf{y}[k]\mathbf{y}^*[k-1] \\
&= \Big(\mathbf{h}[k]\mathbf{x}[k] + \mathbf{n}[k]\Big)\Big(\mathbf{h}^*[k-1]\mathbf{x}^*[k-1] + \mathbf{n}^*[k-1]\Big) \\
&= \underbrace{\big|\mathbf{y}[k-1]\big|^2}_{\tilde{\mathbf{h}}[k]}\mathbf{s}[k] + \tilde{\mathbf{n}}[k] \,,
\end{aligned} \tag{5.36}$$

Note that Eq. (5.36) is the re-constructed version of $\mathbf{y}[k]$, it can be re-arranged as

$$\tilde{\mathbf{y}}[k] = \tilde{\mathbf{h}}[k]\mathbf{s}[k] + \tilde{\mathbf{n}}[k] \ , \tag{5.37}$$

in Eq. (5.37), transmitted symbols are now PSK-modulated symbols prior to differential encoding $\mathbf{s}[k]$, and $\tilde{\mathbf{n}}[k]$ is the new noise term that its variance is doubled to reflect the additional noise introduced during the differential detection. Moreover, $\tilde{\mathbf{h}}[k]$ can be interpreted as the new channel vector.

Calculations in Eq. (5.36) transform the differential transmission model to the absolutely-modulated PSK model. The *a-posteriori* symbol probabilities are generated with PSK Log-MAP demapping utilizing Eq. (5.17) as described in Section 5.2.2.1 and in [129].

5.2.3.3 Semi Non-coherent Approaches Using Estimated Channel

Iterative Non-coherent APP Receiver

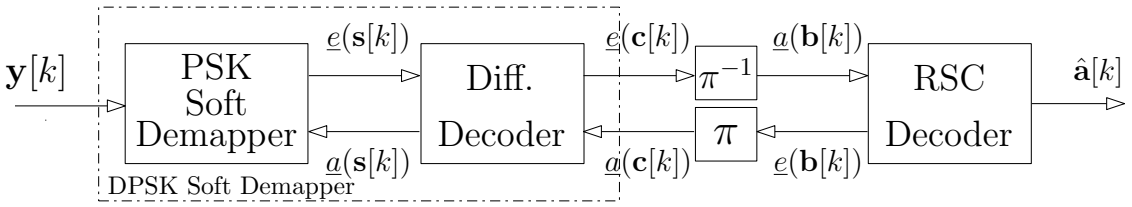

Figure 5.9: The schematic of the proposed iterative non-coherent APP receiver architecture for jointly detecting and decoding the serial concatenation of channel code and DPSK.

As described in Section 5.2.2.1, the differential PSK can be considered as a unity-rate recursive non-systematic convolutional code followed by a conventional memoryless PSK mapper due to the recursive nature of the DPSK encoding. The schematic of a channel-coded DPSK transmitter portrayed in Fig. 5.7 is an analogy to the serially concatenated coding (SCC) scheme.

It is well-known that SCC schemes are capable of achieving infinitesimally low probability of error by using several conventional binary error-correction codes as component codes and decoding the information bits iteratively at the receiver. In channel-coded DPSK scenario, the PSK soft demapper and the FEC decoder serve as the inner and outer

constituent decoders respectively, whereas the differential decoder acts as the intermediate decoder for the proposed joint iterative decoding and detection scheme illustrated in Fig. 5.9. Iterations are conducted among three SISO component demapper and decoders.

Similar to conventional three-stage iterative processing technique, each component decoder/demapper in Fig. 5.9 accepts *a-priori* probabilities or LLRs, denoted as $\underline{a}(.)$, and generates the *extrinsic* probabilities or LLRs $\underline{e}(.)$ utilizing the Log-MAP SISO decoding. In order to eliminate undesirable correlations between neighboring bits, random sequence interleaver and de-interleaver are employed to scramble the LLRs before passing to another SISO module.

Note that for the sake of facilitating the non-coherent reception at the receiver, the coded symbol sequence of length N is divided into several shorter blocks. The first symbol of each block is the reference symbol which is used to initialize the trellis. Moreover, these preambles also provide reference of polarity for the APP channel estimator.

An APP channel estimator as described in Section 5.2.2.2 is incorporated in the inner PSK soft demapper. As mentioned earlier, at the beginning of iterative processing of the received signal, an arbitrary channel coefficient is selected for the PSK soft demapping. The confidence level of the *a-posteriori* symbol probabilities is reinforced after each iteration, a new and up-to-date channel estimate is updated using more accurate *a-posteriori* symbol probabilities calculated by the inner detector.

Non-coherent DFDD-DPSK Soft Demapper

As we can see from the derivation of non-coherent DPSK soft demapper discussed in Section 5.2.3.2, the foundation of this scheme relies upon the assumption that Eq. (5.36) only holds when $\mathbf{h}[k] = \mathbf{h}[k-1]$. In other words, decisions are made upon recent two symbols. Failure of complying with the conception of constant channel coefficients over decision intervals would result in an irreducible error floor. Hence this approach is only valid for slowly or moderately faded Rayleigh channel (normalized Doppler frequency $f_{dop} < 0.02$) and is not favorable in high mobility scenarios.

Moreover, if the f_{dop} becomes too large, a single differential detector is incapable of compensating for the rapid phase variations of the fading process and reliable communication is no longer possible. This problem could be overcome by using a novel non-coherent receiver structure with extended decision intervals. We propose a DFDD aided non-coherent detector in this subsection for recovering data symbols, which is independent of the abovementioned assumption and therefore is able to survive in relatively fast fading channels.

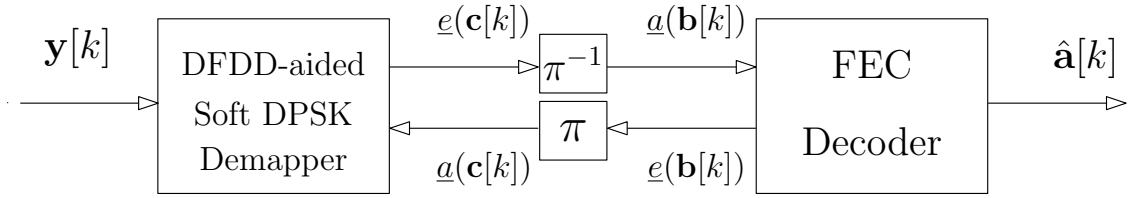

Figure 5.10: Receiver structure for non-coherent DFDD-DPSK soft demapper.

Fig. 5.10 illustrates the structure of the iterative non-coherent soft demapper with embedded DFDD channel estimator in a FEC-coded and interleaved system. The notations $\underline{a}(\cdot)$ and $\underline{e}(\cdot)$ represent the sequences containing the *a-priori* LLRs and *extrinsic* LLRs respectively. In the proposed iterative non-coherent scheme, splitting the data frame into several segments with shorter length is no longer required.

The DFDD aided non-coherent detection is initialized by transmission of n_p number of preambles, the length of which equals to the order of the channel estimator M. With the assistance of M previously-detected data symbols, the *a-posteriori* symbol probabilities can be computed efficiently with DFDD algorithm and Eq. (5.31). The complexity of DFDD channel estimator is linearly proportional to the DPSK constellation size.

DFDD aided Iterative Non-coherent Receiver

The schematic of the proposed DFDD aided three-stage non-coherent iterative detection and decoding scheme is shown in Fig. 5.11.

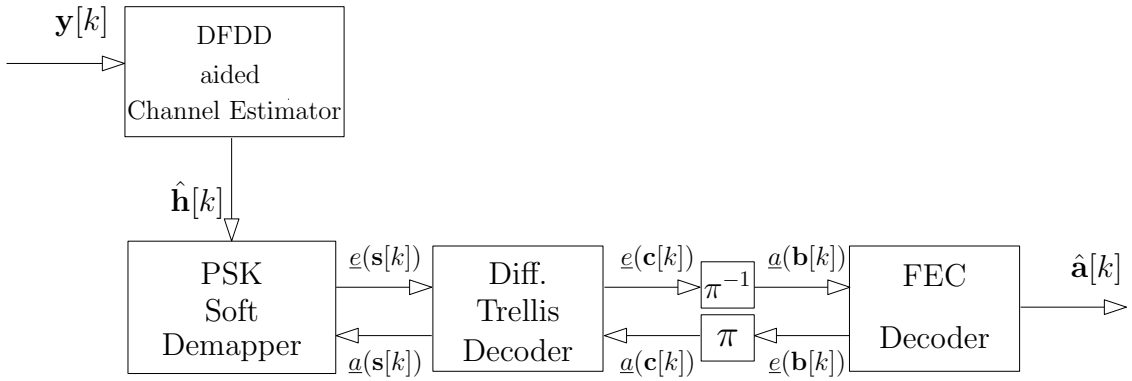

Figure 5.11: The schematic of the proposed DFDD aided iterative non-coherent joint detection and decoding scheme.

The receiver structure as well as decoding principle are very similar to those employed in the iterative non-coherent APP receiver; however the APP channel estimator is replaced with the DFDD channel estimator, the performance of which is more robust in fast fading

channels.

Again, the differential trellis decoder is viewed as the intermediate component decoder in a three-stage concatenated configuration. DFDD algorithm is applied only to acquire the channel estimates employing Eq. (5.24). After channel coefficients $\hat{\mathbf{h}}[k]$ are obtained, the corresponding log-domain metric for hypothesized transmitted symbols $\tilde{\mathbf{x}}_k$ can be calculated as

$$\gamma_k(\tilde{\mathbf{x}}[k]) = -\frac{||\mathbf{y}[k] - \hat{\mathbf{h}}[k]\tilde{\mathbf{x}}[k]||^2}{N_0} \ . \tag{5.38}$$

Following decoding steps including forward and backward recursions proceed in the usual way as in the coherently-detected PSK system.

5.2.3.4 Performance Results and Observations

Performance of Non-coherent DPSK Demapper

In this subsection, Monte-Carlo simulations are conducted to evaluate the BER performance of the serial concatenation of channel code and differential PSK investigated in Section 5.2.3.2. Coherent decoding and detection of coded PSK without differential encoding is also studied in order to provide direct comparisons between the coherent and differential systems.

Recursive systematic convolutional (RSC) code is employed in the proposed schemes as the outer code, which is later extended to non-recursive systematic convolutional (NSC) code as well as Turbo code. In this subsection, for each scheme, two $1/2$-rate RSC codes with different memory elements are considered. The generator polynomial for memory-two RSC is expressed as $[7\ 5]_8$ whereas the memory-four RSC is constructed based on a generator polynomial of $[35\ 23]_8$, both in octal format. Trellis termination is applied to neither RSC codes. Moreover, Gray-labelling is used in both PSK as well as DPSK schemes.

In order to give a fair comparison between different iterative differential schemes, the transmit energy of each scheme is normalized to unity. Moreover, it is assumed that the bit error ratio is defined as the average error rate of 10^5 frames transmitted over correlated Rayleigh fading channels having a normalized Doppler frequency of 0.01, where each frame is fixed to 5000 coded DBPSK symbols.

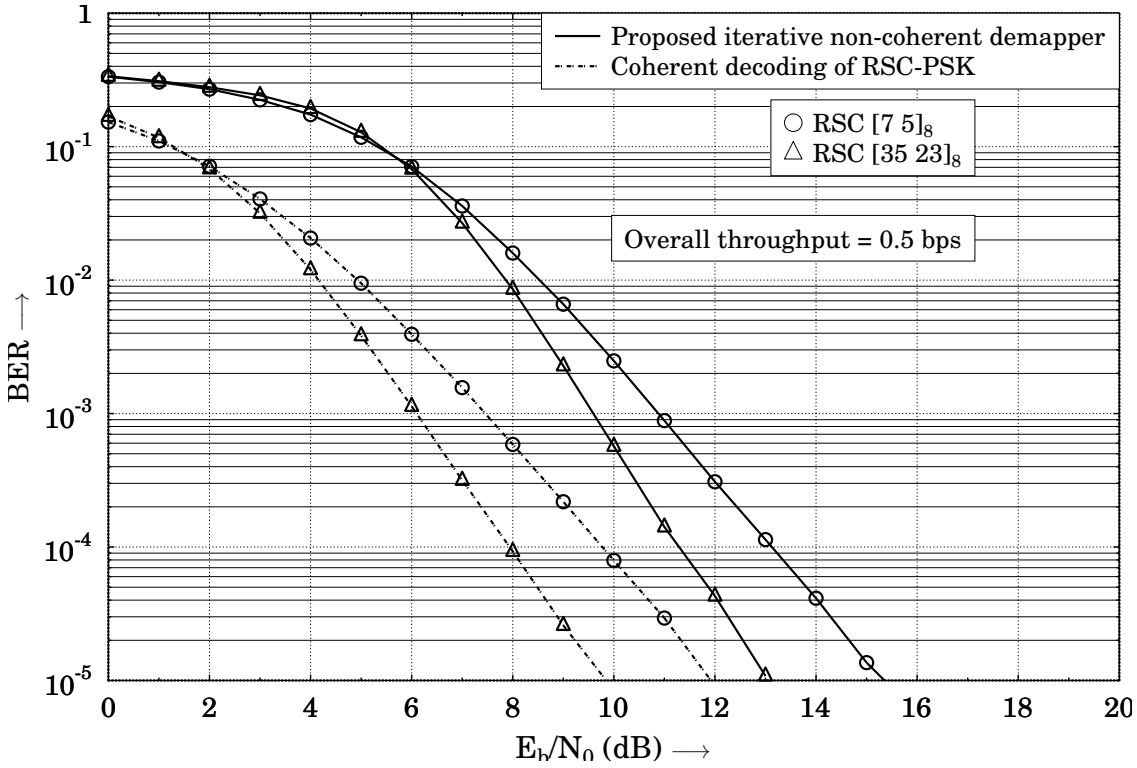

Figure 5.12: BER versus E_b/N_0 performance of the proposed novel iterative non-coherent DPSK demapper for RSC coded DPSK system when communicating over correlated Rayleigh fading channel, where 4 iterations are used between the soft DPSK demapper and RSC decoder.

In Fig. 5.12, the BER performance of non-coherent DPSK demapper is depicted and compared with its coherent counterpart. Four iterations are assumed between the soft DPSK demapper and RSC decoder. As shown in Fig. 5.12, approximately 3.0 dB performance loss is witnessed between the RSC-PSK and RSC-DPSK schemes. Similar observation is also found in conventional non-coherent demodulation schemes without employing any outer code, which implies that the improvement contributed from such receiver structure is very limited as the DPSK demapper is unable to exploit the time diversity introduced by the channel code.

Performance of Iterative Non-coherent APP Receiver

Significant performance improvement is achieved by exploiting the recursive nature inherent in the differential codes. The proposed iterative APP DPSK decoder applies Log-MAP trellis decoding and iterates four times with outer RSC decoder. Discussions commence from a simple scenario assuming perfect channel estimation, the BER versus E_b/N_0 performance of the proposed scheme using memory-two RSC as well as memory-four RSC are illustrated in Fig. 5.13 and Fig. 5.14 respectively. As shown in Fig. 5.13, the slope of curves corresponding to the proposed iterative non-coherent decoder are much steeper due to the time diversity. The performance degradation experienced in the previous system is narrowed down to 2.0 dB after the first iteration, whereas the RSC-DPSK scheme even outperforms the corresponding RSC-PSK by 3.0 dB at BER$= 10^{-4}$ as the number of iterations is increased to two. Further iteration gain of more than 5.0 dB is achieved after four iterations. Similar trend is observed in Fig. 5.14, in which a more sophisticated RSC code with a generator polynomial of $[35\ 23]_8$ is employed. At BER$= 10^{-4}$, the proposed RSC-DPSK scheme is about 3.5 dB superior to the coherent RSC-PSK after only four iterations.

Next, the impact of imperfect channel estimation is taken into consideration. The results shown in Fig. 5.15 are based on the estimated channel coefficients provided by the APP channel estimator. If APP channel estimator is designed with following parameters: forgetting factor $\alpha = 0.99$, $N_w = 30, N_p = 12, N_f = 17$ and block length is 11% of the frame length, imperfect channel coefficients only incur 1.0 dB performance degradation at BER$= 10^{-4}$. For the case of employing memory-four RSC with stronger error-correction capabilities, a slight performance loss of approximately 0.5 dB is expected.

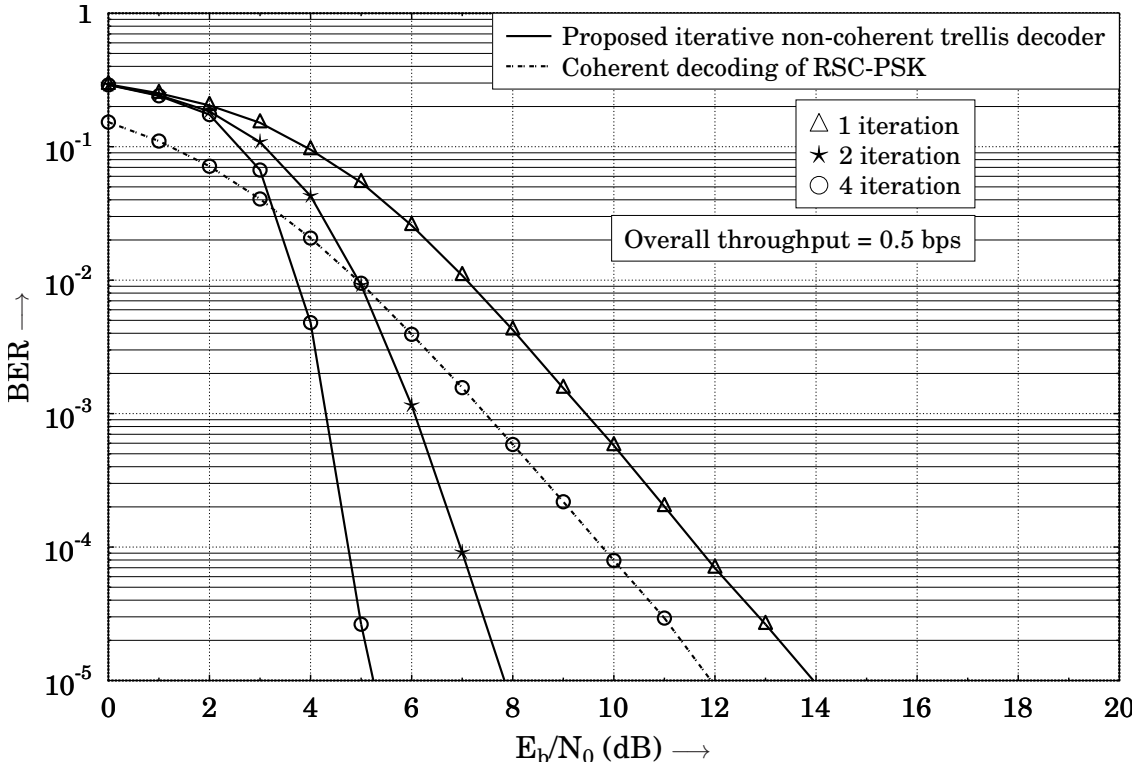

Figure 5.13: BER versus E_b/N_0 performance of the proposed novel iterative non-coherent DPSK trellis decoder for RSC coded DPSK system. Generator polynomial of the RSC encoder is $[7\ 5]_8$ and 4 iterations are used between the DPSK trellis decoder and RSC decoder.

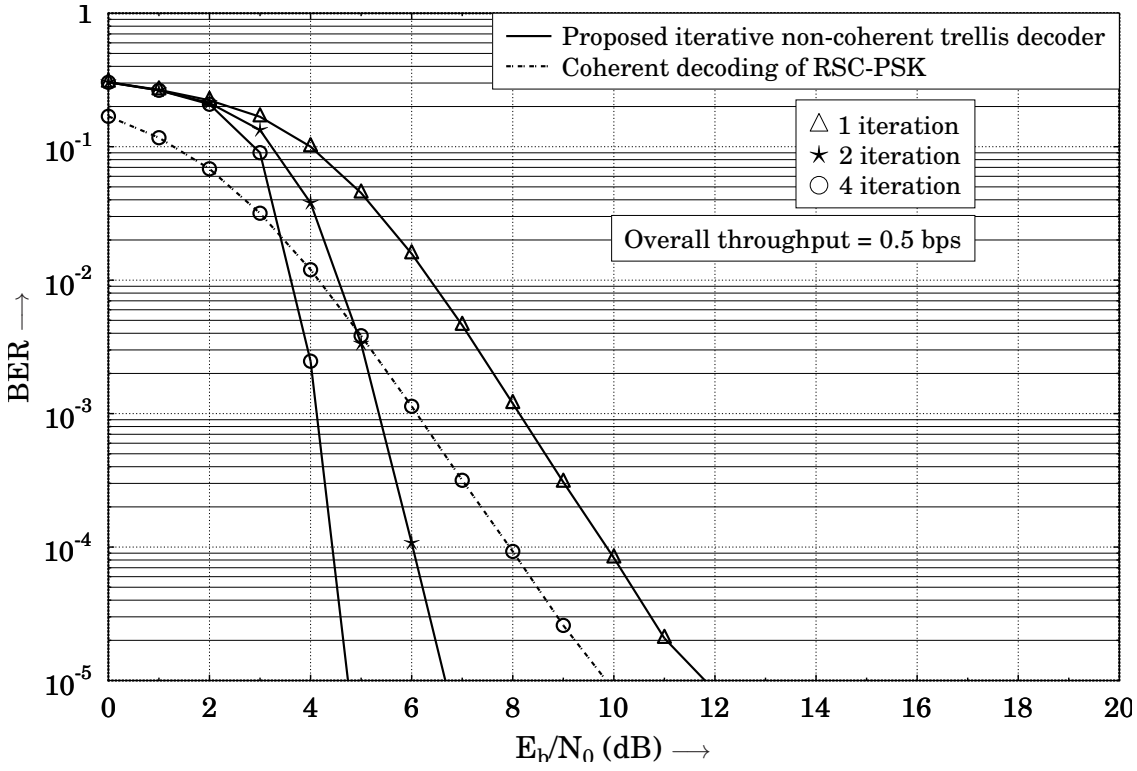

Figure 5.14: BER versus E_b/N_0 performance of the proposed novel iterative non-coherent DPSK trellis decoder for RSC coded DPSK system. Generator polynomial of the RSC encoder is $[35\ 23]_8$ and 4 iterations are used between the DPSK trellis decoder and RSC decoder.

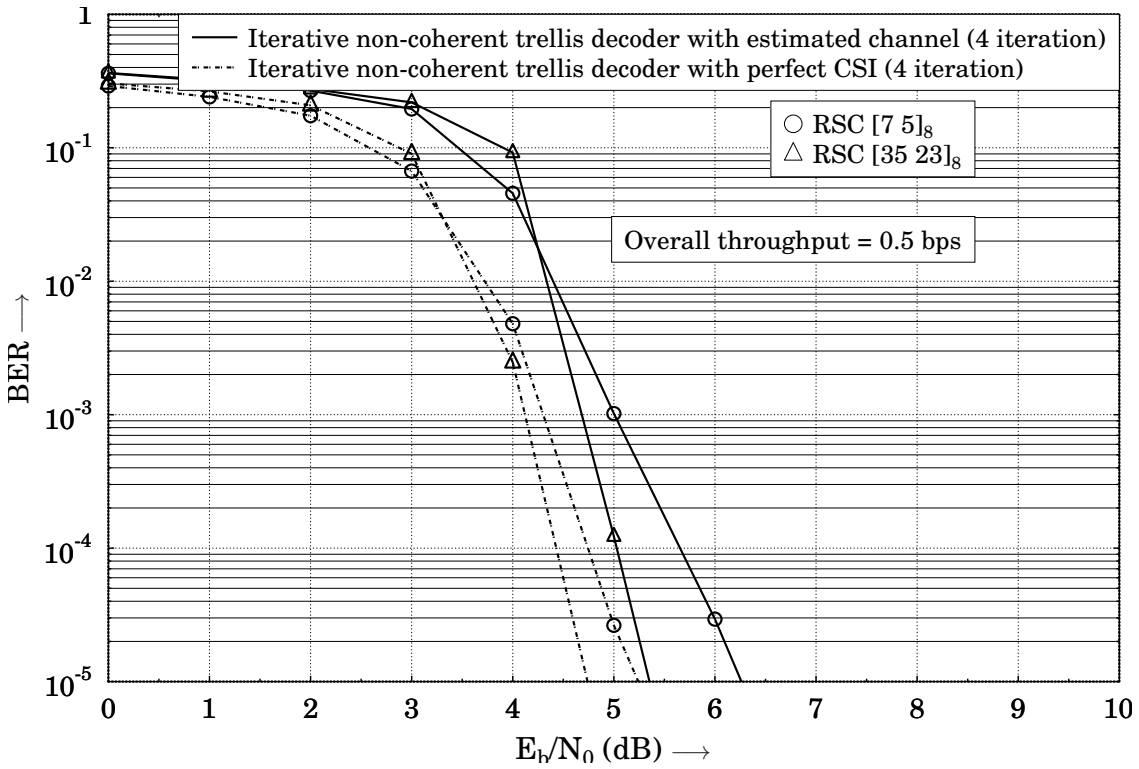

Figure 5.15: Comparison of BER versus E_b/N_0 performance of the proposed novel iterative DPSK trellis decoder with perfect and imperfect CSI. 4 iterations are used between the DPSK trellis decoder and RSC decoder.

Performance of Non-coherent DFDD-DPSK Soft Demapper

Two DFDD aided iterative non-coherent reception schemes for RSC/Turbo-coded DPSK are examined by conducting a series of Monte-Carlo simulations. We focus on the BER performance of the proposed differential schemes under slow and fast fading channels. The discussions in this subsection commence from a slowly-faded Rayleigh channel with normalized Doppler frequency of 0.01, which is later increased up to 0.05 to model a high mobility application. Similarly, simulation results of corresponding coherent counterparts are also provided as performance benchmarks.

For each simulation, the outer code is selected as either a half-rate non-recursive systematic convolutional (NSC) code or a half-rate Turbo code with 2 internal iterations. It is noteworthy that the total number of trellis states used in NSC and Turbo code is identical for a fair comparison. Hence, a memory-six NSC with 64 trellis states as well as a Turbo code constructed by two identical constituent encoders with 32 trellis states for each are considered. Moreover, the generator polynomials employed in the NSC and Turbo code are $[133\ 171]_8$ and $[15\ 17]_8$, both in octal format. Trellis termination is applied to both NSC and Turbo codes. It is assumed that 20000 DQPSK symbols with Gray-labelling are transmitted over correlated Rayleigh fading channels and overall of 10^5 different frames are considered.

Fig. 5.16 demonstrates the BER performance of DFDD-DPSK soft demapper with comparison to the trellis-decoded DFDD-DPSK with perfect channel estimation. It can be seen from Fig. 5.16 that the trellis-decoded DFDD-DPSK is capable of providing substantial amount of iteration gain as well as coding gain so that the error performance approaches that of a coherently-detected convolutional-coded PSK scheme with only four iterations. On the other hand, approximately 2.0 dB degradation is induced in the DFDD-DPSK soft demapping under slow fading case, while further 1.0 dB performance loss is observed in fast fading channel. It is clear that DFDD-DPSK trellis decoder is more appealing in terms of the error performance as it exploits the time diversity made available by the channel code over a time-varying channel.

Performance of DFDD aided Iterative Non-coherent Receiver

The assumption of perfect channel estimation is relaxed in order to examine the impact of estimation error. The DFDD aided channel estimator incorporates at least 11 and 28 previously-detected DQPSK symbols to provide reliable estimation of the channel coef-

ficients under slow and fast fading scenarios respectively. Note that the same number of reference symbols are required at the beginning of each frame to initialize the process; however compared with the relatively large frame length, these preambles are negligible.

As we can see from Fig. 5.17, the proposed DFDD-DPSK trellis decoder with block interleaver is about $1.0-1.5$ dB inferior to its counterpart with perfect channel information. As a remedy, in Fig. 5.18, a sequence interleaver is employed to partly compensate the performance degradation. A direct comparison of Fig. 5.18 to Fig. 6 of [114] confirms that our proposed DFDD-DPSK trellis decoder is capable of performing as well as the linear prediction based scheme in [114], the computational complexity of which is higher than ours by several orders of magnitude.

Our concentration is shifted to fast fading scenario shown in Fig. 5.19, a further performance loss of roughly 2.8 dB is witnessed if compared with the slow fading case at BER$= 10^{-4}$. Therefore, the BER results of the proposed scheme are only 1.0 dB worse than those reported in [114], which is acceptable as it is achieved by a much simpler decoding structure.

In the rest part of this subsection, Turbo code is employed to further narrow down the performance gap caused by imperfect channel estimation. It can be seen from Fig. 5.20, the proposed scheme benefits from substantial amount of improvement in slowly-faded channel and even more performance gain is acquired under fast fading channel due to time diversity provided by the time-varying channel. As expected, at BER$= 10^{-4}$, the Turbo-coded DQPSK scheme outperforms the corresponding NSC-coded systems by 1.0 dB and 2.2 dB for slow and fast fading channels respectively.

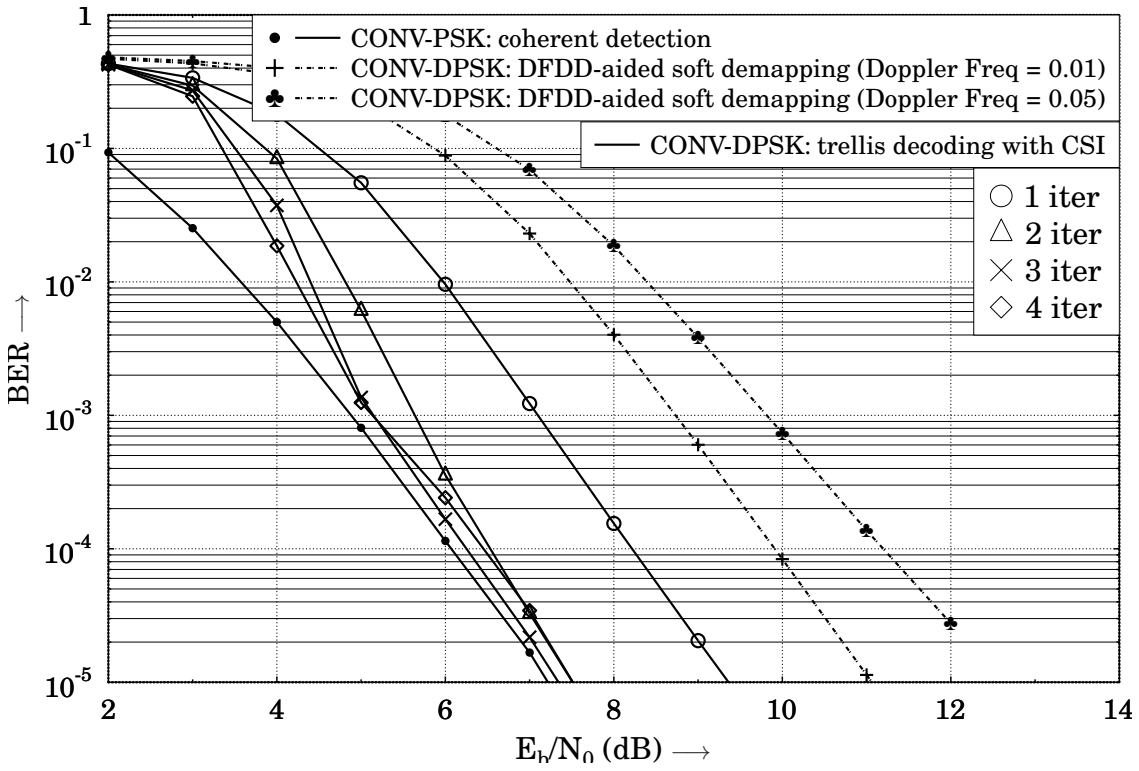

Figure 5.16: BER versus E_b/N_0 performance of the proposed non-coherent DFDD-DPSK soft demapper when communicating over correlated Rayleigh fading channel with normalized Doppler frequency of 0.01 and 0.05. Block interleaver is employed. The solid dot lines are duplicated from [114] for comparison.

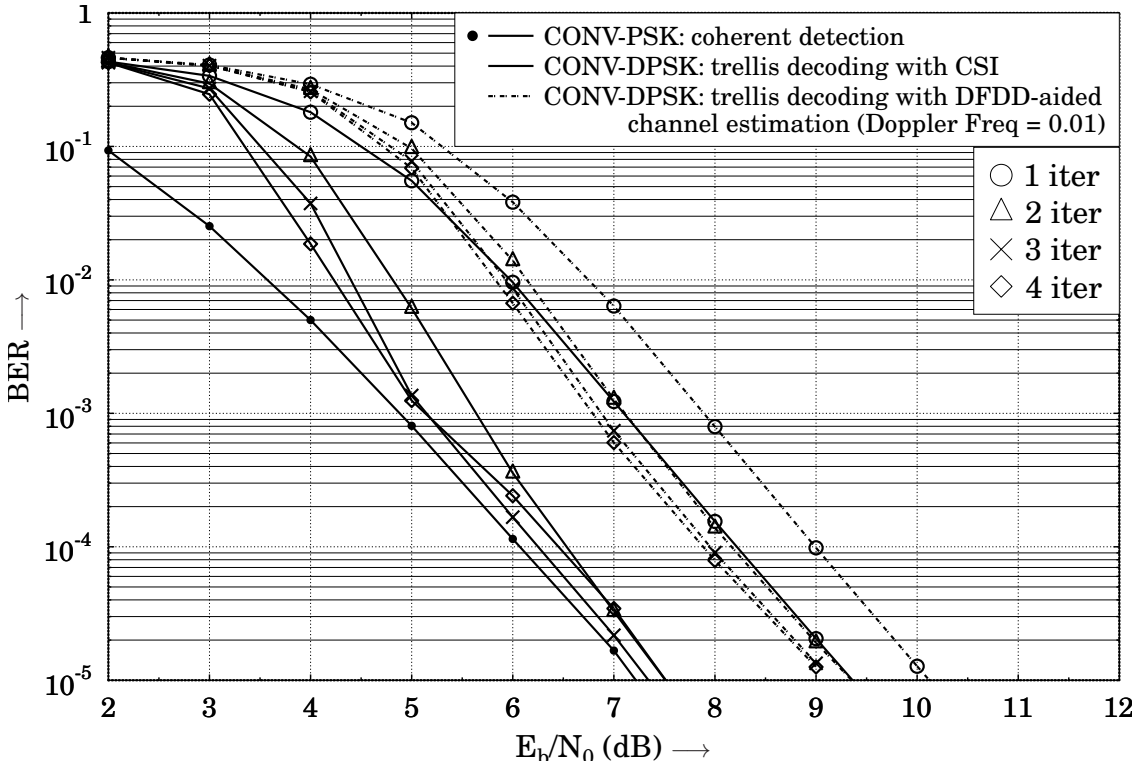

Figure 5.17: BER versus E_b/N_0 performance of the proposed DFDD aided iterative non-coherent trellis detection and decoding of NSC coded DQPSK when communicating over correlated Rayleigh fading channel with normalized Doppler frequency of 0.01. Block interleaver is employed. The solid dot lines are duplicated from [114] for comparison.

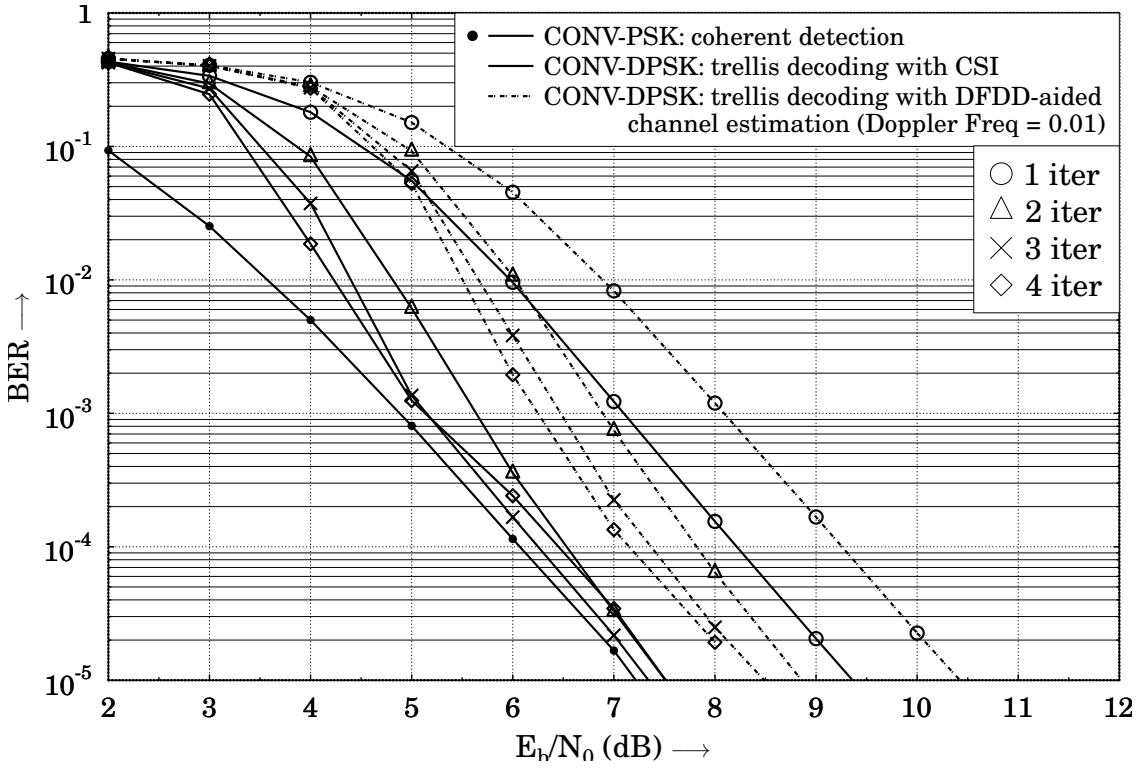

Figure 5.18: BER versus E_b/N_0 performance of the proposed DFDD aided iterative non-coherent trellis detection and decoding of NSC coded DQPSK when communicating over correlated Rayleigh fading channel with normalized Doppler frequency of 0.01. Sequence interleaver is employed. The solid dot lines are duplicated from [114] for comparison.

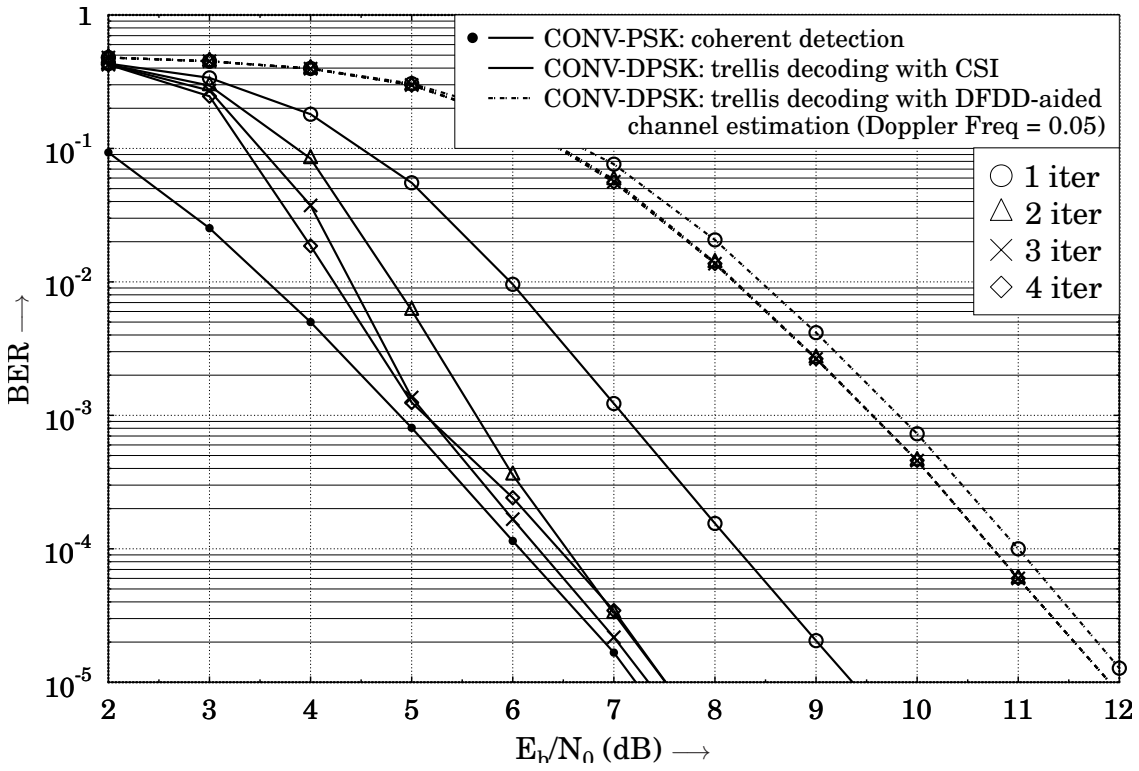

Figure 5.19: BER versus E_b/N_0 performance of the proposed DFDD aided iterative non-coherent trellis detection and decoding of NSC coded DQPSK when communicating over correlated Rayleigh fading channel with normalized Doppler frequency of 0.05. Sequence interleaver is employed.

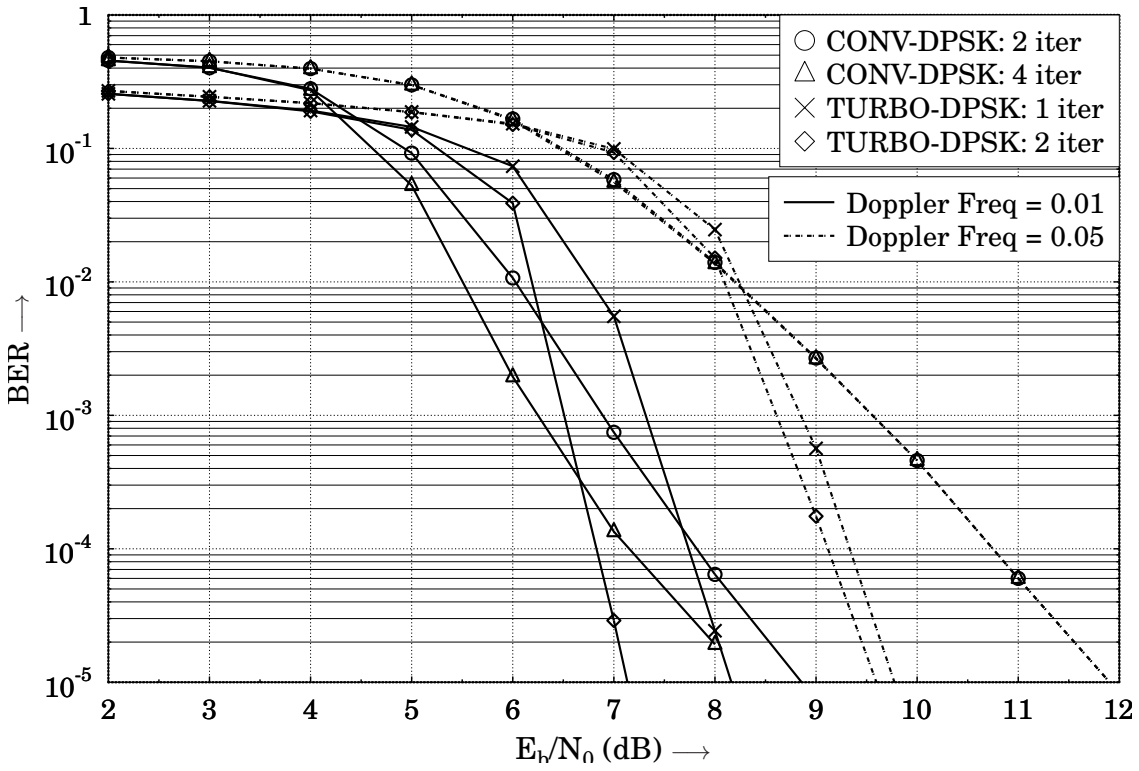

Figure 5.20: BER versus E_b/N_0 performance of the proposed DFDD aided iterative non-coherent trellis detection and decoding of turbo coded DQPSK when communicating over correlated Rayleigh fading channel with normalized Doppler frequency of 0.01 and 0.05. Sequence interleaver is employed.

5.3 Conclusion

In this chapter, we concentrate on improving the error performance of differentially-modulated PSK systems by exploiting iterative non-coherent detection techniques. The benefit of iterative processing allows near-coherent performance when transmitting over slow as well as fast Rayleigh fading channels. DPSK detector essentially works similarly as a unity-rate convolutional decoder that facilitates exchanging *extrinsic* information with other component SISO decoders in an iterative manner like serial/parallel concatenated coding schemes. Some distinguished contributions of this chapter are summarized as follows:

- We first demonstrate that differentially-encoded PSK symbols can be represented by a trellis diagram; therefore, trellis-based SISO decoding algorithm is applicable to provide performance improvement.
- A non-coherent DPSK soft demapper is proposed and studied. By exploiting the connection between current and previous received symbols, proposed scheme is able to calculate the *a-posteriori* symbol probabilities even when the channel information is unavailable at the receiver. Furthermore, the resultant *a-posteriori* symbol probabilities are passed to the outer decoder for the sake of achieving iteration gain. Unfortunately, this approach is only suitable for static or very slowly-faded channels due to the assumption used in the derivation $\mathbf{h}[k] \approx \mathbf{h}[k-1]$.
- A simple APP channel estimator is then investigated. Since it takes advantage of the *a-posteriori* symbol probabilities from the DPSK soft demapper generated by Log-MAP decoding, transmission of training symbols is no longer required. Later, APP channel estimation algorithm is incorporated in an iterative DPSK trellis decoding structure to facilitate iterative processing. Simulation results suggest substantial amount of performance gain is available when differential modulation is combined with error-correction codes and interleaving.
- A different kind of differential decoding approach based on the decision feedback, hence termed DFDD DPSK trellis decoder, is devised and investigated. Although the derivation of DFDD algorithm is very similar to the principle of multi-symbol differential detection, the complexity of our novel DFDD DPSK trellis decoding scheme is linearly proportional to the DPSK constellation size. Furthermore, it is confirmed in simulations that DFDD aided differential decoding scheme is very robust in fast fading channels.

Chapter 6

Conclusions

Contents

6.1 Summary of Work

In this thesis, we primarily concentrate on the design and analysis of low-complexity distributed STBC and distributed differential STBC for unidirectional and bidirectional cooperative networks. PLNC and its non-coherent variant, namely differential PLNC, are investigated and incorporated in our novel distributed coding systems. Furthermore, since the differential techniques generally lead to error rate degradation and poor performance in high mobility applications, several iterative detection and decoding schemes are devised and studied to effectively improve the performance of channel-coded differential PSK under fast fading channels. A brief summary of the contents and major contributions of each chapter is listed below.

1. To begin with, a novel distributed STBC scheme using 'decode-and-forward' relaying protocol for multi-relay assisted two-way cooperative communication systems is presented in Chapter 3. The network topology is similar to the one in [69] where two users simultaneously exchange Alamouti space-time coded signals via a single partner with the aid of PLNC, but we relax the constraint that the source nodes are

supported by multiple co-located antennas. We show that our proposed scheme can still achieve full diversity order when each node acts as a single antenna assisted mobile unit. A simple selection relaying or opportunistic relaying protocol is appropriately designed to effectively circumvent the error propagation inflicted by the relay nodes. More specifically, an error detection code (such as CRC) based selection relaying strategy is proposed to retain the orthogonality of the distributed STBC codewords as well as guarantee the full diversity order is achieved at the destination without employing any sophisticated channel codes to protect the source-to-relay link. PLNC is employed to guarantee that the information exchange between two users via a single or multiple relays could be fulfilled within two time slots. Hence, this novel cooperative communication scheme for two-way relay channels can achieve significant throughput and spectral efficiency improvements. Theoretical end-to-end BEP performance of our proposed distributed STBC scheme over two-way relay channel is investigated using the MGF based approach. Tight upper and lower bounds of the average end-to-end BEP are derived. We then extend our analysis and obtain the exact BEP.

2. In Chapter 4, a novel distributed differential STBC scheme based on 'decode-and-forward' relaying protocol is proposed and investigated in the context of multi-relay assisted cooperative networks. Discussions start from the unidirectional scenario, system model is identical to the one assumed in Chapter 3, in which two users intend to communicate via relay nodes. The encoding and decoding procedures for the distributed differential STBC are elaborated. CRC-based selection relaying protocol is invoked at each relay node to retain the orthogonality of the distributed differential STBC codewords. It is confirmed by both Monte-Carlo simulation results as well as numerical analysis, proposed distributed differential STBC scheme is capable of exploiting full diversity gain with a cluster of single-antenna assisted nodes or users. Furthermore, a Turbo-coded distributed differential STBC scheme is presented to suppress the sensitivity with respect to the frame length. Discussions are later extended to two-way relaying scenario. Novel non-coherent PLNC is also proposed to assist the direct extraction of network-coded symbols without the need of recovering the information from two users explicitly and independently. Consequently, information exchange process between two users via a single or multiple relays can be fulfilled within two time slots, which could result in significant throughput gain.

3. Chapter 5 mostly concentrates on the differential encoding and non-coherent decoding techniques. Two channel estimation methods, namely APP channel estimation as well as DFDD channel estimation, are introduced and incorporated in the uncoded and coded DPSK systems. It is demonstrated in Chapter 5 that the

differential detection is capable of outperforming the coherent counterparts when combined with error-correction codes and interleaving. The APP channel estimator computes the *a-posteriori* symbol probabilities with arbitrary channel coefficients at the beginning of the first iteration. The up-to-date *a-posteriori* symbol probabilities are invoked to update the channel estimates after each iteration. The APP channel estimator is easy to implement yet less robust in fast fading channels. As a result, DFDD channel estimation is presented as a solution, in which the decision of one specific symbol is based on N previously-recovered DPSK symbols. It is shown that differentially-encoded PSK symbols can be represented by a trellis diagram, therefore, standard trellis-based decoding algorithm is feasible. Several concatenated coding schemes using differential encoder as the inner encoder and FEC encoder as the outer encoder are studied. When Turbo code is selected as the outer code, DFDD aided DPSK trellis decoder exhibits its robustness under fast fading channels.

6.2 Future Work

Some suggestions about future work based on this thesis are given as follows.

1. Similar to DPSK, USTM also has recursive nature, hence could be represented by trellis and decoded with trellis decoding algorithm. It is an interesting idea to investigate the application of DFDD channel estimator in a multiple-antenna system.

2. The developed iterative differential decoding techniques can be used in a multi-hop non-coherent cooperative network to reinforce the reliability of cooperating link, especially when fast fading channel is assumed.

3. It is also interesting to investigate if the above-mentioned iterative USTM system is able to work in a distributed way and be extended to two-way relay scenario if possible.

Appendices

Appendix A

Derivation of Upper and Lower Bounds of the Average End-To-End BEP

Take the tight lower bound $P_{EtoE}^{(L)}$ for example, expanding the first term of the left hand side of Eq. (3.34) and after proper arrangements and simplifications based on the symmetrical property of system architecture, we can obtain

$$\begin{aligned}
&\mathbb{E}\left[\left(1-P_{MAC,r_1}^{(U)}\right)\left(1-P_{MAC,r_2}^{(U)}\right)\left(P_{DSTBC}^{t_1}+P_{DSTBC}^{t_2}\right)\right] \\
&=\mathbb{E}\left[2P_{DSTBC}^{t_1}\left(1-P_{MAC,r_1}^{(U)}-P_{MAC,r_2}^{(U)}+P_{MAC,r_1}^{(U)}P_{MAC,r_2}^{(U)}\right)\right] \\
&=\mathbb{E}\left[2P_{DSTBC}^{t_1}-2P_{DSTBC}^{t_1}P_{MAC,r_1}^{(U)}-2P_{DSTBC}^{t_1}P_{MAC,r_2}^{(U)}+2P_{DSTBC}^{t_1}P_{MAC,r_1}^{(U)}P_{MAC,r_2}^{(U)}\right] \\
&=2\mathbb{E}\left[P_{DSTBC}^{t_1}\right]-2\mathbb{E}\left[P_{DSTBC}^{t_1}P_{MAC,r_1}^{(U)}\right]-2\mathbb{E}\left[P_{DSTBC}^{t_1}P_{MAC,r_2}^{(U)}\right] \\
&+2\mathbb{E}\left[P_{DSTBC}^{t_1}P_{MAC,r_1}^{(U)}P_{MAC,r_2}^{(U)}\right], \qquad \text{(A.1)}
\end{aligned}$$

The first term of Eq. (A.1) is the unconditional BEP of conventional Alamouti STBC transmitting over Rayleigh fading channel, its solution is given by [27]

$$\mathbb{E}\left[P_{DSTBC}^{t_1}\right]=\left(\frac{1-\lambda}{2}\right)^2(\lambda+2), \qquad \lambda=\sqrt{\frac{\overline{\gamma}_{DSTBC}}{2+\overline{\gamma}_{DSTBC}}} \qquad \text{(A.2)}$$

where $\overline{\gamma}_{DSTBC}$ is the average received SNR at the destinations when DSTBC scheme is invoked during the BC phase.

The expectation in the second term of Eq. (3.34) can be computed by replacing $P_{MAC,r_1}^{(U)}$

with Eq. (3.29) and taking an integral from 0 to positive infinity, which gives

$$\begin{aligned}
&\mathbb{E}\left[P_{Alamouti}^{T_1} P_{MAC,r_1}^{(U)}\right] \\
&= \int_0^\infty \int_0^\infty P_b(\gamma_{DSTBC}|h_{r_1d_1}, h_{r_2d_1}) P_b(\gamma_{s_1r_1}|h_{s_1r_1}) p(\gamma_{DSTBC}) p(\gamma_{s_1r_1})\, \mathrm{d}\gamma_{s_1r_1}\, \mathrm{d}\gamma_{DSTBC} \\
&+ \int_0^\infty \int_0^\infty P_b(\gamma_{DSTBC}|h_{r_1d_1}, h_{r_2d_1}) P_b(\gamma_{s_2r_1}|h_{s_2r_1}) p(\gamma_{DSTBC}) p(\gamma_{s_2r_1})\, \mathrm{d}\gamma_{s_2r_1}\, \mathrm{d}\gamma_{DSTBC}\,.
\end{aligned} \tag{A.3}$$

The first term of Eq. (A.3) can be addressed using the popular MGF-based approach which is briefly generalized as follows

$$\begin{aligned}
&\int_0^\infty \int_0^\infty P_b(\gamma_{DSTBC}|h_{r_1d_1}, h_{r_2d_1}) P_b(\gamma_{s_1r_1}|h_{s_1r_1}) p(\gamma_{DSTBC}) p(\gamma_{s_1r_1})\, \mathrm{d}\gamma_{s_1r_1}\, \mathrm{d}\gamma_{DSTBC} \\
&= \int_0^\infty \int_0^\infty Q(\sqrt{\gamma_{DSTBC}}) Q(\sqrt{2\gamma_{s_1r_1}}) p(\gamma_{DSTBC}) p(\gamma_{s_1r_1})\, \mathrm{d}\gamma_{s_1r_1}\, \mathrm{d}\gamma_{DSTBC} \\
&= \frac{1}{\pi^2} \int_0^{\frac{\pi}{2}} \int_0^{\frac{\pi}{2}} \left[\int_0^\infty \exp\left(-\frac{\gamma_{DSTBC}}{2\sin^2\varphi}\right) p(\gamma_{DSTBC})\, \mathrm{d}\gamma_{DSTBC}\right] \\
&\qquad\qquad \times \left[\int_0^\infty \exp\left(-\frac{\gamma_{s_1r_1}}{2\sin^2\theta}\right) p(\gamma_{s_1r_1})\, \mathrm{d}\gamma_{s_1r_1}\right] \mathrm{d}\theta\, \mathrm{d}\varphi \\
&= \frac{1}{\pi^2} \int_0^{\frac{\pi}{2}} \int_0^{\frac{\pi}{2}} M_{\gamma_{DSTBC}}\left(-\frac{1}{2\sin^2\varphi}\right) M_{\gamma_{s_1r_1}}\left(-\frac{1}{2\sin^2\theta}\right) \mathrm{d}\theta\, \mathrm{d}\varphi \\
&= \frac{1}{\pi^2} \int_0^{\frac{\pi}{2}} \int_0^{\frac{\pi}{2}} \left(1 + \frac{\overline{\gamma}_{DSTBC}}{2\sin^2\varphi}\right)^{-2} \left(1 + \frac{\overline{\gamma}_{s_1r_1}}{2\sin^2\theta}\right)^{-1} \mathrm{d}\theta\, \mathrm{d}\varphi \\
&= \frac{1}{2}\left(\frac{1-\lambda}{2}\right)^2 (\lambda+2)\left(1 - \sqrt{\frac{\overline{\gamma}_{s_1r_1}}{1+\overline{\gamma}_{s_1r_1}}}\right), \qquad \lambda = \sqrt{\frac{\overline{\gamma}_{DSTBC}}{2+\overline{\gamma}_{DSTBC}}}
\end{aligned} \tag{A.4}$$

where $p(\gamma_{DSTBC})$ denotes the PDF of the instantaneous received SNR γ_{DSTBC} having a chi-squared distribution with $2L$ degrees of freedom and $p(\gamma_{s_1r_1})$ represents the instantaneous received SNR $\gamma_{s_1r_1}$ with an exponentially distributed PDF. If n_T and n_R indicate the number of transmit antennas and receive antennas respectively, we have $L = n_T \times n_R$. Furthermore, by definition, the semi-infinite integrals in square brackets are the MGF of the instantaneous SNR. It is discussed in [16] that the results of $M_{\gamma_{DSTBC}}(s)$ and $M_{\gamma_{s_1r_1}}(s)$ are given by

$$M_{\gamma_{DSTBC}}(s) = (1 - s\overline{\gamma}_{DSTBC})^{-L}, \qquad s > 0 \tag{A.5}$$

$$M_{\gamma_{s_1r_1}}(s) = (1 - s\overline{\gamma}_{s_1r_1})^{-1}, \qquad s > 0 \tag{A.6}$$

where $\overline{\gamma}_{s_1r_1}$ is the average received SNR at relay node r_1. We can solve the rest of terms individually in a similar way and sum up the solution of each term. The final expression for the upper and lower bounds of the average end-to-end BEP for our proposed distributed STBC scheme can be formulated as Eq. (3.35) and Eq. (3.36).

Glossary

4G	The Fourth Generation
AF	Amplify-and-Forward
APP	A Posteriori Probability
AWGN	Additive White Gaussian Noise
BER	Bit Error Ratio
BEP	Bit Error Probability
BLAST	Bell labs LAyered Space Time
BPSK	Binary Phase Shift Keying
BS	Base Station
CCMC	Continuous-input Continuous-output Memoryless Channel
CDMA	Code Division Multiple Access
CRC	Cyclic Redundancy Check
CSI	Channel State Information
D-BLAST	Diagonal BLAST
DCMC	Discrete-input Continuous-output Memoryless Channel
DF	Decode-and-Forward
DFDD	Decision Feedback Differential Detection
DLST	Diagonal Layered Space-Time (Code)
DOSTBC	Differential Orthogonal Space-Time Block Code

DPSK	Differential Phase Shift Keying
DSP	Digital Signal Processing
DSTBC	Differential Space-Time Block Code
DSTC	Differential Space-Time Code
DUSTM	Differential Unitary Space-Time Modulation
FCC	Federal Communications Commission
FEC	Forward-Error-Correction
FER	Frame Error Ratio
GF	Galois Field
GSM	Global System for Mobile communications
HLST	Horizontal Layered Space-Time (Code)
Hz	Hertz
ISI	Inter-Symbol Interference
ITU	International Telecommunication Union
LDC	Linear Dispersion Code
LDPC	Low Density Parity Check
LLR	Log-Likelihood Ratio
LST	Layered Space-Time (Code)
LTE	Long-Term Evolution
MAP	Maximum a Posteriori
MGF	Moment Generating Function
ML	Maximum Likelihood
MIMO	Multiple-Input Multiple-Output
MMSE	Minimum Mean Squared Error
MRC	Maximal Ratio Combining

MS	Mobile Station
MSE	Mean Squared Error
MUD	Multiuser Detection
NC	Network Coding
OSTBC	Orthogonal Space-Time Block Code
PDF	Probability Density Function
PEP	Pairwise Error Probability
PHY	Physical Layer
PLNC	Physical-Layer Network Coding
PSD	Power Spectral Density
PSK	Phase Shift Keying
QAM	Quadrature Amplitude Modulation
QoS	Quality of Service
QOSTBC	Quasi-orthogonal Space-Time Block Code
QPSK	Quadrature Phase Shift Keying
RSC	Recursive-Systematic Code
SCCC	Serially Concatenated Convolutional Codes
SISO	Soft-in Soft-out (Single-Input Sinlge-Output)
SM	Spatial Multiplexing
SNR	Signal to Noise Ratio
SP	Set Partitioning
STBC	Space-Time Block Code
STC	Space-Time Code
STTC	Space-Time Trellis Code
TC	Turbo Code

TLST	Threaded Layered Space-Time (Code)
UMTS	Universal Mobile Telecommunications System
USTM	Unitary Space-Time Modulation
VAA	Virtual Antenna Array
V-BLAST	Vertical BLAST
VLST	Vertical Layered Space-Time (Code)
WCDMA	Wideband Code Division Multiple Access
WSN	Wireless Sensor Network

Bibliography

[1] B. Sanou, "The World in 2013: ICT Facts and Figures," Annual Report, International Telecommunication Union (ITU), 2013. http://www.itu.int/en/ITU-D/Statistics/Documents/facts/ICTFactsFigures2013-e.pdf.

[2] 3GPP, *3rd Generation Patnership Project (3GPP); Technical Specification Group Radio Access Network Physical Channels and Mapping of Transport Channels onto Physical Channels (TDD) (3G TS 25.221 version 3.0.0) (www.3gpp.org)*, October 1999.

[3] "Ofcom Announces Winners of the 4G Mobile Auction," February 2013. http://media.ofcom.org.uk/2013/02/20/ofcom-announces-winners-of-the-4g-mobile-auction/.

[4] B. Sklar, *Digital Communications–Fundamentals and Applications*. Englewood Cliffs, NJ, USA: Prentice-Hall, 2nd ed., 2001.

[5] C. E. Shannon, "A Mathematical Theory of Communication," *Bell Labs Technical Journal*, pp. 379–427, 1948.

[6] C. Berrou and A. Glavieux and P. Thitimajshima, "Near Shannon Limit Error-Correcting Coding and Decoding: Turbo Codes," in *Proceedings of the International Conference on Communications*, (Geneva, Switzerland), pp. 1064–1070, May 1993.

[7] R. Gallager, "Low-Density Parity-Check Codes," *IEEE Transactions on Information Theory*, pp. 21–28, 1962.

[8] D. MacKay and R. Neal, "Near Shannon Limit Performance of Low Density Parity Check Codes," *Electronics Letters*, pp. 457–458, 1997.

[9] E. Telatar, "Capacity of Multi-antenna Gaussian Channels," *European Transactions on Telecommunication*, vol. 10, pp. 585–595, Nov–Dec 1999.

[10] J. Winters, "On the Capacity of Radio Communication Systems with Diversity in a Rayleigh Fading Environment," *IEEE Journal on Selected Areas in Communications*, vol. 5, pp. 0733–8716, June 1987.

[11] A. Paulraj and T. Kailath, "Increasing Capacity in Wireless Broadcast Systems using Distributed Transmission/Directional Reception (DTDR)." U.S. Patent No. 5345599 A, Sep 6, 1994.

[12] J. Winters, J. Salz, and R. Gitlin, "The Impact of Antenna Diversity on the Capacity of Wireless Communication Systems," *IEEE Transactions on Communications*, vol. 42, pp. 1740–1751, March 1994.

[13] G. J. Foschini and M. J. Gans, "On Limits of Wireless Communications in a Fading Environment When Using Multiple Antennas," *Wireless Personal Communications*, vol. 6, pp. 311–335, March 1998.

[14] T. L. Marzetta and B. M. Hochwald, "Capacity of a Mobile Multiple-Antenna Communication Link in Rayleigh Flat Fading," *IEEE Transactions on Information Theory*, vol. 45, pp. 139–157, January 1999.

[15] A. Goldsmith, S. Jafar, N. Jindal, and S. Vishwanath, "Capacity Limits of MIMO Channels," *IEEE Journal on Selected Areas in Communications*, vol. 21, pp. 684–702, June 2003.

[16] M.K. Simon and M.S. Alouini, *Digital Communication over Fading Channels*. Hoboken, NJ, USA: John Wiley & Sons, 2nd ed., 2004.

[17] M. Mouly and M. Pautet, eds., *The GSM System for Mobile Communications*. Olympia, USA: Telecom Publishing, 1992.

[18] A. Wittneben, "Base Station Modulation Diversity for Digital SIMULCAST," in *Proceedings of IEEE Vehicular Technology Conference*, pp. 505–511, May 1993.

[19] N. Seshadri and J. Winters, "Two Signaling Schemes for Improving the Error Performance of Frequency-Division-Duplex (FDD) Transmission Systems Using Transmitter Antenna Diversity," *International Journal of Wireless Information Networks*, vol. 1, pp. 49–60, January 1994.

[20] V. Tarokh, N. Seshadri and A. R. Calderbank, "Space-time Codes for High Data Rate Wireless Communication: Performance Criterion and Code Construction," *IEEE Transactions on Information Theory*, vol. 44, pp. 744–765, March 1998.

[21] S. M. Alamouti, "A Simple Transmit Diversity Technique for Wireless Communications," *IEEE Journal on Selected Areas in Communications*, vol. 16, pp. 1451–1458, October 1998.

[22] V. Tarokh, H. Jafarkhani, and A. R. Calderbank, "Space-Time Block Coding for Wireless Communications: Performance Results," *IEEE Journal on Selected Areas in Communications*, vol. 17, pp. 451–460, March 1999.

[23] V. Tarokh, H. Jafarkhani, and A. R. Calderbank, "Space-time Block Codes from Orthogonal Designs," *IEEE Transactions on Information Theory*, vol. 45, pp. 1456–1467, May 1999.

[24] G. J. Foschini, "Layered Space-Time Architecture for Wireless Communication in a Fading Environment When Using Multi-Element Antennas," *Bell Labs Technical Journal*, vol. 6, no. 2, pp. 41–59, 1996.

[25] L. Zheng and D. Tse, "Diversity and Multiplexing: A Fundamental Tradeoff in Multiple-Antenna Channels," *IEEE Transactions on Information Theroy*, vol. 49, pp. 1073–1096, May 2003.

[26] B. L. Y. L. Hanzo, T. H. Liew, *Turbo Coding, Turbo Equalisation and Space-Time Coding for Transmission over Wireless Channels*. Hoboken, NJ, USA: John Wiley & Sons, 2002.

[27] B. Vucetic and J. Yuan, *Space-Time Coding*. Southern Gate, Chichester, England: John Wiley & Sons, 2003.

[28] E.G. Larsson and P. Stoica, *Space-Time Block Coding for Wireless Communications*. Cambridge, New York, Melbourne, Madrid, Cape Town, Singapore, So Paulo: Cambridge University Press, 2003.

[29] W. C. Jakes, ed., *Microwave Mobile Communications*. New York, USA: John Wiley & Sons, 1974.

[30] Z. Liu, G.B. Giannakis, S. Zhou and B. Muquet, "Space-Time Coding for Broadband Wireless Communications," *Wireless Communications and Mobile Computing*, vol. 1, no. 1, pp. 35–53, 2001.

[31] N. S. A.F. Naguib and A. Calderbank, "Increasing Data Rate over Wireless Channels: Space-time Coding and Signal Processing for High Data Rate Wireless Communications," *IEEE Signal Processing Magazine*, vol. 17, no. 3, pp. 76–92, 2000.

[32] G.J. Foschini, D. Chizhik, M.J. Gans, C. Papadias and R.A. Valenzuela, "Analysis and Performance of Some Basic Space-Time Architectures," *IEEE Journal on Selected Areas in Communications*, vol. 21, pp. 303–320, April 2003.

[33] H. E. Gamal and A. Hammons, "A New Approach to Layered Space-Time Coding and Signal Processing," *IEEE Transactions on Information Theory*, vol. 47, pp. 2321–2334, September 2001.

[34] R. V. G.D. Golden, G.J. Foschini and P. Wolniansky, "Detection Algorithm and Initial Laboratory Results Using V-BLAST Space-Time Communication Architecture," *IEE Electronics Letters*, vol. 35, pp. 14–16, January 1999.

[35] R. V. G.J. Foschini, G.D. Golden and P. Wolniansky, "Simplified Processing for High Spectral Efficiency Wireless Communications Employing Multi-element Arrays," *IEEE Journal on Selected Areas in Communications*, vol. 17, pp. 1841–1852, November 1999.

[36] G. G. P.W. Wolniansky, G.J. Foschini and R. Valenzuela, "V-BLAST: An Architecture for Realizing Very High Data Rates over the Rich-scattering Wireless Cannel,"

in *Proceedings of International Symposium on Signals, Systems and Electronics (ISSSE)*, pp. 295–300, September 1998.

[37] B. Hassibi and B. Hochwald, "High-Rate Codes that Are Linear in Space and Time," *IEEE Transactions on Information Theory*, vol. 48, pp. 1804–1824, July 2002.

[38] H.J. Chen, A. Haimovich and J.A. Sjogren, "Turbo Space-time Codes with Time Varying Linear Transformations," *IEEE Transactions on Wireless Communications*, vol. 6, pp. 486–493, February 2007.

[39] H. G. M.O. Damen and N. Beaulieu, "Linear Threaded Algebraic Space-time Constellations," *IEEE Transactions on Information Theory*, vol. 49, pp. 2372–2388, October 2003.

[40] X. Ma and G. Giannakis, "Full-Diversity Full-Rate Complex-Field Space-Time Coding," *IEEE Transactions on Signal Processing*, vol. 51, pp. 2917–2930, November 2003.

[41] R.H. Gohary and T.N. Davidson, "Design of Linear Dispersion Codes: Asymptotic Guidelines and Their Implementation," *IEEE Transactions on Wireless Communications*, vol. 4, pp. 2892–2906, November 2005.

[42] R. Heath and A. Paulraj, "Linear Dispersion Codes for MIMO Systems Based on Frame Theory," *IEEE Transactions on Signal Processing*, vol. 50, pp. 2429–2441, October 2002.

[43] B. Hassibi and B. Hochwald, "How Much Training Is Needed in Multiple-antenna Wireless Links?," *IEEE Transactions on Information Theory*, vol. 49, pp. 951–963, April 2003.

[44] B. Hochwald and T. Marzetta, "Unitary Spacetime Modulation for Multiple-antenna Communications in Rayleigh Flat Fading," *IEEE Transactions on Information Theory*, vol. 46, pp. 543–564, March 2000.

[45] B.M. Hochwald, T.L. Marzetta, T.J. Richardson, W. Sweldens and R. Urbanke, "Systematic Design of Unitary Spacetime Constellation," *IEEE Transactions on Information Theory*, vol. 46, pp. 1962–1973, September 2000.

[46] B. Hughes, "Differential Space-Time Modulation," *IEEE Transactions on Information Theory*, vol. 46, pp. 2567–2578, November 2000.

[47] B. Hochwald and W. Sweldens, "Differential Unitary Spacetime Modulation," *IEEE Transactions on Communications*, vol. 48, pp. 2041–2052, December 2000.

[48] W. S. K.L. Clarkson and A. Zheng, "Fast Multiple-antenna Differential Decoding," *IEEE Transactions on Communications*, vol. 49, pp. 253–261, February 2001.

[49] T. Himsoon, W. Su and K.J.R Liu, "Differential Unitary Space-time Signal Design Using Matrix Rotation Structure," *IEEE Signal Processing Letters*, vol. 12, pp. 45–48, January 2005.

[50] T.P. Soh, C.S. Ng and P.Y. Kam, "Improved Signal Constellations for Differential Unitary Space-time Modulations with More Than Two Transmit Antennas," *IEEE Communications Letters*, vol. 9, pp. 7–9, January 2005.

[51] S. Cheng, A. Nallanathan and P.Y. Kam, "A New Class of Signal Constellations for Differential Unitary Space-time Modulation (DUSTM)," *IEEE Communications Letters*, vol. 8, pp. 1–3, January 2004.

[52] X.-B. Liang and X.-G. Xia, "Unitary Signal Constellations for Differential Space-time Modulation with Two Transmit Antennas: Parametric Codes, Optimal Designs, and Bounds," *IEEE Transactions on Information Theory*, vol. 48, pp. 2291–2322, August 2002.

[53] V. Tarokh and H. Jafarkhani, "A Differential Detection Scheme for Transmit Diversity," *IEEE Journal on Selected Areas in Communications*, vol. 18, pp. 1169–1174, July 2000.

[54] H. Jafarkhani and V. Tarokh, "Multiple Transmit Antenna Differential Detection from Generalized Orthogonal Designs," *IEEE Transactions on Information Theory*, vol. 47, pp. 2626–2631, September 2001.

[55] G. Ganesan and P. Stoica, "Differential Detection Based on Space-time Block Codes," *Wireless Personal Communications*, vol. 21, pp. 163–180, 2002.

[56] G. Ganesan and P. Stoica, "Differential Modulation Using Space-time Block Codes," *IEEE Signal Processing Letters*, vol. 9, no. 2, pp. 57–60, 2002.

[57] D. Divsalar and M. K. Simon, "Multiple-Symbol Differential Detection of MPSK," *IEEE Transactions on Communications*, vol. 38, pp. 300–308, March 1990.

[58] A. Sendonaris, E. Erkip, and B. Aazhang, "Increasing Uplink Capacity via User Cooperation Diversity," in *Proceedings of IEEE International Symposium on Information Theory*, (Cambridge, MA, USA), August 1998.

[59] A. Sendonaris, E. Erkip, and B. Aazhang, "User Cooperation Diversity Part I: System Description," *IEEE Transactions on Communications*, vol. 51, pp. 1927–1938, November 2003.

[60] A. Sendonaris, E. Erkip, and B. Aazhang, "User Cooperation Diversity Part II: Implementation Aspects and Performance Analysis," *IEEE Transactions on Communications*, vol. 51, pp. 1939–1948, November 2003.

[61] J. N. Laneman, D. N. C. Tse, and G. W. Wornell, "Cooperative Diversity in Wireless Networks: Efficient Protocols and Outage Behavior," *IEEE Transactions on Information Theory*, vol. 50, pp. 3062–3080, December 2004.

[62] E. Zimmermann, P. Herhold and G. Fettweis, "On the Performance of Cooperative Diversity Protocols in Practical Wireless Systems," in *Proceedings of IEEE Vehicular Technology Conference (VTC)*, vol. 4, (Orlando, USA), pp. 2212–2216, October 2003.

[63] H. E. Gamal and D. Aktas, "Distributed Space-Time Filtering for Cooperative Wireless Networks," in *Proceedings of IEEE Global Conference on Communications*, vol. 4, (San Francisco), pp. 1826–1830, December 2003.

[64] J. N. Laneman and G. W. Wornell, "Distributed Space-Time-Coded Protocols for Exploiting Cooperative Diversity in Wireless Networks," *IEEE Transactions on Information Theory*, vol. 49, pp. 2415–2425, October 2003.

[65] M. Dohler and Y. Li, *Cooperative Communications: Hardware, Channel and PHY*. New York, USA: John Wiley & Sons, 2010.

[66] A. H. Bastami and A. Olfat, "Optimal SNR-based Selection Relaying Scheme in Multi-Relay Cooperative Networks with Distributed Space-Time Coding," *IET Communications*, vol. 4, pp. 619–630, April 2010.

[67] T. Cui, F. Gao, T. Ho, and A. Nallanathan, "Distributed Space-Time Coding for Two-Way Wireless Relay Networks," *IEEE Transactions on Signal Processing*, vol. 57, pp. 658–671, February 2009.

[68] Y. Jing and B. Hassibi, "Distributed Space-Time Coding in Wireless Relay Networks," *IEEE Transactions on Wireless Communications*, vol. 5, pp. 3524–3536, December 2006.

[69] D. To, J. Choi, and I. Kim, "Error Probability Analysis of Bidirectional Relay Systems Using Alamouti Scheme," *IEEE Communication Letters*, vol. 14, pp. 758–760, August 2010.

[70] T. Koike-Akino, P. Popovski, and V. Tarokh, "Denoising Maps and Constellations for Wireless Network Coding in Two-Way Relaying Systems," in *Proceedings of Global Conference on Communications (GlobeCom)*, (New Orleans, USA), pp. 3790–3794, December 2008.

[71] C. E. Shannon, "Two-way Communication Channels," in *Proceedings of the Fourth Berkeley Symposium on Mathematical Statistics and Probability*, vol. 1, (Berkeley, USA), pp. 611–644, 1961.

[72] R. Ahlswede, N. Cai, S.-Y. R. Li, and R. W. Yeung, "Network Information Flow," *IEEE Transactions on Information Theory*, vol. 46, pp. 1204–1216, July 2000.

[73] R. Koetter and M. Medard, "An Algebraic Approach to Network Coding," *IEEE/ACM Transactions on Networking*, vol. 11, pp. 782–795, October 2003.

[74] S.-Y. R. Li, R. W. Yeung, and N. Cai, "Linear Network Coding," *IEEE Transactions on Information Theory*, vol. 49, pp. 371–381, February 2003.

[75] P. Popovski and H. Yomo, "Wireless Network Coding by Amplify-and-Forward for Bi-directional Traffic Flows," *IEEE Communication Letters*, vol. 11, pp. 16–18, January 2007.

[76] B. Rankov and A. Wittneben, "Spectral Efficient Protocols for Half-duplex Fading Relay Channels," *IEEE Journal on Selected Areas in Communications*, vol. 25, pp. 379–389, February 2007.

[77] S. Zhang, S. C. Liew, and P. P. Lam, "Physical Layer Network Coding," in *Proceedings of MobiCom'06: The 12th annual international conference on mobile computing and networking*, (New York, NY, USA), pp. 358–365, 2006.

[78] H. Ochiai, P. Mitran, and V. Tarokh, "Design and Analysis of Collaborative Diversity Protocols for Wireless Sensor Networks," in *Proceedings of IEEE Vehicular Technology Conference (VTC)*, (Los Angeles, USA), pp. 4645–4649, 2004.

[79] A. Richardson, *WCDMA Design Handbook*. Cambridge, New York, Melbourne, Madrid, Cape Town, Singapore, So Paulo: Cambridge University Press, 2011 March.

[80] D. W. N. Cam-Winget, R. Housley and J. Walker, "Security Flaws in 802.11 Data Link Protocols," *Communications of the ACM*, vol. 46, pp. 35–39, May 2003.

[81] M. Ju and I. Kim, "Error Performance Analysis of BPSK Modulation in Physical-Layer Network-Coded Bidirectional Relay Networks," *IEEE Transactions on Communications*, vol. 58, pp. 2770–2775, October 2010.

[82] K. Lu, S. Fu, Y. Qian, and H. Chen, "SER Performance Analysis for Physical Layer Network Coding over AWGN Channels," in *Proceedings of Global Conference on Communications (GlobeCom)*, (Honolulu, Hawaii, USA), December 2009.

[83] M. Park, I. Choi, and I. Lee, "Exact BER Analysis of Physical Layer Network Coding for Two-Way Relay Channels," in *Proceedings of IEEE Vehicular Technology Conference (VTC)*, (Budapest, Hungary), May 2011.

[84] R. Freeman, *Fundamentals of Telecommunications*. New York, USA: John Wiley & Sons, 2nd ed., May 2005.

[85] A. Bletsas, A. Khisti, D. P. Reed and A. Lippman, "A simple Cooperative Diversity Method Based on Network Path Selection," *IEEE Journal on Selected Areas in Communications*, vol. 24, pp. 659–672, March 2006.

[86] H. M. P. Tarasak and V. K. Bhargava, "Differential Modulation for Two-User Cooperative Diversity Systems," in *Proceedings of IEEE Global Conference on Communications*, vol. 5, (Dallas), pp. 3389–3393, December 2004.

[87] B. M. Hochwald and W. Sweldens, "Differential Unitary Space-Time Modulation," *IEEE Transactions on Communications*, vol. 48, pp. 2041–2052, December 2000.

[88] S. J. Alabed and M. Pesavento and A. B. Gershman, "Distributed Differential Space-Time Coding Techniques for Two-Way Wireless Relay Networks," in *Proceedings of IEEE International Workshop on Computational Advances in Multi-Sensor Adaptive Processing (CAMSAP)*, (San Juan, Puerto Rico), pp. 1–5, December 2011.

[89] Z. Utkovski and G. Yammine and J. Lindner, "A Distributed Differential Space-Time Coding Scheme for Two-Way Wireless Relay Networks," in *International Symposium on Information Theory*, (Seoul, Korea), pp. 1–5, July 2009.

[90] R1-070462, Ericsson, "QPP Interleaver Design for LTE Turbo Coding," TS 36.212 v8.3.0, 3GPP RAN1, Jan. 14-19, 2007. Sorrento, Italy.

[91] O. Takeshita, "A New Metric for Permutation Polynomial Interleavers," *IEEE International Symposium on Information Theory (ISIT06)*, pp. 1983–1987, July 2006.

[92] , "3GPP Technical Specification: Group Radio Access Network, Evolved Universal Terrestrial Radio Access, Multiplexing and Channel Coding (Release 8)," TS 36.212 v8.3.0, , May 2007. .

[93] S. Lin and D.J. Costello, *Error Control Coding (Second Edition)*. Upper Saddle River, NJ, USA: Prentice Hall, 2004 May.

[94] W. Guan and K. J. R. Liu, "Performance Analysis of Two-Way Relaying with Non-coherent Differential Modulation," *IEEE Transactions on Wireless Communications*, vol. 10, pp. 2004–2014, June 2011.

[95] T. Cui, F. Gao, and C. Tellambura, "Differential Modulation for Two-Way Wireless Communications: A Perspective of Differential Network Coding at the Physical Layer," *IEEE Transactions on Communications*, vol. 57, pp. 2977–2987, October 2009.

[96] M. C. Valenti, D. Torrieri, and T. Ferrett, "Noncoherent Physical-Layer Network Coding with FSK Modulation: Relay Receiver Design Issues," *IEEE Transactions on Communications*, vol. 59, pp. 2595–2604, September 2011.

[97] K. Zhu and A. G. Burr, "Relay Selection aided Distributed Space-Time Block Code for Two-Way Relay Channel with Physical-Layer Network Coding," in *Proceedings of IEEE Vehicular Technology Conference (VTC)*, (Budapest, Hungary), pp. 1–5, May 2011.

[98] P. Robertson, "Illuminating the Structure of Code and Decoder of Systematic (Turbo) Codes," *IEEE Globecom*, pp. 1298–1303, 1994.

[99] L. R. Bahl, J. Cocke, F. Jelinek and J. Raviv, "Optimal Decoding of Linear Codes for Minimal Symbol Error Rate," *IEEE Transactions on Information Theory*, vol. 20, pp. 284–287, March 1974.

[100] G. Forney, "The Viterbi Algorithm," *Proceedings of the IEEE*, vol. 61, pp. 268–278, March 1973.

[101] C. Berrou, A. Glavieux and P. Thitimajshima, "Near Shannon Limit Error-Correcting Coding and Decoding: Turbo Codes," in *Proceedings of IEEE International Conference on Communications*, (Geneva), pp. 1064–1070, May 1993.

[102] P. Robertson, E. Villebrun, and P. Hoher, "A Comparison of Optimal and Sub-optimal MAP Decoding Algorithm Operating in the Log Domain," *International Conference on Communications* , pp. 1009–1013, June 1995.

[103] S. X. Ng, J. Wang and L. Hanzo, "Unveiling Near-Capacity Code Design: The Realization of Shannon's Communication Theory for MIMO Channels," *IEEE International Conference on Communications*, pp. 1415–1419, May 2008.

[104] P. Robertson, E. Villebrun, and P. Hoher, "A Comparison of Optimal and Sub-optimal MAP Decoding Algorithm Operating in the Log Domain," *International Conference on Communications* , pp. 1009–1013, June 1995.

[105] S. Benedetto, D. Divsalar, G. Montorsi and F. Pollara, "A Soft-Input Soft-Output APP Module for Iterative Decoding of Concatenated Codes," *IEEE Communications Letters*, vol. 1, pp. 22–24, January 1997.

[106] S. Benedetto, D. Divsalar, G. Montorsi and F. Pollara, "Soft-Input Soft-Output Modules for the Construction and Distributed Iterative Decoding of Code Networks," *European Transactions on Telecommunications*, vol. 9, pp. 155–172, March 1998.

[107] J. G. Proakis, ed., *Digital Communications*. New York, USA: McGraw-Hill, 4th ed., 2000.

[108] D. Smith, *Digital Transmission Systems*. Boston, USA: Kluwer Academic Publishers, 3rd ed., 2004.

[109] G. Colavolpe and R. Raheli, "The Capacity of the Noncoherent Channel," *European Transactions on Telecommunication*, vol. 12, pp. 289–296, July-August 2001.

[110] D. Makrakis, A. Yongacoglu and K. Feher, "A Sequential Decoder for Differential Detection of Trellis Coded PSK Signals," in *Proceedings of International Conference on Communications (ICC)*, (Philadelphia, PA, USA), pp. 1433–1438, 12-15 June 1988.

[111] F. Adachi and M. Sawahashi, "Viterbi-Decoding Differential Detection of DPSK," *Electronics Letters*, vol. 28, pp. 2196 – 2198, November 1992.

[112] G.M. Vitetta and D.P. Taylor, "Viterbi Decoding of Differentially Encoded PSK Signals Transmitted over Rayleigh Frequency-flat Fading Channels," *IEEE Transactions on Communications*, vol. 43, pp. 1256–1259, April 1995.

[113] D. Makrakis, P.T. Mathiopoulos and D.P. Bouras, "Optimal Decoding of Coded PSK and QAM Signals in Correlated Fast Fading Channels and AWGN: A Combined Envelope, Multiple Differential and Coherent Detection Approach," *IEEE Transactions on Communications*, vol. 42, pp. 63 – 75, January 1994.

[114] P. Hoeher and J. Lodge, "Turbo DPSK: Iterative Differential PSK Demodulation and Channel Decoding," *IEEE Transactions on Communications*, vol. 47, pp. 837–843, June 1999.

[115] M. Peleg, S. Shamai and S. Galan, "Iterative Decoding for Coded Noncoherent MPSK Communications over Phase-noisy AWGN Channel," *IEE Proceedings of Communications*, vol. 147, pp. 87 – 95, April 2000.

[116] D. Divsalar and M. K. Simon, "Maximum-Likelihood Differential Detection of Uncoded and Trellis Coded Amplitude Phase Modulation over AWGN and Fading Channels: Metrics and Performance," *IEEE Transactions on Communications*, vol. 42, pp. 76–89, January 1994.

[117] S.G. Wilson, J. Freebersyser and C. Marshall, "Multi-Symbol Detection of M-DPSK," in *Proceedings of Global Conference on Communications (GlobeCom)*, (Dallas, Texas, USA), pp. 1692–1697, November 1989.

[118] F. Edbauer, "Bit Error Rate of Binary and Quaternary DPSK Signals with Multiple Differential Feedback Detection," *IEEE Transactions on Communications*, vol. 40, pp. 457 – 460, March 1992.

[119] P. Ho and D. Fung, "Error Performance of Multiple-Symbol Differential Detection of PSK Signals Transmitted over Correlated Rayleigh Fading Channels," *IEEE Transactions on Communications*, vol. 40, pp. 1566 – 1569, October 1992.

[120] L. Lampe, R. Schober, V. Pauli, and C. Windpassinger, "Multiple-Symbol Differential Sphere Decoding," *IEEE Transactions on Communications*, vol. 53, pp. 1981–1985, December 2005.

[121] K.R. Narayanan and G.L. Stuber, "A Serial Concatenation Approach to Iterative Demodulation and Decoding," *IEEE Transactions on Communications*, vol. 47, pp. 956 – 961, July 1999.

[122] G. Colavolpe, G. Ferrari and R. Raheli, "Noncoherent Iterative (Turbo) Decoding," *IEEE Transactions on Communications*, vol. 48, pp. 1488 – 1498, September 2000.

[123] S. Howard and C. Schlegel, "Differential Turbo-Coded Modulation with APP Channel Estimation," *IEEE Transactions on Communications*, vol. 54, pp. 1397–1406, August 2006.

[124] C. Lo and S. Su, "SISO FB-MAP Detection for Turbo-Coded Differential PSK Systems," *IEEE Transactions on Vehicular Technology*, vol. 58, pp. 5288–5293, November 2009.

[125] D. Makrakis and K. Feher, "Optimal Noncoherent Detection of PSK Signals," *IEE Electronics Letters*, vol. 26, pp. 398 – 400, March 1990.

[126] K.M. Mackenthun, Jr., "A Fast Algorithm for Multiple-Symbol Differential Detection of MPSK," *IEEE Transactions on Communications*, vol. 42, pp. 1471 – 1474, April 1994.

[127] M. Peleg and S. Shamai, "Iterative Decoding of Coded and Interleaved Noncoherent Multiple Symbol Detected DPSK," *IEE Electronics Letters*, vol. 33, pp. 1018 – 1020, June 1997.

[128] V. Pauli, L. Lampe, and R. Schober, "Turbo DPSK: Using Soft Multiple-Symbol Differential Sphere Decoding," *IEEE Transactions on Information Theory*, vol. 52, pp. 1385–1398, April 2006.

[129] S. ten Brink, J. Speidel and R.H. Han, "Iterative Demapping for QPSK Modulation," *IEE Electronics Letters*, vol. 34, pp. 1459 – 1460, July 1998.